



THESIS
3
2009

LIBRARY
Michigan State
University

This is to certify that the
dissertation entitled


CATALYZED HYDROGEN PEROXIDE PROPAGATIONS: STUDY
OF HYDROGEN PEROXIDE DECOMPOSITION, HYDROXYL
RADICAL PRODUCTION, AND BYPRODUCT FORMATION FROM
THE REMEDIATION OF AROMATIC HYDROCARBONS.

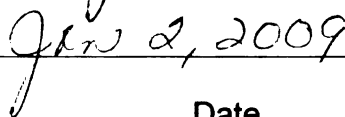
presented by

Carlos A. Sanlley Pagan

has been accepted towards fulfillment
of the requirements for the

Doctoral degree in Environmental Engineering


Major Professor's Signature


Date

MSU is an Affirmative Action/Equal Opportunity Employer

PLACE IN RETURN BOX to remove this checkout from your record.
TO AVOID FINES return on or before date due.
MAY BE RECALLED with earlier due date if requested.

DATE DUE	DATE DUE	DATE DUE

CATALYZED HYDROGEN PEROXIDE PROPAGATIONS: STUDY OF
HYDROGEN PEROXIDE DECOMPOSITION, HYDROXYL RADICAL
PRODUCTION, AND BYPRODUCT FORMATION FROM THE REMEDIATION OF
AROMATIC HYDROCARBONS.

By

Carlos A. Sanlley Pagan

A DISSERTATION

Submitted to
Michigan State University
in partial fulfillment of the requirements
for the degree of

DOCTOR OF PHILOSOPHY

Environmental Engineering

2009

ABSTRACT

CATALYZED HYDROGEN PEROXIDE PROPAGATIONS: STUDY OF HYDROGEN PEROXIDE DECOMPOSITION, HYDROXYL RADICAL PRODUCTION, AND BYPRODUCT FORMATION FROM THE REMEDIATION OF AROMATIC HYDROCARBONS

By

Carlos A. Sanlley Pagan

Catalyzed hydrogen peroxide propagations have been studied in order to determine the role of hydrogen peroxide decomposition and hydroxyl radical production during *in situ* remediation, as well as the byproducts obtained from the oxidation of aromatic hydrocarbons. Three types of catalyzed systems have been studied: ferrous catalyzed, ferric catalyzed, and goethite catalyzed reactions.

Hydrogen peroxide decomposition appears to be dependent only hydrogen peroxide concentration regardless of the catalyzer used. The rate of hydrogen peroxide decomposition is higher for reactions catalyzed with ferrous ion as opposed to ferric ion, while maintaining a similar yield for oxygen production. Goethite catalyzed reactions are slower, with a 24-hour reaction period required to achieve peak yield, versus a few minutes for soluble iron reactions.

Hydroxyl radical production from goethite catalyzed systems appears to be out competed by hydrogen peroxide decomposition, resulting in an increase in hydroxyl radical yield after 24 hours of reaction. Reactions at pH 3 appear to produce more hydroxyl radicals than reactions at pH 7 under the same experimental conditions. The total yield of hydroxyl radicals could not be determined due to the production of byproducts in the

reactions, some of which have been identified. Hydroxyl radical production from soluble iron reactions was estimated using kinetic modeling.

Pyrene was removed from both aqueous and slurry systems using catalyzed hydrogen peroxide. Pyrene removal was greater in slurry systems than in aqueous systems, possibly because of limitations due to the water solubility of pyrene. Ferric catalyzed systems achieved better removal rates than ferrous catalyzed reactions at the same experimental conditions. Goethite catalyzed reactions appear to be the most efficient achieving similar removal rates while using lower hydrogen peroxide concentrations. Byproducts were found for all reactions; 12 of these products have been identified. The byproducts range from hydroxylation reactions to ring cleaved products. By the use of parameter estimation software we have found that the aqueous solubility, and therefore their mobility, of some of these byproducts is orders of magnitude larger than that of pyrene; causing a potential threat to the environment. Byproducts found in this study are similar to those found from gaseous ozonation of pyrene.

Dedication

To my family and friends

Acknowledgements

I have come from afar and withstood many ordeals to reach this summit, but one constant is that I was never alone. I would like to thank through this section the many individuals and organizations that helped me achieve this feat. First and foremost I would like to thank Dr. Susan Masten for her encouragement, help, and understanding throughout my studies at Michigan State University. Dr. Masten was a teacher, a friend, family and a mentor, for that I am eternally grateful.

I would also like to thank the members of my research committee: Dr. Phanikumar Mantha, Dr. Volodymyr Tarabara, and Dr. Brian Teppen for their help and contributions to my work.

I was very fortunate to receive the support of LASPAU and the William H. Fulbright Scholarship program, which enabled me to study in the United States and fulfill one of my life dreams.

Once I reached Michigan State University I required financial support and received it from the East and West Michigan Chapters of the Air and Waste Management Association. My research funding was obtained from McMaster University, and NIEHS Superfund Grant 2P42ESO4911-05; thank you for your support.

There were many people involved in my life at MSU to which I would like to show my appreciation by naming them here: Lori Hasse, Laura Taylor, Mary Mroz and Linda Steinman; Joseph Nguyen and Yiliang Pan, Dr. Shuguang Li, Dr. Rick Lyles, Dr. Neeraj Buch and Dr. Sayed Hashsham, from the CEE department; Dr. Paul Jones and Patrick Bradley from Department of Food Toxicology; Shawn McElmurry, the unofficial member of my committee; Dr. Daniel Jones, Beverly Chamberlain and Li-Jun from the Mass Spectrometry Facility; and Dr. Simon Davies from Agricultural Engineering.

I have to give great thanks to Dr. Mackenzie Davis for being an inspiration, a mentor and a friend throughout my years at MSU. I have learned a great deal from you and I am still enjoying the fruits of our many conversations.

To Dr. Roger Wallace, thank you for being my friend, teacher, and collaborator. Your poise, knowledge and presence have always been greatly appreciated.

Finally, I would like to thank Geneva, without whom I would not have made it this far. I am thankful for your support, your caring and your belief in me. Your light gave me strength and guided me through the days. Thank you, you are and always will be the love of my life.

TABLE OF CONTENTS

List of Tables.....	x
List of Figures.....	xii
Objectives and Hypotheses	1
Objectives	1
Hypotheses.....	2
Chapter 1. Background.....	4
Polycyclic Aromatic Hydrocarbons.....	4
In-Situ Chemical Oxidation	6
Permanganate.....	6
Ozone.....	7
Persulfate.....	7
Catalyzed Hydrogen Peroxide	9
Conclusion	14
References.....	15
Chapter 2. Hydrogen Peroxide Decomposition	20
Introduction.....	20
Decomposition of hydrogen peroxide from reaction with mineral Iron: Goethite...	22
Method and Materials	23
Preliminary Experiments	23
Gravimetric Tests: Oxygen Evolution	24
Effect of a chelating agent on Oxygen Evolution.....	25
Effect of aquifer Material on Hydrogen Peroxide Decomposition.....	26
Results.....	26
Goethite.....	35
Discussion.....	39
Soluble Iron.....	39
Temperature.....	41
Ottawa Sand Slurries.....	43
Soluble iron.....	43
EDTA experiments	43
Goethite.....	44
Conclusions.....	48
References.....	50

Chapter 3. Hydroxyl Radical Production	55
Introduction.....	55
Method and Materials:	57
Materials	57
Soluble Iron Experiments	57
Goethite experiments:	58
Salicylic Acid Determination.....	59
Time dependent SA reactions	59
Byproduct Identification	60
GC/MS	60
LC/MS.....	60
Atomic Absorption.....	61
Results:.....	62
Soluble Iron.....	62
Goethite.....	63
Time Dependent Reactions	72
Byproducts	73
GC/MS	75
Discussion	76
Sorption of SA to Goethite	76
Salicylic Acid Degradation by Goethite Catalyzed CHPs.....	77
Byproducts	82
Conclusions.....	95
References.....	97
 Chapter 4. Oxidation of Pyrene in Soil	 107
Pyrene	107
Method and Materials	108
Determining Pyrene Concentration.....	109
Results.....	111
Organic Matter Soil:	112
Discussion:	116
Ottawa Sand:	117
MSU soil:	119
Sodium Dodecyl Sulfate	120
MGP Site Soil	122
Conclusions.....	125
References.....	126
 Chapter 5. Byproduct formation from the oxidation of Pyrene by Catalyzed Hydrogen Peroxide Propagations	 128
Introduction.....	128
Method and Materials	131
Byproduct Structure Identification	133

Sample preparation	133
Results.....	134
Byproduct Formation.....	136
Discussion.....	143
Byproduct formation between different Catalyzers.....	144
Comparison to PAH byproducts found from Fenton's Reagent Reactions	148
Comparison to PAH Byproducts from other Remediation Techniques.....	149
Electrolytic Aeration of pyrene.....	149
Photolysis of Pyrene	150
Biodegradation of Pyrene and other PAHs.....	150
Ozonation of Pyrene	152
Environmental Impact of PAH remediation	154
Mobility.....	154
Toxicity.....	155
Conclusions:.....	157
References.....	161
 Chapter 6. Modeling.....	 167
Introduction.....	167
Kinetic Model	167
Temperature	170
Modeling Iron Species and Concentration.....	172
Oxidation of Ferrous ion by Oxygen	173
RMSE.....	174
Results.....	175
Discussion.....	184
Conclusions.....	186
References.....	187
 Chapter 7. Conclusions	 189
 Appendix A: Pyrene Oxidation Byproducts	 195
Appendix B: Salicylic Acid Byproducts.....	220
Appendix C: HPLC Chromatograms	238
Appendix D: MATLAB Code for Kinetic Model:	248

List of Tables

Table 2-1: Regression analysis for oxygen produced during CHP reactions. The terms a, b, c, and d refer to the coefficients in equation 13. CI is the 95% confidence interval for the preceding variable.	33
Table 2-2: Values for coefficients for equation 11 obtained from normalized solution temperature fits.	33
Table 2-3: Coefficients and 95% confidence intervals for Oxygen production from Goethite experiments for an exponential regression fit.	37
Table 2-4: Coefficients found form linear regression of data from gravimetric experiments during Goethite catalyzed CHPs.	38
Table 3-1: Results for the removal of 100 ppm of salicylic acid (SA) from solution using Goethite catalyzed reactions at pH 7. Shown are the amounts of Goethite weighed for each trial and its subsequent concentration, the total surface area in each sample vial the amount of salicylic acid found in each sample, the amount of salicylic acid sorbed onto the mineral and the percent removal of salicylic acid from the sample (corrected by sorption). The final column is an estimate of hydroxyl radicals produced calculated from the amount of salicylic acid removed after 72 hours	66
Table 3-2: Results for the removal of 100 ppm of salicylic acid (SA) from solution using Goethite catalyzed reactions at pH 3. Shown are the amounts of Goethite weighed for each trial and its subsequent concentration, the total surface area in each sample vial the amount of salicylic acid found in each sample, the amount of salicylic acid sorbed onto the mineral and the percent removal of salicylic acid from the sample (corrected by sorption). The final column is an estimate of hydroxyl radicals produced calculated from the amount of salicylic acid removed after 72 hours.	67
Table 4-1: Physicochemical properties of Pyrene ¹	107
Table 4-2 Results from oxidation of 50 grams of MGP soil with 120,000 ppm of hydrogen peroxide with and without soluble iron addition. LOD: Limit of Detection	115
Table 5-1: Table showing m/z found in the combined extracts from the different CHP tested.	136
Table 5-2: Byproducts identified by LC/MS/MS with a list of major m/z peaks found in the spectra	137
Table 5-3: Estimated parameters for each one of the byproducts found as well as the SMILES characters used to represent them in the parameter estimation software.	158

Table 5-4: Byproducts found from CHP, gaseous ozonation and bioremediation remediation of pyrene.	159
Table 6-1: Best fit for normalized temperature for soluble iron catalyzed reactions. Molar concentrations of iron and hydrogen peroxide are given along with the coefficients for the regression line and the R^2	171
Table 6-2: Rate Constants for Reaction of Fe^{2+} Species with O_2 from Morel 1993 ⁴⁴ ...	174
Table 6-3: Values for the hydrogen peroxide decomposition rate constant determined from the optimization of the objective function in equation 63 for reactions corrected and not corrected for temperature.	177

List of Figures

Figure 2-1: Volume of Oxygen produced during a CHP with high end hydrogen peroxide concentration (0.5M) catalyzed by ferric ion (0.01M). Measured by water displacement on an inverted cylinder.	27
Figure 2-2: Hydrogen peroxide concentration back calculated from the volume of oxygen collected in the inverted cylinder shown in Figure 1.	28
Figure 2-3: Moles of oxygen produced during reactions catalyzed with ferrous and ferric soluble iron for varying hydrogen peroxide concentrations. The graph shows that oxygen production is independent of catalyzer concentration.	29
Figure 2-4: Relation between regression coefficients and the initial hydrogen peroxide concentration for oxygen production for soluble iron catalyzed reactions.....	30
Figure 2-5: Change in temperature of solution during reaction normalized by initial temperature for three different hydrogen peroxide concentrations catalyzed by 0. 3 M Ferric ion.	31
Figure 2-6: Comparison between solution temperature for ferrous and ferric catalyzed systems, normalized by the initial temperature.....	32
Figure 2-7: Relation between regression coefficients and the initial hydrogen peroxide concentration for normalized temperature for soluble iron catalyzed reactions.....	34
Figure 2-8: Comparison of Oxygen production between reactions with and without Ottawa sand and with and without EDTA.	35
Figure 2-9: Oxygen production form Goethite catalyzed reactions.....	36
Figure 3-1: Pathway for the reaction of hydroxyl radicals with salicylic acid and its products ⁵⁴	56
Figure 3-2: Plot of the change in hydrogen peroxide concentration as a function of time for ferric ion concentration of 0.06 M. Hydrogen peroxide was measured by iodometric titration. The initial concentration of hydrogen peroxide is shown in the legend.....	62
Figure 3-3: Response surface obtained from equation 1 for the removal of salicylic acid at pH 7 using goethite catalyzed reactions. The x-axis represents H from equation 2 and the y-axis represents F from equation 3. The color scheme represents the region at which a specific removal efficiency can be found and is delineated by the isoresponse lines shown in the figure.	68

Figure 3-4: Response surface obtained from equation 4 for the removal of salicylic acid at pH 3 using goethite catalyzed reactions. The x-axis represents H from equation 2 and the y-axis represents F from equation 3. The color scheme represents the region at which a specific removal efficiency can be found and is delineated by the isoresponse lines shown in the figure.	70
Figure 3-5: Plot of SA concentration over time for different hydrogen peroxide and Goethite concentrations for pH 3 reactions. Initial SA concentration of 100 ppm...	72
Figure 3-6: Plot of SA concentration over time for different hydrogen peroxide and Goethite concentrations for pH 7 reactions. Initial SA concentration of 100 ppm...	73
Figure 3-7: Oxidation of salicylic acid 100 ppm over time for pH 3 and pH 7 reactions with 0.0263 g/L goethite and an initial concentration of hydrogen peroxide of 0.13M.	74
Figure 3-8: Comparison of SA removal in pH3 and pH 7 samples at different SA concentrations.	78
Figure 3-9: Typical chromatographic spectra from LC/MS analysis in negative ion mode for pH 3 reactions, showing the total ion count for negative ion data acquisitions. And the peaks for m/z 153 ⁻ found in the samples.	83
Figure 3-10: Mass spectra for pH 3 samples showing m/z 153 ⁻ and 169 ⁻ , that are believed to be dihydroxy and trihydroxy benzoic acids.	85
Figure 3-11: Chromatographic peak of m/z 169 ⁻ believed to be THBA, as compared to the total ion count on the LC/MS for pH 3 samples	87
Figure 3-12: LC/MS spectra for retention time 5.17minutes for pH 7 samples, showing m/z 153 ⁻ and 169 ⁻ ; which are believed to be DHBA And THBA.....	89
Figure 3-13: Chromatographic peak of byproduct m/z 153 ⁻ shown here to compare its abundance versus total ion counts, in positive and negative ion mode for pH 7 sample during LC/MS analysis. It is possible to see from the first scan that three isomers may exist.....	91
Figure 3-14: Possible structure for the byproduct m/z 169 ⁻ found in the LC/MS spectra in Figures 3-8 and Figure 3-10.....	93
Figure 3-15: GC/MS identified byproducts found from the oxidation of salicylic acid by Goethite catalyzed CHPs for both pH 3 and pH 7.	94
Figure 4-1: Structure of model PAH, Pyrene showing double bonds and fused benzene rings.....	107

Figure 4-2: Results from the Oxidation of Pyrene in Ottawa Sand using CHP. The graph shows the percent oxidation achieved at the different hydrogen peroxide concentrations used under Ferrous and Goethite catalyzed systems.	111
Figure 4-3: Summary of results in soil containing organic matter. Percent of pyrene oxidation Vs hydrogen peroxide concentrations using both soluble Fe^{2+} and natural minerals of the Soil. Results shown are averages of triplicates.	113
Figure 4-4 : Pyrene oxidation in soil containing organic matter catalyzed with soluble Fe^{2+} (Percent Oxidation vs. Hydrogen Peroxide Concentration).	114
Figure 4-5: Pyrene oxidation in soil containing organic matter catalyzed with mineral iron (Percent Oxidation vs. Hydrogen Peroxide Concentration).	114
Figure 4-6: Contaminated soil being extracted from geo-probes during sampling at the Grand Ledge, MI former MGP site.	123
Figure 5-1: Percent removal of pyrene from CHPs for solution and Ottawa sand reactions. The initial iron catalyst concentration was held at 0.06 M, while the initial hydrogen peroxide concentration was 0.11 M.	135
Figure 5-2: LC/MS Electrospray mass spectra for m/z 233 obtained from the oxidation of Pyrene in solution by Goethite. This m/z was found in the hexane extract.	138
Figure 5-3: MS/MS spectra showing fragment ions from m/z 233, obtained from the hexane extract of Goethite catalyzed CHPs.	139
Figure 5-4: Byproducts identified from the oxidation of Pyrene by CHPs in water and soil slurries, using mineral and soluble iron catalyzed reactions. *3 isomers of the structure were found, but not readily distinguished.	141
Figure 5-5: Proposed pathway for hydroxyl radical degradation of Pyrene by CHPs... ..	142
Figure 5-6: a) Pyrene molecule with numbered carbons and b) showing p-orbitals around the center region of the molecule.	147
Figure 6-1: Plot showing the result from the optimization of the kinetic model described by equations 11-17 for an initial hydrogen peroxide concentration of 0.1 M and ferric ion concentration of 0.06 M. The lines represent the simulated concentrations obtained by the model and the Δ represent the hydrogen peroxide concentration obtained from iodometric titration.	176
Figure 6-2: Plot showing the result from the optimization of the kinetic model described by equations 11-17 for an initial hydrogen peroxide concentration of 0.57 M and ferric ion concentration of 0.07 M. The lines represent the simulated concentrations	

obtained by the model and the Δ represent the hydrogen peroxide concentration obtained from iodometric titration.....	177
Figure 6-3: Graph showing the change in concentration for Ferrous and Ferric ions during CHP reactions with initial hydrogen peroxide concentration of 0.1 M and ferric ion initial concentration of 0.07 M for reactions modeled with equations 11-17 with temperature correction. The graph illustrates the cycling of ferric ion to ferrous ion and back.	178
Figure 6-4: Graphs showing the concentrations of hydroxyl radical, perhydroxyl radical, and Superoxide formed during CHP reactions for initial hydrogen peroxide concentration of 0.1 M and initial ferric ion concentration of 0.07 M. Model is described by equations 11-17 with temperature correction.	180
Figure 6-5: Comparison of the oxygen production calculated by the kinetic model and experimental data collected for hydrogen peroxide concentration of 0.57 M and ferric ion concentration of 0.07 M	182

Objectives and Hypotheses

Objectives

Chemical oxidation, used as an in-situ remediation technique, is a highly complex system that is commonly treated as a black box. This research attempts to shed light on the mechanisms that occur in catalyzed hydrogen peroxide systems while creating tools that can be applied for estimating the outcomes from this treatment. To complement these tools, byproduct identification from the oxidation of aromatic compounds during such reactions has been performed. The fate of these byproducts in the environment has also been estimated.

The following objectives have been studied:

- 1) The conditions under which hydrogen peroxide decomposition inhibits hydroxyl radical production in catalyzed hydrogen peroxide reactions have been determined.
- 2) A kinetic model for hydroxyl radical production during catalyzed hydrogen peroxide reactions has been developed.
- 3) Byproducts formed from oxidation of pyrene in aqueous and soil matrices have been identified for the following oxidative treatments:
 - a) Ferrous ion (Fe^{2+}) catalyzed hydrogen peroxide. (Classic Fenton's Reagent)
 - b) Ferric ion (Fe^{3+}) catalyzed hydrogen peroxide. (Modified Fenton's Reagent I)

c) Mineral iron (Goethite) catalyzed hydrogen peroxide. (Modified Fenton's Reagent II)

4) A model that can be used to determine the potential fate of the identified by-products in the environment has been developed.

Hypotheses

The following hypotheses for this proposed study have been tested:

1) Based on the known theories of hydroxyl radical interaction with aromatic species, in-situ chemical oxidation of polycyclic aromatic hydrocarbons *in aqueous systems* using catalyzed hydrogen peroxide, Fenton's Reagent, will produce hydroxylated, quinonic, hydroquinonic and ring-cleaved by-products, whose physical-chemical properties (e.g., water solubility) will differ from the parent compound.

2) Based on the known theories of hydroxyl radical interaction with aromatic species, in-situ chemical oxidation of polycyclic aromatic hydrocarbons *in soil matrices* using catalyzed hydrogen peroxide, Fenton's Reagent, will produce hydroxylated, quinonic, hydroquinonic and ring-cleaved by-products, whose physical-chemical properties will differ from the parent compound. The extent of byproduct formation will be greater than that of the aqueous system.

- 3) The catalyzer selected to promote hydroxyl radical formation during Fenton system reactions will affect the structure of the by-product formed and/or the rate of by-product formation.
- 4) A mathematical model can be constructed in order to predict the type of byproduct formed under specified matrix conditions; specifically what will be the dominant species in the system. The environmental fate of the byproducts that result from the chemical oxidation of pyrene using Fenton's Reagent may be predicted by computational modeling; using the properties of the by-products formed (i.e., mobility, sorptive behavior) or the properties of model compounds with similar structures.
- 5) Hydrogen peroxide decomposition into oxygen, a parallel competitive reaction occurring in Fenton systems during both homogeneous and heterogeneous catalysis, inhibits maximum hydroxyl radical production.
- 6) Oxygen production from hydrogen peroxide decomposition during Fenton reactions can be quantified and may be used as a tool to predict hydroxyl radical production during in-situ chemical reactions.

Chapter 1.

Background

Polycyclic Aromatic Hydrocarbons

Polycyclic Aromatic Hydrocarbons (PAHs) are a group of common environmental contaminants comprised of 2 or more fused benzene rings. These compounds are formed during the incomplete combustion of organic matter and fossil fuels, and are found in petroleum derived products, such as diesel, kerosene, and gasoline^{1, 2}.

PAHs are characterized as being recalcitrant. The mobility of these compounds is limited due to their low water solubility (log water solubility at 25°C ranging from -3.61 to -8.22)³; with solubility decreasing as their molecular weight or hydrophobic surface area increases³. PAHs also have a strong affinity toward soil organic matter (log K_{ow} from 3.36 to 6.5)⁴. As a result, PAHs are stable in the environment for long periods of time.

The recalcitrant nature of the PAHs as well as their mutagenic/carcinogenic potential, makes them potential health risks and therefore they are listed as priority pollutants⁵ by the U.S. Environmental Protection Agency (U.S.EPA). The U.S. EPA states that at least 8 out the 16 PAHs listed as priority pollutants may produce skin, liver and/or lung cancer in humans.

PAHs are associated with industrial activities where fossil fuels are used, leading to their presence in highly industrialized areas. The formation of PAHs during the combustion of fossil fuels and their subsequent release into the atmosphere has allowed for their

widespread distribution in air, water, soil and sediments ². The presence of PAHs in the atmosphere varies due to seasonal fluxes as fossil fuel consumption increases during winter months. The contaminant may move to a different medium by wet or dry deposition from the atmosphere. PAHs may also reach the environment through leaching from wastes, leaking underground storage tanks or direct contact of petroleum derived products with soil or water ¹. Manufactured Gas Plant (MGP) sites, for example, have been found to contain PAH contamination ⁶; occurring from mismanagement of coal tar wastes, as well as direct dumping of these wastes into soil (U.S. EPA).

Current efforts for the remediation of these compounds in soil and water include: soil washing, in-situ and ex-situ chemical oxidation and biodegradation ^{1, 2, 7, 8}. Ex-situ treatments involve the pumping of water from the contaminated site or the excavation of the contaminated soil/aquifer material in order to remove the contaminant; the U.S. EPA promotes the use of incineration for soils extracted from sites that contain PAH contamination. In-situ treatment may include the use of chemical agents to neutralize or oxidize the contaminant in place. Bioremediation, which can be performed both ex-situ and in-situ, includes bioaugmentation or biostimulation of bacteria or fungi that degrade PAHs. Bioremediation may degrade these chemicals by utilizing them as a carbon source for the bacteria or the contaminant may be cometabolized ².

Sims and Overcash ⁹ (1983) found that one, two, and three ring PAHs are believed to be acutely toxic and that four and five ring PAHs may be genotoxic. Using Gap Junction

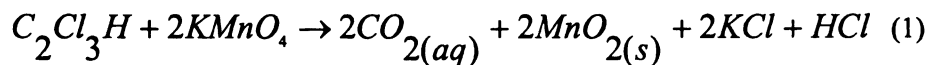
Intercellular Communication (GJIC), the epigenetic toxicity of some PAHs and their derivatives was studied by Luster-Teasley et al.¹⁰, Herner et al. (ref), and Upham et al.¹¹. The studies found that GJIC was inhibited by both the PAHs and their ozonated derivatives; with some derivatives creating greater inhibition than the parent compound.

In-Situ Chemical Oxidation

In-Situ Chemical Oxidation or ISCO has evolved as an effective process to remediate organic chemicals from soils, especially in places where infrastructure impedes other treatment techniques¹². ISCO involves the addition of a strong oxidant; often ozone, catalyzed hydrogen peroxide, potassium permanganate or persulfate; into the soil matrix. The goal of chemical oxidation is to change the valence state of the chemical species, ultimately breaking carbon bonds and forming carbon dioxide and water. The effectiveness of these remediation schemes is dependent on the site characteristics, distribution of the oxidant in the matrix, the target compound, and the oxidant used^{12, 13}.

Permanganate

There are two forms of permanganate used for ISCO: potassium permanganate (KMnO_4) or sodium permanganate (NaMnO_4)^{13, 14}. Sodium permanganate is sold as a 40% solution, while potassium permanganate is sold in bulk as a solid. Permanganate is known to oxidize a wide variety of chemicals, such as phenols, cresols, and cyanides; and is believed to react more effectively with olefins than with aliphatic compounds. It is especially reactive with double bonds. Permanganate is commonly used to remediate water contaminated with chlorinated chemicals, such as trichloroethylene:



Permanganate produces manganese dioxide as a product from the oxidation reactions and in most cases the dioxide will coat soil grains and reduce soil matrix permeability. Gates-Anderson, 2001¹⁵ used permanganate as an oxidizer for PAHs and found that the system could achieve the similar results to those of catalyzed hydrogen peroxide (about 90% disappearance).

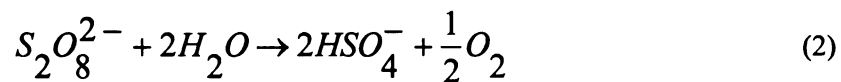
Ozone

Ozone is a very reactive and unstable species of oxygen. It is used as an oxidizer and a disinfectant. Ozone is a gas with a half-life of 30 seconds in distilled water at 20 °C. The solubility of ozone in water is three times that of oxygen at the same temperature or about 24 ppm at 20 °C. The use of ozone as a remediation agent requires an on-site generator to produce the gas, which entails high capital costs for treatment. Ozone gas has been studied as a remediation agent for PAHs in both water and soil; and the byproducts obtained from this system have been also identified and studied^{10, 16-20}.

Persulfate

Sodium persulfate (Na₂S₂O₈) has been recently employed as a chemical oxidant for in-situ remediation. The persulfate ion is a slow reacting oxidant considered more powerful than hydrogen peroxide, whose reactivity is a function of pH and concentration²¹.

Neutral



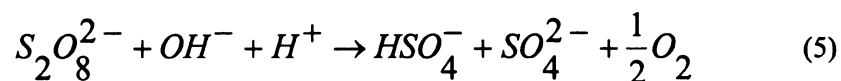
Dilute acid (pH 3-7)



Strong acid



Alkaline



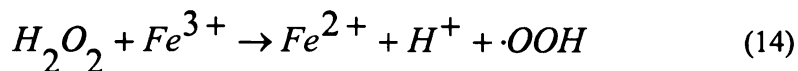
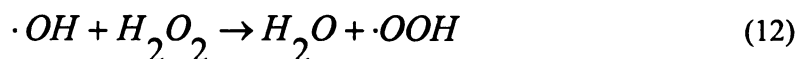
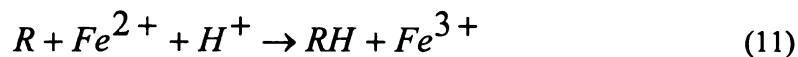
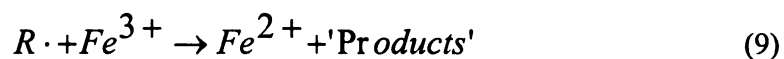
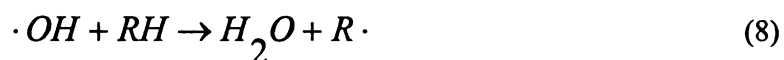
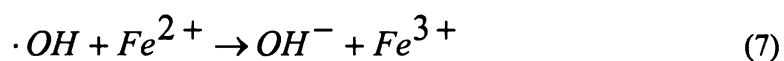
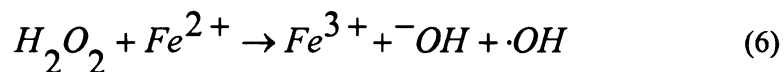
The oxidative strength of persulfate may be increased with the addition of heat or ferrous salts (although copper, silver or manganese can be used). The increase in strength is believed to result from the formation of sulfate radicals ($SO_4^{\cdot-}$), which are oxidation potency comparable to the hydroxyl radical. The half life of the sulfate radical is believed to be approximately 4 seconds at 40°C.

Persulfate is activated at high pH, where it is capable of degrading chlorinated compounds and has been used in acid conditions to remove VOC's from groundwater.

The system does not have the capability of degrading chlorinated solvents in acid conditions. The catalytic effect of metals in the persulfate system decreases over time and the distance from the injection point, limiting the application of this oxidizer.

Catalyzed Hydrogen Peroxide

In 1894, H.J. Fenton reported that ferrous ion promoted the oxidation of malic acid by hydrogen peroxide. This discovery jumpstarted the study of the chemical system that now bears his name, Fenton's Reagent. It was not until 1934 that Haber and Weiss proposed that the addition of the ferrous ion catalyzes the decomposition of hydrogen peroxide, producing a highly oxidative radical species known as the hydroxyl radical ²². The catalytic reaction and the subsequent reactions that occur in the presence of an oxidizable substrate are shown below ^{23, 24}



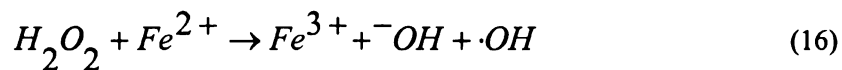
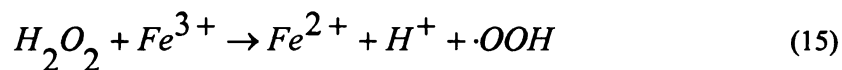
Fenton's Reagent is defined as a dilute hydrogen peroxide solution catalyzed by ferrous **iron**. A dilute hydrogen peroxide solution is considered to be less than 300 ppm (0.03%)

of the oxidizer. In in-situ applications, these dilute conditions may not be achieved and higher concentrations (4-20%) of peroxide are typically used. Adding to this discrepancy, the ferric ion produced during the reaction may precipitate out of solution at pH values greater than 5, which prompted the addition of chelating agents into the system to maintain iron solubility. Watts et al. have proposed the use of the term Catalyzed Hydrogen Peroxide Propagations (CHP) as a collective title for the new Fenton hybrid systems^{25, 26}. The contaminant removal efficiency using these CHPs is varied and dependent on the chemical properties of the contaminant, the matrix and the CHP formulation used. The use of the original Fenton's composition is commonly referred to as Classical Fenton's Reagent.

Hydroxyl radicals are highly reactive, nonspecific oxidizing agents²⁷. Walling et al.²⁸ studied the reaction of the hydroxyl radical with several substituted benzene compounds and found that reactions would either cause hydroxylation of the aromatic ring forming phenolic compounds, leading to ring cleavage, or cause a dimerization of the molecule forming a biphenyl group. The hydroxylation of the aromatics was found to have a first-order dependence on the concentration of the compound and that ring deactivating groups such as bromide and chloride have a positive effect on the hydroxylation²⁹. Casero et al.³⁰ found that the ratio of ferrous to ferric ions (or excess hydrogen peroxide) affected the intermediates and end products formed during the oxidation of aromatic amines. If the iron species is predominantly in its ferric state the formation of dimers was favored, while the predominance of ferrous ion led to ring cleavage byproducts.

Not all hydroxyl radicals formed by CHPs may be free in solution, some are caged or become complexed before they interact with the target molecule ³¹. Walling found that high concentrations of hydroxyl radical scavengers did not completely prevent the oxidation of mandelic acid (α -hydroxy benzeneacetic acid), and therefore concluded that some of the hydroxyl radicals were not entering the bulk phase of the solution, but still reacting with the target compound.

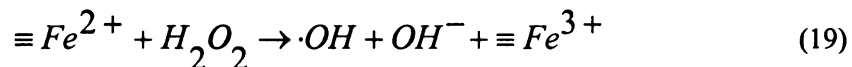
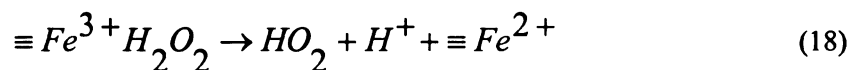
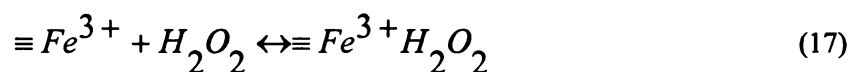
Hydrogen peroxide decomposition may be catalyzed by polyvalent metal ions other than the ferrous ion to create hydroxyl radical formation. Copper (Cu^{2+}), titanium (Ti^{3+}), and manganese (Mn^{2+} , Mn^{3+}) all produce Fenton-like chemistry when used as catalyzers ^{23, 24, 28, 31, 32}. Fenton systems may also be catalyzed by other iron species, such as ferric ion ³³, mineral iron ³³⁻³⁵ and chelated iron ^{24, 36}. The studies performed by Watts ³³ and by Pignatello ³⁷ utilize the ferric ion as the main catalyzer in CHP reactions. Ferric ion creates reactions that differ from the classical system by the formation of a greater amount of perhydroxyl ions ($\text{HO}_2\cdot$ or $\cdot\text{OOH}$). The ferric ion catalyzed system reactions are described by Walling, 1974, as:



This ferric ion catalyzed system was found to be dependent on the stability of the carbonium ions formed during oxidation of an organic compound ^{24, 29}. Pignatello also **points** out that due to the rapid oxidation of the ferrous ion to ferric ion (95% oxidation in

2.8 minutes in a 2:/1 mM ferrous : hydrogen peroxide ion solution) most of the actual studies performed on the degradation of organics may have been actually ferric ion catalyzed and not ferrous ion catalyzed ³⁷. This same study found that the ferric system resulted in the mineralization of 2,4 dichlorophenoxyacetic acid (2,4-D) while with the ferrous ion system, 2,4-D reacted more rapidly, but mineralization was not achieved.

Mineral iron catalyzed reactions utilize the natural iron species found in soils as a catalyzer ³⁵. Goethite is one of the most common minerals used as catalysts ^{33-35, 38}. These minerals usually contain a mixture of both ferric and ferrous ions and thus the reactions that occur are a combination of ferric/ferrous systems. For insoluble minerals Kwan et al. ³⁸ proposed Fenton's Reagent initiation reactions that occur on the mineral surface:



Since the reaction is dependent on the extent of contact between the surface and hydrogen peroxide, and the binding of hydrogen peroxide to iron atoms on the surface; it is reasonable to assume that these reactions will be slower than those that contain soluble iron.

Fenton chemistry has been found to be pH dependent, being most effective at pH 2-3³⁷; with its oxidizing efficiency decreasing as the pH increases. For this reason, chelated iron species such as ferrous/ferric-EDTA^{24, 36, 40, 41} are sometimes used to create Fenton-like reactions at higher pH. The chelated species are expected to prevent the precipitation of the iron from the solution, and thus avoid the pH adjustment that would be necessary for the reaction to take place effectively.

No published study has looked at byproduct or intermediate product formation from Fenton's Reagent systems catalyzed by mineral iron. Some studies lacked effort in determining byproducts; Chen et al.⁴² stated no byproducts were found in GC analysis from the oxidation of n-hexadecane, 2-methylnaphthalene, and Diesel Fuel after 24 hour oxidation; but only looked at low mass products in the GC. The extraction of these byproducts was performed with a Soxhlet method, which uses hexane as the extracting solvent. Hexane would only extract non-polar compounds and if hydroxylation is the principle means of attack for hydroxyl radicals, then polar compounds would be expected to a major fraction of the products formed.

A study performed by Bowers et al.^{43, 44} on the oxidation 2,4-dichlorophenol and dinitro-ortho-cresol with Fenton's Reagent concluded that not all the hydrogen peroxide was used to convert the organic matter into carbon dioxide, but that the parent compounds were altered leaving byproducts in the solution.

Conclusion

Polycyclic aromatic hydrocarbons are widespread environmental contaminants. Their carcinogenic potential has made them priority pollutants in the U.S. and therefore contaminated areas must be treated in order to minimize potential health risks. In situ chemical oxidation (ISCO) is one of the most common techniques used for treatment of PAH contaminated sites. Of the four ISCO chemicals used, Fenton's reagent is the most common because of its availability, cost, and versatility. Recent work has shown that PAH remediation with ozone produces byproducts that are in some instances more soluble and hazardous than the parent compound. The following work has looked at the potential problems that arise from the use of Fenton's Reagent as remediation tool and the potential byproducts that are formed from the chemical oxidation of PAHs by this technique.

References

1. Kostecki, P. T.; Calabrese, E. J., *Petroleum Contaminated Soils: Remediation Techniques, Environmental Fate, and Risk Assessment*. 3rd ed.; Lewis Publishers, Inc.: Chelsea, MI, 1989; Vol. 1.
2. Juhasz, A. L.; Naidu, R., Bioremediation of High Molecular Weight Polycyclic Aromatic Hydrocarbons: A Review of Microbial Degradation of Benzo[a]pyrene. *International Biodeterioration & Biodegradation* **2000**, *45*, 57-88.
3. Schwarzenbach, R. P.; Gschwend, P. M.; Imboden, D. M., *Environmental Organic Chemistry*. 1st ed.; Wilkey-Interscience, John Wiley & Sons Inc: New York, 1993.
4. Chiou, C. T.; McGroddy, S. E.; Kile, D. E., Partition Characteristics of Polycyclic Aromatic Hydrocarbons on Soils and Sediments. *Environmental Science and Technology* **1998**, *32*, (2), 264-269.
5. Keith, L. H.; Telliard, W. A., Priority Pollutants: Prospective View. *Environmental Science and Technology* **1979**, *13*, (4), 416-424.
6. Srivastava, V. J.; Kelley, R. L.; Paterek, J. R.; Hayes, T. D.; Nelson, G. L.; Golchin, J., A Field Scale Demonstration of Novel Bioremediation Process for MGP Sites. *Applied Biochemistry and Biotechnology* **1994**, *45*, (6), 741-756.
7. Heitkamp, M. A.; Freeman, J. P.; Cerneglia, C. E., Napthalene Biodegradation in Environmental Microcosms: Estimates of Degradation Rates and Characterization of Metabolites. *Applied and Environmental Microbiology* **1987**, *53*, (1), 129-136.
8. Nam, K.; Rodriguez, W.; Kukor, J. J., Enhanced Degradation of Polycyclic Aromatic Hydrocarbons by Biodegradation Combined with a Modified Fenton Reaction. *Chemosphere* **2001**, *45*, (2001), 11-20.
9. Sims, R. C.; Overcash, M. R., Fate of Polycyclic Aromatic Compounds (PNAs) in Soil-Plant Systems. *Residue Reviews* **1983**, *88*, 1-68.

10. Luster-Teasley, S. L.; Yao, J. J.; Herner, H. H.; Trosko, J. E.; Masten, S. J., Ozonation of Chrysene: Evaluation of By-Product Mixtures and Identification of Toxic Constituent. *Environmental Science and Technology* **2002**, 36, (5), 869-876.
11. Upham, B. L.; Masten, S. J.; Lockwood, B. R.; Trosko, J. E., Nongenotoxic Effects of Polycyclic Aromatic Hydrocarbons and Their Ozonation By-Products on Intercellular Communication of Rat Liver epithelial Cells. *Fundamental and Applied Toxicology* **1994**, 23, 470-475.
12. Yin, Y.; Allen, H. E., In Situ Chemical Treatment. July 1999
13. Group, I. T. a. R. C. W. Technology Overview Dense Non-Aqueous Phase Liquids (DNPL): Review of Emerging Characterization and Remediation Technologies. <http://www.itrcweb.org/DNAPL-1.pdf>
14. Gates-Anderson, D. D.; Siegreist, R. L.; Cline, S. R., Comparison of Potassium Permanganate and Hydrogen Peroxide as Chemical Oxidants for Organically Contaminated Soils. *Journal of Environmental Engineering* **2001**, 337-347.
15. Beltran, F. J.; Ovejeor, G.; Rivas, J., Oxidation of Polycyclic Aromatic Hydrocarbons in Water.4. Ozone Combined with Hydrogen Peroxide. *Industrial Engineering and Chemistry Research* **1996**, 35, (3), 891-898.
16. Luster-Teasley, S. The Use of Gaseous Ozone to remediate Pyrene Contaminated Soils: A study of By-Product Production, Environmental effects on Remediation Efforts, and Scale-Up Volume I & II. Dissertation for the Degree of Ph. D., Michigan State University, East Lansing, MI, 2003.
17. Yao, J.-J.; Huang, Z.-H.; Masten, S. J., Ozonation of Benz[a]anthracene: Pathway and Product Identification. *Water Research* **1998**, 32, (11), 3235-3244.
18. Yao, J.-J.; Huang, Z.-H.; Masten, S. J., The Ozonation of Pyrene: Pathway and Product Identification. *Water Research* **1998**, 32, (10), 3001-3012.
19. Benitez, F. J.; Beltran-Heredia, J.; Acero, J. L.; Rubio, F. J., Chemical Decomposition of 2,4,6-Trichlorophenol by Ozone, Fenton's Reagent and UV Radiation. *Industrial Engineering and Chemistry Research* **1999**, 38, (1999), 1341-1349.

20. Haber, F.; Weiss, J., Catalytic Decomposition of Hydrogen Peroxide by Iron Salts. *Proceedings of The Royal Society, London* **1934**, 147, 332-351.
21. Jones, C. W., *Applications of Hydrogen Peroxide*. The Royal Society of Chemistry: Cambridge, 1999.
22. Walling, C., Fenton's Reagent Revisited. *Accounts of Chemical Research* **1974**, 8, 125-131.
23. Watts, R. J.; Teel, A. L., Chemistry of Modified Fenton's Reagent (Catalyzed H₂O₂ Propagations-CHP) for In Situ Soil and Groundwater Remediation. *Journal of Environmental Engineering* **2005**, 131, (4), 612-622.
24. Watts, R. J.; Teel, A. L., Treatment of Contaminated Soils and Groundwater Using ISCO. *Practice Periodical of Hazardous, Toxic, and Radioactive Waste Management* **2006**, 10, (1), 2-9.
25. Buxton, G. V.; Greenstock, C. L.; Helman, W. P.; Ross, A. B. *Critical Review Constants for Reactions of Hydrated Electrons Hydrogen Atoms and Hydroxyl Radicals (•OH/O•) in Aqueous Solution.*; 1988.
26. Walling, C.; Johnson, R. A., Fenton's Reagent V. Hydroxylation and Side-Chain Cleavage of Aromatics. *Journal of the American Chemical Society* **1974**, 97, (2), 363-367.
27. Augusti, R.; Dias, A. O.; Rocha, L. L.; Lago, R. M., Kinetics and Mechanism of Benzene Derivative Degradation with Fenton's Reagent in Aqueous Medium Studied by MIMS. *Journal of Physical Chemistry* **1998**, 102, (52), 10723-10727.
28. Casero, I.; Sicilia, D.; Rubio, S.; Perez-Bendito, D., Chemical Degradation of Aromatic Amines By Fenton's Reagent. *Water Research* **1997**, 31, (8), 1985-1995.
29. Walling, C.; Amarnath, K., Oxidation of Mandelic Acid by Fenton's Reagent. *Journal of the American Chemical Society* **1982**, 104, (5), 1185-1189.

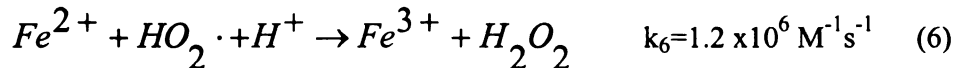
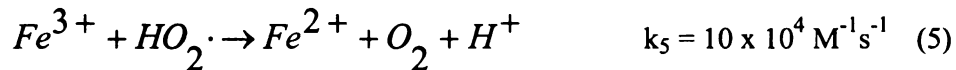
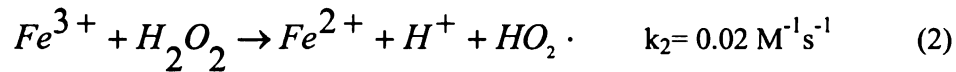
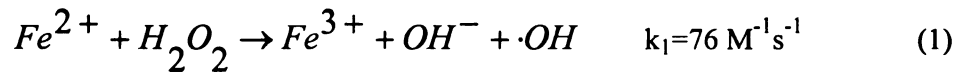
30. Walling, C.; El-Taliawi, Fenton's Reagent III. Addition of Hydroxyl Radicals to Acetylenes and Redox Reactions of Vinyl Radicals. *Journal of the American Chemical Society* **1973**, 95, (3), 848-850.
31. Teel, A. L.; Warberg, C. R.; Atkinson, D. A.; Watts, R. J., Comparison of Mineral and Soluble Iron Fenton's Catalysts for the Treatment of Trichloroethylene. *Water Research* **2001**, 35, (4), 977-984.
32. Kong, S.-H.; Watts, R. J.; Choi, J.-H., Treatment of Petroleum-Contaminated Soils Using Iron Mineral Catalyzed Hydrogen Peroxide. *Chemosphere* **1998**, 37, (8), 1473-1482.
33. Watts, R. J.; Stanton, P. C.; Howsawkung, J.; Teel, A. L., Mineralization of a Sorbed Polycyclic Aromatic Hydrocarbon in Two Soils using Catalyzed Hydrogen Peroxide. *Water Research* **2002**, 36, 4283-4292.
34. Kakarla, P. K.; Andrews, T.; Greenberg, R. S.; Zervas, D. S., Modified Fenton's Processes For Effective In-Situ Chemical Oxidation-Laboratory and Field Evaluation. *Remediation* **2002**, Autumn, 23-36.
35. Pignatello, J. J., Dark and Photoassisted Fe³⁺ Catalyzed Degradation of Chlorophenoxy Herbicides by Hydrogen Peroxide. *Environmental Science and Technology* **1992**, 26, (5), 944-951.
36. Kwan, W. P.; Voelker, B. M., Rates of Hydroxyl Radical Generation and Organic Compound Oxidation in Mineral-Catalyzed Fenton-like Systems. *Environmental Science and Technology* **2003**, 37, (6), 1150-1158.
37. Tyre, B. W.; Watts, R. J.; Miller, G. C., Treatment of Four Biorefractory Contaminants in Soils Using Catalyzed Hydrogen Peroxide. *Journal of Environmental Quality* **1991**, 20, (October-December), 832-838.
38. Pignatello, J. J.; Baehr, K., Ferric Complexes as Catalysts for "Fenton" Degradation of 2,4-D and Metolachlor in Soil. *Journal of Environmental Quality* **1994**, 23, (March-April), 365-370.

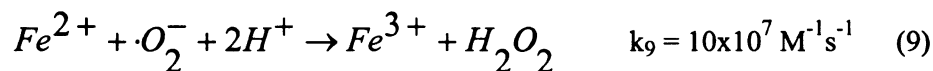
39. Yamazaki, I.; Piette, L., EPR Spin Trapping Study on the Oxidizing Species Formed in the Reaction of The Ferrous Ion with Hydrogen Peroxide. *Journal of the American Chemical Society* **1991**, 113, (20), 7588-7593.
40. Chen, C. T.; Tafuri, A. N.; Rahman, M.; Foerst, M. B., Chemical Oxidation Treatment of Petroleum Contaminated Soil Using Fenton's Reagent. *Journal of Environmental Science and Health* **1998**, A33, (6), 987-1008.
41. Bowers, A. R.; Gaddipati, P.; Eckenfelder Jr., W. W.; Monsen, R. M., Treatment of Toxic or Refractory Wastewaters with Hydrogen Peroxide. *Water Science and Technology* **1989**, 21, 477-486.
42. Morel, F. M.; Hering, J. G., *Principles and Applications of Aquatic Chemistry*. John Wiley & Sons, Inc.: New York, 1993; p 588.

Chapter 2. Hydrogen Peroxide Decomposition

Introduction

Fenton's Reagent is a complex set of reactions in which a dilute solution of hydrogen peroxide is catalyzed by polyvalent metals, usually iron, to form hydroxyl radicals. The catalyst is recycled back its original state through a series of complex reactions. Fenton's Reagent has seen a large increase in demand as an in situ remediation technique but with modifications to the catalyzer and oxidant used. The modified Fenton Reagent systems are becoming known as Catalyzed Hydrogen Peroxide Propagations (CHP). CHP systems utilize higher hydrogen peroxide concentrations than those used in traditional Fenton's reactions; this increase in concentration is usually done as a means of compensating for the nonselective nature of hydroxyl radicals and the amount of oxidizable material present in project sites. The typical reactions in a Fenton Reagent system are:





Hydrogen peroxide decomposes to oxygen over time; this process is accelerated by the presence of soluble iron and other polyvalent metals, as well as by certain minerals that may be present in the soil. The kinetic rate constant for hydrogen peroxide decomposition to oxygen is rarely found in the literature, nor is the equation ever incorporated in the Fenton's Reagent system.



Studies of Fenton's Reagent reactions avoid the issue of hydrogen peroxide decomposition by using low end concentrations of both hydrogen peroxide and soluble iron (1μM-1mM), where oxygen evolution is minimal. In field applications much greater peroxide concentrations are commonly used. Typically solutions of 4%-15% hydrogen peroxide injected into the soil or surface water²¹. Oxygen production in these systems would be significant wherever soluble iron species exceeds mM concentrations or where mineral iron is found, and thus the limiting reactant in CHPs, hydrogen peroxide, would decrease at a faster rate than expected, resulting in a decrease in the removal efficiency of the system.

Another factor that affects the remediation process is that hydrogen peroxide decomposition is an exothermic reaction releasing 98 kJ/mole of energy; this energy is transformed to heat, which then increases the temperature of the solution accelerating all reactions in the system including kinetic, sorptive and decomposition reactions.

Decomposition of hydrogen peroxide from reaction with mineral Iron:

Goethite

Hydrogen peroxide decomposition on mineral surfaces is easily seen due to the formation of oxygen bubbles on the surface and the diffusion of these throughout the liquid phase.

This decomposition rate was found to be zero order by Watts⁴⁵, which is the expected reaction order for surface catalyzed reactions. Lin and Guro⁴⁶ found a relationship for hydrogen peroxide decomposition on goethite to follow the empirical equation:

$$k_d = k_o(\text{FeOOH})^n \quad (11)$$

where

$$n = 1$$

FeOOH is the concentration of Goethite (g/L)

k_o has an empirical value of 0.037, dimensionless.

k_d is the decomposition rate constant in 1/(Ls/mole)

In a subsequent paper Lin and Guro⁴⁷ give a value for a hydrogen peroxide decomposition rate, k_d , on goethite that does not match the value the authors would get from equation 11. The reason for this discrepancy may be due to the equation being incomplete. Using the goethite concentration in g/L would not work because the surface

area (SA) and number of available kinetic sites (S) would differ on samples of goethite not obtained from the same manufacturing process, where the size and shape of the particles will vary from batch to batch. The equation found is unique to the goethite used for that particular experiment. For that reason, the goethite concentration (g/L) should be substituted for the effective surface area of the goethite (m^2/g) in the sample.

Method and Materials

Chemicals: All chemicals used were A.C.S reagent grade unless stated otherwise. Ferrous perchlorate, ferric perchlorate, Ethyldiamine acetic acid disodium salt (EDTA), salicylic acid, potassium iodide, bipyridine, goethite ($\alpha\text{-FeOOH}$, 30-50 mesh), and perchloric acid were obtained from Sigma-Aldrich (St. Louis, Mo). Stabilized hydrogen peroxide 30% solution was obtained from Fisher Scientific (Hampton, NH).

The hydrogen peroxide concentrations greater than $1\mu\text{M}$ were determined by iodometric titration with sodium thiosulfate⁴⁸. Concentrations of hydrogen peroxide less than $1\mu\text{M}$ were titrated by peroxidase catalyzed oxidation of N,N-diethyl-*p*-phenylenediamine (DPD) as described by Bader et al.⁴⁹ and modified by Voelker and Sulzberger⁵⁰ to minimize interference by ferrous and ferric ions.

Preliminary Experiments

Experiments were designed to determine the decomposition rate of hydrogen peroxide to oxygen in CHP systems and how the rate of decomposition varies with the concentration of catalyzer, Fe^{2+} , Fe^{3+} , and/or goethite. The tests were performed by measuring water

displacement on an inverted graduated cylinder. Borosilicate vials (40 mL) were completely filled with the desired catalyzer solution and capped with a Teflon liner to which the desired amount of hydrogen peroxide was injected through the liner. The liner was cut and fit with a Teflon tube with a gas sparger at the other end. The sparger was placed inside an inverted graduated cylinder filled with water held inverted inside a tub of water (Torricelli Experiment). As oxygen was produced in the 40 mL vial it flowed through the tube and into the graduated cylinder the gas then displaced water and a volume reading was recorded from the cylinder.

The volume of water displaced was then used to back calculate the hydrogen peroxide concentration using the ideal gas law to determine the moles of oxygen produced from the volume reading, and the rate of oxygen production versus hydrogen decomposition of 2 to one to determine the hydrogen peroxide concentration.

$$-\frac{dH_2O_2}{dt} = \frac{1}{2} \frac{dO_2}{dt} \quad (12)$$

Gravimetric Tests: Oxygen Evolution

Experiments were conducted to measure the change in mass that occurred in the reactive samples over time using an analytical scale. CHP reactions were carried out in 40 mL borosilicate vials containing 25 mL of an aqueous catalyzer solution. Before initiating the reaction the weight of the vials was recorded. To start the reaction a previously weighed and titrated hydrogen peroxide solution was added to the catalyzer mixture and allowed to react for 2 minutes before the first measurement was taken. The 2 minute time frame was given to allow the aqueous solution to become saturated with the oxygen produced,

thus creating steady state conditions for mass loss in the system. For this data to be of significance we have to assume that the only mass leaving the system would be that of the oxygen produced during the reaction. The mass difference over time was used to calculate the moles of oxygen produced by:

$$\text{Moles of Oxygen} = \frac{\Delta \text{Mass}}{32 \text{ g } O_2 / \text{mole}} \quad (13)$$

Because the decomposition of hydrogen peroxide to oxygen is an exothermic reaction the temperature of the reaction was monitored and recorded throughout the experiments with the use of temperature probe attached to a Jenway 4330 pH/Conductivity meter.

The pH of the solution was also monitored during reactions, but no buffer was added. The pH of the samples was adjusted using 0.1 M perchlorate acid or 0.1M sodium hydroxide solutions.

The experiments were carried out for a wide range of catalyzer and oxidant concentrations (10^{-5} to 1M), for the three catalyzer systems used: ferric ion, ferrous ion and Goethite. Goethite experiments were carried out at pH 7, were Watts et al.⁴⁵ determined was the pH with the greatest oxygen production.

Effect of a chelating agent on Oxygen Evolution

CHP reactions often use the addition of a complexing agent to solubilize the ferrous or ferric ion at pH values greater than 3. For this reason, EDTA was added as desired and the effect this complexing agent had on oxygen evolution was recorded. EDTA (0.1 M)

was added to the reaction vials containing the soluble iron species and allowed to interact with the iron for 20 minutes before the start of the experiments.

Effect of aquifer Material on Hydrogen Peroxide Decomposition

To determine the effect that aquifer material might have on the production of oxygen during CHP reactions, the experiments were also carried out as soil slurries using 20 g of Ottawa sand. Experiments were conducted with the soil either partially or fully saturated with water/catalyst solution. Results from all experiments are averages of at least triplicates.

Results

Preliminary tests using water displacement as an oxygen production measure show that the rate of decomposition of hydrogen peroxide may be 1st order for CHPs using soluble ferric ion as seen in

Figure 2-1 and Figure 2-2. Water displacement experiments were replaced with gravimetric tests to improve on precision and accuracy.

The displacement of water by oxygen showed a region during the reaction phase in which the oxygen production followed a linear trend. This time frame was then selected for further experiments with soluble iron catalyst.

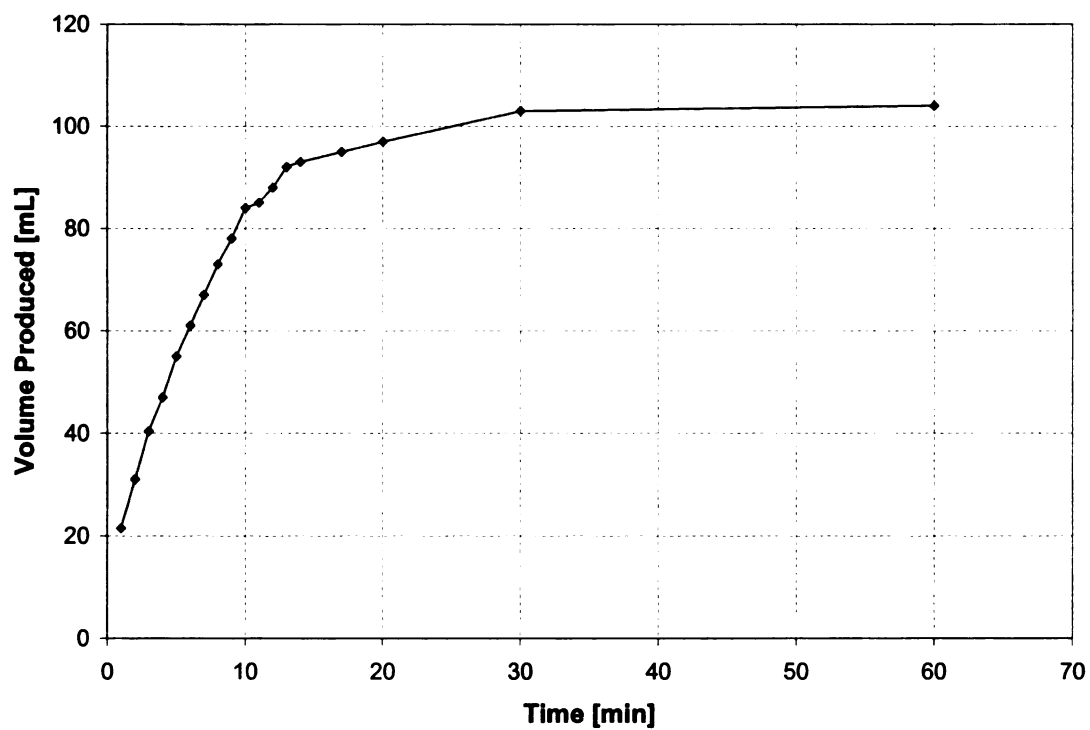


Figure 2-1: Volume of Oxygen produced during a CHP with high end hydrogen peroxide concentration (0.5M) catalyzed by ferric ion (0.01M). Volume of air was measured by water displacement on an inverted cylinder.

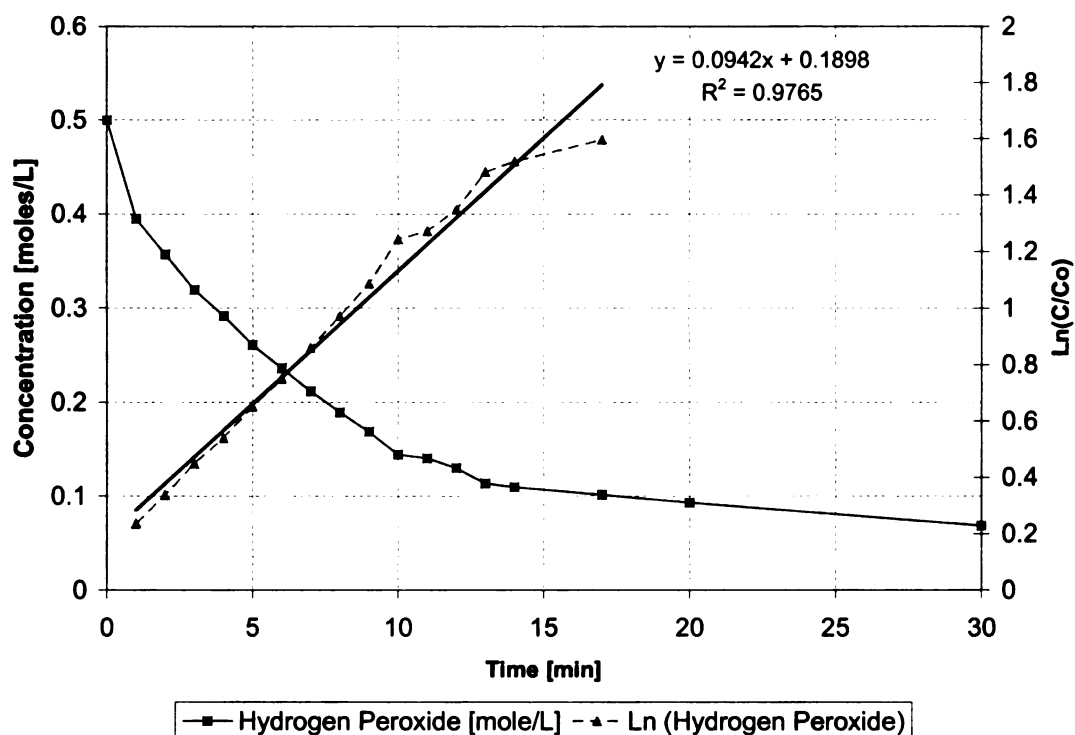


Figure 2-2: Hydrogen peroxide concentration over time, back calculated from the volume of oxygen collected in the inverted cylinder shown in Figure 1. The figure also shows the linear relationship between log concentration and time for the reaction

The change in mass in the reaction vials was measured for several hydrogen peroxide and soluble iron concentrations as seen in Figure 2-3. The data was corrected for evaporation by weighing blanks; 40 ml borosilicate vials containing water, catalyzer solution; and diluted hydrogen peroxide were used as evaporation blanks. The change in mass that occurred in these vials, if any, over the experimental time frame was subtracted from the change in mass of the reactions.

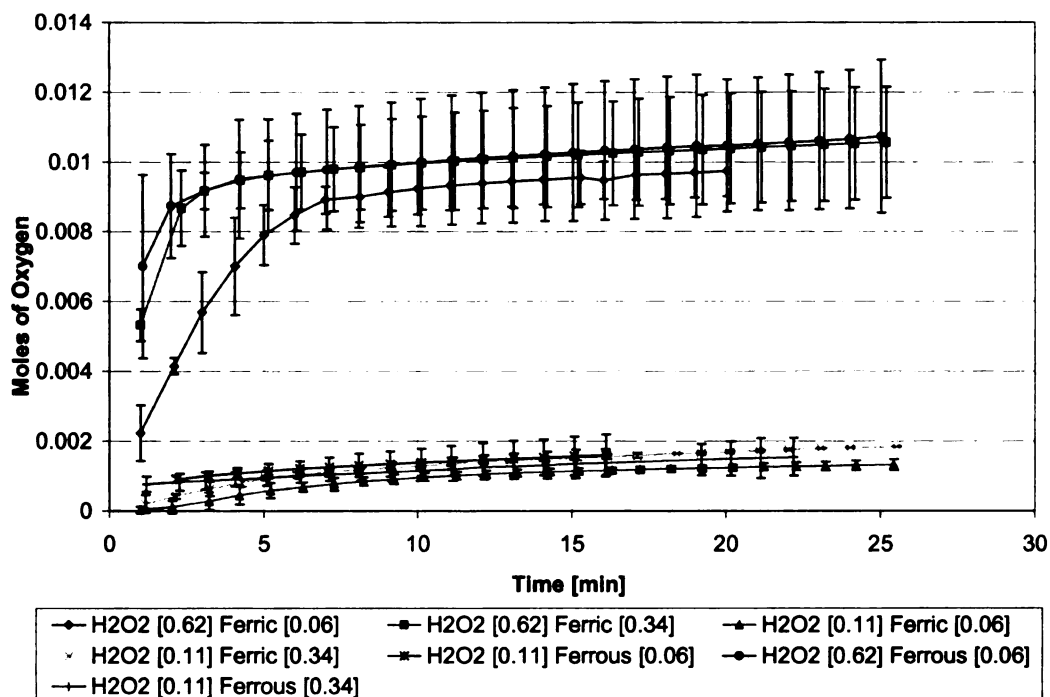


Figure 2-3: Moles of oxygen produced during reactions catalyzed with ferrous and ferric soluble iron for varying hydrogen peroxide concentrations. The graph shows that oxygen production is independent of catalyzer concentration.

The oxygen production curves were generated from the data collected from soluble iron gravimetric tests. The best fit for the curves and the coefficients found from these fits are found in Table 2-1. The best fit for the curves was found using equation 14.

$$\text{Moles } O_2 \text{ produced}(t) = a \cdot e^{b \cdot t} + c \cdot e^{d \cdot t} \quad (14)$$

The coefficients from Table 2-1 were then graphed versus the initial hydrogen peroxide concentration to try and establish a correlation between the concentrations of oxidant and catalyzer used, as shown in Figure 2-4.

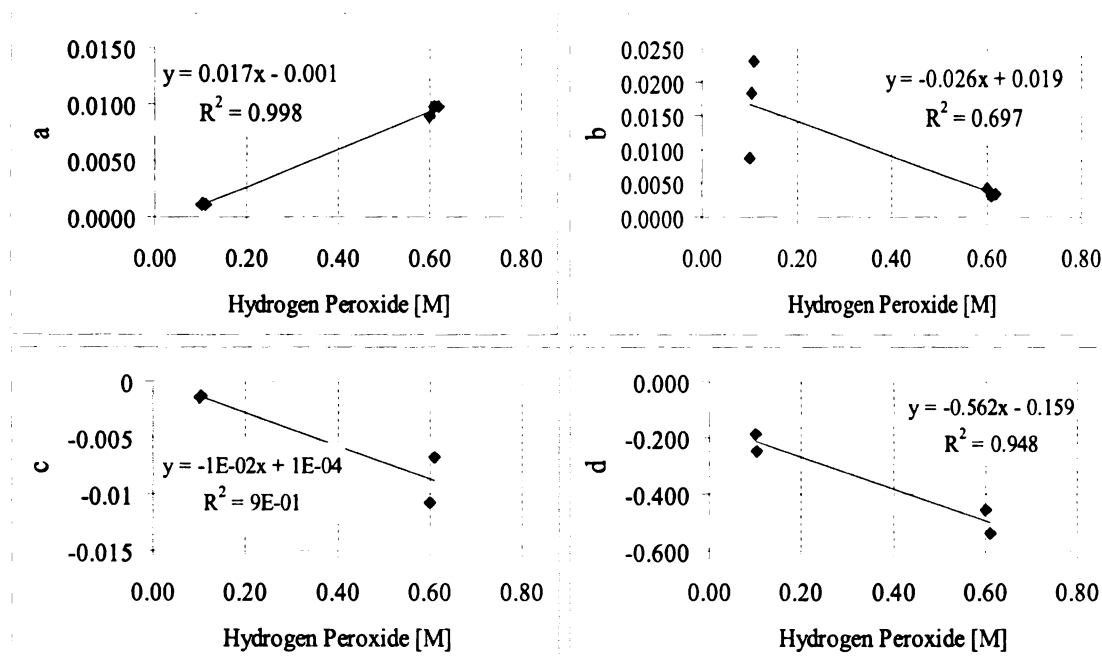


Figure 2-4: Relation between regression coefficients and the initial hydrogen peroxide concentration for oxygen production for soluble iron catalyzed reactions

The temperature of the solution during the reaction period was also monitored and a plot of normalized temperature over the experimental time for ferric catalyzed systems can be seen in Figure 2-5. Only three of the trials are shown for clarity. A comparison for the temperature profiles between ferrous and ferric catalyzed reactions is seen in Figure 2-6.

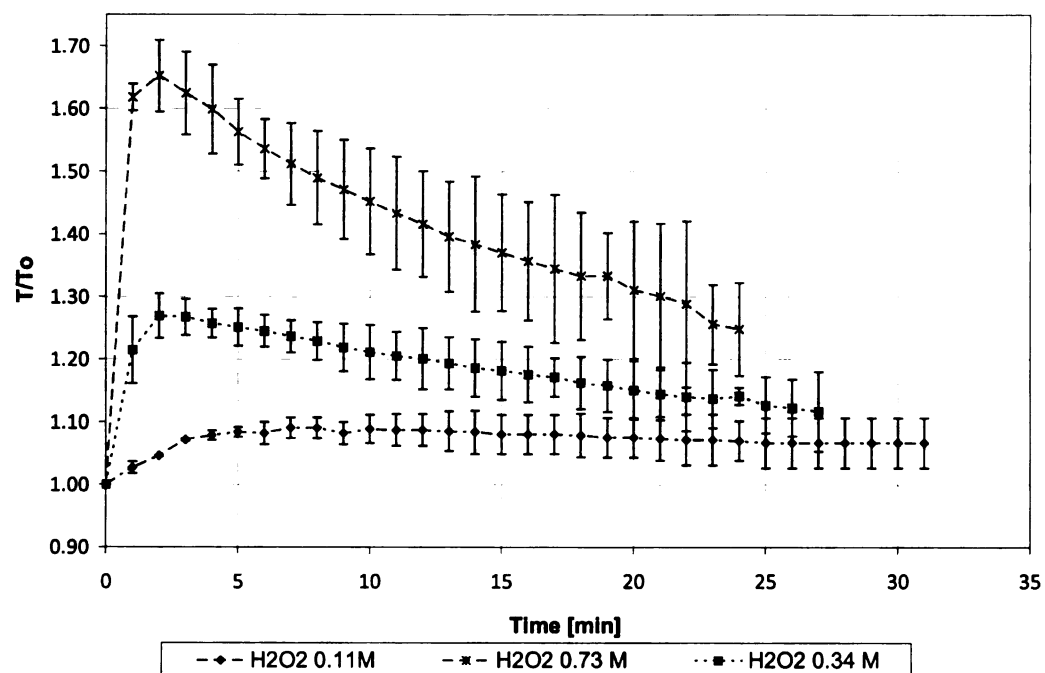


Figure 2-5: Temperature of the solution was measured during reactions. Here the temperature data is normalized by initial temperature for initial hydrogen peroxide concentrations of 0.11, 0.34 and 0.73 M. The ferric ion concentration used in all experiments was 0.3 M at a pH ranging between 2-3.

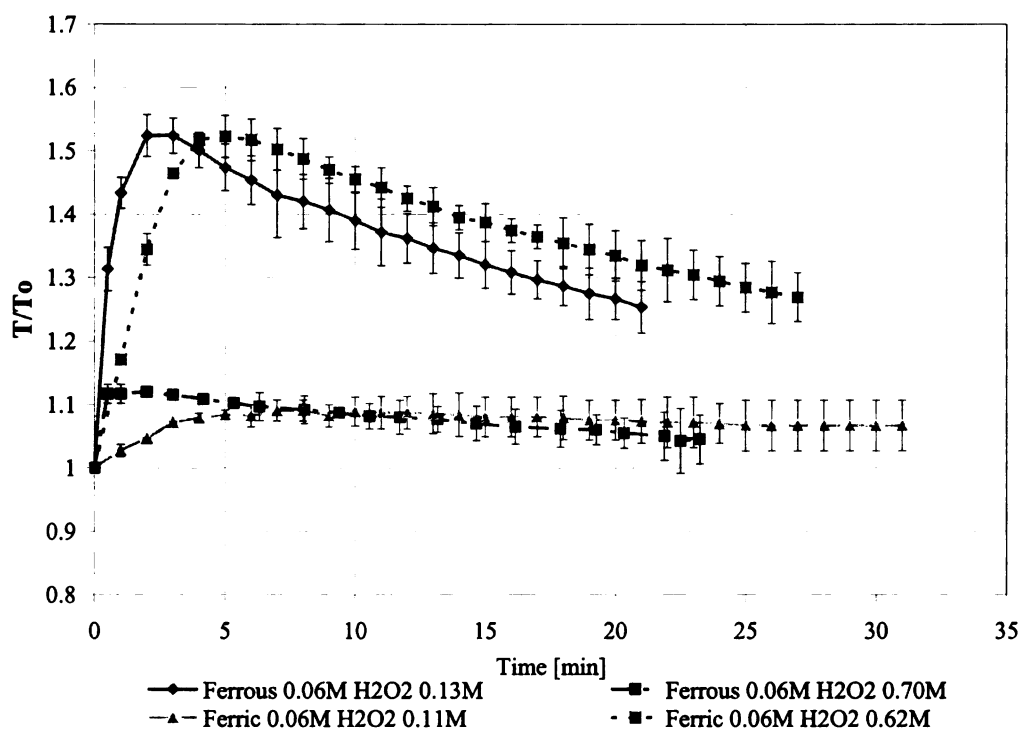


Figure 2-6: Comparison between solution temperature for ferrous and ferric catalyzed systems, normalized by the initial temperature at 2-3 pH range.

As with the oxygen production, the normalized temperature curves were fit through regression analysis, and the values for the best fit equation are shown in Table 2-2. The best fit was found using the equation:

$$\frac{T}{T_0} = a \cdot e^{b \cdot t} + c \cdot e^{d \cdot t} \quad (15)$$

Table 2-1: Regression analysis for oxygen produced during CHP reactions. The terms a, b, c, and d refer to the coefficients in equation 13. CI is the 95% confidence interval for the preceding variable.

	H ₂ O ₂	Fe	a	CI	b	CI	c	CI	d	CI	R ²
Ferric											
Trial1	0.10	0.06	0.0011	1.68E-04	0.0087	0.0066	-0.00138	1.37E-04	-0.187	0.042	0.99
Trial2	0.60	0.06	0.0089	2.33E-04	0.0042	0.0016	-0.01072	3.90E-04	-0.459	-0.047	1.00
Trial3	0.10	0.34	0.0012	3.90E-05	0.0182	0.0015	-0.00134	4.10E-05	-0.246	0.020	1.00
Trial4	0.61	0.34	0.0098	4.11E-04	0.0031	0.0024	-0.00669	1.50E-03	-0.538	-0.178	0.95
Ferrous											
Trial1	0.11	0.06	0.0011	4.80E-05	0.0230	0.0026	-0.00049	3.69E-05	-0.277	0.066	1.00
Trial2	0.62	0.06	0.0098	4.08E-04	0.0035	0.0024	-0.00338	8.08E-04	-0.377	0.183	0.94

Table 2-2: Values for coefficients for equation 11 obtained from normalized solution temperature fits.

	H ₂ O ₂	Fe	a	CI	b	CI	c	CI	d	CI	R ²
Ferric											
Trial1	0.11	0.06	1.102	0.004	-0.0012	0.0002	-0.105	0.006	-0.406	0.053	0.98
Trial2	0.62	0.06	1.612	0.032	-0.0094	0.0011	-0.639	0.047	-0.539	0.086	0.97
Trial3	0.11	0.34	1.096	0.004	-0.0013	0.0002	-0.096	0.006	-0.694	0.099	0.98
Trial4	0.62	0.34	1.505	0.013	-0.0090	0.0005	-0.506	0.029	-1.739	0.315	0.99
Trial6	0.73	0.20	1.696	0.017	-0.0122	0.0008	-0.659	0.038	-3.525	1.935	0.99
Trial8	0.37	0.41	1.282	0.005	-0.0053	0.0002	-0.283	0.012	-1.622	0.200	0.99
Trial9-13	0.37	0.20	1.331	0.005	-0.0054	0.0001	-0.332	0.010	-1.833	0.119	1.00
Ferrous											
Trial1	0.11	0.06	1.122	3.0E-04	-0.0031	0.0002	-0.122	0.007	-7.343	4.100	0.99
Trial2	0.59	0.06	1.557	0.013	-0.0011	0.0006	-0.558	0.023	-1.734	0.165	0.99

The coefficients from Table 2-2 were then graphed versus the initial hydrogen peroxide concentration to determine if there was any correlation between them, as shown in Figure 2-7.

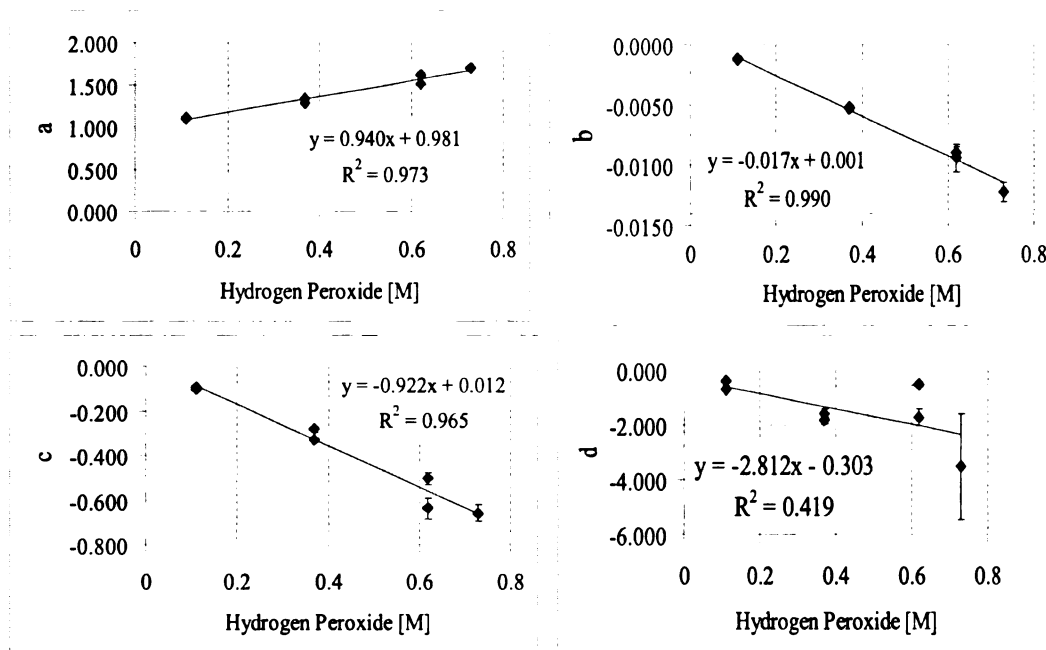


Figure 2-7: Relation between regression coefficients and the initial hydrogen peroxide concentration for normalized temperature for soluble iron catalyzed reactions.

The results for the experiments with Ottawa sand slurries and EDTA experiments are shown together in Figure 2-8

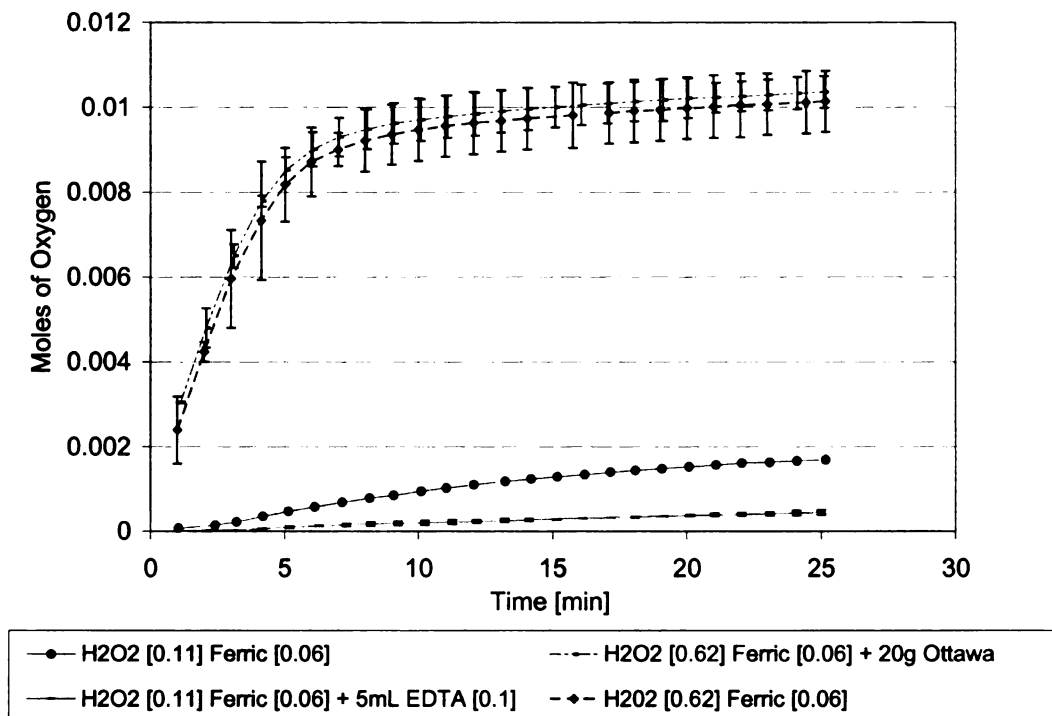


Figure 2-8: Comparison of Oxygen production between reactions with and without Ottawa sand and with and without EDTA.

Goethite

Results from the gravimetric experiments for hydrogen peroxide catalyzed by goethite can be found in Figure 2-8. Fits for the regression analysis on data can be found in Table 2-3 for an exponential regression using equation 14. Table 2-4 shows the coefficients for the same data fit through linear regression.

$$\text{Moles of } O_2 \text{ Produced} = a \cdot x + b \quad (16)$$

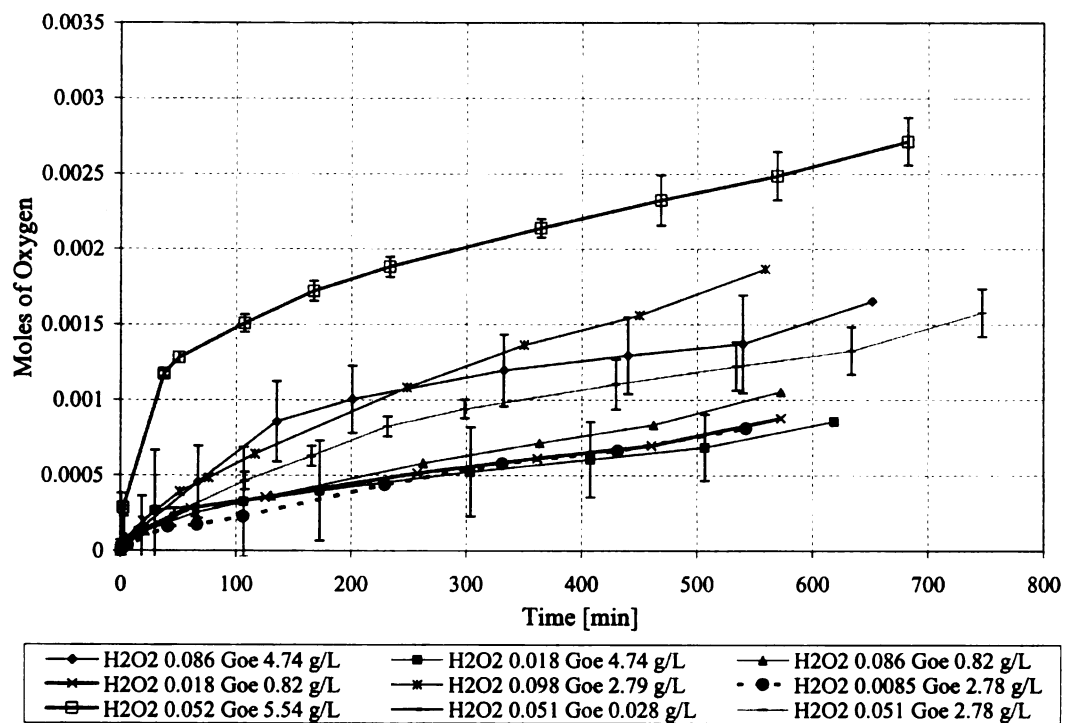


Figure 2-9: Oxygen production form Goethite catalyzed reactions

Table 2-3: Coefficients and 95% confidence intervals for Oxygen production from Goethite experiments for an exponential regression fit.

Exp.	H2O2 [M]	Goe (gm)	Fe3+ [M]	SA [m ²]	a	CI	b	CI	c	CI	d	CI	R ²
Trial1	0.086	0.0945	0.0425	7.04	9.07E-04	2.30E-04	8.66E-04	5.30E-04	-9.17E-04	2.30E-04	-1.07E-02	6.00E-03	0.994
	0.086	0.0951	0.0428	7.08	9.12E-04	2.18E-04	6.76E-04	4.44E-04	-8.84E-04	2.16E-04	-1.17E-02	6.64E-03	0.990
	0.086	0.0948	0.0427	7.06	1.05E-03	1.68E-04	6.38E-04	3.03E-04	-1.04E-03	1.68E-04	-1.28E-02	4.90E-03	0.995
Trial2	0.018	0.0950	0.0428	7.08	4.70E-04	1.36E-04	1.27E-03	6.02E-04	-4.22E-04	1.83E-04	-3.10E-02	4.34E-02	0.974
	0.018	0.0947	0.0426	7.05	3.00E-04	9.10E-05	1.84E-03	5.99E-04	-2.67E-04	1.26E-04	-2.52E-02	3.90E-02	0.973
	0.018	0.0948	0.0427	7.06	3.76E-04	3.10E-04	1.27E-03	1.04E-03	-3.17E-04	3.09E-04	-9.27E-03	2.03E-02	0.969
Trial4	0.018	0.0164	0.0074	1.22	3.52E-04	5.04E-05	1.74E-03	3.03E-04	-3.37E-04	5.92E-05	-1.96E-02	9.64E-03	0.996
	0.017	0.0162	0.0073	1.21	4.10E-04	2.85E-04	1.28E-03	1.29E-03	-3.65E-04	2.75E-04	-7.96E-03	1.19E-02	0.980
	0.017	0.0163	0.0073	1.21	3.23E-04	1.83E-04	1.40E-03	1.10E-03	-2.86E-04	1.83E-04	-1.08E-02	1.60E-02	0.974
Trial6	0.008	0.0553	0.0249	4.12	2.22E-04	1.56E-04	1.75E-03	1.27E-03	-2.00E-04	1.49E-04	-6.37E-03	9.49E-03	0.990
	0.008	0.0552	0.0248	4.11	3.16E-04	3.17E-04	1.68E-03	1.76E-03	-2.77E-04	2.99E-04	-5.95E-03	1.21E-02	0.985
Trial7	0.052	0.1114	0.0501	8.30	7.68E-04	1.22E-04	1.08E-03	2.56E-04	-7.29E-04	1.18E-04	-8.26E-03	2.85E-03	0.998
	0.052	0.1103	0.0496	8.22	9.63E-04	9.94E-05	9.14E-04	1.95E-04	-9.00E-04	1.10E-04	-1.60E-02	4.99E-03	0.996
Trial9-13	0.052	0.0555	0.0250	4.13	6.50E-04	1.43E-04	1.05E-03	3.06E-04	-6.00E-04	1.35E-04	-6.13E-03	-2.90E-03	0.996
	0.052	0.0554	0.0249	4.13	7.20E-04	7.32E-05	9.85E-04	1.58E-04	-6.96E-04	7.22E-05	-8.71E-03	1.04E-02	0.998

Table 2-4: Coefficients found form linear regression of data from gravimetric experiments during Goethite catalyzed CHPs.

Linear	H2O2 [M]	Goe [g]	Fe ³⁺ [M]	SA [m ²]	a	Cl	b	Cl	R ²
Trial 1	0.086	0.095	0.0425	7.04	1.71E-06	5.99E-07	5.39E-04	2.36E-04	0.90
	0.086	0.095	0.0428	7.08	1.37E-06	5.91E-07	5.94E-04	2.34E-04	0.85
	0.086	0.095	0.0427	7.06	1.47E-06	6.40E-07	7.09E-04	2.52E-04	0.85
Trial2	0.018	0.095	0.0428	7.08	8.15E-07	1.05E-07	4.61E-04	3.95E-05	0.99
	0.018	0.095	0.0426	7.05	1.02E-06	1.03E-07	2.48E-04	3.80E-05	0.99
	0.018	0.095	0.0427	7.06	9.64E-07	1.07E-07	2.26E-04	3.92E-05	0.99
Trial 3	0.085	0.016	0.0073	1.21	1.62E-06	1.49E-07	1.81E-04	4.97E-05	0.99
	0.085	0.017	0.0074	1.23	1.59E-06	1.50E-07	1.35E-04	4.97E-05	0.99
	0.086	0.017	0.0074	1.23	1.50E-06	1.52E-07	1.48E-04	5.03E-05	0.99
Trial4	0.018	0.016	0.0074	1.22	1.34E-06	2.26E-07	1.89E-04	7.45E-05	0.97
	0.017	0.016	0.0073	1.21	1.22E-06	2.75E-07	1.71E-04	6.88E-05	0.97
	0.017	0.016	0.0073	1.21	1.02E-06	2.25E-07	1.59E-04	7.39E-05	0.96
Trial5	0.098	0.055	0.0249	4.12	3.00E-06	3.30E-07	2.45E-04	9.90E-05	0.99
	0.098	0.056	0.0253	4.19	2.97E-06	5.30E-07	3.00E-04	1.57E-04	0.96
	0.098	0.056	0.0252	4.16	2.62E-06	3.52E-07	2.41E-04	1.03E-04	0.98
Trial6	0.008	0.055	0.0249	4.12	9.16E-07	7.67E-08	7.40E-05	2.37E-05	0.99
	0.009	0.056	0.0252	4.17	1.33E-06	1.36E-07	1.03E-04	4.23E-05	0.99
	0.008	0.055	0.0248	4.11	1.20E-06	8.10E-08	1.14E-04	2.48E-05	1.00
Trial7	0.051	0.110	0.0495	8.19	2.27E-06	3.09E-07	1.24E-03	1.27E-04	0.97
	0.052	0.111	0.0501	8.30	2.00E-06	2.73E-07	3.14E-04	1.01E-04	0.98
	0.052	0.110	0.0496	8.22	1.85E-06	4.39E-07	6.10E-04	1.65E-04	0.93
Trial 9-13	0.052	0.056	0.0250	4.13	1.78E-06	2.13E-07	1.57E-04	7.74E-05	0.96
	0.052	0.055	0.0249	4.13	1.72E-06	2.67E-07	2.95E-04	1.07E-04	0.95

Discussion

Soluble Iron

Water displacement experiments show, as seen in

Figure 2-1 and Figure 2-2, that hydrogen peroxide decomposition in the presence of soluble iron may be first order. Since the decomposition of hydrogen peroxide is exothermic, the temperature of the solution increases as hydrogen peroxide decomposes, thus the rate of decomposition is accelerated. Because of this issue, the water displacement experiment was replaced with a gravimetric test that did not depend on temperature and the precision of the measurements could be improved.

As seen in Figure 2-3 the gravimetric data collected show that hydrogen peroxide decomposition with soluble iron is independent of the catalyzer concentration and the oxidation state of the soluble iron. Results from reactions containing 0.06 M and 0.34 M ferric ion concentration and 0.11 M hydrogen peroxide concentration show no significant difference within 95% confidence for the rate of oxygen production. Figure 2-3 also shows that hydrogen peroxide concentration appears to control the rate of oxygen production, and that higher hydrogen peroxide concentrations produce oxygen at a higher rate for the same catalyzer concentration. It can be seen in this figure that the moles of oxygen produced by an initial hydrogen peroxide concentration of 0.62 M is significantly higher than those produced from an initial hydrogen peroxide 0.11 M concentration for either ferric ion concentrations of 0.06 or 0.34 M. This finding is also consistent with a first order rate expression with respect to hydrogen peroxide decomposition.

Oxygen production from ferrous ion catalyzed systems was not significantly different from ferric ion catalyzed systems for the same catalyzer and hydrogen peroxide concentrations. The reason for this is that the Fenton system initiation reaction, equation 1, is faster than the decomposition reaction; thus most, if not all, of the ferrous ions react with hydrogen peroxide to form ferric ion and hydroxyl radicals, before the hydrogen peroxide decomposes. This leads to reactions being catalyzed mostly by ferric ion, even if, initially, iron ions were in the ferrous state.

The data obtained from oxygen production with both ferrous and ferric ions, was fitted with a regression line to better understand the process. The best fit curve for the data is a double exponential expression shown in equation 13. The coefficients from this fit were then graphed versus the initial hydrogen peroxide and iron concentrations to determine if any correlation between them existed. No correlation was found between iron concentration and any of the coefficients, but there appeared to be a strong correlation between hydrogen peroxide concentration and the coefficients, seen in Figure 2-4, this finding is consistent with what has been described in the previous paragraph about Figure 2-3. The value of coefficient “a” for this system increases as hydrogen peroxide concentration in what appears to be a linear trend. Inversely coefficient “b” decreases linearly as hydrogen peroxide concentration is increased.

These results appear to indicate that the first term of the equation and coefficient “a” are related to the decomposition of hydrogen peroxide into oxygen as it reacts with the catalyzer; while the second term of the equation may be dependent on either the release

of oxygen from solution; or the reaction of hydrogen peroxide with the ration of iron catalyzer that is cycling back to its initial state.

Temperature

The reason why the best fit for the oxygen production is an exponential equation may be because of the increase in solution temperature that results as hydrogen peroxide decomposes. The temperature of the solutions was monitored throughout the experiments, in order to correct the rate constant obtained from oxygen production for hydrogen peroxide decomposition. Figure 2-5 shows the normalized temperature profiles between three different initial hydrogen peroxide concentrations catalyzed with 0.3 M ferric ion. As expected the higher hydrogen peroxide concentration produces the highest temperature increase in the solution. The normalized temperature profiles show that the maximum reaction temperature is reached early in the reaction period, before 5 minutes, after which the solution is slowly cooled down by the release of oxygen, which absorbs energy; and convection processes, due to the difference between ambient temperature and solution temperature.

Normalized temperature profiles for the reactions between ferrous and ferric catalyzed systems appear to differ only in their initial increase in temperature. Ferrous catalyzed reactions reach maximum temperature earlier than ferric catalyzed systems, shown in Figure 2-6. This difference in temperature increase causes ferrous reactions to be more violent than ferric catalyzed reactions, making ferrous catalyzed systems more dangerous to work with. This rate of temperature increase also leads to an increase in the initial rate

of hydrogen peroxide decomposition and sometimes forces the reactions to become diffusion limited when certain concentrations of hydrogen peroxide and the catalyzer are mixed. The solutions become diffusion limited when the reactions occur faster than the hydrogen peroxide can mix in the solution. By testing certain hydrogen peroxide and ferrous catalyzer ratios, it was found that concentrations higher than 0.5M ferrous ion in solution combined with concentrations 8% or higher of hydrogen peroxide produce diffusion limited reactions.

Ferrous and ferric catalyzed systems only differ, in terms of hydrogen peroxide decomposition, by the steepness of the temperature elevation at the start of the experiment. This could mean that hydrogen peroxide is preferentially decomposed when the ferrous ion is present, explaining why the ferric ion reactions were observed to be less violent than those catalyzed by ferrous ion. Ferric catalyzed systems require that the reaction shown in equation 2 occur before hydrogen peroxide decomposes or catalyzes to hydroxyl radical. The decomposition of hydrogen peroxide may only be occurring when the iron cycling process produces ferrous ion in the solution. Since the ending point for reactions in both systems appears to be the same, this point may be irrelevant when comparing oxygen production.

The temperature profiles from the reactions were fit with a regression analysis like those performed for oxygen production. The best fit for this regression was found with equation 14. This appears to indicate that the oxygen production and the temperature of the solution are directly related. As before, the coefficients from this regression analysis were graphed versus catalyzer and initial hydrogen peroxide concentration, and found that the

latter appears to have strong correlation to the coefficients presented in Table 2-4. This is expected as well because the cause for temperature increase is the decomposition of hydrogen peroxide.

Ottawa Sand Slurries

Soluble iron

Ottawa sand was saturated with water by adding 4.5 mL of water/catalyzer solution to 20 gm of sand. Under completely saturated conditions reactions in Ottawa sand reactions with soluble iron catalysts were found not to be significantly different from that observed in solutions without Ottawa sand, as shown in Figure 2-8. This means that under these conditions the sand did not interfere or interact with the CHP reactions and did not affect oxygen production. Results from reactions with unsaturated Ottawa sand could not be reproduced, because of oxygen was not released freely into the atmosphere during reaction. Throughout the experiments with unsaturated sand, air bubbles were seen forming inside the sand matrix, and it appeared that the sand particles prevented the release of the oxygen being produced.

EDTA experiments

Oxygen production in CHP reactions decreased with the addition of EDTA, and continued to decrease as the EDTA concentration increased. At EDTA concentrations less than 2.5 mM, no significant effect on oxygen production was observed when compared to reactions conducted in the absence of EDTA, as seen in Figure 2-8. When the concentration of EDTA reached 2.5 mM, oxygen production decreased. The oxygen

production continued to decrease as more EDTA was added, with oxygen production becoming negligible when the EDTA concentration reached 25 mM. Figure 2-8 shows the oxygen production for a solution containing 12.5 mM of EDTA. The oxygen production rate found may be only due to uncomplexed iron reacting with the hydrogen peroxide. Further experiments and modeling iron speciation under these conditions may shed more light on this phenomenon. Pignatello and Baehr ⁴⁰ have shown that hydroxyl radicals are generated during Fenton reactions catalyzed by ferric-complexes. Ferric complexes are used as a substitute catalyzer because these do not precipitate with an increase in pH. By using ferric complexes we may be able to carry out CHPs while using high hydrogen peroxide concentrations without the risk of losing a significant amount of the oxidant due to oxygen decomposition. Inadvertently we may be also able to diminish the decomposition of hydrogen peroxide, allowing for the use of higher concentrations of the oxidant.

Goethite

Oxygen production from goethite catalyzed CHPs appears to be dependent on the mineral concentration, and thus surface area, as shown in Figure 2-9. The rate of oxygen production, over a 24 hour reaction time, for all samples goes through an initial exponential production stage and later settles into a linear production stage. The initial production stage occurs within the first hour of commencement of the reaction. The main difference between the different catalyzer to oxidant ratios tested appears to be this initial stage of the reaction.

A regression analysis of the data in Table 2-4 was conducted to determine the relationship between the oxidant concentration and catalyzer concentration. The coefficients obtained from the regression analysis along with their 95% confidence interval are given in Tables 2-3 and 2-4. Table 2-3 is a compilation of the coefficients from an exponential fit using equation 13. The first term of the equation refers to the initial surge in oxygen production. Coefficient “b” in Table 2-3 is the exponent of the first term which may be related to the hydrogen peroxide decomposition rate constant (k_{10}), if we compare the two terms in equation 13 as two first order reaction rate equations in integrated form. By the same analogy, the second term of the equation may refer to the stabilization of the reaction where the oxygen production is now limited by the number of sites interacting in the mineral surface. Since the decomposition reaction and the hydroxyl radical reaction both occur at the mineral surface, the reactions compete for the active sites available at the mineral surface.

The coefficients for the first term of equation 13, in Table 2-3, may be dependent on both hydrogen peroxide and goethite concentration, not just goethite concentration. By analyzing the data from Trials 1 and 2 we can see that a decrease in hydrogen peroxide concentration from 0.086M to 0.018M, with the same goethite concentration, resulted in a decrease in the value of “a” by a factor of 2. Meanwhile the value of “b” increases by the same factor for these same reactions. This finding suggests that low concentrations of hydrogen peroxide decompose at a faster rate than higher concentrations for the same goethite concentration.

Watts et. al⁴⁵ and Lin and Gurol⁴⁶ found that the decomposition of hydrogen peroxide on goethite follows zero order kinetics. If we ignore the first 2 data points for each experiment, the data appears to follow a linear trend. By fitting a straight line to the data we obtain the regression coefficients and their respective, 95% confidence intervals, as shown in Table 2-4. From this data we can see that the rate constant for oxygen production, for all goethite and hydrogen peroxide concentrations used in this study, is relatively constant with a value of $1.62 \times 10^{-6} \pm 2.25 \times 10^{-7} \text{ M min}^{-1}$ ($2.70 \times 10^{-8} \pm 3.75 \times 10^{-9} \text{ M s}^{-1}$) for 24 hours of reaction. The elimination of the first two data points from the analysis may be justified by the fact that the solution required this time to equilibrate or to reach oxygen saturation at which point the oxygen production and desorption should reach steady state conditions.

Lin and Gurol's equation for hydrogen decomposition from goethite catalysis, does not appear to hold true for our experiments, because the value of the decomposition constant obtained from equation 11, would vary for each of our experiments due to the different goethite concentrations used. The decomposition constant according to Lin and Gurol, would range from 0.029 to 0.178 M s^{-1} for the range of goethite concentrations used. These results are obtained by substituting the value of FeOOH in equation 11. In our experiments we observed a decomposition rate which is 2 to 3 orders of magnitude less than the rate constants found by Lin and Gurol. It should be noted that the value we found only takes into account the decomposition of hydrogen peroxide to oxygen and does not take into account the catalysis of hydrogen peroxide into hydroxyl radicals, which is also a major hydrogen peroxide sink in the system. Since Lin and Gurol determined their rate

constant by hydrogen peroxide titration, they have incorporated the hydroxyl radical formation into their rate constant.

The data collected for oxygen production from all the experiments can be used to generate kinetic models for the CHPs tested. These models are developed in Chapter 6.

Conclusions

The decomposition of hydrogen peroxide into oxygen is an important hydrogen peroxide sink during CHP reactions, especially when high concentrations of hydrogen peroxide are used. This reaction should be added to any models that account for hydrogen peroxide loss. There is a limit to the concentrations that can be used for CHPs that are catalyzed by soluble iron. Solutions having high concentrations of hydrogen peroxide ($\geq 8\%$ or 2.5×10^{-3} M) and high soluble ferrous ion concentrations (0.5 M) become diffusion limited toward hydrogen peroxide, thus creating a boundary to which these chemicals can be mixed to form an effective remediation tool

The empirical relationship determined in this study can be used to predict the decomposition rate of hydrogen peroxide or the formation rate of oxygen in an in-situ environment. The relationship can help in creating kinetic models and to better assess the chemical concentrations that can be used in CHP remediation systems.

The rate of oxygen production was found to be independent of the concentration and oxidative state of soluble iron used. Hydrogen peroxide decomposition was found to be first order.

The temperature of the reaction can be determined from the empirical equations obtained in this study, which could also help for in situ remediation modeling by enabling us to correct for the effect of temperature during the reactions.

The use of a complexing agent like EDTA would help minimize the loss of hydrogen peroxide by decomposition when soluble iron catalysts are used.

Oxygen production is not affected by Ottawa sand in completely saturated conditions, when soluble iron is used as the catalyzer. If the solution is not saturated the reactions suffer from channeling and surface-bubble interactions that affect the reproducibility of the experiments.

Goethite catalyzed systems appear to have two oxygen production reaction rates; an initial rate which occurs during the first hour of reaction, and a secondary linear rate, which was found to be constant for all hydrogen peroxide and goethite concentrations studied. The rate constant was found to be $2.70 \times 10^{-8} \text{ M s}^{-1}$.

References

1. Kostecki, P. T.; Calabrese, E. J., *Petroleum Contaminated Soils: Remediation Techniques, Environmental Fate, and Risk Assessment*. 3rd ed.; Lewis Publishers, Inc.: Chelsea, MI, 1989; Vol. 1.
2. Juhasz, A. L.; Naidu, R., Bioremediation of High Molecular Weight Polycyclic Aromatic Hydrocarbons: A Review of Microbial Degradation of Benzo[a]pyrene. *International Biodeterioration & Biodegradation* **2000**, *45*, 57-88.
3. Schwarzenbach, R. P.; Gschwend, P. M.; Imboden, D. M., *Environmental Organic Chemistry*. 1st ed.; Wilkey-Interscience, John Wiley & Sons Inc: New York, 1993.
4. Chiou, C. T.; McGroddy, S. E.; Kile, D. E., Partition Characteristics of Polycyclic Aromatic Hydrocarbons on Soils and Sediments. *Environmental Science and Technology* **1998**, *32*, (2), 264-269.
5. Keith, L. H.; Telliard, W. A., Priority Pollutants: Prospective View. *Environmental Science and Technology* **1979**, *13*, (4), 416-424.
6. Srivastava, V. J.; Kelley, R. L.; Paterek, J. R.; Hayes, T. D.; Nelson, G. L.; Golchin, J., A Field Scale Demonstration of Novel Bioremediation Process for MGP Sites. *Applied Biochemistry and Biotechnology* **1994**, *45*, (6), 741-756.
7. Heitkamp, M. A.; Freeman, J. P.; Cerneglia, C. E., Naphthalene Biodegradation in Environmental Microcosms: Estimates of Degradation Rates and Characterization of Metabolites. *Applied and Environmental Microbiology* **1987**, *53*, (1), 129-136.
8. Nam, K.; Rodriguez, W.; Kukor, J. J., Enhanced Degradation of Polycyclic Aromatic Hydrocarbons by Biodegradation Combined with a Modified Fenton Reaction. *Chemosphere* **2001**, *45*, (2001), 11-20.
9. Sims, R. C.; Overcash, M. R., Fate of Polycyclic Aromatic Compounds (PNAs) in Soil-Plant Systems. *Residue Reviews* **1983**, *88*, 1-68.

10. Luster-Teasley, S. L.; Yao, J. J.; Herner, H. H.; Trosko, J. E.; Masten, S. J., Ozonation of Chrysene: Evaluation of By-Product Mixtures and Identification of Toxic Constituent. *Environmental Science and Technology* **2002**, 36, (5), 869-876.
11. Upham, B. L.; Masten, S. J.; Lockwood, B. R.; Trosko, J. E., Nongenotoxic Effects of Polycyclic Aromatic Hydrocarbons and Their Ozonation By-Products on Intercellular Communication of Rat Liver epithelial Cells. *Fundamental and Applied Toxicology* **1994**, 23, 470-475.
12. Yin, Y.; Allen, H. E., In Situ Chemical Treatment. July 1999, 1999.
13. Group, I. T. a. R. C. W. Technology Overview
Dense Non-Aqueous Phase Liquids (DNPL): Review of Emerging Characterization and Remediation Technologies. <http://www.itrcweb.org/DNAPL-1.pdf>
14. Carvel, D. D.; Cartwright, R. T. In *Measuring in situ Fenton's application success*, Proceedings of the Third International Conference on Remediation of Chlorinated and Recalcitrant Compounds, Monterrey, CA, United States of America, May 20-23 2002, 2002; Press, B., Ed. Battelle Press: Monterrey, CA, United States of America, 2002; pp 1173-1178.
15. Gates-Anderson, D. D.; Siegreest, R. L.; Cline, S. R., Comparison of Potassium Permanganate and Hydrogen Peroxide as Chemical Oxidants for Organically Contaminated Soils. *Journal of Environmental Engineering* **2001**, 337-347.
16. Beltran, F. J.; Ovejeor, G.; Rivas, J., Oxidation of Polycyclic Aromatic Hydrocarbons in Water.4. Ozone Combined with Hydrogen Peroxide. *Industrial Engineering and Chemistry Research* **1996**, 35, (3), 891-898.
17. Luster-Teasley, S. The Use of Gaseous Ozone to remediate Pyrene Contaminated Soils: A study of By-Product Production, Environmental effects on Remediation Efforts, and Scale-Up Volume I & II. Dissertation for the Degree of Ph. D., Michigan State University, East Lansing, MI, 2003.
18. Yao, J.-J.; Huang, Z.-H.; Masten, S. J., Ozonation of Benz[a]anthracene: Pathway and Product Identification. *Water Research* **1998**, 32, (11), 3235-3244.
19. Yao, J.-J.; Huang, Z.-H.; Masten, S. J., The Ozonation of Pyrene: Pathway and Product Identification. *Water Research* **1998**, 32, (10), 3001-3012.

20. Benitez, F. J.; Beltran-Heredia, J.; Acero, J. L.; Rubio, F. J., Chemical Decomposition of 2,4,6-Trichlorophenol by Ozone, Fenton's Reagent and UV Radiation. *Industrial Engineering and Chemistry Research* **1999**, 38, (1999), 1341-1349.
21. Council, I. T. R. *Technical and Regulatory Guidelines for In-Situ Chemical Oxidation of Contaminated Soil and Groundwater 2nd ed. ISCO-2*; Interstate Technology & Regulatory Council: Washington, D.C., 2005.
22. Haber, F.; Weiss, J., Catalytic Decomposition of Hydrogen Peroxide by Iron Salts. *Proceedings of The Royal Society, London* **1934**, 147, 332-351.
23. Jones, C. W., *Applications of Hydrogen Peroxide*. The Royal Society of Chemistry: Cambridge, 1999.
24. Walling, C., Fenton's Reagent Revisited. *Accounts of Chemical Research* **1974**, 8, 125-131.
25. Watts, R. J.; Teel, A. L., Chemistry of Modified Fenton's Reagent (Catalyzed H₂O₂ Propagations-CHP) for In Situ Soil and Groundwater Remediation. *Journal of Environmental Engineering* **2005**, 131, (4), 612-622.
26. Watts, R. J.; Teel, A. L., Treatment of Contaminated Soils and Groundwater Using ISCO. *Practice Periodical of Hazardous, Toxic, and Radioactive Waste Management* **2006**, 10, (1), 2-9.
27. Buxton, G. V.; Greenstock, C. L.; Helman, W. P.; Ross, A. B. *Critical Review Constants for Reactions of Hydrated Electrons Hydrogen Atoms and Hydroxyl Radicals (•OH/O•) in Aqueous Solution.*; 1988.
28. Walling, C.; Johnson, R. A., Fenton's Reagent V. Hydroxylation and Side-Chain Cleavage of Aromatics. *Journal of the American Chemical Society* **1974**, 97, (2), 363-367.
29. Augusti, R.; Dias, A. O.; Rocha, L. L.; Lago, R. M., Kinetics and Mechanism of Benzene Derivative Degradation with Fenton's Reagent in Aqueous Medium Studied by MIMS. *Journal of Physical Chemistry* **1998**, 102, (52), 10723-10727.
30. Casero, I.; Sicilia, D.; Rubio, S.; Perez-Bendito, D., Chemical Degradation of Aromatic Amines By Fenton's Reagent. *Water Research* **1997**, 31, (8), 1985-1995.

31. Walling, C.; Amarnath, K., Oxidation of Mandelic Acid by Fenton's Reagent. *Journal of the American Chemical Society* **1982**, 104, (5), 1185-1189.
32. Walling, C.; El-Taliawi, Fenton's Reagent III. Addition of Hydroxyl Radicals to Acetylenes and Redox Reactions of Vinyl Radicals. *Journal of the American Chemical Society* **1973**, 95, (3), 848-850.
33. Teel, A. L.; Warberg, C. R.; Atkinson, D. A.; Watts, R. J., Comparison of Mineral and Soluble Iron Fenton's Catalysts for the Treatment of Trichloroethylene. *Water Research* **2001**, 35, (4), 977-984.
34. Kong, S.-H.; Watts, R. J.; Choi, J.-H., Treatment of Petroleum-Contaminated Soils Using Iron Mineral Catalyzed Hydrogen Peroxide. *Chemosphere* **1998**, 37, (8), 1473-1482.
35. Watts, R. J.; Stanton, P. C.; Howsawheng, J.; Teel, A. L., Mineralization of a Sorbed Polycyclic Aromatic Hydrocarbon in Two Soils using Catalyzed Hydrogen Peroxide. *Water Research* **2002**, 36, 4283-4292.
36. Kakarla, P. K.; Andrews, T.; Greenberg, R. S.; Zervas, D. S., Modified Fenton's Processes For Effective In-Situ Chemical Oxidation-Laboratory and Field Evaluation. *Remediation* **2002**, Autumn, 23-36.
37. Pignatello, J. J., Dark and Photoassisted Fe³⁺ Catalyzed Degradation of Chlorophenoxy Herbicides by Hydrogen Peroxide. *Environmental Science and Technology* **1992**, 26, (5), 944-951.
38. Kwan, W. P.; Voelker, B. M., Rates of Hydroxyl Radical Generation and Organic Compound Oxidation in Mineral-Catalyzed Fenton-like Systems. *Environmental Science and Technology* **2003**, 37, (6), 1150-1158.
39. Tyre, B. W.; Watts, R. J.; Miller, G. C., Treatment of Four Biorefractory Contaminants in Soils Using Catalyzed Hydrogen Peroxide. *Journal of Environmental Quality* **1991**, 20, (October-December), 832-838.
40. Pignatello, J. J.; Baehr, K., Ferric Complexes as Catalysts for "Fenton" Degradation of 2,4-D and Metolachlor in Soil. *Journal of Environmental Quality* **1994**, 23, (March-April), 365-370.

41. Yamazaki, I.; Piette, L., EPR Spin Trapping Study on the Oxidizing Species Formed in the Reaction of The Ferrous Ion with Hydrogen Peroxide. *Journal of the American Chemical Society* **1991**, 113, (20), 7588-7593.
42. Chen, C. T.; Tafuri, A. N.; Rahman, M.; Foerst, M. B., Chemical Oxidation Treatment of Petroleum Contaminated Soil Using Fenton's Reagent. *Journal of Environmental Science and Health* **1998**, A33, (6), 987-1008.
43. Bowers, A. R.; Gaddipati, P.; Eckenfelder Jr., W. W.; Monsen, R. M., Treatment of Toxic or Refractory Wastewaters with Hydrogen Peroxide. *Water Science and Technology* **1989**, 21, 477-486.
44. Morel, F. M.; Hering, J. G., *Principles and Applications of Aquatic Chemistry*. John Wiley & Sons, Inc.: New York, 1993; p 588.
45. Watts, R. J.; Foget, M. K.; Kong, S.-H.; Teel, A. L., Hydrogen Peroxide Decomposition in Model Subsurface Systems. *Journal of Hazardous Materials* **1999**, 69, (2), 229-243.
46. Lin, S.-S.; Gurol, M. D., Heterogeneous Catalytic Oxidation of Organic Compounds by Hydrogen Peroxide. *Water Science and Technology* **1996**, 34, (9), 57-64.
47. Lin, S.-S.; Gurol, M. D., Catalytic Decomposition of Hydrogen Peroxide on Iron Oxide: Kinetics, Mechanism, and Implications. *Environmental Science and Technology* **1998**, 32, (10), 1417-1423.
48. Christian, G. D., *Analytical Chemistry*. 5th ed.; John Wiley & Sons, Inc.: New York, 1994; p 812.
49. Bader, H.; Sturzenegger, V.; Hoigne, J., Photometric Method for the Determination of Low Concentrations of Hydrogen Peroxide by the Peroxidase Catalyzed Oxidation of N,N-Diethyl-p-Phenylenediamine (DPD). *Water Research* **1988**, 22, (9), 1109-1115.
50. Voelker, B. M.; Sulzberger, B., Effects of Fulvic acid on Fe(II) Oxidation by Hydrogen Peroxide. *Environmental Science and Technology* **1996**, 30, (4), 1106-1114.

Chapter 3.

Hydroxyl Radical Production

Introduction

Hydroxyl radical ($\cdot\text{OH}$) production experiments using catalyzed hydrogen peroxide propagations were performed in order to obtain the optimum concentrations of catalyzer and reagent required to generate a maximum yield of radicals. Hydroxyl radicals can be determined by indirect measurement, in which a probe compound reacts with the $\cdot\text{OH}$ and the concentration of the probe is measured and related to the concentration of OH radicals. Probe compounds are chemicals with high rates of reaction (10^9 - $10^{10} \text{ M}^{-1} \text{ s}^{-1}$) with $\cdot\text{OH}$, which form byproducts that are easily measured after reaction. Chemicals such as benzoic acid ⁵¹, n-propanol ⁵¹, dimethyl sulfoxide (DMSO) ^{52, 53}, salicylic acid ⁵⁴⁻⁵⁶, D-phenylalanine ⁵⁷, terephthalate ⁵⁸, 3-chloro benzoic acid ⁵⁹, 4-hydroxy benzoic acid ⁶⁰ and formic acid ⁶¹ have been used to quantify the $\cdot\text{OH}$. The change in concentration of the probe over time can be correlated to the $\cdot\text{OH}$ concentration if we assume that only hydroxyl radicals react with the probe.

Salicylic Acid (SA) has been found to be a very selective $\cdot\text{OH}$ probe ⁵⁴, making it the frontrunner for $\cdot\text{OH}$ determination. The selectivity of SA is due to the effect the hydroxyl and carboxyl substitutions have on an aromatic ring. The hydroxyl group is in the ortho position with respect to the carboxyl group in the SA molecule. The position of these structures forces hydroxyl radicals to act on carbons 3 and 5 of the ring, thus creating 2,3

and 2,5 dihydroxy benzoic acids as the initial products of the reaction of hydroxyl radical and SA. These dihydroxy benzoic acids along with catechol have been found as byproducts of the reaction^{54, 62}. The reaction rate for the hydroxylation of the aromatic ring in SA was found to be $2.7 \times 10^{10} \text{ L mol}^{-1} \text{ s}^{-1}$ by Amphlett and Adams⁶³ using pulse radiolysis.

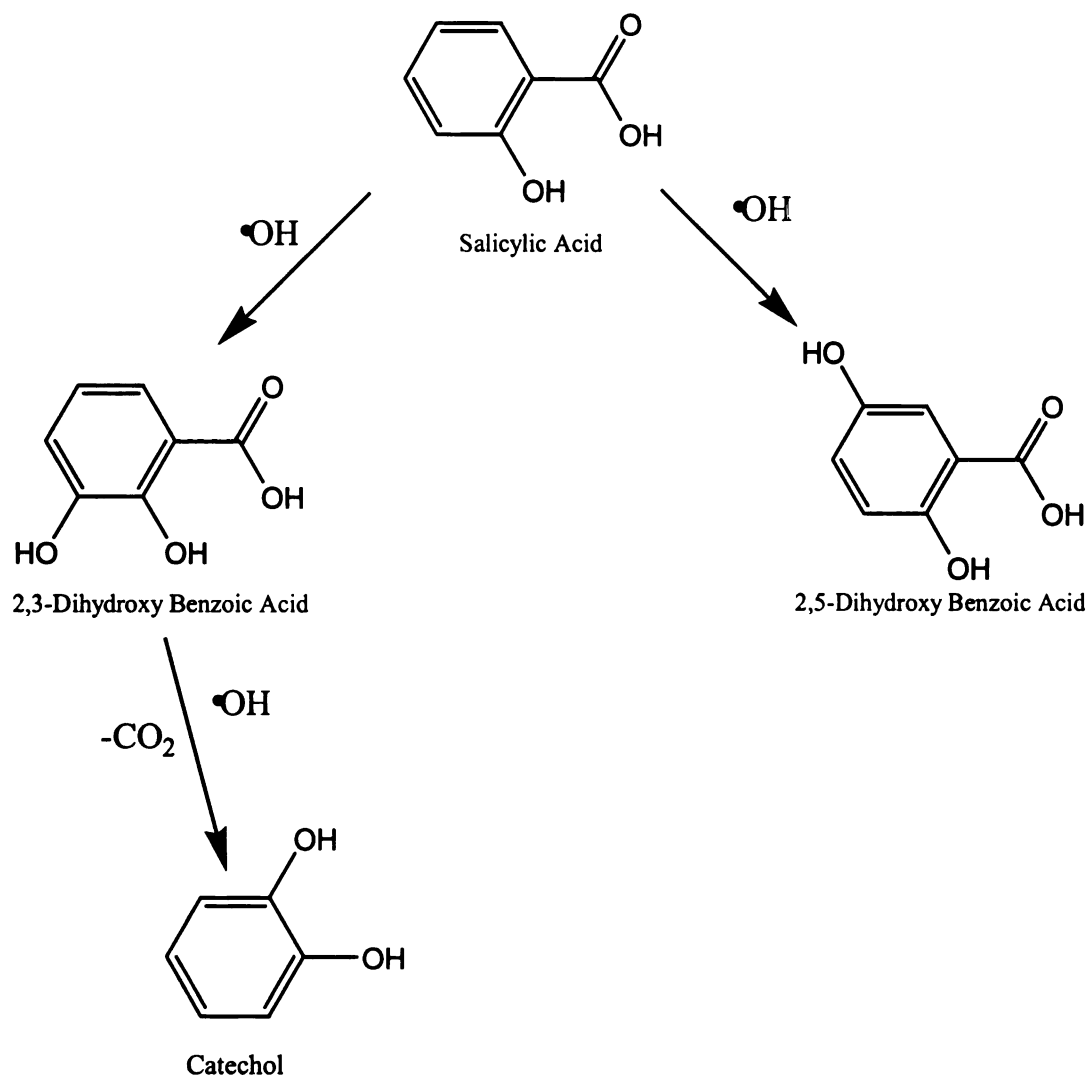


Figure 3-1: Pathway for the reaction of hydroxyl radicals with salicylic acid and its products⁵⁴.

Method and Materials:

Materials

Chemicals: All chemicals used were A.C.S reagent grade unless stated otherwise. Ferrous perchlorate, ferric perchlorate, salicylic acid, potassium iodide, bipyridine, goethite (α -FeOOH, 30-50 mesh), and perchloric acid were obtained from Sigma-Aldrich (St. Louis, MO). Stabilized hydrogen peroxide 30% solution was obtained from Fisher Scientific (Hampton, NH).

Soluble Iron Experiments

Experiments were designed to determine hydroxyl radical concentrations during soluble iron catalyzed reactions in both aqueous solutions and in Ottawa sand soil slurries. No suitable hydroxyl radical probe was found for soluble iron reactions (ferric and ferrous) at the concentrations used. Most of the above mentioned probes either complexed with iron in solution (formic acid, SA, 4-hydroxybenzoic acid, propanol) or were not sufficiently soluble (benzoic acid) to obtain a measurable amount in solution. Finally DMSO could not be used because the iron concentration caused interference during analysis.

Hydrogen peroxide concentrations were measured during these reactions, using the DPD⁴⁹ method modified to decrease iron interference⁵⁰, and the data collected was used to calibrate a kinetic model. The kinetic model was then used to estimate of hydroxyl radical concentration for the reactions. These results are presented in Chapter 6.

Goethite experiments:

Goethite catalyzed hydrogen peroxide propagations were carried out in solution and in aqueous suspensions of Ottawa sand. Salicylic acid was used as the $\cdot\text{OH}$ probe. Central Composite designs, first employed by Watts³⁵ and described by Diamond⁶⁴, were used to obtain the optimal oxidizer to catalyzer ratio for SA removal. Concentrations of hydrogen peroxide greater than 3% were used.

Stock solutions of salicylic acid were made fresh each week. Solution reactions were carried out at pH 3 and pH 7. All solutions and suspensions were buffered using a 10 mM phosphate. A total volume of 20 mL of solution was used for all OH/goethite experiments in aqueous solution (no Ottawa sand).

Prior to use, goethite was cleaned by rinsing the mineral with DI water to remove any iron dust from the surface; the mineral was then dried in an oven at 105 °C and later placed at 550 °C for 2 hours to remove any organic material present. Surface area for the goethite was measured using BET analysis and found to be 74.5 m²/gm.

For Ottawa sand, 20 grams of sand were used. Goethite was added to each vial while being shaken in a Mistral multimixer to help distribute the mineral throughout the sand. 4.5 mL of water containing the desired SA concentration was added to each vial. The system was allowed to equilibrate for 24 hours in a dark hood prior to the start of reactions. After the addition of hydrogen peroxide, the vials were mixed gently (at 85 cycles/hour for the duration of the experiment) in an orbital shaker.

The vials were covered to prevent photo-catalyzed reactions from occurring. pH was monitored during the reaction and any pH adjustments required were performed by adding drop wise 1M perchloric acid solution or 1M sodium hydroxide solution.

Salicylic Acid Determination

Salicylic acid concentrations were measured by RP-HPLC using an isocratic mobile phase consisting of 60% acetonitrile and 40% water at a 0.5 mL per minute flow rate, with a total runtime of 15 minutes. A Waters 2487 Dual absorbance UV detector set at 234 nm was used for detection along with a Waters MODEL fluorescence detector set at excitation and emission wavelengths of 310 and 400 nm, respectively. The detection limit for the UV detector was 0.59 ppm, while the detection limit with the fluorescence detector was 2.2 ppb.

Time dependent SA reactions

Experiments were performed to determine how SA concentrations changed over time and to determine the rate of hydroxyl radical production. The experiments were carried out using the same methodology as described earlier, while 100 μ L samples were taken at 5 minutes, 30 minutes, 4 hours, 24 hours and 72 hours after the addition of hydrogen peroxide to the system.

Byproduct Identification

GC/MS

Samples were decanted after 72 hours of reaction time, in order to remove the solution phase from the goethite. No additional reagents were added to quench reactions, because the reaction will not take place if goethite was not present in the vial.

The samples collected were placed under nitrogen gas until they were completely dry. After drying 50 μ L of BSTFA (O-bis(trimethylsilyl)acetamide) with 1% TMS (trimethylsilyl), and 15 μ L of pyridine were added to each sample and placed in an oven at 100°C for 2 hours to allow derivatization to occur. Five micro liters (5 μ L) of the solution were then injected into the GC/MS fitted with a DB-5 capillary column.

LC/MS

A Shimadzu LC-20AD HPLC with a Waters Z-spray electrospray ion source was used in this study. Data acquisitions were performed in both positive and negative ion modes. A 150 mm length 1mm diameter, 5 μ Thermo Hypersil-Keystone BetaBasic-18 PIONEER column was used. The LC used a gradient program with acetonitrile and water containing 0.15% formic acid as mobile phase and a flow rate of 0.1 mL per minute. The initial phase of the gradient program contained 10% acetonitrile, which was increased linearly to 60% over 30 minutes, after which the acetonitrile concentration is increased to 100% over ten minutes. At this time, the concentration of acetonitrile was decreased to 60% over ten minutes, and finally the concentration was decreased immediately to 10% and held at this concentration for 5 minutes. The program had a total run time of 60 minutes.

The LC/MS detector was set with a cone voltage of 40 V and a capillary voltage of 3.17 kV. The desolvation and cone gas (N_2) had flow rates of 400 L/hr and 10 L/hr, respectively.

To extract SA from Ottawa sand, 10 mL of water were added to the slurry and mixed thoroughly for 4 hours before sampling. The sample was filtered through a 22 μ m membrane filter to remove any suspended material.

Atomic Absorption

Atomic absorption analysis was performed on samples after 72 hours of reaction time. A Perkin Elmer AAnalyst 400 using flame ionization and hollow cathode iron lamp (DL3uNxFeE6) was used for the analysis at a 280 nm wavelength. A 1 mL sample of the water was passed through the flame, the difference in absorption was measured and the concentration determined using a previously created calibration curve. The calibration curve standards ranged from 0.5 to 25 μ g of iron, and were checked before each run. The data collected proved that less than 3 μ g of iron, the detection limit for our method, were dissolved in solution after 72 hours of reaction at pH 3.

Results:

Soluble Iron

The concentration of hydrogen peroxide over time for soluble iron reactions was measured, an example of which can be seen in Figure 3-2. This data was then used in combination with a kinetic model to obtain a value for the rate constant for the decomposition of hydrogen peroxide, k_d .

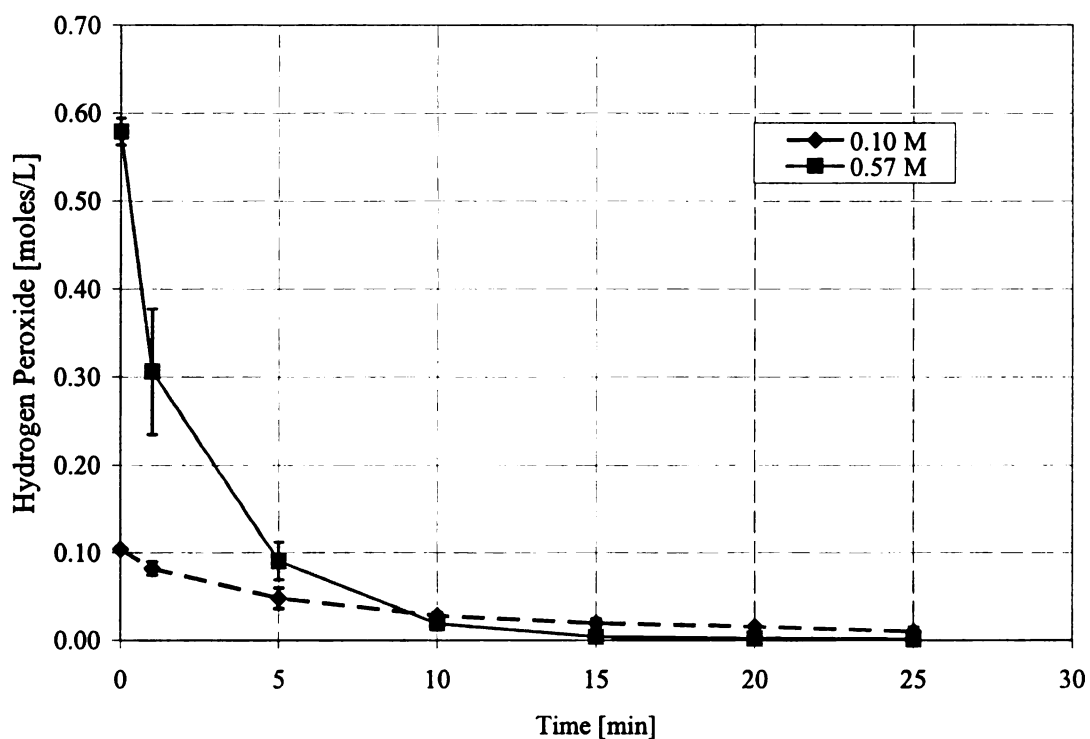


Figure 3-2: Plot of the change in hydrogen peroxide concentration as a function of time for initial ferric ion concentration of 0.06 M. Hydrogen peroxide was measured by iodometric titration. The initial concentration of hydrogen peroxide is shown in the legend

Goethite

During experimentation reaction blanks were run in parallel to account for the loss of salicylic acid by sorption onto the mineral. All concentrations have been adjusted by this value. At pH 7, in absence of hydrogen peroxide, $16.3 \pm 1.98\%$ salicylic acid sorbed onto 8.89 g/L of goethite, while at pH 3, $38.7 \pm 3.2\%$ was lost to sorption.

Salicylic acid removal efficiency appeared to differ between pH 3 and pH 7. A comparison of SA removal between pH 3 and 7, for different SA concentrations (and the same oxidant/catalyzer ratio) can be seen in Figure 3-8. For an initial SA concentration of 10 ppm, the removal efficiencies were found to be $56 \pm 2\%$ and $64 \pm 0.5\%$ respectively; while at an SA concentration of 100 ppm SA was removed $57 \pm 1\%$ and $16 \pm 2\%$ by the same oxidizer/catalyzer ratio.

The concentrations of hydrogen peroxide studied ranged from 0.001 to 0.85 M, while goethite was held between 2×10^{-4} and 0.1 M as ferric ion. Table 3-1 shows the data for aqueous phase experiments at pH 7 for the oxidation of 100 ppm SA. The trial number in the table represents the points required for the Central Composite Design analysis. This table also details the hydrogen peroxide and iron concentrations used for each trial along with the weighed amount of mineral and the corrected values of iron concentration present. The Results section of Table 3-1 gives the concentration of SA found in each vial, the amount of SA lost due to absorption into the mineral and the percent removal achieved after 72 hours of reaction time. The estimated moles of hydroxyl radicals

produced over the course of the experiment are shown in the last column of Table 3-1. This value was estimated from the concentration of salicylic acid removed; assuming one mole of SA is removed by one mole of $\cdot\text{OH}$.

The percent removal shown in Table 3-1 was then used to generate a regression equation to help predict the potential removal of SA from solution at pH 7, as described by the central composite design method⁶⁴ This regression equation was found to be:

$$Z(H,F) = 0.16 - 0.084H + 0.039F - 0.0022H^2 \quad (1)$$

H and F are dependent on the hydrogen peroxide and goethite concentration as ferric ion, and can be found by:

$$H = \frac{[H_2O_2] - 0.43}{-0.30} \quad (2)$$

$$F = \frac{[Fe] - 0.05}{-0.0353} \quad (3)$$

Using this regression line a contour plot, shown in Figure 3-3, for the response of the system to different hydrogen peroxide and goethite concentrations was made. The iso-response lines show the decimal value of SA removal and represent the boundaries at which a combination of hydrogen peroxide and goethite will achieve a given removal.

The data for pH 3 are recorded in a similar manner, as shown in Table 3-2. The regression obtained from this data is shown in Equation 4, and contour plot generated from the equation can be seen as Figure 3-4. The regression equation for pH 3 data was found to be

$$B(H, F) = 0.57 - 0.105H + 0.06F - 0.067H^2 - 0.086F^2 + 0.051HF \quad (4)$$

H and F are determined using equations 2 and 3.

This regression analysis can be better expressed as a function of surface area of goethite. Since the reactive properties of a mineral are dependent of the number of features on its surface⁶⁵, this implies that the total surface area of the mineral is more important than the mass of mineral present. In order to do this we can substitute F in equation 1 for F_s .

$$F_s = \frac{\text{Surface Area} - 6.65}{-4.67} \quad (5)$$

Table 3-1: Results for the removal of 100 ppm of salicylic acid (SA) from solution using goethite catalyzed reactions at pH 7. Shown are the amounts of goethite weighed for each trial and its subsequent concentration, the total surface area in each sample vial the amount of salicylic acid found in each sample, the amount of salicylic acid sorbed onto the mineral and the percent removal of salicylic acid from the sample (corrected by sorption). The final column is an estimate of hydroxyl radicals produced calculated from the amount of salicylic acid removed after 72 hours

Trial	H2O2	Fe	Goethite		Results			OH radical
			Weighted	Corrected Concentration [M]	Surface Area [m ²]	SA in sample [ppm]	Mass of SA sorbed [ppm]	Total Moles Produced
1	0.73	0.0854	0.1515	0.0852	11.286	65.8	13.43	1.47E-04
2	0.13	0.0854	0.1523	0.0857	11.345	83.4	13.50	1.83E-05
3	0.73	0.0148	0.0261	0.0147	1.944	70.4	2.31	1.94E-04
4	0.13	0.0148	0.0260	0.0146	1.937	88.5	2.30	6.24E-05
5	0.85	0.0501	0.0892	0.0502	6.645	69.5	7.91	1.60E-04
6	0.0010	0.0501	0.0889	0.0500	6.622	91.7	7.88	0.00E+00
7	0.43	0.1000	0.1779	0.1001	13.252	76.1	15.77	5.50E-05
8	0.43	0.0002	0.0004	0.0002	0.030	78.9	0.04	1.48E-04
9	0.43	0.0501	0.0891	0.0501	6.637	78.6	7.90	9.43E-05
10	0.43	0.0501	0.0893	0.0502	6.652	76.8	7.92	1.07E-04
11	0.43	0.0501	0.0887	0.0499	6.607	76.3	7.86	1.11E-04
12	0.43	0.0501	0.0890	0.0501	6.630	74.0	7.89	1.28E-04
13	0.43	0.0501	0.0892	0.0502	6.645	74.9	7.91	1.21E-04

Goethite Corrected Concentration calculated from:
$$\frac{\text{Weight} \times \% \text{ Fe}}{56 \text{ gm/mole} \times \text{volume (mL)}} \times 1000 \frac{\text{mL}}{\text{L}}$$
 Goethite is 63% iron by weight.

Table 3-2: Results for the removal of 100 ppm of salicylic acid (SA) from solution using goethite catalyzed reactions at pH 3. Shown are the amounts of goethite weighed for each trial and its subsequent concentration, the total surface area in each sample vial the amount of salicylic acid found in each sample, the amount of salicylic acid sorbed onto the mineral and the percent removal of salicylic acid from the sample (corrected by sorption). The final column is an estimate of hydroxyl radicals produced calculated from the amount of salicylic acid removed after 72 hours.

			Goethite		Results			OH radical	
			Weight [g]	Corrected Concentration [M]	Surface Area [m ²]	SA in sample [ppm]	Mass of SA sorbed [ppm]	Removal	Total Moles Produced
Trial	H2O2	Fe							
1	0.73	0.0854	0.1517	0.0853	11.301	21.9	33.08	45%	6.45E-06
2	0.13	0.0854	0.1515	0.0852	11.286	47.4	33.04	19%	2.75E-06
3	0.73	0.0148	0.0264	0.0149	1.967	37.5	5.76	56%	8.14E-06
4	0.13	0.0148	0.0263	0.0148	1.959	42.8	5.73	51%	7.38E-06
5	0.85	0.0501	0.0893	0.0502	6.652	21.9	19.47	58%	8.41E-06
6	0.0010	0.0501	0.0889	0.0500	6.622	59.2	19.39	21%	3.02E-06
7	0.43	0.1000	0.1780	0.1001	13.260	24.7	38.81	36%	5.21E-06
8	0.43	0.0002	0.0006	0.0003	0.045	60.3	0.13	39%	5.66E-06
9	0.43	0.0501	0.0892	0.0502	6.645	24.4	19.45	56%	8.06E-06
10	0.43	0.0501	0.0892	0.0502	6.645	25.0	19.45	55%	7.97E-06
11	0.43	0.0501	0.0891	0.0501	6.637	22.1	19.43	58%	8.40E-06
12	0.43	0.0501	0.0889	0.0500	6.622	21.5	19.39	59%	8.49E-06
13	0.43	0.0501	0.0889	0.0500	6.622	23.9	19.39	56%	8.14E-06

Goethite Corrected Concentration calculated from:
$$\frac{\text{Weight} \times \% \text{ Fe}}{56 \text{ gm/mole} \times \text{volume (mL)}} \times 1000 \frac{\text{mL}}{\text{L}}$$
 Goethite is 63% iron by weight.

Figure 3-3: Response surface obtained from equation 1 for the removal of salicylic acid at pH 7 using goethite catalyzed reactions. The x-axis represents H from equation 2 and the y-axis represents F from equation 3. The space between the lines represents the region at which a specific removal efficiency can be found and is delineated by the isoresponse lines shown in the figure.

Figure 3-4: Response surface obtained from equation 4 for the removal of salicylic acid at pH 3 using goethite catalyzed reactions. The x-axis represents H from equation 2 and the y-axis represents F from equation 3. The ν represents the region at which a specific removal efficiency can be found and is delineated by the isoresponse lines shown in the figure.

Time Dependent Reactions

The results from the measurement of salicylic acid concentration over the 72 hour time frame are shown in Figures 3-5 and 3-6. The graphs show an increase in the rate of SA disappearance after 24 hours of reaction time.

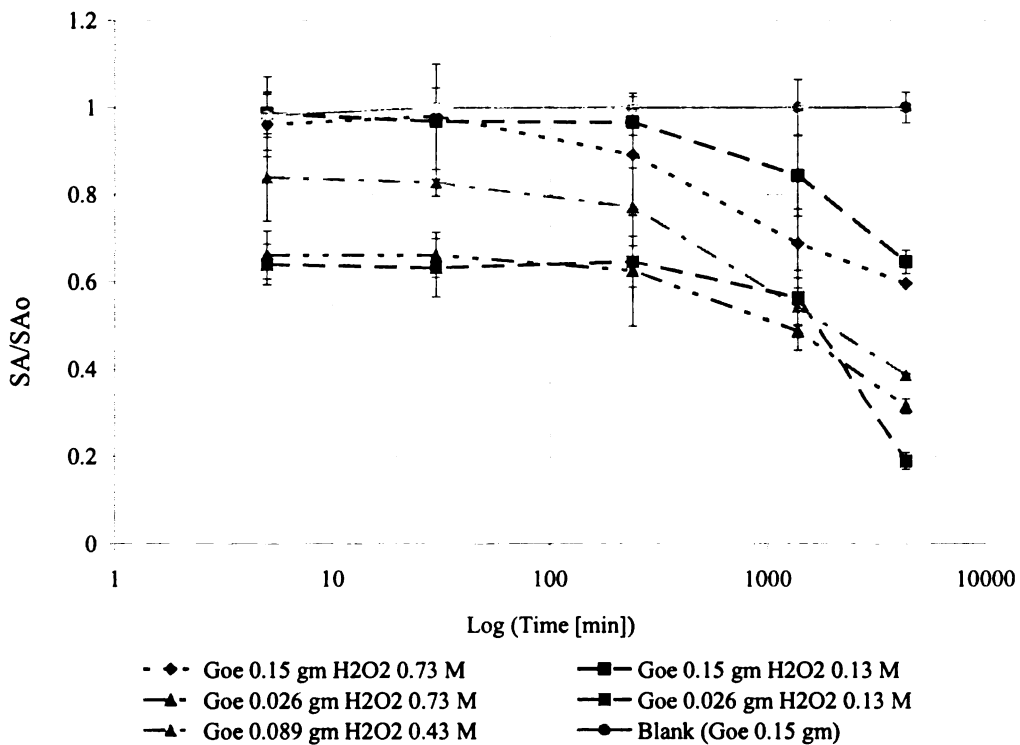


Figure 3-5: Plot of SA concentration over time for different hydrogen peroxide and Goethite concentrations for pH 3 reactions. Initial SA concentration of 100 ppm.

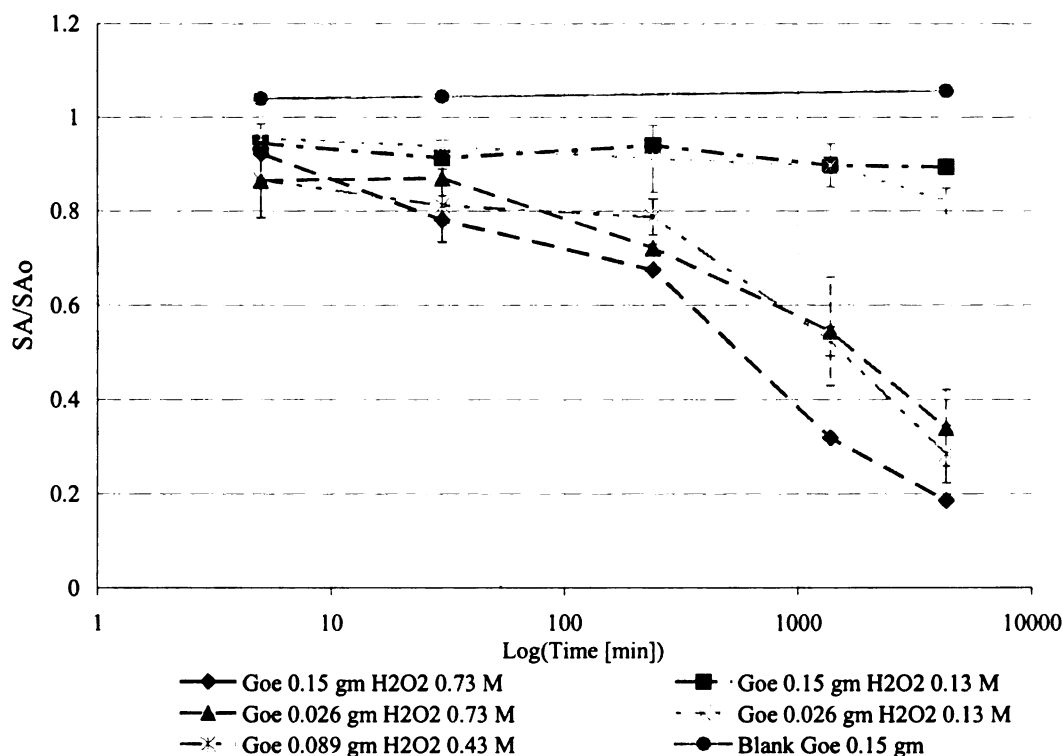


Figure 3-6: Plot of SA concentration over time for different hydrogen peroxide and Goethite concentrations for pH 7 reactions. Initial SA concentration of 100 ppm

Byproducts

Byproducts from the reaction of hydroxyl radicals with salicylic acid have been found in the samples during and after the 72 hr time frames. During experiments where SA concentration was measured over time, the formation of these byproducts was observed at pH 3 and 7, with the use of an HPLC/UV detector as described earlier.

Samples were analyzed by LC/MS and GC/MS to determine the products resulting from the reaction of hydroxyl radical and SA. The formation of these byproducts can be seen for both pH regimes in Figure 3-7

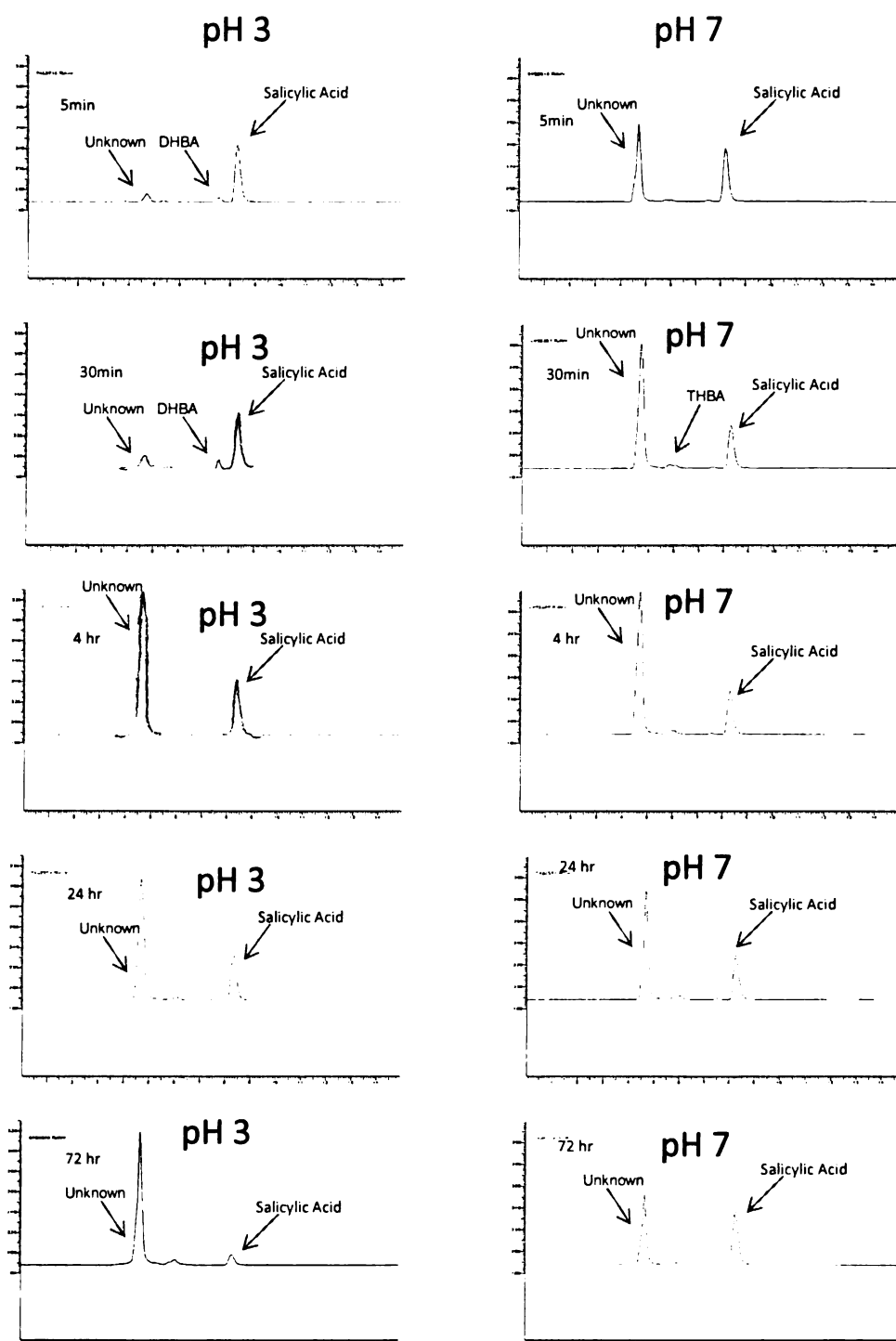


Figure 3-7: Oxidation of salicylic acid 100 ppm over time for pH 3 (left column) and pH 7 (right column) reactions with 0.0263 g/L goethite and an initial hydrogen peroxide concentration of 0.13M, analyzed through HPLC/UV at 234 nm. Shown in the figure are peaks formed during the 72 hours of reaction time. Dihydroxy benzoic acid (DHBA) and trihydroxy benzoic acid (THBA) peaks have been identified.

Results from LC/MS data are shown in Figures 3-9 thru 3-13. Samples from LC/MS analysis had prominent peaks in the negative ion mode and show that dihydroxy (m/z 153) and trihydroxy (m/z 169) benzoic acids are formed and were present in both pH 3 and 7 experiments. Peaks 99-, 109-, represent the loss of COO⁻ and ⁻OH from the molecular ion (M-1).

GC/MS

GC/MS analysis of the samples revealed different byproducts than those observed from the LC/MS results. The products found were more oxidized versions of SA and its known products. The structures of these byproducts can be seen in Figure 3-15.

Discussion

Sorption of SA to Goethite

Mineral catalyzed systems, like all heterogeneous catalyzed systems, require that both the oxidant and the contaminant are in close proximity to active sites on the mineral surface⁶⁵. Because of this, before any reaction can occur, the compound must sorb to the reactive surface. In both systems SA was found to sorb to the mineral, although it sorbed to a greater extent at pH 3 (38%) than at pH 7 (16%). We may be able to explain this result by the findings from Evanko and Dzombak⁶⁶, who found that alterations to the functional group of carboxylic acids influenced their sorption to goethite. He et. al⁶⁷ found that SA complexes with goethite. A change in pH will influence both the SA's functional group and the charge on the mineral surface. The pKa for SA is 2.97, which is close to the pH of 3 used for reactions. As such, about half of the SA found in solution would be present in its protonated form and the other half would be unprotonated. On the contrary, at pH 7, about 99.99% of the SA would be unprotonated as the salicylate ion, which may not sorb as readily to the mineral surface. This conclusion contradicts the findings by Karnik et al⁶⁸, who found that there was no significant sorption of SA to a hematite coated membrane at pH range of 2.5-3, but a high sorption of SA at pH of 7. A pH 3 solution could also affect the mineral surface by dissolving some of the iron and obstructing a portion of the reaction sites with dust; precipitating iron phosphate that sometimes formed during experimentation; or inversely by activating sites that were not

available to react. Because the disappearance of SA was greater at pH 3 than pH 7, site activation appears more likely.

Salicylic Acid Degradation by Goethite Catalyzed CHPs

The removal efficiency of SA by goethite catalyzed CHPs increased as the initial SA concentration was increased, at both pH 3 and 7. Figure 3-8 shows a comparison of SA removal for initial SA concentrations of 10 and 100 ppm, at pH 3 and 7, at the same initial hydrogen peroxide and goethite concentration. Since SA removal depends on the diffusion of the contaminant to the mineral surface, an increase in concentration would allow more SA to be in proximity to the mineral, ergo an increase in removal is expected. Another explanation might be that SA degradation occurs according to a pseudo first order reaction on the mineral surface. The mineral surface should not change appreciably over the course of the experiment, leading to a pseudo-first order hypothesis.

1
2
3
4
5
6
7
8
9
10
11
12
13
14
15
16
17
18
19
20
21
22
23
24
25
26
27
28
29
30
31
32
33
34
35
36
37
38
39
40
41
42
43
44
45
46
47
48
49
50
51
52
53
54
55
56
57
58
59
60
61
62
63
64
65
66
67
68
69
70
71
72
73
74
75
76
77
78
79
80
81
82
83
84
85
86
87
88
89
90
91
92
93
94
95
96
97
98
99
100

Fig
20

Ta

et

us

go

la

by

go

co

rea

ex

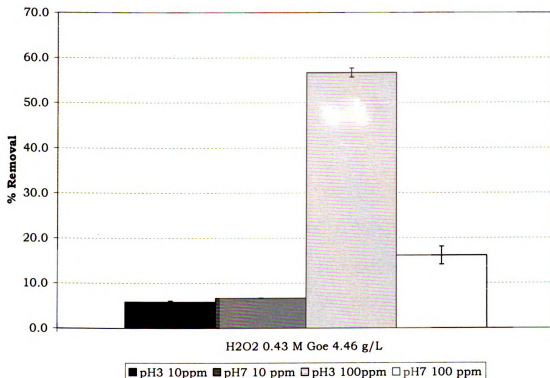


Figure 3-8: Comparison of SA removal in pH 3 and pH 7 samples at different SA concentrations.

The results from Table 3-2 show that at pH 3, CHP resulted in similar removal efficiencies for SA after 72 hours for all goethite and hydrogen peroxide combinations used. On the contrary, at pH 7, the efficacy of SA removal varied for the different goethite and hydrogen peroxide combinations used. This may be due to the saturation of the goethite surface by the oxidant and thus the active sites on the mineral produced hydroxyl radicals to its fullest extent. The linear regression fits for oxygen production in goethite catalyzed systems at pH 7, found in Chapter 2, appear to corroborate this conclusion; where oxygen production appeared to reach a constant rate after 1 hour of reaction time for all hydrogen peroxide and goethite concentrations tested. Another explanation is that the byproducts produced are consuming hydroxyl radicals. The true

amount of $\cdot\text{OH}$ formed from these experiments cannot be measured unless the concentration of one or more byproducts is measured as well; in part because competing reactions would occur as byproducts are formed, consuming $\cdot\text{OH}$ before they interact with SA.

The data obtained from SA removal experiments was used to generate a response surface for SA degradation for a wide range of hydrogen peroxide and goethite concentrations. This response surface can be a useful tool for estimating the desired range of oxidant to catalyzer ratio necessary to remove a contaminant. This data becomes especially useful for field applications where a range of concentrations is more applicable than a lone single value for the required ratio of oxidant to catalyzer. From Figure 3-8 the maximum SA removal achieved at pH 7 was 30% ($[\text{SA}]_0 = 100$ ppm) for a 0.43 M hydrogen peroxide concentration. On the other hand, at pH 3, 60% removal of SA was achieved at initial concentrations of 100 ppm and 0.43 M for SA and H_2O_2 , respectively. The maximum SA removal at pH 7, 30%, was achieved with concentrations of 0.77-0.85 M hydrogen peroxide and goethite concentrations between 0.021 and 1.78 g/L (2.27×10^{-4} M and 0.02 M as Fe, respectively). In contrast, at pH 3, a hydrogen peroxide concentration between 0.51 and 0.77 M with a goethite concentration between 2.48 to 4.9 g/L (0.035 and 0.055 M as Fe) was required to obtain maximum percent removal (60%). Reactions at pH 3 achieve SA removal that is 200% higher than reactions at pH 7 (60% removal vs. 30% removal, respectively) under the same experimental conditions and range of concentrations. To achieve this maximum removal, pH 3 reactions were carried

out at the same hydrogen peroxide concentrations as pH 7 reactions; but reactions at pH 7 require higher goethite concentrations.

The use of surface area as a surrogate for active reaction sites on the surface of a mineral can also be used to estimate hydroxyl radical production. According to Kwan and Voelker³⁸, the amount of hydroxyl radicals produced by goethite over a period of time can be estimated by the surface area of the mineral and the hydrogen peroxide concentration:

$$V_{OH} = 10^{-7} [\text{Surface Area}] [\text{H}_2\text{O}_2] \quad (6)$$

V_{OH} = hydroxyl radical production over time.

From this equation we can see that hydrogen peroxide concentration will be the limiting factor in determining $\cdot\text{OH}$ production. Since hydrogen peroxide decomposes on the surface of goethite and produces oxygen, the rate of decomposition needs to be known in order to estimate $\cdot\text{OH}$ production. Because Kwan and Voelker used concentrations of hydrogen peroxide of 5 mM, they may have been able to ignore the decomposition of hydrogen peroxide to oxygen at the mineral surface; at least there is no mention of this reaction in their paper, and it's difficult to know if the hydrogen peroxide concentration in equation 6 takes this reaction into account. According to the authors, at a constant goethite concentration, the steady state hydroxyl radical concentration does not depend on hydrogen peroxide concentration, allowing them to use a fixed hydrogen peroxide value. It is our belief that hydroxyl radical production will vary with time because the hydrogen peroxide concentration varies with time.

By using the data presented in Table 3-2 and 3-3, showing the number of moles of hydroxyl radicals produced over the 72 hour time frame, and assuming the OH radical production was constant throughout that time we can determine that the rate of OH radical produced in our system at pH 3 is approximately $1 \times 10^{-9} \text{ M s}^{-1}$, while at pH 7 the production rate was found to be $4 \times 10^{-10} \text{ M s}^{-1}$. Watts et al⁴⁵ found that the rate of OH radical production for goethite in soil slurries at pH 7 was $2.94 \times 10^{-8} \text{ M s}^{-1}$, which is 2 orders of magnitude greater than our rate. If we take into account the hydroxyl radicals that are consumed when forming byproducts, and we add this mass to the calculated production rates from our study, we may find that the hydroxyl radical production rate in our experiments is similar or higher than the rates found by other authors.

Figure 3-5 and 3-6 show the removal of SA over the 72 hours for several hydrogen peroxide and goethite concentrations. It can be observed in both figures that SA removal increases significantly for most reactions after 24 hours in both pH 3 and pH 7 systems. Since the majority of the oxygen production occurs in the first 24 hours (Chapter 2) we may conclude that hydrogen peroxide decomposition is affecting hydroxyl radical production. The figures also show that reactions containing the same hydrogen peroxide concentration but different goethite concentrations have similar rates of SA removal at pH 7 but reactions at pH 3 depend on both hydrogen peroxide and goethite concentrations.

In Chapter 2 we found that oxygen is produced at a rate of $2.70 \times 10^{-8} \pm 3.75 \times 10^{-9} \text{ M s}^{-1}$. Using this decomposition rate and the data for hydroxyl radical production presented

elsewhere in this chapter we may be able to hypothesize the mechanism by which hydrogen peroxide reacts at the mineral surface.

Byproducts

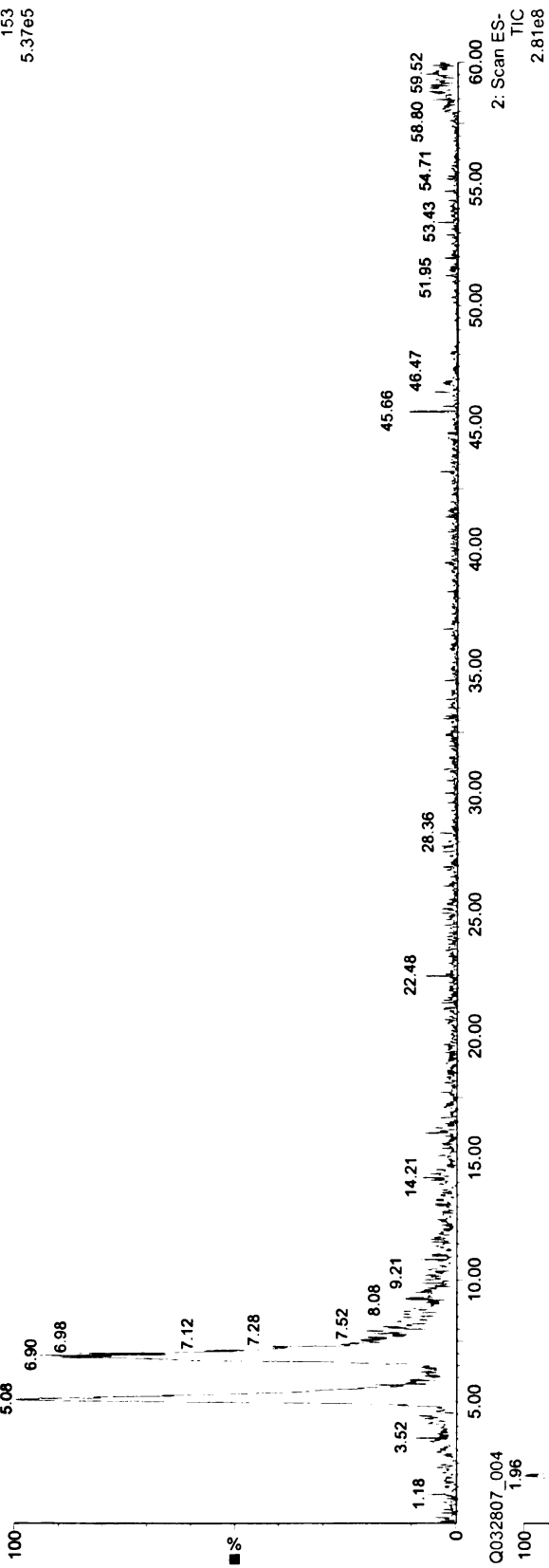
Previous studies have shown that the byproducts formed from the reactions of hydroxyl radicals with SA include 2,3 hydroxybenzoic acid (2,3-DHBA) and 2,5 dihydroxybenzoic acid (2,5-DHBA) and catechol⁵⁴. During the oxidation of SA with CHP, several byproducts were formed. Using both LC and GC/MS analysis, some of these byproducts were identified.

LC/MS analysis showed the presence of DHBA as well as a trihydroxy benzoic acid (THBA) after 72 hours of reaction. The spectra for these byproducts are seen in Figures 7-11. Although LC/MS spectra did not provide extensive information about the THBA found, a possible structure has been developed and is shown in Figure 3-14.

Figure 3-9: Typical chromatographic spectra from LC/MS analysis in negative ion mode for pH 3 reactions, showing the total ion count for negative ion data acquisitions. And the peaks for m/z 153- found in the samples.

Salicylic Acid pH3
Q032807_004

2: Scan ES-
153
5.37e5



Q032807_004

2: Scan ES-
TIC
2.81e8

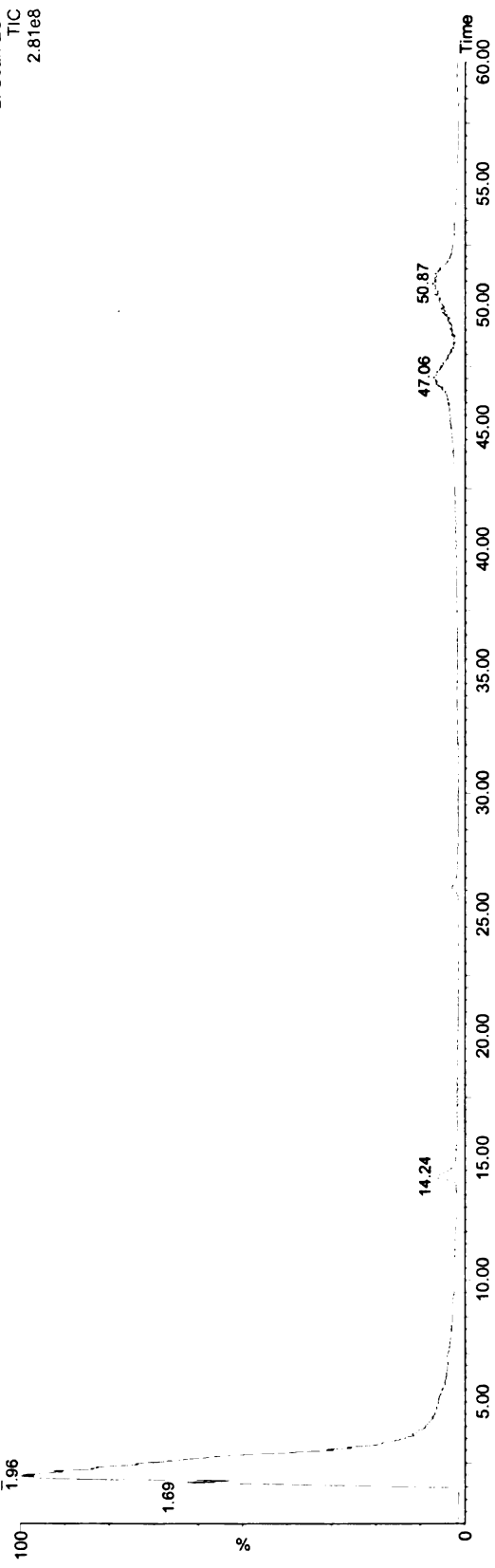


Figure 3-10: Mass spectra obtained from pH 3 samples showing m/z 153⁻ and 169⁻, which are believed to be dihydroxy and trihydroxy benzoic acids.

28-Mar-2007
2: Scan ES-
3.39e5

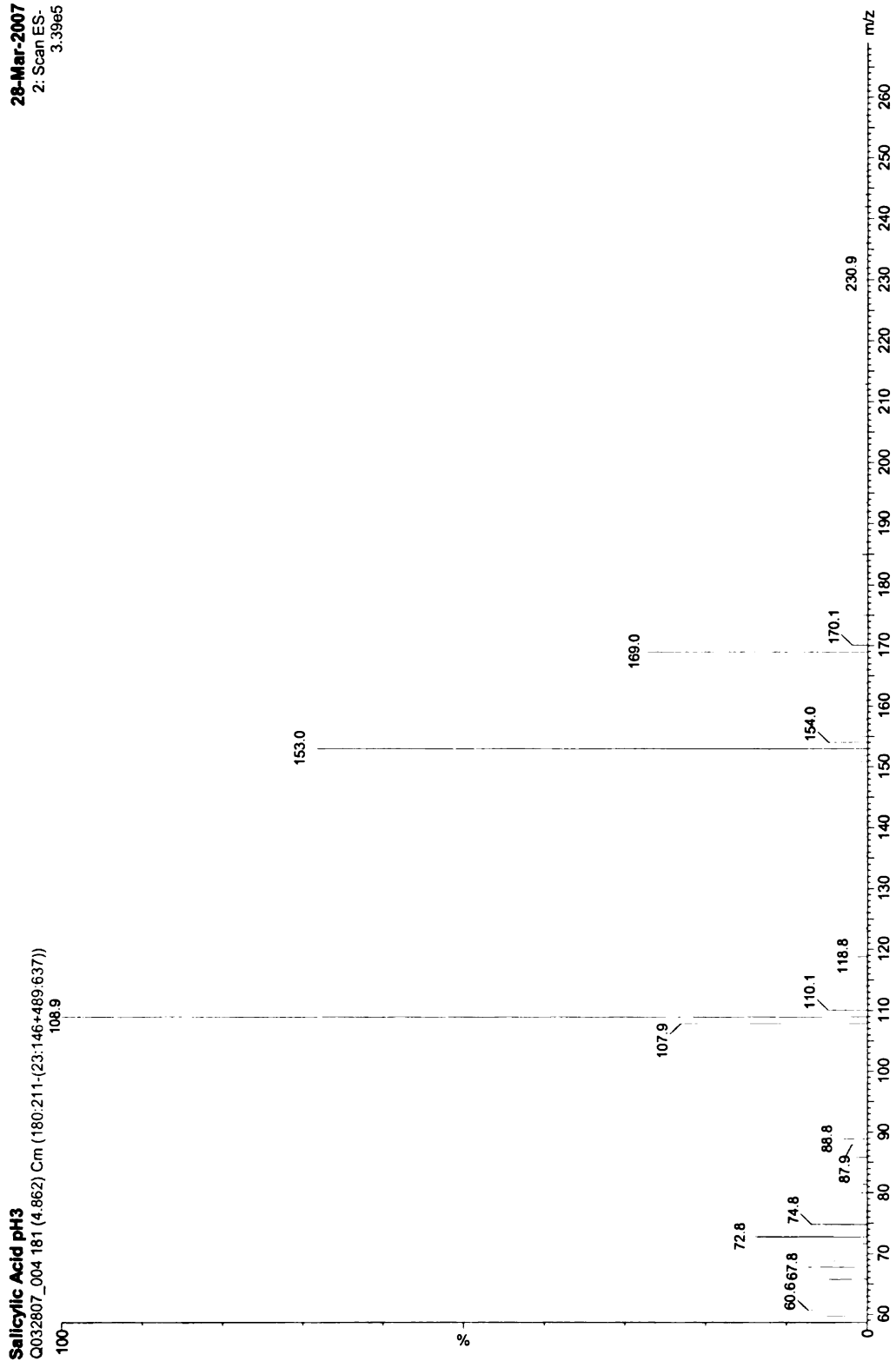


Figure 3-11: Chromatographic peak of m/z 169⁻ shown on the upper part of the figure believed to be trihydroxy benzoic acid (THBA), compared to the total ion count (TIC), lower part of the figure, for pH 3 samples by LC/MS analysis. The intensity of the THBA peak is 2 orders of magnitude less than the total intensity of ions detected signifying that it may not be the most prominent by product formed.

Salicylic Acid pH3
0032607.D

28-Mar-2007
2: Scan ES-
1.3398

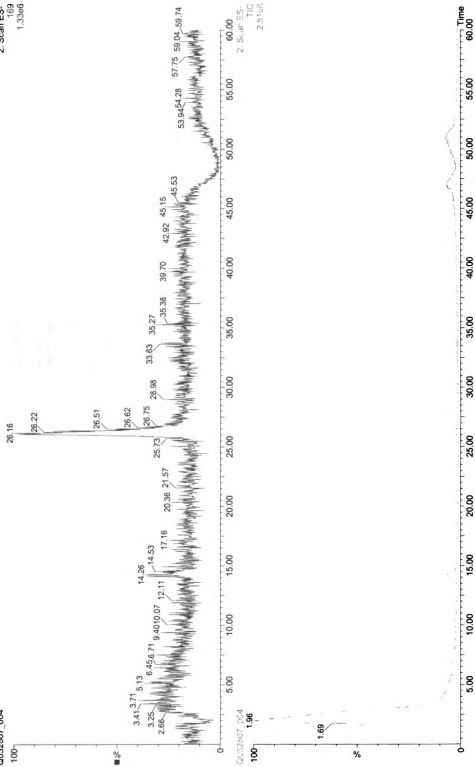


Figure 3-12: LC/MS spectra for peaks eluding at a retention time of 5.17minutes (from LC/MS column) for pH 7 samples. In the spectra m/z 153⁻ and 169⁻ are visible; these peaks are believed to be dihydroxy benzoic acid (DHBA) and trihydroxy benzoic acid (THBA).

28-Mar-2007
2: Scan ES-
6.30e5

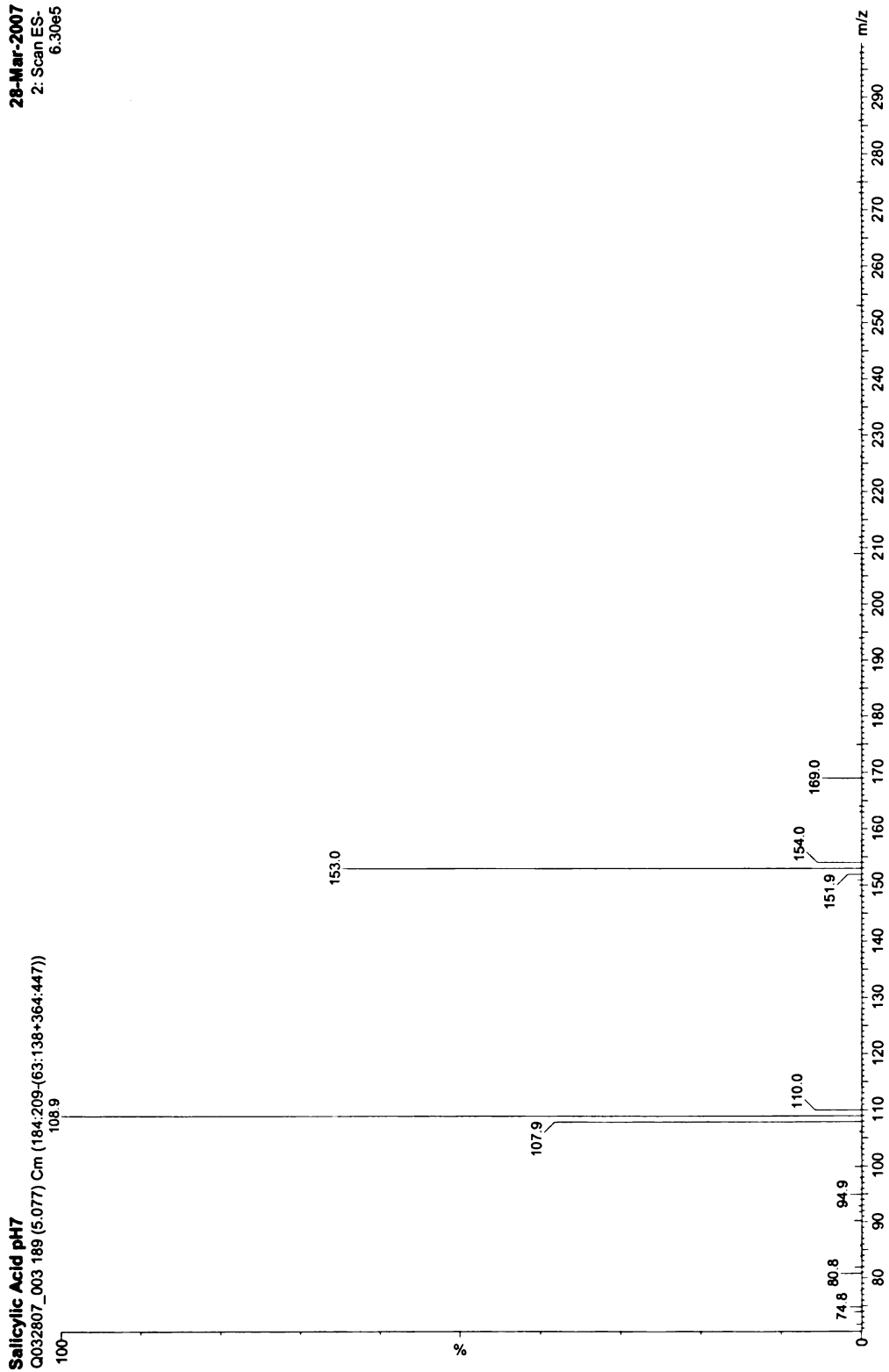
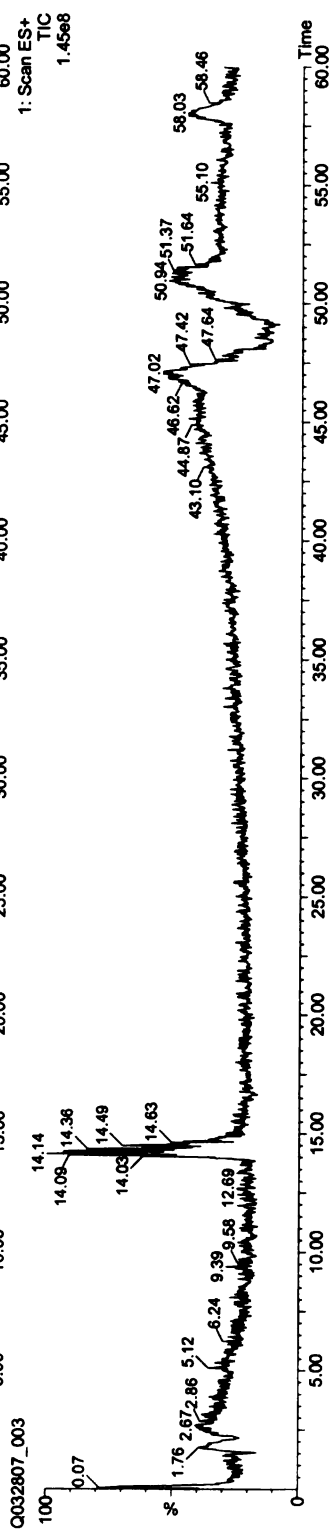
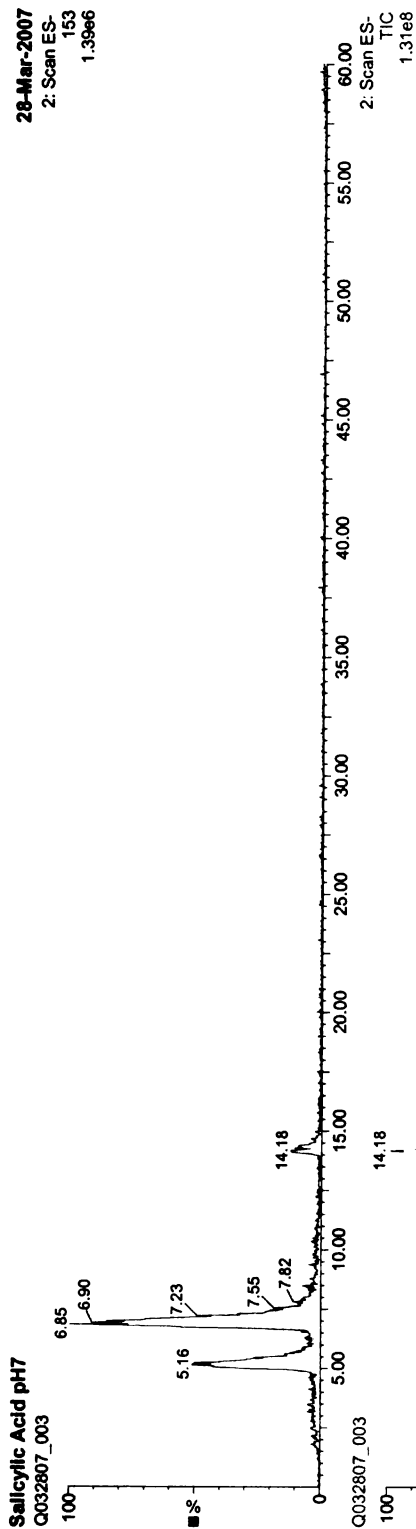


Figure 3-13: Chromatographic peak of byproduct having m/z 153⁻ shown here to compare its abundance versus total ion counts, in positive and negative ion mode for pH 7 sample during LC/MS analysis. It is possible to see from the first scan that three isomers may exist.

28-Mar-2007
2: Scan ES-
153
1.39e6



Fi
E

Fi

Fi

Fi

Fi

Fi

Fi

Fi

Fi

Fi

Fi

Fi

Fi

Fi

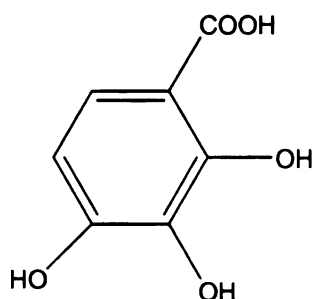


Figure 3-14: Possible structure for the byproduct m/z 169⁻ found in the LC/MS spectra in Figures 8 and Figure 10.

The presence of these byproducts indicate that some of the hydroxyl radicals produced did not selectively interact with SA in solution, instead reacting with any possible species found in solution, including other byproducts. As a result, the use of SA removal efficiencies to determine OH radical production may result in an under-prediction of the actual amount of radicals produced.

GC/MS analysis revealed byproducts that had a higher degree of oxidation than the byproducts found by LC/MS. Figure 3-15 shows the structure of the byproducts found from GC/MS. Some of the byproducts found are more volatile and have lower molecular weights than the parent compound, which explains why they were found by GC and not LC analysis. The formation of these byproducts show that the actual yield of hydroxyl radical production may be significantly higher than that estimated from SA removal alone. The formation of hydroxyl and dihydroxy acetic acid requires the reaction of SA with multiple radical species to obtain that degree of oxidation.

Fig
Ga

Li

cy

200

200

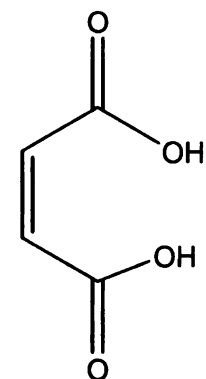
bet

by

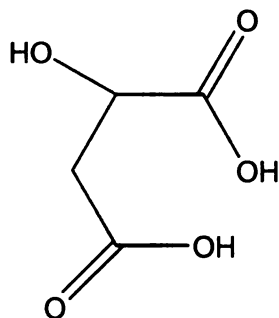
of

able

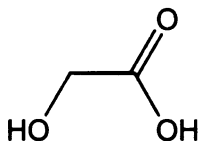
by



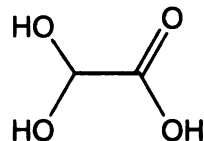
Maleic Acid



Malic Acid



2-hydroxy Acetic Acid



2, 2 di-hydroxy acetic acid

Figure 3-15: GC/MS identified byproducts found from the oxidation of salicylic acid by Goethite catalyzed CHPs for both pH 3 and pH 7.

In Figure 3-7 one can see the presence of a large peak labeled “unknown” throughout the experimentation. Although multiple attempts were made to determine the structure of this compound, the exact nature of the byproduct could not be determined. A UV spectral purity analysis of the peak was performed using a diode array detector set to scan between 200 and 300 nm. The analysis showed that the peak may be mixture of byproducts as its initial (at the time it starts to show in the chromatogram), central (apex of the chromatogram) and spectra from the peak tail, do not match. Although we were not able to separate the peaks with our system, we may have identified the structure of the byproducts that form the peak inadvertently with the GC/MS analysis.

Con

At

h

at

at

H

at

at

at

at

at

B

at

at

C

at

at

at

at

Conclusions

At the high iron concentrations employed in this study, it was not possible to quantify the hydroxyl radical concentration for soluble iron experiments. Unfortunately we were not able to identify a hydroxyl radical probe that did not complex with the soluble iron or was able to be maintained in solution at the pH required.

Hydroxyl radicals can be measured with SA as a radical probe in mineral iron catalyzed reactions. The mass of hydroxyl radicals produced during the reactions was found to be at least 2×10^{-6} moles for reactions at pH 3. At pH 7, the mass of hydroxyl radicals produced was found to be between 1×10^{-11} to 2×10^{-6} moles after 72 hours. Reactions at pH 7 were less efficient at removing SA than reactions carried out at pH 3. It is our belief that the protonation of SA at lower pH may be the key to this difference.

Byproducts are formed during CHP reactions at both pH 3 and pH 7. Six different byproducts (Dihydroxy benzoic acid, trihydroxybenzoic acid, malic acid, maleic acid, 2 hydroxy acetic acid, and 2,2 dihydroxyl acetic acid) were identified using LC and GC/MS analysis, some of which are more oxidized forms than those found in the literature. One of the byproducts found 2,3 DHBA is a known byproduct of the reaction of hydroxyl radicals with salicylic acid. In order to determine the actual amount of hydroxyl radicals produced we need to quantify all the byproducts formed and determine the concentration of at least one them.

In mineral catalyzed reactions the oxygen production rate appears out-compete hydroxyl radical production rate during the first 24 hours of reaction. By comparing the hydroxyl radical time dependent reactions from this chapter to the oxygen production experiments from Chapter 2, we found that the major oxygen production surge occurs in the first 24 hours of reaction time, while hydroxyl radical production increases notably after 24 hours of reaction,

References

1. Kostecki, P. T.; Calabrese, E. J., *Petroleum Contaminated Soils: Remediation Techniques, Environmental Fate, and Risk Assessment*. 3rd ed.; Lewis Publishers, Inc.: Chelsea, MI, 1989; Vol. 1.
2. Juhasz, A. L.; Naidu, R., Bioremediation of High Molecular Weight Polycyclic Aromatic Hydrocarbons: A Review of Microbial Degradation of Benzo[a]pyrene. *International Biodeterioration & Biodegradation* **2000**, 45, 57-88.
3. Schwarzenbach, R. P.; Gschwend, P. M.; Imboden, D. M., *Environmental Organic Chemistry*. 1st ed.; Wilkey-Interscience, John Wiley & Sons Inc: New York, 1993.
4. Chiou, C. T.; McGroddy, S. E.; Kile, D. E., Partition Characteristics of Polycyclic Aromatic Hydrocarbons on Soils and Sediments. *Environmental Science and Technology* **1998**, 32, (2), 264-269.
5. Keith, L. H.; Telliard, W. A., Priority Pollutants: Prospective View. *Environmental Science and Technology* **1979**, 13, (4), 416-424.
6. Srivastava, V. J.; Kelley, R. L.; Paterek, J. R.; Hayes, T. D.; Nelson, G. L.; Golchin, J., A Field Scale Demonstration of Novel Bioremediation Process for MGP Sites. *Applied Biochemistry and Biotechnology* **1994**, 45, (6), 741-756.
7. Heitkamp, M. A.; Freeman, J. P.; Cerneglia, C. E., Naphthalene Biodegradation in Environmental Microcosms: Estimates of Degradation Rates and Characterization of Metabolites. *Applied and Environmental Microbiology* **1987**, 53, (1), 129-136.
8. Nam, K.; Rodriguez, W.; Kukor, J. J., Enhanced Degradation of Polycyclic Aromatic Hydrocarbons by Biodegradation Combined with a Modified Fenton Reaction. *Chemosphere* **2001**, 45, (2001), 11-20.
9. Sims, R. C.; Overcash, M. R., Fate of Polycyclic Aromatic Compounds (PNAs) in Soil-Plant Systems. *Residue Reviews* **1983**, 88, 1-68.

10. Luster-Teasley, S. L.; Yao, J. J.; Herner, H. H.; Trosko, J. E.; Masten, S. J., Ozonation of Chrysene: Evaluation of By-Product Mixtures and Identification of Toxic Constituent. *Environmental Science and Technology* **2002**, 36, (5), 869-876.
11. Upham, B. L.; Masten, S. J.; Lockwood, B. R.; Trosko, J. E., Nongenotoxic Effects of Polycyclic Aromatic Hydrocarbons and Their Ozonation By-Products on Intercellular Communication of Rat Liver epithelial Cells. *Fundamental and Applied Toxicology* **1994**, 23, 470-475.
12. Yin, Y.; Allen, H. E., In Situ Chemical Treatment. July 1999, 1999.
13. Group, I. T. a. R. C. W. Technology Overview
Dense Non-Aqueous Phase Liquids (DNPL): Review of Emerging Characterization and Remediation Technologies. <http://www.itrcweb.org/DNAPL-1.pdf>
14. Carvel, D. D.; Cartwright, R. T. In *Measuring in situ Fenton's application success*, Proceedings of the Third International Conference on Remediation of Chlorinated and Recalcitrant Compounds, Monterrey, CA, United States of America, May 20-23 2002, 2002; Press, B., Ed. Battelle Press: Monterrey, CA, United States of America, 2002; pp 1173-1178.
15. Gates-Anderson, D. D.; Siegreist, R. L.; Cline, S. R., Comparison of Potassium Permanganate and Hydrogen Peroxide as Chemical Oxidants for Organically Contaminated Soils. *Journal of Environmental Engineering* **2001**, 337-347.
16. Beltran, F. J.; Ovejeor, G.; Rivas, J., Oxidation of Polycyclic Aromatic Hydrocarbons in Water.4. Ozone Combined with Hydrogen Peroxide. *Industrial Engineering and Chemistry Research* **1996**, 35, (3), 891-898.
17. Luster-Teasley, S. The Use of Gaseous Ozone to remediate Pyrene Contaminated Soils: A study of By-Product Production, Environmental effects on Remediation Efforts, and Scale-Up Volume I & II. Dissertation for the Degree of Ph. D., Michigan State University, East Lansing, MI, 2003.
18. Yao, J.-J.; Huang, Z.-H.; Masten, S. J., Ozonation of Benz[a]anthracene: Pathway and Product Identification. *Water Research* **1998**, 32, (11), 3235-3244.
19. Yao, J.-J.; Huang, Z.-H.; Masten, S. J., The Ozonation of Pyrene: Pathway and Product Identification. *Water Research* **1998**, 32, (10), 3001-3012.

20. Benitez, F. J.; Beltran-Heredia, J.; Acero, J. L.; Rubio, F. J., Chemical Decomposition of 2,4,6-Trichlorophenol by Ozone, Fenton's Reagent and UV Radiation. *Industrial Engineering and Chemistry Research* **1999**, 38, (1999), 1341-1349.
21. Council, I. T. R. *Technical and Regulatory Guidelines for In-Situ Chemical Oxidation of Contaminated Soil and Groundwater 2nd ed. ISCO-2*; Interstate Technology & Regulatory Council: Washington, D.C., 2005.
22. Haber, F.; Weiss, J., Catalytic Decomposition of Hydrogen Peroxide by Iron Salts. *Proceedings of The Royal Society, London* **1934**, 147, 332-351.
23. Jones, C. W., *Applications of Hydrogen Peroxide*. The Royal Society of Chemistry: Cambridge, 1999.
24. Walling, C., Fenton's Reagent Revisited. *Accounts of Chemical Research* **1974**, 8, 125-131.
25. Watts, R. J.; Teel, A. L., Chemistry of Modified Fenton's Reagent (Catalyzed H₂O₂ Propagations-CHP) for In Situ Soil and Groundwater Remediation. *Journal of Environmental Engineering* **2005**, 131, (4), 612-622.
26. Watts, R. J.; Teel, A. L., Treatment of Contaminated Soils and Groundwater Using ISCO. *Practice Periodical of Hazardous, Toxic, and Radioactive Waste Management* **2006**, 10, (1), 2-9.
27. Buxton, G. V.; Greenstock, C. L.; Helman, W. P.; Ross, A. B. *Critical Review Constants for Reactions of Hydrated Electrons Hydrogen Atoms and Hydroxyl Radicals (•OH/O•) in Aqueous Solution.*; 1988.
28. Walling, C.; Johnson, R. A., Fenton's Reagent V. Hydroxylation and Side-Chain Cleavage of Aromatics. *Journal of the American Chemical Society* **1974**, 97, (2), 363-367.
29. Augusti, R.; Dias, A. O.; Rocha, L. L.; Lago, R. M., Kinetics and Mechanism of Benzene Derivative Degradation with Fenton's Reagent in Aqueous Medium Studied by MIMS. *Journal of Physical Chemistry* **1998**, 102, (52), 10723-10727.
30. Casero, I.; Sicilia, D.; Rubio, S.; Perez-Bendito, D., Chemical Degradation of Aromatic Amines By Fenton's Reagent. *Water Research* **1997**, 31, (8), 1985-1995.

31. Walling, C.; Amarnath, K., Oxidation of Mandelic Acid by Fenton's Reagent. *Journal of the American Chemical Society* **1982**, 104, (5), 1185-1189.
32. Walling, C.; El-Taliawi, Fenton's Reagent III. Addition of Hydroxyl Radicals to Acetylenes and Redox Reactions of Vinyl Radicals. *Journal of the American Chemical Society* **1973**, 95, (3), 848-850.
33. Teel, A. L.; Warberg, C. R.; Atkinson, D. A.; Watts, R. J., Comparison of Mineral and Soluble Iron Fenton's Catalysts for the Treatment of Trichloroethylene. *Water Research* **2001**, 35, (4), 977-984.
34. Kong, S.-H.; Watts, R. J.; Choi, J.-H., Treatment of Petroleum-Contaminated Soils Using Iron Mineral Catalyzed Hydrogen Peroxide. *Chemosphere* **1998**, 37, (8), 1473-1482.
35. Watts, R. J.; Stanton, P. C.; Howsawheng, J.; Teel, A. L., Mineralization of a Sorbed Polycyclic Aromatic Hydrocarbon in Two Soils using Catalyzed Hydrogen Peroxide. *Water Research* **2002**, 36, 4283-4292.
36. Kakarla, P. K.; Andrews, T.; Greenberg, R. S.; Zervas, D. S., Modified Fenton's Processes For Effective In-Situ Chemical Oxidation-Laboratory and Field Evaluation. *Remediation* **2002**, Autumn, 23-36.
37. Pignatello, J. J., Dark and Photoassisted Fe³⁺ Catalyzed Degradation of Chlorophenoxy Herbicides by Hydrogen Peroxide. *Environmental Science and Technology* **1992**, 26, (5), 944-951.
38. Kwan, W. P.; Voelker, B. M., Rates of Hydroxyl Radical Generation and Organic Compound Oxidation in Mineral-Catalyzed Fenton-like Systems. *Environmental Science and Technology* **2003**, 37, (6), 1150-1158.
39. Tyre, B. W.; Watts, R. J.; Miller, G. C., Treatment of Four Biorefractory Contaminants in Soils Using Catalyzed Hydrogen Peroxide. *Journal of Environmental Quality* **1991**, 20, (October-December), 832-838.
40. Pignatello, J. J.; Baehr, K., Ferric Complexes as Catalysts for "Fenton" Degradation of 2,4-D and Metolachlor in Soil. *Journal of Environmental Quality* **1994**, 23, (March-April), 365-370.

41. Yamazaki, I.; Piette, L., EPR Spin Trapping Study on the Oxidizing Species Formed in the Reaction of The Ferrous Ion with Hydrogen Peroxide. *Journal of the American Chemical Society* **1991**, 113, (20), 7588-7593.
42. Chen, C. T.; Tafuri, A. N.; Rahman, M.; Foerst, M. B., Chemical Oxidation Treatment of Petroleum Contaminated Soil Using Fenton's Reagent. *Journal of Environmental Science and Health* **1998**, A33, (6), 987-1008.
43. Bowers, A. R.; Gaddipati, P.; Eckenfelder Jr., W. W.; Monsen, R. M., Treatment of Toxic or Refractory Wastewaters with Hydrogen Peroxide. *Water Science and Technology* **1989**, 21, 477-486.
44. Morel, F. M.; Hering, J. G., *Principles and Applications of Aquatic Chemistry*. John Wiley & Sons, Inc.: New York, 1993; p 588.
45. Watts, R. J.; Foget, M. K.; Kong, S.-H.; Teel, A. L., Hydrogen Peroxide Decomposition in Model Subsurface Systems. *Journal of Hazardous Materials* **1999**, 69, (2), 229-243.
46. Lin, S.-S.; Gurol, M. D., Heterogeneous Catalytic Oxidation of Organic Compounds by Hydrogen Peroxide. *Water Science and Technology* **1996**, 34, (9), 57-64.
47. Lin, S.-S.; Gurol, M. D., Catalytic Decomposition of Hydrogen Peroxide on Iron Oxide: Kinetics, Mechanism, and Implications. *Environmental Science and Technology* **1998**, 32, (10), 1417-1423.
48. Christian, G. D., *Analytical Chemistry*. 5th ed.; John Wiley & Sons, Inc.: New York, 1994; p 812.
49. Bader, H.; Sturzenegger, V.; Hoigne, J., Photometric Method for the Determination of Low Concentrations of Hydrogen Peroxide by the Peroxidase Catalyzed Oxidation of N,N-Diethyl-p-Phenylenediamine (DPD). *Water Research* **1988**, 22, (9), 1109-1115.
50. Voelker, B. M.; Sulzberger, B., Effects of Fulvic acid on Fe(II) Oxidation by Hydrogen Peroxide. *Environmental Science and Technology* **1996**, 30, (4), 1106-1114.

51. Lindsey, M. E.; Tarr, M. A., Quantitation of Hydroxyl radicals During Fenton Oxidation following a single Addition of Iron and Peroxide. *Chemosphere* **2000**, 41, (2000), 409-417.
52. Yang, X.-F.; Guo, X.-Q., Study of Nitroxide-Linked Naphthalene as a Fluorescence Probe for Hydroxyl Radicals. *Analytica Chimica Acta* **2001**, 434, 169-177.
53. Steiner, M. G.; Babbs, C. F., Quantitation of the Hydroxyl Radical By Reaction with Dimethyl Sulfoxide. *Archives of Biochemistry and Biophysics* **1990**, 278, (2), 478-481.
54. Punchard, N. A.; Kelly, F. J., *Free Radicals: A Practical Approach*. Oxford University Press: New York, 1996; p 310.
55. Yang, X.; Zhan, M.-j.; Kong, L.-r.; Wang, L.-s., Determination of Hydroxyl Radicals with Salicylic Acid in Aqueous Nitrate and Nitrite Solutions. *Journal of Environmental Sciences* **2004**, 16, (4), 687-689.
56. Diez, L.; Livertoux, M.-H.; Stark, A.-A.; Wellman-Rousseau, M.; Leroy, P., High Performance Liquid Chromatographic Assay of Hydroxyl Free Radical using Salicylic Acid Hydroxylation During In Vitro Experiments Involving Thiols. *Journal of Chromatography B* **2001**, 763, 185-193.
57. Bailey, S. M.; Fauconnet, A.-L.; Reinke, L. A., Comparison of Salicylate and D-phenylalanine for detection of Hydroxyl Radicals in Chemical and Biological Reactions. *Redox Report* **1997**, 3, (1), 17-22.
58. Saran, M.; Summer, K. H., Assaying for Hydroxyl Radicals: Hydroxylated Terephthalate is Superior Marker than Hydroxylated Benzoate. *Free Radical Research* **1999**, 31, 429-436.
59. Elovitz, M. S.; Von Guten, U., Hydroxyl Radical/Ozone Ratios During Ozonation Process I. Rct Concept. *Ozone Science & Engineering* **1999**, 21, 239-260.
60. Duesterberg, C. K.; Waite, T. D., Kinetic Modeling of the Oxidation of p-Hydroxybenzoic Acid by Fenton's Reagent: Implications of the Role of Quinones in the Redox Cycling of Iron. *Environ. Sci. Technol.* **2007**, 41, (11), 4103-4110.

61. Duesterberg, C. K.; Cooper, W. J.; Waite, T. D., Fenton-Mediated Oxidation in the Presence and Absence of Oxygen. *Environ. Sci. Technol.* **2005**, 39, (13), 5052-5058.
62. Albarran, G.; Schuler, R. H., Concerted Effects in the Reaction of OH Radicals with Aromatics: Radiolytic Oxidation of Salicylic Acid. *Radiation Physics and Chemistry* **2003**, 67, 279-285.
63. Amphlett, C. B.; Adams, G. E.; Michael, B. D., *Advances in Chemistry Series* **1968**, 81, 231-250.
64. Diamond, W. J., *Practical Experimental Designs for Engineers and Scientists*. Lifetime Learning Publications, Wadsworth Inc.: Belmont, 1989.
65. Steinfeld, J., *Chemical Kinetics and Dynamics*. 2nd ed.; Prentice Hall: Upper Saddle River, N.J., 1999.
66. Evanko, C. R.; Dzombak, D. A., Influence of Structural Features on Sorption of NOM-analogue Organic Acids to Goethite. *Environmental Science Technology* **1998**, 32, 2846-2855.
67. He, J.; Ma, W.; Song, W.; Zhao, J.; Qian, X.; Zhang, S.; Yu, J. C., Photoreaction of Aromatic Compounds at Goethite/H₂O interface in the Presence of H₂O₂: Evidence for Organic-Goethite Surface Complex. *Water Research* **2005**, 39, 119-128.
68. Karnik, B. S.; Davies, S. H.; Baumann, M. J.; Masten, S. J., Use of Salicylic Acid as a Model Compound to Investigate Hydroxyl Radical Reaction in Ozonation-Membrane Filtration Hybrid Process. *Journal of Environmental Engineering Science* **2007**, 6, (5).
69. Huling, S.; Pivetz, B. E. *Engineering Issue Paper: In-Situ Chemical Oxidation*; 600R06072; Environmental Protection Agency: Ada, Oklahoma, July 28 2006, 2006; p 60.
70. Belkin, S.; Steiber, M.; Tiehm, a.; Frimmel, F. H.; Abeliovich, A.; Werner, P.; Ulitzur, S., Toxicity and Genotoxicity Enhancement during Polycyclic Aromatic Hydrocarbon Degradation. *Environmental Toxicology and Water Quality* **1994**, 9, (4), 303-309.

71. Bogan, B. W.; Trbovic, V., Effect of Sequestration on PAH degradability with Fenton's Reagent: Roles of Total Organic Carbon, Humic and Soil Porosity. *Journal of Hazardous Materials* **2003**, B100, 285-300.
72. Bogan, B. W.; Trbovic, V.; Paterek, R. J., Inclusion of Vegetable oils in Fenton's Chemistry for Remediation of PAH-Contaminated Soils. *Chemosphere* **2003**, 50, 15-21.
73. Kawahara, F. K.; Davila, B.; Al-Abed, S. R.; Vesper, S. J.; Ireland, J. C.; Rock, S., Polycyclic Aromatic Hydrocarbon (PAH) release from Soil during Treatment with Fenton's Reagent. *Chemosphere* **1995**, 31, (9), 4131-4142.
74. Saxe, J. K.; Allen, H. E.; Nicol, G. R., Fenton Oxidation of Polycyclic Aromatic Hydrocarbons after Surfactant-Enhanced Soil Washing. *Environmental Engineering Science* **2000**, 17, 233-244.
75. Flotron, V.; Delteil, C.; Bermond, A.; Camel, V., Remediation of Matrices Contaminated by Polycyclic Aromatic Hydrocarbons: Use of Fenton's Reagent. *Polycyclic Aromatic Compounds* **2003**, 23, 353-376.
76. Martens, D. A.; T, F. j. W., Enhanced Degradation of Polycyclic Aromatic Hydrocarbons in Soil Treated with Advance Oxidative Process- Fenton's Reagent. *Journal of Soil Contamination* **1995**, 4, (2), 1-14.
77. Huang, H.-H.; Lu, M.-C.; Chen, J.-N., Catalytic Decomposition of Hydrogen Peroxide and 2-Chlorophenol with Iron Oxides. *Water Research* **2001**, 35, (9), 2291-2299.
78. Sedlak, D. L.; Andren, A. W., Oxidation of Chlorobenzene with Fenton's Reagent. *Environmental Science and Technology* **1991**, 25, (4), 777-782.
79. Beltran, F. J.; Gonzalez, M.; Rivas, F. J.; Alvarez, P., Fenton Reagent Advanced Oxidation of polycyclic Aromatic Hydrocarbons in Water. *Water Air and Soil Pollution* **1998**, 105, (1998), 685-700.
80. Lindsey, M. E.; Tarr, M. A., Inhibited Hydroxyl radical Degradation of Aromatic Hydrocarbons in the presence of Dissolved Fulvic Acid. *Water Research* **2000**, 34, (8), 2385-2389.

81. Lee, B.-D.; Nakai, S.; Hosomi, M., Application of Fenton Oxidation To Remediate Polycyclic Aromatic Hydrocarbons-Contaminated Soil. *Journal of Chemical Engineering of Japan* **2002**, 35, (6), 582-586.
82. Walling, C., Intermediates in the Reactions of Fenton Type Reagents. *Accounts of Chemical Research* **1998**, 31, (4), 155-157.
83. Masten, S. J. In *Use of In-Situ Ozonation For the Removal of VOCs and PAHs from Unsaturated Soils*, Proceedings of the Symposium on Soil Venting, Houston, Texas, 1991; U.S. Environmental Protection Agency: Houston, Texas, 1991; pp 29-45.
84. Liang, Y. In *Biodegradation of Pyrene in Soil Microcosms: Identification of a Toxic Intermediate*, EWRI 2005: Impacts of Global Climate Change, Anchorage, Alaska, 2005; Environmental and Water Resources Institute: Anchorage, Alaska, 2005.
85. Chen, R.; Pignatello, J. J., Role of Quinone Intermediates as Electron Shuttles in Fenton and Photoassisted Fenton Oxidations of Aromatic Compounds. *Environmental Science and Technology* **1997**, 31, (8), 2399-2406.
86. Goel, R. K.; Flora, J. R. V.; Ferry, J., Mechanisms for Naphthalene Removal during Electrolytic Aeration. *Water Research* **2003**, 37, 891-901.
87. Zeng, K.; Hwang, H.-M.; Fu, P. P.; Yu, H., Identification of 1-Hydroxypyrene Photoproducts and Study of the Effect of Humic Substances on its Photolysis. *Polycyclic Aromatic Compounds* **2002**, 22, 459-467.
88. Heitkamp, M. A.; Freeman, J. P.; Miller, D. W.; Cerniglia, C. E., Pyrene Degradation by *Mycobacterium* sp.: Identification of Ring Oxidation and Ring Fission Products. *Applied and Environmental Microbiology* **1988**, 54, (10), 2556-2565.
89. Alexander, M., *Biodegradation and Bioremediation*. second ed.; Academic Press: New York, 1999.
90. Liang, Y.; Gardner, D. R.; Miller, C. D.; Chen, D.; Anderson, A.; Weimer, B. C.; Sims, R. C., Study of Biochemical Pathways and Enzymes Involved in Pyrene Degradation by *Mycobacterium* sp. Strain KMS. *Applied and Environmental Microbiology* **2006**, 72, (12), 7821-7828.

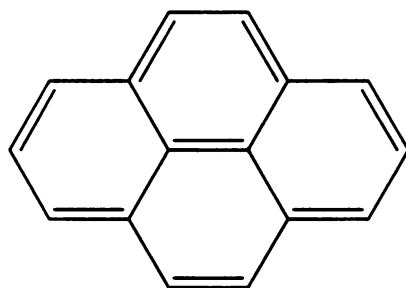
91. Herner, H. A.; Trosko, J. E.; Masten, S. J., The Epigenetic Toxicity of Pyrene and Related Ozonation Byproducts Containing an Aldehyde Functional Group. *Environmental Science and Technology* **2001**, 35, (17), 3576-3583.
92. Satoh, A. Y.; Trosko, J. E.; Masten, S. J., Epigenic Toxicity of Hydroxylated Biphenyls and Hydroxylated Polychlorinated Biphenyls on Normal Rat Liver Epithelial Cells. *Environmental Science and Technology* **2003**, 37, (12), 2727-2733.
93. Sedlak, D. L. The Abiotic Reactions of Polychlorinated Biphenyls (PCBs). Doctoral Dissertation, University of Wisconsin, Madison, 1992.
94. Hauser, B.; Schrader, G.; Bahadir, M., Dependence of Genotoxicity of Benzo[a]pyrene Suspensions in MutaTox Test on Dissolved Concentration and S9 Addition. *Ecotoxicology and Environmental Safety* **1997**, 38, (3), 224-226.
95. Lambert, M.; Kremer, S.; Anke, H., Antimicrobial, Phytotoxic, Nematicidal, Cytotoxic, and Mutagenic Activities of 1-Hydroxypyrene, the Initial Metabolite in Pyrene Metabolism by the Basidiomycete *Crinipellis stipitaria*. *Bulletin of Environmental Contamination and Toxicology* **1995**, 55, (2), 251-257.

Chapter 4.

Oxidation of Pyrene in Soil

Pyrene

Pyrene was chosen as the model PAH for this study because of the information available regarding byproduct formation from the remediation of the contaminant through multiple techniques. Pyrene is a symmetrical molecule as seen in Figure 4-1. A list of chemical and physical properties for pyrene is shown in Table 4-1.



Pyrene

Figure 4-1: Structure of model PAH, Pyrene showing double bonds and fused benzene rings.

Table 4-1: Physicochemical properties of Pyrene¹

Property	Value/Units
Molecular Weight	202 gm/mol
Melting Point	149° C
Boiling Point	360° C
Water Solubility	0.14 mg/L
Vapor Pressure @ 20° C	9.16E-5 Pa
Log Kow	5.32
Kom	10 ^{4.5} kg om/L

Method and Materials

Chemicals: All chemicals were ACS grade unless stated otherwise. Pyrene (98% purity) and ferrous ammonium sulfate were purchased from Sigma Chemical Company.(St. Louis, MO). HPLC grade acetonitrile was obtained from J.T. Baker Company (MG Scientific Inc. Pleasant Prairie, WI). Sodium dodecyl sulfate (lauryl) was obtained from Pierce Chemical Company (Perbio) (Rockford, Il.). Hydrogen Peroxide 30% was purchased from Fisher Company (Pittsburgh, PA).

The initial concentrations of hydrogen peroxide and soluble iron used in this study were determined by comparison to the available literature on PAH oxidation using Fenton's reagent ²⁻⁸. The experiments were set-up as soil slurry or suspension type systems. The reaction time for our experiment was also taken from comparisons between the literatures, where 24 hours was the conventional reaction time. An experiment involving 60,000 ppm of hydrogen peroxide was carried out for 72 hours and found that at 95% confidence level, the removal was not different from a 24 reaction at the same concentration. All authors ²⁻⁸ adjusted the pH before adding the hydrogen peroxide in order to create ideal conditions for Fenton's chemistry to occur.

All reactions were run in borosilicate glass vials using a single addition of hydrogen peroxide to start the reaction. The vials were cleaned in a 1% hydrochloric acid wash, rinsed in ultrapure water and allowed to dry; to remove organics, the vials were placed in an oven at 550°C for 2 hours.

CHP reactions using soluble iron were allowed to continue for 24 hours and were quenched by adding sodium hydroxide 1M solution to precipitate iron. Reactions using goethite as the catalyzer were allowed to react for 72 hours and quenched by decanting the solution from the catalyzer.

Organic matter soil was collected from the MSU campus during construction of the Spartan Child Development Center. The soil was sieved through a 40 mesh strainer to remove any debris and rocks. The soil was then analyzed for organic matter content, which was found to be 0.8%.

For Ottawa sand and organic matter soil experiments a pyrene stock solution was added drop wise to vials in a multishaker containing Ottawa sand. The vials were then placed in a dark fume hood for 24 hours to allow the solvent to evaporate. The initial pyrene concentration was held constant at 300 mg/kg sand.

Determining Pyrene Concentration

Pyrene was extracted from water or soil by adding 10 ml of hexane and placing the vials in on a tumble shaker for 24 hours. The concentration of pyrene in the hexane was then measured. If dilution was necessary, aliquots were taken from hexane extract and added to a 2 mL auto sampler vial containing 1mL of hexane. This dilution was repeated until an absorbance similar to the absorbance of a 10 mg/L calibration standard was achieved.

A Perkin-Elmer 200 series RP-HPLC coupled with UV and fluorescence detectors was used to determine the pyrene concentration. A Supelco C18 5 μ 25 cm column was used

for the separation, using water and acetonitrile as the LC mobile phase with a flow rate of 1 mL per minute. HPLC program used an initial acetonitrile: water ratio of 25% held for 3 minutes; a linear gradient over ten minutes increased acetonitrile to 90% concentration and held for 10 minutes, after which the acetonitrile is reduced linearly over a 5 minute span to 25%; the total run time was 28 minutes. Under these conditions, pyrene eluted at 19.44 ± 0.14 min. A Waters 2487 Dual wavelength absorbance UV detector measured absorbance at 254 nm, while a Waters fluorescence detector with excitation wavelength of 295 nm and an emission wavelength 375 were used to detect pyrene. The fluorescence detector was used to increase the sensibility of the experiments for pyrene concentrations lower than 1 ppm.

Manufactured Gas Plant Soil

Samples were collected from a former manufactured gas plant site in Grand Ledge, Michigan. Three bore holes were dug and the contaminated soil extracted was analyzed for PAH contamination.

The HPLC method used for the analysis of the MGP soil allowed for the resolution of 16 PAH peaks. This method has an initial a 25% acetonitrile concentration which was increased using a linear gradient over a period of 3 minutes to 90%. This condition was then linearly increased to 100% acetonitrile mobile phase and held for 20 minutes. Finally the acetonitrile concentration was linearly decreased back to the original 25% over an 8 minute time frame.

Results

A maximum removal efficacy of $88.1 \pm 1.8\%$ was achieved for Ottawa sand with an initial hydrogen peroxide concentration of 300 g/kg and 3 g/kg ferrous ammonium sulfate. Without the addition of ferrous ammonium sulfate, only $46.1 \pm 5.8\%$ removal of pyrene was obtained. Contaminated soil from a former Manufactured Gas Plant site containing 16 polycyclic aromatic hydrocarbons was treated under the same conditions as the previous soils. Removal efficiencies were less than 80% and accompanied by high experimental errors. Experiments carried out with sodium dodecyl sulfate (SDS), added to enhance the solubility of pyrene, resulted in less removal than those observed in experiments under the same conditions but without SDS.

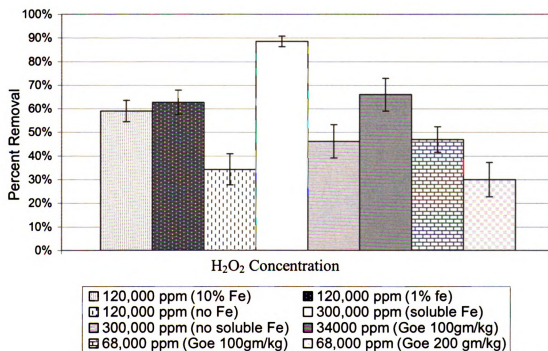


Figure 4-2: Results from the Oxidation of Pyrene in Ottawa Sand using CHP. The graph shows the percent oxidation achieved at the different hydrogen peroxide concentrations used under Ferrous and Goethite catalyzed systems.

Organic Matter Soil:

Pyrene contaminated MSU soil was allowed to react using different concentrations of hydrogen peroxide as shown in Figure 4-3. Pyrene concentrations decreased as hydrogen peroxide concentration increased reaching a maximum oxidation level of $75.9 \pm 19.8\%$ with soluble iron addition and $79.9 \pm 13.6\%$ oxidation with no soluble iron added. The results are separated for each CHP condition; Figure 4-4 for soluble iron catalyzed reactions and Figure 4-5 for reactions catalyzed by mineral iron.

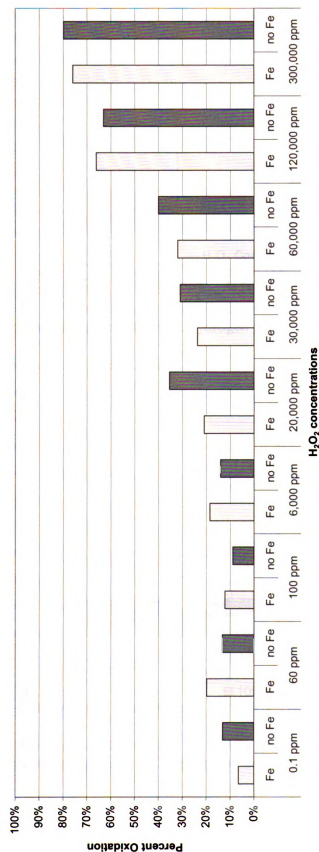


Figure 4-3: The figure shows the percent of pyrene oxidized vs. hydrogen peroxide dosage for reactions involving MSU soil, both with the addition and in the absence of soluble ferrous iron.

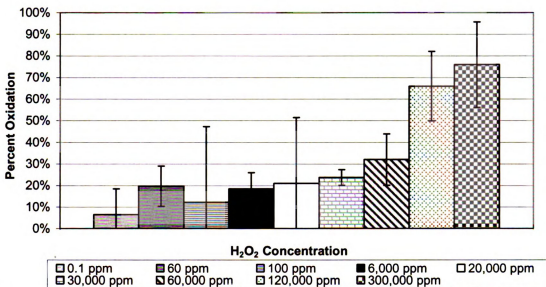


Figure 4-4 : Pyrene oxidation in soil containing organic matter catalyzed with soluble ferrous iron (percent oxidation vs. hydrogen peroxide concentration).

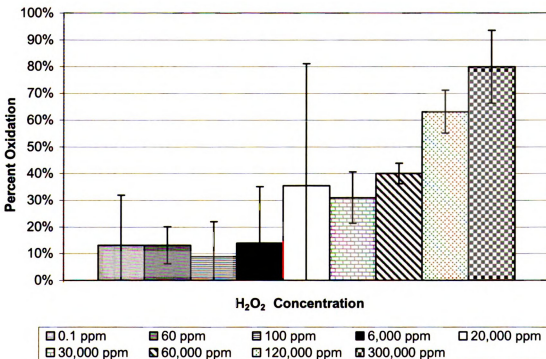


Figure 4-5: Pyrene oxidation in soil containing organic matter catalyzed with mineral iron (percent oxidation vs. hydrogen peroxide concentration).

Table 4-2 Results from oxidation of 50 grams of MGP soil with 120,000 ppm of hydrogen peroxide with and without soluble iron addition. Sample 1 taken at a depth of 10 feet, while Sample 3 was taken at a depth of 8 feet.

Polynuclear Aromatic Hydrocarbon	Concentration in Soil mg/kg of soil (extracted before H2O2 treatment)	Extracted from	Concentration after Treatment with H2O2 mg/kg of soil	Percent Reduced
Naphthalene	< LOD	-	< LOD	-
Acenaphthylene	4,539	Sample 1	1670* (Fe Added)	63 ± 32%
Acenaphthene	4566*	Sample 1	1591* (Fe Added)	65 ± 70%
			2510* (no Fe Added)	45 ± 26%
Fluorene	1093	Sample 3	776* (no Fe Added)	29 ± 14%
Phenanthrene	1567	Sample 1	1132 (Fe Added)	27.8 ± 30%
			1261 (no Fe Added)	19.5 ± 27%
Anthracene	542	Sample 1	396 (Fe Added)	27 ± 29%
	1175	Sample 3	455 (no Fe Added)	16 ± 36%
			259 (Fe Added)	78 ± 49%
Fluoranthene	3351	Sample 3	921 (no Fe Added)	22 ± 7%
			1279 (Fe Added)	61.8 ± 17%
Pyrene	4938	Sample 1	2813 (no Fe Added)	16 ± 20%
	10927	Sample 3	3945 (Fe Added)	24 ± 32%
			4068 (no Fe Added)	18 ± 27%
Chrysene	263	Sample 1	2891 (Fe Added)	73 ± 12%
	579	Sample 3	6389 (no Fe Added)	41 ± 19%
			151 (Fe Added)	42 ± 39%
			229 (no Fe Added)	23 ± 36%
Benzo(b) fluoranthene	< LOD	-	98.37 (Fe added)	83 ± 16%
			329 (no Fe Added)	43 ± 39%
Benzo(k) fluoranthene	837	Sample 3	< LOD	-
			215 (Fe Added)	74.3 ± 7%
			532 (no Fe Added)	36.4 ± 19%
Benzo(a)pyrene	< LOD	-	< LOD	-
Indeno(1,2,3-cd)pyrene	< LOD	-	< LOD	-
Dibenzo(a,h)anthracene	< LOD	-	< LOD	-
Benzo(g,h,i)perylene	< LOD	-	< LOD	-

* Estimated from values < LOQ and > LOD

D

R

d

V

a

r

C

a

w

S

Q

h

co

pl

se

st

se

con

The

/me

alib

Discussion:

Reactions that occurred in soluble iron-containing suspensions appeared to react differently when compared to that in suspensions that did not contain added soluble iron. White-grayish fumes, most likely NH_3 emitted from the vials containing ferrous ammonium sulfate during reaction, which were visible during the first 30 minutes of the reaction. These same fumes were visible for a shorter period of time in experiments with Ottawa sand containing added ferrous iron. Reactions with soluble iron were also violent, and exothermic and resulted significant increase in the temperature of the container; while no noticeable change in temperature was noted in suspensions that did not contain soluble iron. A dark-red compound was formed during the reaction in suspensions containing ferrous iron; this compound seemed to act as a pH-buffer. The pH after 24 hours of reaction time was found to remain less than 3 in suspensions where the compound was formed, while in suspensions where the compound was not visible, the pH increased to greater than 4 after the same time period. The addition of 20 ml of a 2 N sodium hydroxide solution were required to raise the pH to neutral conditions in the suspensions where the compound was visible; on the other hand, just a few drops of the same solution were required to reach neutral pH in suspensions lacking the red compound.

The temperature rose during the soluble iron catalyzed reactions, reaching up to 90°C (measured by placing a thermometer in the flask while the reaction was taking place); although the temperature generally remained at $\sim 70^\circ\text{C}$. Because a simple glass

thermometer was used, these measurements may have been recorded in the liquid-bubble interface, and the temperature in the bulk of the soil may not have been as high. Nevertheless the released energy from the reactions created an increase in temperature that may affect the oxidation process.

The increase in temperature at the liquid–bubble interface will likely have large effects in field applications, especially when dealing with compounds whose flash point may be exceeded during the reaction. Temperature monitoring during field scale applications should be performed.

Reactions in Ottawa sand had one noticeable difference to those of MSU soil and soil obtained from the MGP site; the reactions in the low organic content soils seemed faster than reactions in the other soils. Bubbling was visible in the regular soil samples for hours; while this bubbling was visible in Ottawa sand for only a few minutes.

Ottawa Sand:

The presence of soluble iron in Ottawa sand samples increased the contaminant removal efficiency. A possible explanation is the formation or lack thereof, of hydroxyl radicals in the system. Suspensions with no added iron would require the interaction of hydrogen peroxide with trace metals found in the sand to produce hydroxyl radicals. Alternatively pyrene may be oxidized by hydrogen peroxide, a weak oxidant when not catalyzed^{6, 9}.

On the other hand, samples with added soluble iron were able to produce a Fenton reaction, thereby producing sufficient hydroxyl radicals to oxidize the contaminant.

When the initial oxidant concentration was increased to 300,000 ppm from 120,000 ppm, a 40% increase in the removal efficiency of the contaminant (88.1%, compared to 62.8%) was achieved when soluble iron was present. Meanwhile, at the same concentration, in suspensions with no added iron, removal was much less (46.1%). If we assume that these soils contain few hydroxyl radical scavengers, the hydroxyl radicals formed should have few obstacles to prevent contaminant removal, thus these hydrogen peroxide concentrations should be able to oxidize the contaminant present. If hydroxyl radical formation is inefficient, contaminant removal is not likely to occur. From the results, we can determine that Ottawa sand in the absence of added soluble iron did not create the required conditions for pyrene oxidation. It appears that in Ottawa sand suspensions without added soluble iron, hydrogen peroxide is the major oxidizing compound. Oxidation by hydrogen peroxide is a much slower reaction than oxidations by hydroxyl radicals. Although some reaction occurred in these suspensions, a large portion of the hydrogen peroxide must not have reacted, resulting in lower removal efficiencies. This was evident by the release of gas during agitation after the given reaction time had elapsed.

Oxidation reactions of pyrene in Ottawa sand produced consistent results due to the very controlled nature of the reactions taking place. With very few radical scavengers present, the possible side reactions appear to be minimal, therefore allowing straight Fenton's chemistry to occur.

MSU soil:

From Figure 4-3 we may conclude that the addition of soluble iron did not increase the removal efficiencies in the MSU soil samples, in contrast to what was observed with the Ottawa sand. The major difference between these two types of soil was the amount of hydroxyl radical scavengers present. MSU soil had components (including organic matter and metals, including mineral iron) that may have influenced the reactions and had some apparent effect on the pyrene removal efficiency.

Suspensions with soluble iron could have reacted in the following manner: the iron in solution made it possible for the hydrogen peroxide to generate hydroxyl radicals and convert all ferrous ions present, into ferric ions. The reactions at this point become ferric ion catalyzed and depend on how fast the ferric ion cycles back to its ferrous state to produce new hydroxyl radicals^{4, 10}. The initial surge of hydroxyl radicals formed would have reacted with any scavengers encountered, including other hydroxyl radicals, limiting the effectiveness of the Fenton chemistry on pyrene removal. The exothermic nature of the reactions also could have caused a loss of hydrogen peroxide, forcing any unreacted hydrogen peroxide to decompose into water and oxygen. The cumulative effect of these factors may be represented in the lower removal of pyrene when compared to suspensions with the same oxidant concentration in the absence of added soluble iron.

Reactions in suspensions where ferrous ammonium sulfate was not added should and did behave differently because of their dependence on the availability of the iron mineral present in the soil to react with the hydrogen peroxide. The mineral iron in the soil slowly

dissolved, allowing the hydroxyl radical to slowly form and interact with scavengers and with the contaminants. This effect apparently helped the process; a less violent reaction occurred, allowing a smaller net loss of hydrogen peroxide from the solution by decomposition or volatilization; reducing the extent to which hydroxyl radicals reacted with each other. These effects resulted in improved oxidation in suspensions that had no added iron.

Due to the heterogeneous nature of soil samples, the analytical error increased, as seen in Figure 4-4 and Figure 4-5, in samples from the MSU soil. This increase in error could be due to the side reactions that are more likely to predominate in more complex soils. Hydroxyl radical scavengers and soil organic matter present interact with the oxidation reactions, making it difficult for radicals to attack the contaminant directly. The number of side reactions that may occur in the field could be too numerous to model or account for, therefore high analytical errors can be expected.

Sodium Dodecyl Sulfate

In experiments containing SDS a great amount of foam was produced specially in those suspensions that contained soluble iron, and if carelessly attended, the foam would spill out of the containers.

The addition of SDS to both Ottawa sand resulted in a decrease in the removal of the contaminant and an increase in the experimental error. The experiments yielded 16-59%

removal and errors between 17-54%. The soil samples that had been treated with SDS before oxidation clumped up and became difficult to dry.

Experiments with SDS in MSU soil yielded less oxidation of pyrene than observed in experiments without SDS. The oxidations resulted in a $32.2 \pm 21\%$ removal when soluble iron was added and $45.5 \pm 2.1\%$ with mineral iron was used as catalyzer. It appears that the violent nature of the reactions with added soluble iron in combination with the added SDS, affected the ability to obtain consistent results. Surfactants are known to affect the surface tension of the fluid, if gas is being released and bubbles formed, the material trapped in these bubbles maybe taken out of the solution and not allowed to react, thus affecting the reproducibility of these reactions.

SDS was added as a means to enhance the partitioning of pyrene to partition into solution and increase the oxidation efficiency of the hydroxyl radical, but results obtained do not show this, since no improvement was seen in the oxidation. Martens et al.² found a 400-fold increase in pyrene oxidation (from 8% to 55%) after the addition of 5 mM SDS solution to his samples. Our results do not confirm Marten's results.

SDS in our system appeared to be detrimental to the oxidation process, acting as a hydroxyl radical scavenger. The rate constant for the reaction of hydroxyl radical with dodecylsulfate ions in aqueous solutions (8.2×10^9) is comparable to that of known hydroxyl radical sinks, such as bicarbonate (8.6×10^8) and carbonate (3.9×10^8) ions¹¹. This may explain the decrease in removal efficiency found in our samples. Furthermore,

the product of the rate constant (k) and the initial molar concentration of our components can be calculated; using the rate constant for pyrene (the documented range of PAH-OH radical rate constants is 5×10^9 to 5×10^{10})¹¹ and the solubility of pyrene at 25°C (6.76×10^{-7})¹:

Reaction with SDS:

$$k_{\text{SDS}}[\text{dodecylsulfate}] = 8.2 \times 10^9 [5 \times 10^{-6}] = 4.1 \times 10^4$$

Reaction with Pyrene

$$k_{\text{pyr}}[\text{pyrene}] = 5 \times 10^9 [6.76 \times 10^{-7}] = 3.38 \times 10^3$$

or using the higher reaction rate for hydroxyl radicals with PAHs

$$k_{\text{pyr}}[\text{pyrene}] = 5 \times 10^{10} [6.76 \times 10^{-7}] = 3.38 \times 10^4$$

We can conclude from these equations that hydroxyl radical reactions with SDS in aqueous solutions are very competitive when compared to the reactions between pyrene and hydroxyl radicals. This competition could yield results like the ones obtained, although they do not explain Martens' results.

MGP Site Soil

The soils obtained from the Grand Ledge former MGP site were difficult to work with. The samples were heterogeneous, containing: gravel, sand, brick, tar, and water (Figure 4-6). The samples were homogenized to the greatest extent possible.

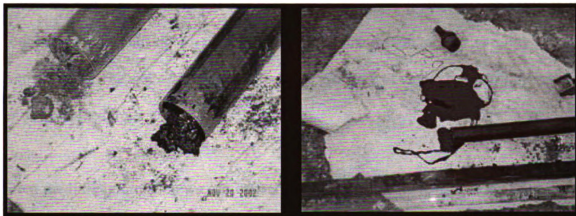


Figure 4-6: Contaminated soil being extracted from geo-probes during sampling at the Grand Ledge, MI former MGP site

The results of experiments with MGP soil are shown in Table 4-2. No quantifiable data could be obtained using our method from Sample 2 (4-6 ft depth). This data was then discarded from further analysis/discussion.

Results from the oxidation of the MGP soil, as shown in Table 4-2, were variable and were accompanied by large errors. The degree of contamination and the complexity of the matrix involved in the reactions lowered the degree of precision that could be obtained. This uncertainty was also present in the analyses performed on the soil by Consumers Energy, where concentrations of some PAHs were noticeably different between two sets of analyses performed in a 7 month time frame. Naphthalene concentration, for example, in Sample 1 was found to be 2.2 g/kg of soil based on analysis performed on November 2002; this same location was re-sampled in June 2003 and the naphthalene concentration was 4.4 g/kg of soil. Similarly pyrene was first reported at 820 mg/kg of soil and was later reported at 1,400 mg/kg for the same location.

Given the fact that the MGP site has been closed since the 1930s, such an increase in concentration is unlikely to result from new contamination or the mobility of the contaminants. The site's complexity affects the accuracy of any experiments performed on soil obtained from it.

From the little information we can extract from the results, it seems that the addition of soluble iron assisted the oxidation process. Although iron was present in the soils excavated, it appears that the iron was not available to assist Fenton reactions. The inefficiency of oxidation is also clear; no contaminant was removed to a 90% level. With errors found in the system, removal efficiencies were poor.

Conclusions

PAHs can be removed from soil using catalyzed hydrogen peroxide reactions. Pyrene was removed from several soil matrices with removal efficiency decreasing with increasing matrix complexity. Reactions in Ottawa sand achieved the highest level of removal ($88.1 \pm 1.8\%$), followed by reactions in soil containing organic matter ($75.9 \pm 19.8\%$) and finally MGP site soil ($61.8 \pm 17\%$ for fluoranthene).

Temperature becomes increasingly important in hydrogen peroxide catalyzed systems. As noted here the temperature of the matrix may increase substantially during reaction, this may cause an acceleration of all the reactions involved, including hydrogen peroxide decomposition.

Catalyzed hydrogen peroxide systems do not appear to be the most sensible solution when dealing with highly contaminated soils like those found in MGP sites. The non-specificity of the hydroxyl radical plus the strictly aqueous environment required the use of higher chemical doses than might be expected from stoichiometry.

References

1. Schwarzenbach, R. P.; Gschwend, P. M.; Imboden, D. M., *Environmental Organic Chemistry*. 1st ed.; Wilkey-Interscience, John Wiley & Sons Inc: New York, 1993.
2. Martens, D. A.; T, F. j. W., Enhanced Degradation of Polycyclic Aromatic Hydrocarbons in Soil Treated with Advance Oxidative Process- Fenton's Reagent. *Journal of Soil Contamination* **1995**, 4, (2), 1-14.
3. Kong, S.-H.; Watts, R. J.; Choi, J.-H., Treatment of Petroleum-Contaminated Soils Using Iron Mineral Catalyzed Hydrogen Peroxide. *Chemosphere* **1998**, 37, (8), 1473-1482.
4. Watts, R. J.; Stanton, P. C.; Howsawkeng, J.; Teel, A. L., Mineralization of a Sorbed Polycyclic Aromatic Hydrocarbon in Two Soils using Catalyzed Hydrogen Peroxide. *Water Research* **2002**, 36, 4283-4292.
5. Kawahara, F. K.; Davila, B.; Al-Abed, S. R.; Vesper, S. J.; Ireland, J. C.; Rock, S., Polynuclear Aromatic Hydrocarbon (PAH) release from Soil during Treatment with Fenton's Reagent. *Chemosphere* **1995**, 31, (9), 4131-4142.
6. Beltran, F. J.; Gonzalez, M.; Rivas, F. J.; Alvarez, P., Fenton Reagent Advanced Oxidation of polynuclear Aromatic Hydrocarbons in Water. *Water Air and Soil Pollution* **1998**, 105, (1998), 685-700.
7. Kakarla, P. K.; Andrews, T.; Greenberg, R. S.; Zervas, D. S., Modified Fenton's Processes For Effective In-Situ Chemical Oxidation-Laboratory and Field Evaluation. *Remediation* **2002**, Autumn, 23-36.
8. Nam, K.; Rodriguez, W.; Kukor, J. J., Enhanced Degradation of Polycyclic Aromatic Hydrocarbons by Biodegradation Combined with a Modified Fenton Reaction. *Chemosphere* **2001**, 45, (2001), 11-20.
9. Tyre, B. W.; Watts, R. J.; Miller, G. C., Treatment of Four Biorefractory Contaminants in Soils Using Catalyzed Hydrogen Peroxide. *Journal of Environmental Quality* **1991**, 20, (October-December), 832-838.

10. Pignatello, J. J.; Baehr, K., Ferric Complexes as Catalysts for "Fenton" Degradation of 2,4-D and Metolachlor in Soil. *Journal of Environmental Quality* **1994**, 23, (March-April), 365-370.

11. Buxton, G. V.; Greenstock, C. L.; Helman, W. P.; Ross, A. B. *Critical Review Constants for Reactions of Hydrated Electrons Hydrogen Atoms and Hydroxyl Radicals ($^{\bullet}\text{OH}/\text{O}^-$) in Aqueous Solution.*; 1988.

Chapter 5.

Byproduct formation from the oxidation of Pyrene by Catalyzed Hydrogen Peroxide Propagations

Introduction

In recent years Fenton's Reagent and its hybrid successor, Catalyzed Hydrogen Peroxide Propagations (CHP), have seen a surge in their use as in-situ remediation technologies^{1, 2}. CHPs consist of the addition of 30% hydrogen peroxide, accompanied by a metal ion catalyzer, usually an iron species^{3, 4}. Fenton's reagent on the other hand consists of a dilute hydrogen peroxide solution (~0.03% solution), catalyzed by ferrous iron (soluble salt). Catalyzed hydrogen peroxide systems could be an ideal technique for in-situ remediation of contaminated sites: the system produces a strong, albeit, non-specific, oxidizing agent; the system is aqueous, allowing for its application to both soil and natural water systems; the catalyzer is readily found in natural soils; and unreacted hydrogen peroxide decomposes naturally to water and oxygen, usually saturating the matrix, which helps the proliferation of natural biota after remediation. These reasons have allowed CHP to be used for the remediation of sites containing: PAHs⁵⁻¹³, halogenated compounds¹⁴⁻¹⁹, petroleum derived products²⁰⁻²², and other hazardous chemicals. The system has also been used in combination with other remediation processes such as bioremediation and is a common part of advanced oxidation processes²³⁻²⁵. A number of consulting companies utilize CHPs as their primary method of in-situ site remediation.

The oxidation efficiency of this technique is based on the hydroxyl radical formation. Lindsey et al.^{26, 27} studied the effect of fulvic acid and humic acid on hydroxyl radical formation from Fenton's Reagent, and found that hydroxyl radical concentration was four times lower in natural water samples when compared to samples with no dissolved organic matter. We can extrapolate from this that the formation of hydroxyl radicals in soil samples will decrease as well, due in part to the presence of soil organic matter, as well as metals (copper, manganese, mineral iron), carbonate and bicarbonate, ammonium and nitrite and any other oxidizable species in the soil. The expected outcome is that partially oxidized products will exist after treatment. Nam et al.¹³, stated: "very little study has been done on whether partially oxidized organic compounds pose fewer hazards than the parent compound."

Fenton remediation was performed on soil contaminated with 3-,4-, and 5-ring PAHs by Lee et al.²⁸. PAHs were extracted from the matrix using ethanol, and Fenton's Reagent was added to the ethanol extract. Several PAH diones were identified using GC/MS from this experiments, but it is unclear how the Fenton's Reagent system behaves in an ethanol matrix and if the byproducts come from the interactions with organic radicals formed from ethanol or from Fenton oxidation directly.

Walling et al.²⁹⁻³¹ were the first to critically analyze Fenton's Reagent and hydroxyl radical interactions with known contaminants. Walling found that hydroxylation of aromatic compounds with hydroxyl radicals was common. Walling theorized the reaction pathways and reaction rates for these compounds, for Fenton systems that were catalyzed

by fe

mas

Fen

hyd

gro

Lus

the

baa

The

the

app

Al

ren

Ko

fac

inc

the

me

by

app

PA

by ferrous, ferric and cuprous ions. Augusti et al.³² found through membrane introduced mass spectrometry (MIMS) that the oxidation/mineralization of benzene derivatives with Fenton's Reagent proceeded via hydroxylation producing phenolic, hydroquinonic (*p*-hydroxy phenol) and quinonic (1,4 dioxy-benzene) intermediates. Similar functional groups were found after the oxidation of PAHs by Fenton's Reagent.

Luster-Teasley³³, Upham et al.³⁴, and Yao et. al.³⁵ identified byproducts obtained from the ozonation of pyrene in soils. The byproducts found had biphenyl and anthracene backbone structures containing multiple, hydroxyl, carboxylic, and aldehyde groups. These byproducts, especially those with bay regions, were found to be more toxic than the original contaminant, leading to the question of what would be created in field applications if the contaminant were not completely mineralized during treatment.

Although studies have been performed to measure the effectiveness of CHPs and FR in remediating polycyclic aromatic hydrocarbons (e.g., see Kakarla et. al.³⁶, Beltran et. al.²³, Kong et al.²¹, Watts et al.⁹), the end products from these reactions are unclear. If the only factor measured is the disappearance of a compound, then there may be a risk of increased toxicity in the environment after remediation, due to byproduct formation. In this study we have identified the byproducts formed from CHP reactions with pyrene as a model PAH, as well as their formation rate and estimated the potential fate of these byproducts in the environment. The knowledge gained from these studies can be readily applied and should identify potential hazards that may arise during or after remediation of PAHs is performed.

Method and Materials

A single addition of hydrogen peroxide was used for all experiments. All reactions were carried out in borosilicate glass vials. The vials were cleaned in a 1% hydrochloric acid wash, rinsed in ultrapure water and allowed to dry. To remove organics, the vials were placed in an oven at 550 °C for 2 hours.

CHP reactions using soluble iron were allowed to react for 24 hours and quenched by adding sodium hydroxide (1M) to precipitate iron. Reactions using goethite as a catalyzer were allowed to react for 72 hours and quenched by decanting the supernatant solution from the catalyzer.

Goethite used in the experiments was rinsed under a deionized water stream to remove iron dust from the surface and dried in an oven at 105°C. Finally, the goethite was cleansed of any organic contamination by placing it in an oven at 550°C for two hours, prior to use.

Pyrene oxidation was carried out in two systems, water and Ottawa sand. For reactions in water, acetonitrile was used as a co-solvent to enhance the solubility of pyrene. The volumetric amount of acetonitrile in the solution was not allowed to exceed 3% (or about 1 ml in 20 ml of solution) because of reactions that occurred between the solvent and hydroxyl radicals. The effect acetonitrile had on pyrene solubility can be calculated by the Morris equation³⁷:

$$\text{Log} \left(\frac{C_{mix}^{sat}}{C_w^{sat}} \right) = (a \log K_{ow} + b)(f_c) \quad (1)$$

where,

C_{mix}^{sat} is saturated concentration of the solute in the mixture

C_w^{sat} is the saturated concentration of the solute in water

K_{ow} is the water-octanol partition coefficient for the solute,

f_c is the volume fraction of co-solvent, and

a and b are coefficients unique to the solvent. For acetonitrile, these coefficients are 0.9 and 0.83 respectively³.

According to this equation, the solubility of pyrene should increase by 48% to about 0.21 mg/L. Initial pyrene concentrations were 100 mg/L, resulting in a suspension with the water.

A pyrene stock solution was prepared by dissolving 0.5 grams of the compound in 200 mL of acetonitrile. This solution was then diluted as appropriate.

Ottawa sand was rinsed with acidic ultrapure water and allowed to dry prior to use. These experiments were carried out in the absence of acetonitrile. The pyrene stock solution was added drop by drop to a vial containing 20 grams (dry weight) of sand while being

mixed by a Mistral Multimixer (Model 4600, Lab-Line Instruments Inc.). The vials were placed in a dark hood for 24 hours to allow the solvent to evaporate before commencing the experiments. The initial pyrene concentration was held at 300 mg/kg of sand.

Ottawa sand reactions were carried out as aqueous slurries. The soil (20 g dry weight) was saturated by adding 4.5 mL of water, which contained iron at a concentration ranging from 0.001 to 0.06 moles/kg of soil. For reactions with mineral iron, goethite was added to the dry sand while being mixed, to allow homogenization of the mineral in the matrix, before the addition of water.

Byproduct Structure Identification

Sample preparation

Samples from the oxidation experiments were placed under a gentle nitrogen gas stream until completely dry. Hexane (5 mL) was added and the vial was placed on an orbital shaker (Lab-Line, Model 3590) for 1 hr. The hexane was then decanted and 5 mL of acetonitrile was added to the vial and placed on the shaker. This process was repeated with 5 mL of 0.1 M sodium hydroxide solution followed by 5mL of 0.1 M perchloric acid solution. The extracts were then taken for LC/MS analysis.

A Shimadzu LC-20AD HPLC was used coupled with a Waters Quattro micro API mass spectrometer. The LC used a 5 μ Thermo Hypersil-Keystone BetaBasic-18 PIONEER column with dimensions of 150 by 1mm. The LC used a gradient program with

acetonitrile and water, containing 0.15% formic acid, as the mobile phase and the flow rate was 0.1 mL/min. At the start, the ratio of acetonitrile to water was 10:90, the ratio was increased linearly to 60:40 over 30 minutes, and then continually increased to 100% acetonitrile over ten minutes. At this time the concentration of acetonitrile was decreased to 60% over ten minutes, after which the concentration was decreased immediately to 10%, with this concentration held for 5 minutes. This program had a total run time of 60 minutes.

The LC/MS used a Waters Z-spray electrospray ion source with acquisitions performed in both positive and negative ion modes with a cone voltage of 40 V and a capillary voltage of 3.17 kV. The desolvation and cone gas (N₂) had flow rates of 400 L/hr and 10 L/hr respectively. For MS/MS analysis, the collision energy was held between 25 and 35 eV.

Results

CHPs catalyzed by ferrous ion are more violent and exothermic than those catalyzed by ferric ion, because the rate of hydrogen peroxide decomposition into oxygen is faster when ferrous ion is present, leading to a rapid loss of hydrogen peroxide from the system (as described in Chapter 2).

Pyrene was oxidized by CHPs in both soil slurries and water systems. Reactions that occurred in solution achieved only moderate removals as compared to those in soil slurries described in Chapter 3. As seen in Figure 5-1, reactions with soluble ferrous iron resulting in 9.4% removal; while reactions with ferric ion achieved 15.2% removal in

aqueous solutions. Pyrene removal increased for both of these ions in Ottawa sand slurry reactions, with ferrous ion catalyzed reactions achieving 36.1 % removal and ferric ion catalyzed reactions resulting in 49.8% removal.

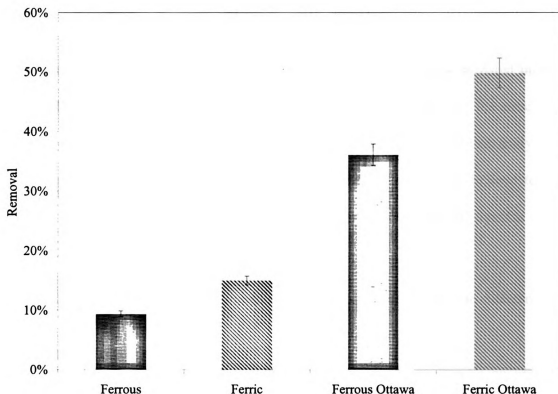


Figure 5-1: Percent removal of pyrene from CHPs for solution and Ottawa sand reactions. The initial iron catalyst concentration was held at 0.06 M, while the initial hydrogen peroxide concentration was 0.11 M.

Goethite catalyzed reactions also displayed the trend found from the reactions with soluble iron, higher pyrene removal in Ottawa sand experiments as compared to reactions in aqueous systems. For reactions with a Goethite equivalent of 0.06 M ferric ion, the pyrene concentration was found to be below our analytical detection limit for Ottawa sand slurries, while reactions in aqueous solutions resulted in less than 1% removal.

Byproduct Formation

Byproducts from the oxidation of pyrene with both soluble and mineral iron catalyzed CHPs have been found and identified. Several compounds having different mass to charge ratios (m/z) were found in hexane and acetonitrile extracts, while no byproducts were found in the water extracts. The full range of compounds found is listed in Table 5-1. MS/MS analysis was performed in order to obtain information about the structure of the compounds formed. Figure 5-2 and Figure 5-3 show an example of this analysis the electrospray mass spectra and MS/MS spectra for m/z 233 which is believe to be a pyrene-quinone structure. The complete set of electrospray and MS/MS spectra for the compounds found can be seen in Appendix A.

Table 5-1: Table showing m/z found in the combined extracts from the different CHP tested.

Hydrogen Peroxide [M]	Catalyzer		m/z
	Concentration [M]	Catalyzer Used	
Water/Acetonitrile			
0.01	0.001	Goe	241, 219
		Ferric	208, 233, 207, 235, 315, 275, 247, 234, 251, 221, 267
		Ferrous	223, 429, 233, 235, 251, 331, 315, 281, 301, -299, -341
0.11	0.06	Goe	241, 219
		Ferric	233, 257, 255, 249, 251, 331, -485
		Ferrous	233, 257, 249, 251
0.10	0.01	Ferric	208,149,217,233,260,249,227,301,218,225,265,282, 255,331,271,221
0.38	0.06	Goe	205,221,233,267,217,219,260,208,225,223,203,204, 433,204,295,239
Ottawa Sand			
0.11	0.06	Goe	233, 241, 221, 217, 203, 204, 219
		Ferric	233, 353, 271, -329, -285, -315
		Ferrous	233, 271, -286

Table 5-2: Byproducts identified by LC/MS/MS with a list of major m/z peaks found in the spectra

Byproduct	m/z	Major Fragments
FI	219ES+	219, 201, 191
FII	217ES-	271/216, 189
FIII	235ES+	235, 217, 207, 192, 179, 164
FIV	251ES+	251, 233, 205
FV	233ES+	233, 205, 177/176, 151
FVI	249ES+	249, 221, 203, 192/193, 165
FVII	221ES+	220, 177/176, 165, 151, 77
FVIII	267ES+	267, 249, 239, 221, 193, 165
FIX	247ES+	247, 218, 201, 190/189
FX	204ES+	204, 203, 202, 176, 151
FXI	223ES+	223, 205, 177/176, 152/151, 98, 63
Pyrene	203ES+	203, 202, 201

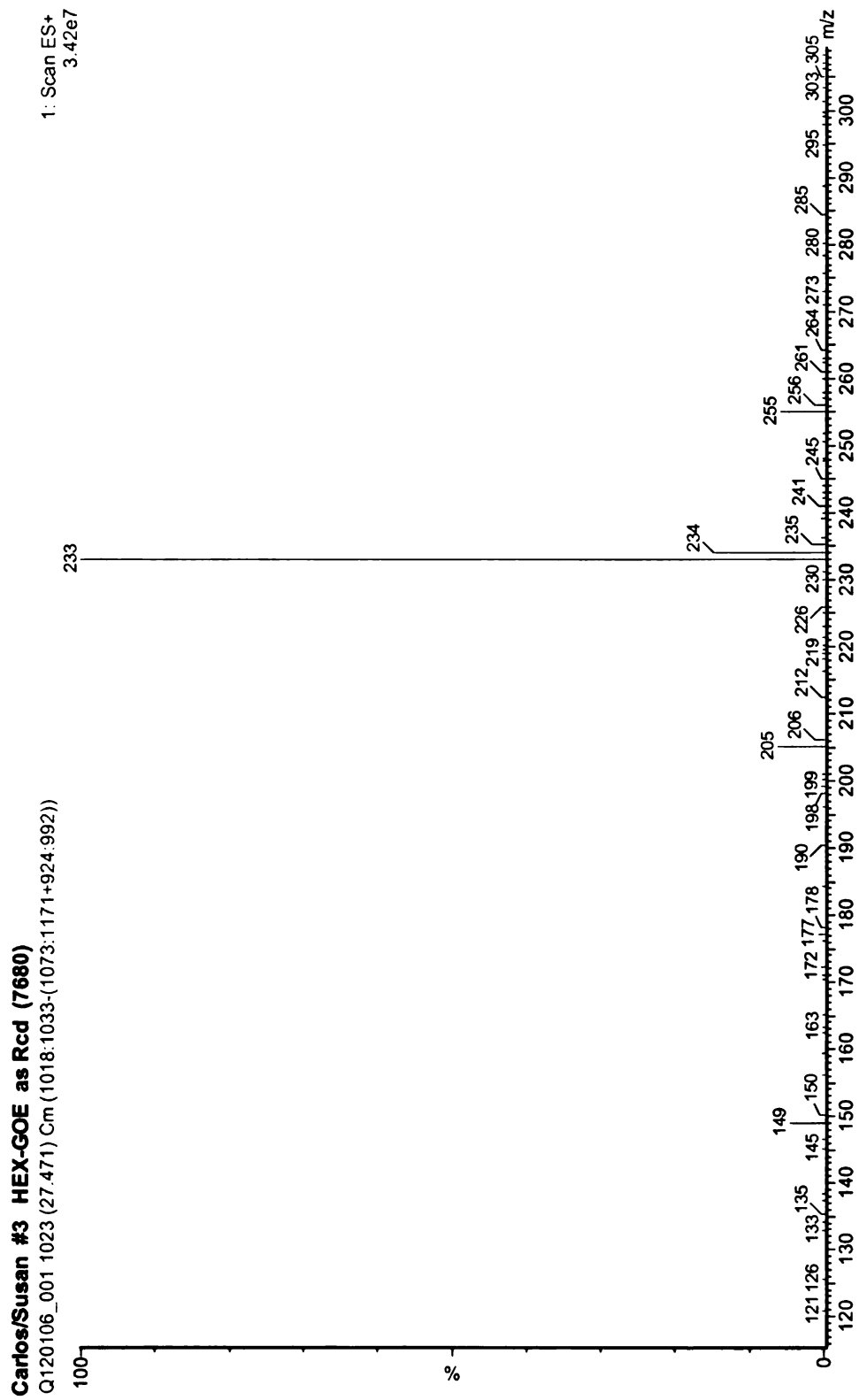


Figure 5-2: LC/MS Electrospray mass spectra for m/z 233 obtained from the oxidation of pyrene in solution by goethite. This m/z was found in the hexane extract.

Carlos/Susan #3 HEX-GOE as Rcd (7680) MSMS
Q121306_001 155 (24.887) Cm (143:160-(7.91+185.297))

8: Daughters of 233ES+
4.04e5

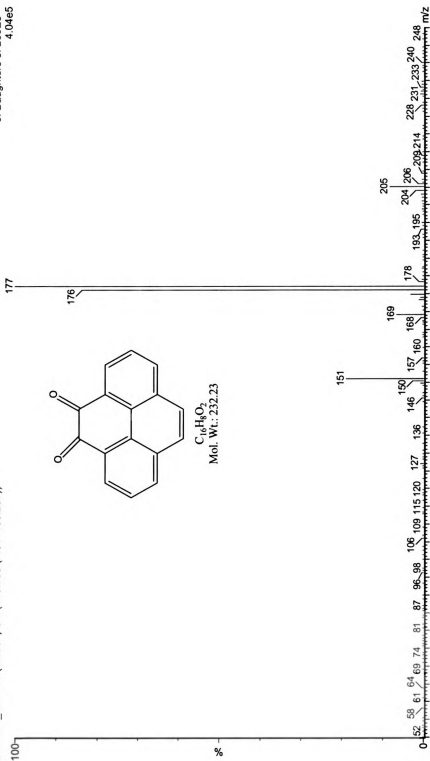


Figure 5-3: MS/MS spectra showing fragment ions from m/z 233, obtained from the hexane extract of goethite catalyzed CHPs.

Electrospray ionization produces both negative and positive ions; negatively charged ions have been highlighted in Table 1. Electrospray ionization creates adducts with positive ions such as $[M+H]^+$ formed by cation attachment, , while negative ions are often formed by deprotonation to give $[M-H]^-$. Any m/z found would require the addition or subtraction of 1 Dalton to establish its molecular mass.

Not all m/z found could be identified as byproducts from the reactions because they did not produce sufficient ions from the electrospray process to allow identification. For other structures, such as m/z 233 ($[M+H]^+$ of pyrenequinone), insufficient information was available to identify the specific structural isomer, but molecular ion and fragment ion masses in MS/MS spectra were consistent with its assignment as pyrenequinone. There is as well the possibility that some byproducts may have been lost during the drying of the sample with nitrogen gas, or were irreversibly sorbed to the walls of the reaction vials ¹¹. The structures for the byproducts identified can be found in Figure 5-4 and in the first column in Table 5-4.

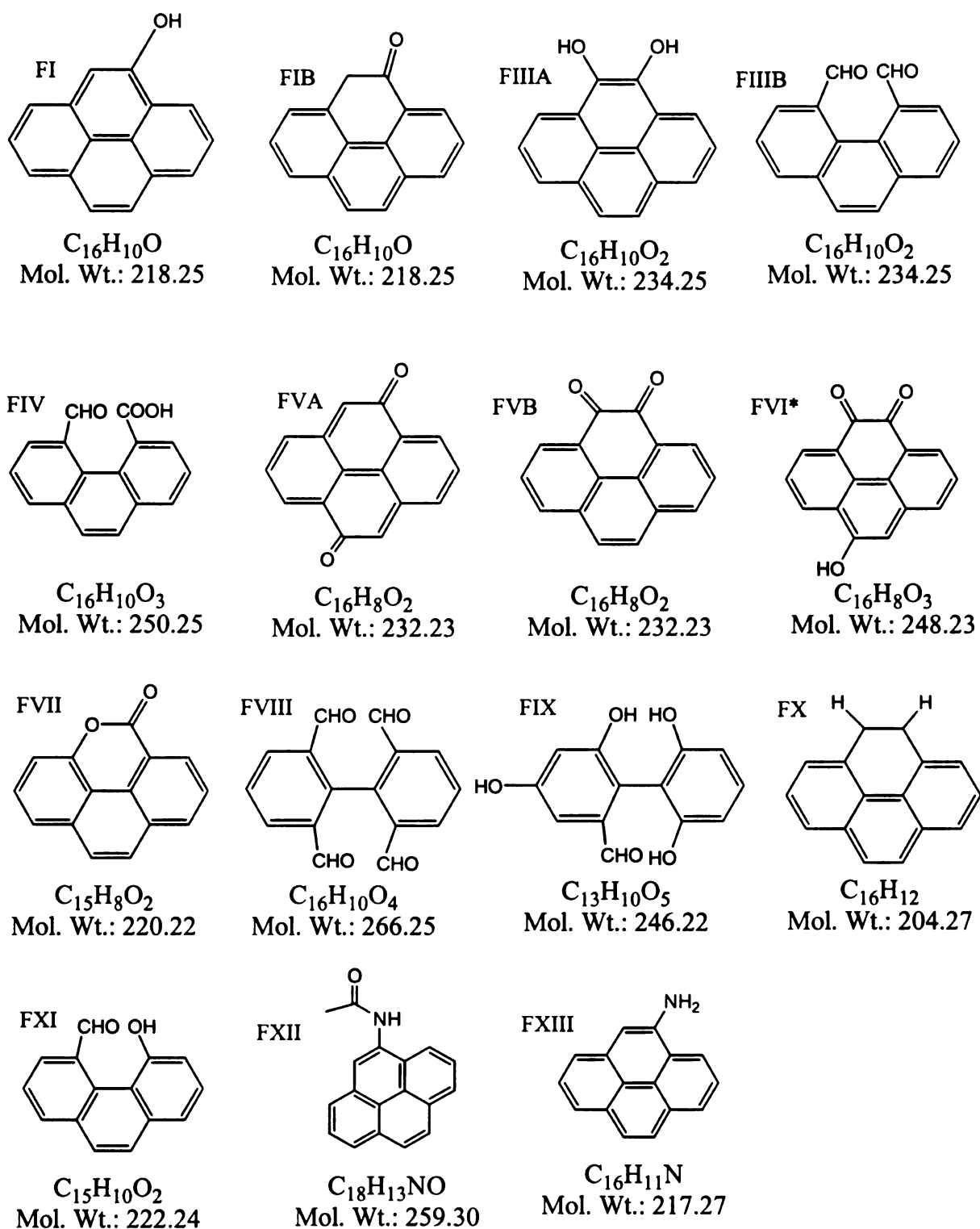


Figure 5-4: Byproducts identified from the oxidation of pyrene by CHPs in water and soil slurries, using mineral and soluble iron catalyzed reactions. *3 isomers of the structure were found, but not readily distinguished.

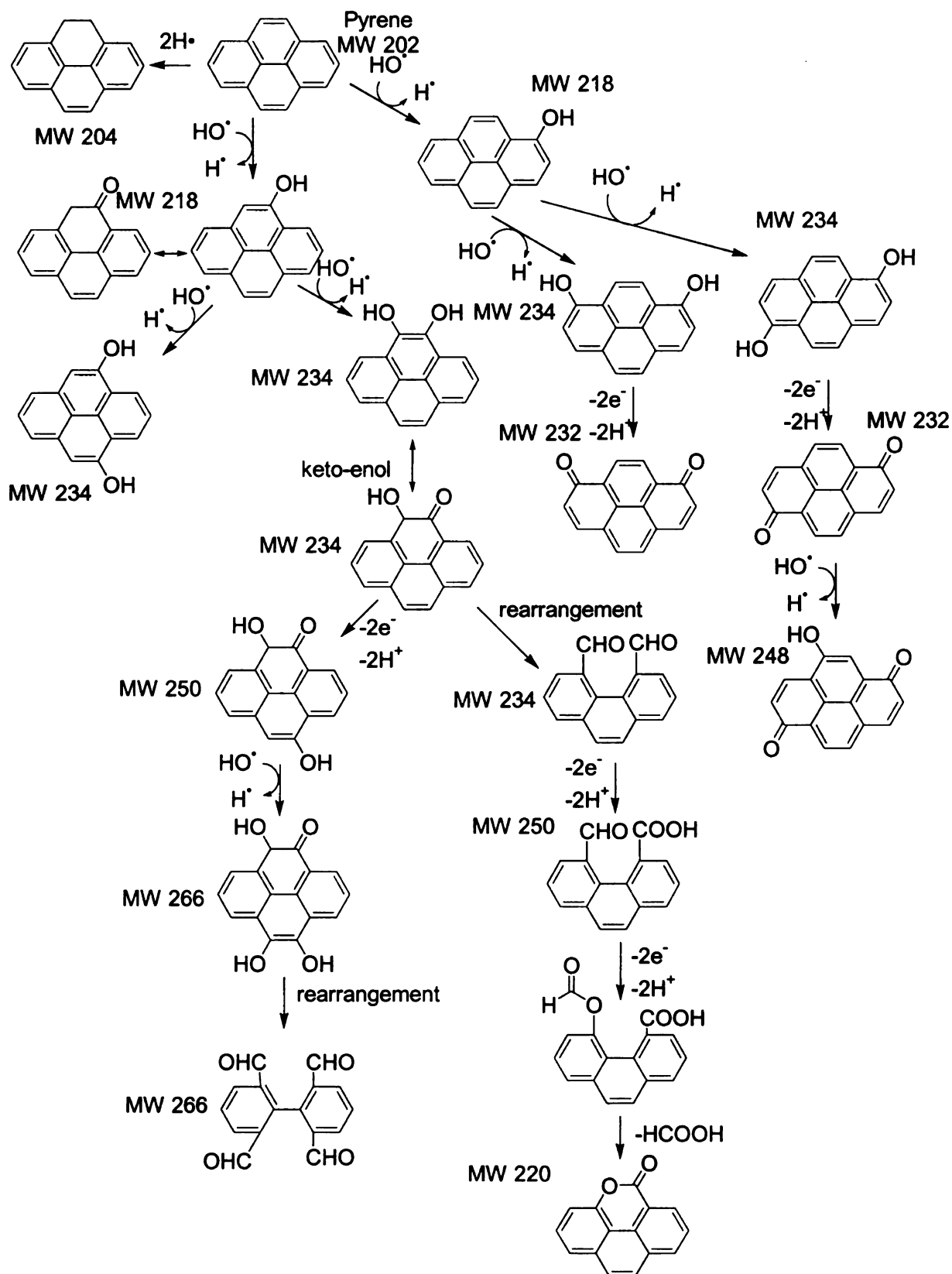


Figure 5-5: Proposed pathway for hydroxyl radical degradation of pyrene by CHPs

Discussion

A greater extent of removal was obtained in the presence of Ottawa sand as compared to aqueous solutions. Pyrene solubility may have had a major role in this result, because although the addition of acetonitrile increased its solubility, the amount of acetonitrile added may have been insufficient to ensure that pyrene was solubilized and available to interact with the hydroxyl radicals produced, instead hydrogen peroxide may have decomposed and the excess hydroxyl radicals reacted with the other species in the reaction (ferric ion, ferrous ion, and hydrogen peroxide). The fact that pyrene was present in a greater amount in a suspension and not in the solution, would have prevented most of the pyrene, from reacting with the oxidant. It is thought that pyrene was more available to react in Ottawa sand slurries because it may have sorbed to sand particles allowing any hydroxyl radicals formed nearby to interact directly with the contaminant. These results are consistent with findings from Masten³⁸, where PAH removal by ozonation was greater in soils slurries than in aqueous solutions.

Pyrene oxidation byproducts were found for both soluble and mineral iron catalyzed CHPs. The byproducts tentatively identified range from pyrene substituted with a hydroxyl group to quinone to ring cleavage products. All of the byproducts found appear to have been formed from the reaction of hydroxyl radicals with pyrene and are thus oxidized versions of the contaminant. The byproducts found were formed from a single addition of hydrogen peroxide, which could have limited the degree and/or extent of oxidation that was achieved, in comparison the continuous addition of hydrogen peroxide

would likely have resulted in the formation of a continuous supply of radicals into the system, producing more highly degraded products.

Figure 5-5 shows the proposed pathway for hydroxyl radical interaction with pyrene. The pathway was based on the assumption that hydroxyl radicals were the only species present in the system capable of oxidizing the contaminant. Numerous studies have found that hydroxyl radicals interact with aromatic compounds by hydroxylating the ring. This is the first step in the mechanism, from there on the nonspecific nature of the hydroxyl radicals can form multiple byproducts and isomers, leading to phenolic (FI), ketonic (FIB), quinonic (FVA and FVB), carboxylic (FIV); and ultimately, biphenyl structures are formed (FVIII and FIX).

Byproduct formation between different Catalyzers

The byproduct formation varied under the three catalyzers used, as seen in Table 5-1. As a general trend we can conclude that an increase in hydrogen peroxide concentration (oxidant) increased the extent of oxidation of products found in solutions catalyzed by goethite. For the three concentration schemes used only the combination of 0.38 M hydrogen peroxide with a 0.06 M (as ferric ion) goethite concentration achieved significant byproduct formation. Under these concentrations we were able to find 16 different products (m/z), while under concentrations of hydrogen peroxide (0.01 and 0.11 M) combined with goethite concentrations of 0.06 and 0.001M only two products were found m/z 241 and 219. The difference in the number of products found can be attributed to the nature of goethite catalyzed reactions. Heterogeneous catalysis of hydrogen

peroxide is a surface reaction that requires the diffusion of hydrogen peroxide and pyrene to the goethite surface. If undissolved pyrene covered the surface of the catalyzer it may have impeded the diffusion of hydrogen peroxide to the active sites, and thus less of the oxidation reaction may have taken place; an increase in oxidant concentration appeared to force its way into the catalyzer surface thus increasing oxidation.

Both ferrous and ferric catalyzed systems created byproducts, but the byproducts identified in ferric catalyzed reactions appeared to be more oxidized than those from ferrous systems. As a result, byproducts FVIII and FIX, corresponding to the two byproducts with the highest degree of oxidation, were found in ferric systems. In ferrous systems the most oxidized byproducts found were FIV and FVI, which are a few oxidizing steps behind the ultimate products found by ferric catalysis, as seen in Figure 3. An increase in hydrogen peroxide and iron concentration in both systems resulted in less byproduct formation. This decrease in byproduct formation may be due to an increase in hydrogen peroxide decomposition at these concentrations of iron, with ferrous systems having the highest decomposition rate between the two. This result is consistent with the results from oxygen decomposition described in Chapter 2.

Ottawa sand experiments resulted in fewer byproducts than those found in the aqueous solution experiments. This result may be due to several factors: the byproducts may have been sorbed to the soil particles; the impurities extracted from the sand may have masked byproducts and thus we could not separate them during analysis; or the extraction method

used may not have been the optimal. Although any of these reasons may be true, byproduct m/z 233 (pyrenequinone) was produced by all three catalyzers in this system.

Pyrenequinone (FV, m/z 233) was found throughout all the experiments, making it the most likely byproduct to be found in remediation of pyrene contaminated sites. The formation of pyrenequinone has special significance because: (i) pyrenequinone is known to be toxic³⁹, (ii) its presence validates that oxidation is indeed occurring; and (iii) Chen and Pignatello⁴⁰ found that the presence of quinone intermediates helped catalyze CHP reactions by converting the ferric ion into ferrous ion. Many different isomers of pyrenequinone may be formed and the byproducts shown in Figure 1 (FVA and FVB) represent two of the most stable isomers that may be formed. Unfortunately, insufficient information was obtained from the MS/MS data to distinguish between the possible isomers. A sample LC/MS chromatogram showing the ion abundance peak for m/z 233 (pyrenequinone or FVA or FVB) versus the total ion count, and its molecular ion peak is shown in Figure 5-2. Figure 5-3 shows the MS/MS product ion mass spectrum obtained from this m/z with the fragment ions formed arising from successive losses of CO (28 Da) that are consistent with a quinonic structure on the pyrene ring.

The reason structures FVA and FVB were selected as the most probable isomers is because hydroxyl radicals are most likely to react with carbons 4,5 and 11, 12, which have a greater electron activity present. The increased electron activity in the area is due to the π - π bonds located here, which create a larger electron cloud, and thus making these

carbons more likely to interact with radicals. The byproducts found from the ozonation of pyrene³³ confirm that these are the most reactive bonds.

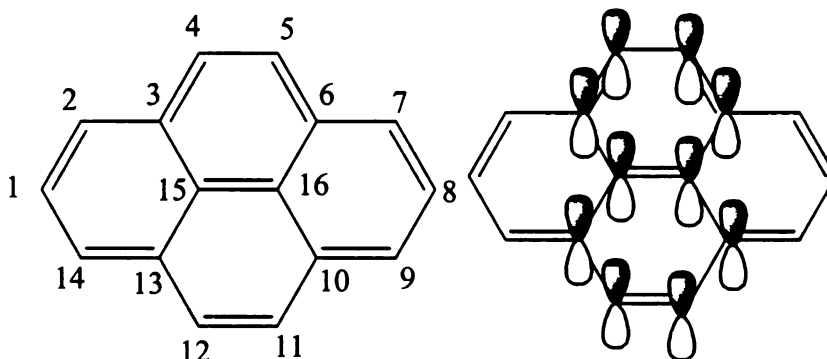


Figure 5-6: a) Pyrene molecule with numbered carbons and b) showing p-orbitals around the center region of the molecule.

Byproduct FX is an interesting compound because it is a product of a reduction reaction rather than an oxidation reaction. The most likely scenario is that of pyrene reacting with excess hydrogen peroxide or with superoxide to reduce one of the double bonds forming hydro and di-hydro pyrene. These compounds were readily found in all CHP reactions investigated. Byproduct FX was easy to find because it fluoresced at the same excitation and emission wavelengths used for pyrene but had a different retention time compared to that of pyrene.

Byproducts FXII and FXIII are products resulting from the reaction of acetonitrile, a co-solvent in aqueous reactions, with hydrogen peroxide or hydroxyl radicals. These byproducts, although unexpected, may be of significance because of the multitude of contaminants and chemical species present in the natural environment. Coal tar contaminated soils contain benzene, naphthalene and aliphatic compounds that may be involved in the reactions to form a multitude of byproducts. The structures found

illustrate that other radical species may be formed during CHP reactions and these radicals can react with the contaminant of interest to form other byproducts.

A compound with m/z 208 was found, but could not be positively identified. Enough information was present in the mass spectra to determine that the structure was comprised of an acetamide group attached to a highly oxidized bi-phenyl structure. The acetamide group was formed from the reaction of hydroxyl radicals with acetonitrile (co-solvent) making it a similar reaction to the one that formed byproducts FXII and FXIII.

Comparison to PAH byproducts found from Fenton's Reagent Reactions

Beltran et al.^{23, 25} identified byproducts from Fenton's Reagent reactions and hydrogen peroxide/ozone reactions with PAHs (fluorene, phenanthrene and acenaphthene) in water by GC/MS. Beltran et al.²³ reported 11 different byproducts including phenolic and quinonic derivatives; but researchers were unable to identify 16 other byproducts. These byproducts found by Beltran are similar to those found in this study. From the 11 identified products three were a form of the hydroxylated PAH (9-phenanthrenol, 9-fluorenol, 1-naphthol 2-,ethyl), one was a ketone (9-fluorenone) and 2 were biphenyl structures (o-hydroxybiphenyl and 2(H)-1-benzopyran-2-one,3,4-dihydro-). These byproducts are similar to the structures identified for byproducts FI and FIII (hydroxylated), FIB and FV (ketonic or quinonic), FVIII and FIX (biphenyl). These structures are also consistent with the proposed pathway, shown in Figure 5-5, of degradation by hydroxyl radicals, where an initial hydroxylation leads to phenolic

compounds, and a second reaction leading to ketonic structures. The final products of these reactions are substituted biphenyls which were found by Beltran and this study. Beltran unfortunately does not go into discussion about the byproducts formed, but states that a smaller quantity of byproducts was found from oxidations using Fenton's Reagent than with oxidation using ozone, but was not sure why this happened. The major difference between ozone and CHP reactions is that the former can react directly with the contaminant while the latter goes thru a series of transformations to form the radicals that attack the molecule. Ozone is also capable of forming hydroxyl radicals; the result is then that more of the contaminant reacts in the ozone system, when compared to a Fenton's reaction, for the same dose of oxidant.

Comparison to PAH Byproducts from other Remediation Techniques.

PAH byproducts from other remediation techniques have been identified. Byproducts have been found from, electrolytic aeration⁴¹, photolysis⁴², , biodegradation^{39, 43, 44} and ozonation^{33, 35, 45}.

Electrolytic Aeration of pyrene

Goel⁴¹ has shown found that naphthalene is degraded by electrolytic aeration in a similar manner as pyrene, in the proposed pathway, starting with phenolic structures and leading to ketonic and quinonic byproducts. Goel indentified 1,4 naphthaquinone and, 1-napthol as byproducts.

Phot

Zeng

in a

alon

prop

four

qui

Ze

py

B

B

b

c

e

c

Photolysis of Pyrene

Zeng et al.⁴² used 1-hydroxypyrene as a model PAH to study the irradiation of UV light in a water/acetonitrile system. The authors identified two pyrenequinone byproducts along with a pyrene quinone dimer. The byproducts in this study are consistent with the proposed mechanism shown in Figure 5-5. The only difference between the byproducts found in this study and the byproducts found by Zeng is that the actual location of the quinonic groups was not determined in this study but both of the structures found by Zeng can be found in the proposed mechanism as possible results from the oxidation of pyrene by hydroxyl radicals.

Biodegradation of Pyrene and other PAHs

Byproducts (metabolites) from the biodegradation of pyrene by *Mycobacterium sp.* have been identified by Heitkamp⁴⁴ and are shown in the third column of Table 2. The degradation of PAHs by aerobic bacteria follows hydroxyl radical interaction through enzymatic catalysis; oxygen from the atmosphere is transformed by a di-oxygenase enzyme into hydroxyl radicals (and sometimes, superoxide) that attack the contaminant^{46, 47}. These metabolites are similar to byproducts found by CHP oxidation. As seen in Table 2, hydroxypyrene is found in both systems (structures FI and BI). Pyrenone (FIB), which is found in CHP treatment, is one oxidative step away from this structure. Phenanthrene carboxylic acid (BIV), also found after ozonation (OIV), has a similar structure to byproducts FIIIB, FIV and FVII found in CHPs. Byproduct FIIB and FIV are one oxidative step away from becoming phenanthrene carboxylic acid, while FVII is a

tautomerization of this product. This implies that both biodegradation and CHP treatment follow similar schemes for the oxidation of PAHs.

An important aspect of bioremediation that should be taken into consideration is that enzymatic processes are selective, while hydroxyl radicals generated from CHP treatments are not. Metabolites from biodegradation and byproducts from CHPs should differ because of this, since hydroxyl radicals in a CHP reaction would not selectively form one structure over another. The selective nature of enzymatic processes allows them to become more efficient oxidizing systems than those that are non-selective. Hydroxyl radicals generated during CHP reactions will react with any species present in solution, instead of just reacting with previously oxidized species.

Liang^{39, 48} found 4,5 pyrene quinone (BVI) from the biodegradation of pyrene in soil microcosms containing *Mycobacterium sp.* This byproduct was also found in the CHP remediation of pyrene in water and Ottawa sand (FV). The byproduct found by Liang indicates that biodegradation in soils is similar to that of the PAHs in solution and the metabolites found by Heitkamp should also be present in the Liang experiments. This finding supports the proposed pathway, because the structure produced is a product of hydroxyl radical reaction with the most reactive bonds of the molecule as stated earlier in this paper.

The biodegradation of naphthalene and benzanthracene yielded similar byproducts as compared to those obtained from the bioremediation and CHP treatment of pyrene.

Salicylic acid, catechol and naphthol have been found from the oxidation of naphthalene⁴³, while two dihydrodiols of benzantracene were found from bezanthrazene degradation. Both of these studies confirm that biodegradation of PAHs follows the phenolic, ketonic/quinonic pathway that has been proposed.

Ozonation of Pyrene

Most of the information on byproduct formation from the remediation of PAHs comes from chemical oxidation using gaseous ozone. Studies by Luster-Teasley et al.³³ and Yao et al.^{35, 49} give an extensive look into the byproducts formed from the oxidation of PAHs with gaseous ozone. The studies found that the ozonation of pyrene resulted in the oxidation of specific bonds forming aldehyde, and carboxylic acid functional groups and later ring cleavage byproducts, in which biphenyl structures are seen and bay regions are formed, as shown in the second column of Table 3. Most of the byproducts found from ozonation are more oxidized than those from CHPs in this study. Two byproducts found in this study, the substituted biphenyls (FVIII and FIX), are similar to those formed from ozonation (OV and OXII). In general, CHP oxidations formed precursor byproducts to the substituted biphenyls found by Luster-Teasley and Yao, but more of these biphenyl structures would likely have been formed if more hydrogen peroxide had been added. As seen in Table 3, byproducts FIIB, FIV, FVII and FVIII are homologous to byproducts OIII, OIV, OVI and OVII found from ozonation.

The difference in byproducts produced in the two systems, CHP and ozonation, may be explained by the reaction pathway. Ozonation results in two types of reactions, direct

(molecular) ozone reactions and hydroxyl radical reactions. CHP reacts only through hydroxyl radical interactions and thus for similar oxidant doses, reaction byproducts found from ozone remediation will have a greater degree of oxidation than those from CHP reactions. If we would continue to add hydrogen peroxide we may achieve the same degree of oxidation in CHP systems as those found in ozone systems, byproducts FVIII and FIX may be indicators of this possibility.

PAHs partition to the non-polar region of a matrix⁵⁰; in soil this region is the soil organic matter. If the molecules are bound to the soil organic matter and do not solubilize well to the water phase, then a strict aqueous system like CHP, may not reach the contaminant to the extent required for mineralization. Ozone when used in its gaseous state may reach the contaminant more freely because it would not require water as a means of transport to the contaminant. As Luster-Teasley found, the humidity of the soil affected the rate of oxidation, the rate of pyrene disappearance decreased as the percent humidity increased obtaining differences of 6% and 12% for soil conditions of 5% and 10% humidity respectively, when compared to dry soil³³. The experiments also found that an increase in pH accompanied by an increase of humidity in the matrix resulted in a decrease of up to 40% in the extent of oxidation (found at pH 6-8). These results would indicate that ozone may not produce complete oxidation of the contaminant if the contaminant is in an aqueous phase, unless the ozone dosage is increased, and that byproducts will most likely be present after the treatment is finished.

Environmental Impact of PAH remediation

Mobility

The hydroxylation of contaminants may cause an increase in the mobility of the molecule, by increasing the polarity of the molecule and the means to form hydrogen bonds with water. By using the SPARC estimation software available from the University of Georgia, Chemdraw Ultra (CambridgeSoft) and EPISuite available from EPA, some physical chemical properties for the byproducts found were estimated and seen in Table 5-3.

In general an increase in mobility or aqueous solubility could cause a concern for in-situ chemical oxidation (ISCO) remediation. Since the agent is pumped into a groundwater system per se, then the fluids in the matrix will be forced into motion. If the contaminant becomes more soluble; then the end result is the spreading of the contaminant and the amplification of the treatment zone and potential threat. If the structure of the byproducts is known and the conditions that create these byproducts are also known, then determining the environmental fate of these byproducts during and after remediation should be accomplished.

Parameters were estimated for two different pyrenequinone structures as well as the two isomers for FIII since we could not determine the correct structure from our data. The aqueous solubility of the byproducts FIB and FIX are about one order of magnitude greater than that of pyrene. Byproducts FVII, FVIII and FXI have aqueous solubilities that are least 2 orders of magnitude greater than that of pyrene. All byproducts with

exception of compounds FIIIA and FX have a lower K_{ow} than pyrene. All byproducts also show a lower K_{om} value than pyrene with the exception of FX, dihydropyrene.

These findings suggest that most byproducts will have a tendency partition to the aqueous phase as opposed to an organic matter or solvent (perhaps a DNAPL) as pyrene would. Byproducts FVII, FVIII and FXI are very soluble, which means their mobility in the environment is likely to be greater than that of pyrene.

The SPARC estimated data (water solubility, K_{ow} , diffusion coefficient) are very dependent on the melting point used. If we assume that all byproducts have the same melting point as pyrene then the solubilities of all compounds would increase by at least one order of magnitude. The melting points used for these estimations, were all estimated from EPISuite, which relies on functional group contribution to estimate the melting points. This method may have its limitations; byproducts FIIIA, FVI, and FIX all have the same estimated melting point even though they are different in structure. Byproducts, such as FVI which has isomers, will have different melting points depending on the isomer and as such, the estimated data may not be accurate.

Toxicity

Luster-Teasley et al.⁴⁵ and Herner et al.⁵¹ found that byproducts formed from the oxidation of PAHs with gaseous ozone inhibited gap junction intercellular communication (GJIC) of rat-liver epithelial cells, leading to the conclusion that some daughter products formed during remediation were in fact more toxic than the parent

compounds. They also concluded that byproducts that contained a bay region (like biphenyl groups) were more toxic than compounds that did not have this structure present. Little is known about the toxicity of byproducts formed from Fenton's Reagent reactions. As Bowers et al.⁵² described intermediates from the remediation of wastewater contaminated with refractory chemicals may be more toxic than the parent compound if the reaction does not completely mineralize the contaminant. Satoh et al.⁵³ studied the epigenetic toxicity of hydroxylated biphenyls and hydroxylated polychlorinated biphenyls (PCB), all potential products from Fenton's Reagent and CHP reactions with biphenyls and PCBs, and found that the hydroxylated products were in most cases equal or more toxic than the parent compound. Sedlak⁵⁴ found and identified several hydroxylated PCBs after the oxidation of chlorobenzene with Fenton's Reagent. The PCBs were apparently of hydroxylated chlorobenzenes formed during reaction. The formation of these could increase the toxicity of the solutions once reactions are terminated.

We have found 11 byproducts relating to the oxidation of pyrene by CHP reactions. Some of these compounds are known to be toxic. Byproduct FI (1-hydroxypyrene) is known to be acutely toxic and genotoxic⁵⁵, it is commonly used as a biomarker for exposure to PAH contamination⁵. This first byproduct is also known to be toxic to numerous to other organisms⁵⁶. Products FIIIB, FIV, FVIII, FIX and FXI all contain a bay region with an aldehyde group, which is known to increase the toxicity of the molecule⁵¹. Byproducts that have quinonic structures like FIB, FVA, FVB and FVI may be toxic to other forms of life, including bacteria³⁹.

Conclusions:

The remediation of PAHs using CHP systems in both aqueous solutions and soil slurries produce byproducts. Eleven byproducts have been identified from the chemical oxidation of pyrene in these systems. The byproducts found are similar in structure to those found in from bioremediation and ozonation of pyrene in the same systems.

Three different catalyzers were used for the CHP reactions in the two matrices. Byproducts were found in all of the systems, therefore we may conclude that byproducts are produced whenever CHPs are used for the remediation of PAHs.

The byproducts found are consistent with hydroxyl radical interaction with aromatics. A proposed pathway that may lead to the products found has been developed.

Parameter estimation software has been used to estimate the potential fate of the byproducts found. The results show a general trend of decreasing K_{ow} for all byproducts when compared to that of pyrene. Aqueous solubility some cases increased by 3 orders of magnitude, leading to the belief that the byproducts formed may be more mobile than the parent compound.

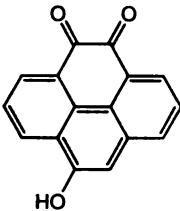
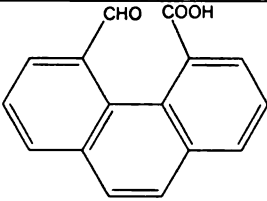
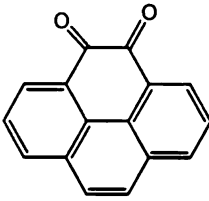
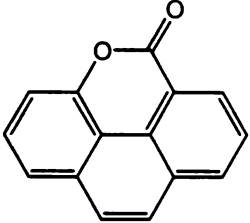
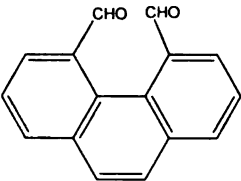
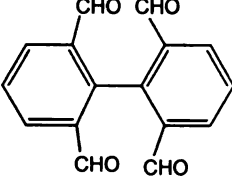
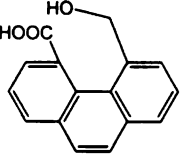
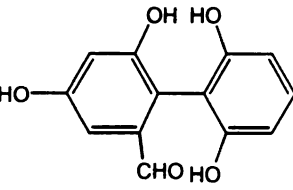
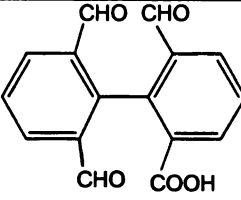
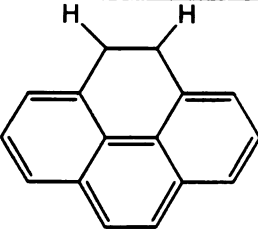
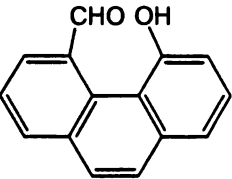
Some of the byproducts found are known to be toxic or to interrupt GJIC communication. This leads us to believe that CHP reactions yield products whose toxicity is greater than that of the parent compound.

Table S-3: Estimated parameters for each one of the byproducts found as well as the SMILES characters used to represent them in the

Table 5-4: Byproducts found from CHP, gaseous ozonation and bioremediation remediation of pyrene.

CHP	Gaseous Ozonation	Bioremediation by <i>Mycobacterium</i> sp.
<p>FI</p>	<p>OI</p>	<p>BI</p>
<p>FIB</p>	<p>OII</p>	<p>BII</p>
<p>FIII</p>	<p>I OII</p>	<p>BIII</p>
<p>FIV</p>	<p>OIV</p>	<p>BIV</p>
<p>FV</p>	<p>V</p>	<p>BV</p>

Table 5-4 Continued

CHP	Gaseous Ozonation	Bioremediation by <i>Mycobacterium</i> sp.
 <p>FVI</p>	 <p>VI</p>	 <p>BVI</p>
 <p>FVII</p>	 <p>I</p>	
 <p>FVIII</p>	 <p>OVIII</p>	
 <p>FIX</p>	 <p>X</p>	
 <p>FX</p>		
 <p>FXI</p>		

References

1. Council, I. T. R. *Technical and Regulatory Guidelines for In-Situ Chemical Oxidation of Contaminated Soil and Groundwater 2nd ed. ISCO-2*; Interstate Technology & Regulatory Council: Washington, D.C., 2005.
2. Huling, S.; Pivetz, B. E. *Engineering Issue Paper: In-Situ Chemical Oxidation*; 600R06072; Environmental Protection Agency: Ada, Oklahoma, July 28 2006, 2006; p 60.
3. Watts, R. J.; Teel, A. L., Chemistry of Modified Fenton's Reagent (Catalyzed H₂O₂ Propagations-CHP) for In Situ Soil and Groundwater Remediation. *Journal of Environmental Engineering* **2005**, 131, (4), 612-622.
4. Watts, R. J.; Teel, A. L., Treatment of Contaminated Soils and Groundwater Using ISCO. *Practice Periodical of Hazardous, Toxic, and Radioactive Waste Management* **2006**, 10, (1), 2-9.
5. Belkin, S.; Steiber, M.; Tiehm, a.; Frimmel, F. H.; Abeliovich, A.; Werner, P.; Ulitzur, S., Toxicity and Genotoxicity Enhancement during Polycyclic Aromatic Hydrocarbon Degradation. *Environmental Toxicology and Water Quality* **1994**, 9, (4), 303-309.
6. Bogan, B. W.; Trbovic, V., Effect of Sequestration on PAH degradability with Fenton's Reagent: Roles of Total Organic Carbon, Humic and Soil Porosity. *Journal of Hazardous Materials* **2003**, B100, 285-300.
7. Bogan, B. W.; Trbovic, V.; Paterek, R. J., Inclusion of Vegetable oils in Fenton's Chemistry for Remediation of PAH-Contaminated Soils. *Chemosphere* **2003**, 50, 15-21.
8. Kawahara, F. K.; Davila, B.; Al-Abed, S. R.; Vesper, S. J.; Ireland, J. C.; Rock, S., Polynuclear Aromatic Hydrocarbon (PAH) release from Soil during Treatment with Fenton's Reagent. *Chemosphere* **1995**, 31, (9), 4131-4142.
9. Watts, R. J.; Stanton, P. C.; Howsawkung, J.; Teel, A. L., Mineralization of a Sorbed Polycyclic Aromatic Hydrocarbon in Two Soils using Catalyzed Hydrogen Peroxide. *Water Research* **2002**, 36, 4283-4292.

10. Saxe, J. K.; Allen, H. E.; Nicol, G. R., Fenton Oxidation of Polycyclic Aromatic Hydrocarbons after Surfactant-Enhanced Soil Washing. *Environmental Engineering Science* **2000**, 17, 233-244.
11. Flotron, V.; Delteil, C.; Bermond, A.; Camel, V., Remediation of Matrices Contaminated by Polycyclic Aromatic Hydrocarbons: Use of Fenton's Reagent. *Polycyclic Aromatic Compounds* **2003**, 23, 353-376.
12. Martens, D. A.; T, F. j. W., Enhanced Degradation of Polycyclic Aromatic Hydrocarbons in Soil Treated with Advance Oxidative Process- Fenton's Reagent. *Journal of Soil Contamination* **1995**, 4, (2), 1-14.
13. Nam, K.; Rodriguez, W.; Kukor, J. J., Enhanced Degradation of Polycyclic Aromatic Hydrocarbons by Biodegradation Combined with a Modified Fenton Reaction. *Chemosphere* **2001**, 45, (2001), 11-20.
14. Carvel, D. D.; Cartwright, R. T. In *Measuring in situ Fenton's application success*, Proceedings of the Third International Conference on Remediation of Chlorinated and Recalcitrant Compounds, Monterrey, CA, United States of America, May 20-23 2002, 2002; Press, B., Ed. Battelle Press: Monterrey, CA, United States of America, 2002; pp 1173-1178.
15. Benitez, F. J.; Beltran-Heredia, J.; Acero, J. L.; Rubio, F. J., Chemical Decomposition of 2,4,6-Trichlorophenol by Ozone, Fenton's Reagent and UV Radiation. *Industrial Engineering and Chemistry Research* **1999**, 38, (1999), 1341-1349.
16. Huang, H.-H.; Lu, M.-C.; Chen, J.-N., Catalytic Decomposition of Hydrogen Peroxide and 2-Chlorophenol with Iron Oxides. *Water Research* **2001**, 35, (9), 2291-2299.
17. Pignatello, J. J., Dark and Photoassisted Fe³⁺ Catalyzed Degradation of Chlorophenoxy Herbicides by Hydrogen Peroxide. *Environmental Science and Technology* **1992**, 26, (5), 944-951.
18. Sedlak, D. L.; Andren, A. W., Oxidation of Chlorobenzene with Fenton's Reagent. *Environmental Science and Technology* **1991**, 25, (4), 777-782.
19. Teel, A. L.; Warberg, C. R.; Atkinson, D. A.; Watts, R. J., Comparison of Mineral and Soluble Iron Fenton's Catalysts for the Treatment of Trichloroethylene. *Water Research* **2001**, 35, (4), 977-984.

20. Chen, C. T.; Tafuri, A. N.; Rahman, M.; Foerst, M. B., Chemical Oxidation Treatment of Petroleum Contaminated Soil Using Fenton's Reagent. *Journal of Environmental Science and Health* **1998**, A33, (6), 987-1008.
21. Kong, S.-H.; Watts, R. J.; Choi, J.-H., Treatment of Petroleum-Contaminated Soils Using Iron Mineral Catalyzed Hydrogen Peroxide. *Chemosphere* **1998**, 37, (8), 1473-1482.
22. Kostecki, P. T.; Calabrese, E. J., *Petroleum Contaminated Soils: Remediation Techniques, Environmental Fate, and Risk Assessment*. 3rd ed.; Lewis Publishers, Inc.: Chelsea, MI, 1989; Vol. 1.
23. Beltran, F. J.; Gonzalez, M.; Rivas, F. J.; Alvarez, P., Fenton Reagent Advanced Oxidation of polynuclear Aromatic Hydrocarbons in Water. *Water Air and Soil Pollution* **1998**, 105, (1998), 685-700.
24. Srivastava, V. J.; Kelley, R. L.; Paterek, J. R.; Hayes, T. D.; Nelson, G. L.; Golchin, J., A Field Scale Demonstration of Novel Bioremediation Process for MGP Sites. *Applied Biochemistry and Biotechnology* **1994**, 45, (6), 741-756.
25. Beltran, F. J.; Ovejeor, G.; Rivas, J., Oxidation of Polynuclear Aromatic Hydrocarbons in Water.4. Ozone Combined with Hydrogen Peroxide. *Industrial Engineering and Chemistry Research* **1996**, 35, (3), 891-898.
26. Lindsey, M. E.; Tarr, M. A., Quantitation of Hydroxyl radicals During Fenton Oxidation following a single Addition of Iron and Peroxide. *Chemosphere* **2000**, 41, (2000), 409-417.
27. Lindsey, M. E.; Tarr, M. A., Inhibited Hydroxyl radical Degradation of Aromatic Hydrocarbons in the presence of Dissolved Fulvic Acid. *Water Research* **2000**, 34, (8), 2385-2389.
28. Lee, B.-D.; Nakai, S.; Hosomi, M., Application of Fenton Oxidation To Remediate Polycyclic Aromatic Hydrocarbons-Contaminated Soil. *Journal of Chemical Engineering of Japan* **2002**, 35, (6), 582-586.
29. Walling, C., Fenton's Reagent Revisited. *Accounts of Chemical Research* **1974**, 8, 125-131.

30. Walling, C., Intermediates in the Reactions of Fenton Type Reagents. *Accounts of Chemical Research* **1998**, 31, (4), 155-157.
31. Walling, C.; Johnson, R. A., Fenton's Reagent V. Hydroxylation and Side-Chain Cleavage of Aromatics. *Journal of the American Chemical Society* **1974**, 97, (2), 363-367.
32. Augusti, R.; Dias, A. O.; Rocha, L. L.; Lago, R. M., Kinetics and Mechanism of Benzene Derivative Degradation with Fenton's Reagent in Aqueous Medium Studied by MIMS. *Journal of Physical Chemistry* **1998**, 102, (52), 10723-10727.
33. Luster-Teasley, S. The Use of Gaseous Ozone to remediate Pyrene Contaminated Soils: A study of By-Product Production, Environmental effects on Remediation Efforts, and Scale-Up Volume I & II. Dissertation for the Degree of Ph. D., Michigan State University, East Lansing, MI, 2003.
34. Upham, B. L.; Masten, S. J.; Lockwood, B. R.; Trosko, J. E., Nongenotoxic Effects of Polycyclic Aromatic Hydrocarbons and Their Ozonation By-Products on Intercellular Communication of Rat Liver epithelial Cells. *Fundamental and Applied Toxicology* **1994**, 23, 470-475.
35. Yao, J.-J.; Huang, Z.-H.; Masten, S. J., The Ozonation of Pyrene: Pathway and Product Identification. *Water Research* **1998**, 32, (10), 3001-3012.
36. Kakarla, P. K.; Andrews, T.; Greenberg, R. S.; Zervas, D. S., Modified Fenton's Processes For Effective In-Situ Chemical Oxidation-Laboratory and Field Evaluation. *Remediation* **2002**, Autumn, 23-36.
37. Schwarzenbach, R. P.; Gschwend, P. M.; Imboden, D. M., *Environmental Organic Chemistry*. 1st ed.; Wilkey-Interscience, John Wiley & Sons Inc: New York, 1993.
38. Masten, S. J. In *Use of In-Situ Ozonation For the Removal of VOCs and PAHs from Unsaturated Soils*, Proceedings of the Symposium on Soil Venting, Houston, Texas, 1991; U.S. Environmental Protection Agency: Houston, Texas, 1991; pp 29-45.
39. Liang, Y. In *Biodegradation of Pyrene in Soil Microcosms: Identification of a Toxic Intermediate*, EWRI 2005: Impacts of Global Climate Change, Anchorage, Alaska, 2005; Environmental and Water Resources Institute: Anchorage, Alaska, 2005.

40. Chen, R.; Pignatello, J. J., Role of Quinone Intermediates as Electron Shuttles in Fenton and Photoassisted Fenton Oxidations of Aromatic Compounds. *Environmental Science and Technology* **1997**, 31, (8), 2399-2406.
41. Goel, R. K.; Flora, J. R. V.; Ferry, J., Mechanisms for Naphthalene Removal during Electrolytic Aeration. *Water Research* **2003**, 37, 891-901.
42. Zeng, K.; Hwang, H.-M.; Fu, P. P.; Yu, H., Identification of 1-Hydroxypyrene Photoproducts and Study of the Effect of Humic Substances on its Photolysis. *Polycyclic Aromatic Compounds* **2002**, 22, 459-467.
43. Heitkamp, M. A.; Freeman, J. P.; Cerniglia, C. E., Naphthalene Biodegradation in Environmental Microcosms: Estimates of Degradation Rates and Characterization of Metabolites. *Applied and Environmental Microbiology* **1987**, 53, (1), 129-136.
44. Heitkamp, M. A.; Freeman, J. P.; Miller, D. W.; Cerniglia, C. E., Pyrene Degradation by *Mycobacterium* sp.: Identification of Ring Oxidation and Ring Fission Products. *Applied and Environmental Microbiology* **1988**, 54, (10), 2556-2565.
45. Luster-Teasley, S. L.; Yao, J. J.; Herner, H. H.; Trosko, J. E.; Masten, S. J., Ozonation of Chrysene: Evaluation of By-Product Mixtures and Identification of Toxic Constituent. *Environmental Science and Technology* **2002**, 36, (5), 869-876.
46. Juhasz, A. L.; Naidu, R., Bioremediation of High Molecular Weight Polycyclic Aromatic Hydrocarbons: A Review of Microbial Degradation of Benzo[a]pyrene. *International Biodeterioration & Biodegradation* **2000**, 45, 57-88.
47. Alexander, M., *Biodegradation and Bioremediation*. second ed.; Academic Press: New York, 1999.
48. Liang, Y.; Gardner, D. R.; Miller, C. D.; Chen, D.; Anderson, A.; Weimer, B. C.; Sims, R. C., Study of Biochemical Pathways and Enzymes Involved in Pyrene Degradation by *Mycobacterium* sp. Strain KMS. *Applied and Environmental Microbiology* **2006**, 72, (12), 7821-7828.
49. Yao, J.-J.; Huang, Z.-H.; Masten, S. J., Ozonation of Benz[a]anthracene: Pathway and Product Identification. *Water Research* **1998**, 32, (11), 3235-3244.

50. Chiou, C. T.; McGroddy, S. E.; Kile, D. E., Partition Characteristics of Polycyclic Aromatic Hydrocarbons on Soils and Sediments. *Environmental Science and Technology* **1998**, 32, (2), 264-269.
51. Herner, H. A.; Trosko, J. E.; Masten, S. J., The Epigenetic Toxicity of Pyrene and Related Ozonation Byproducts Containing an Aldehyde Functional Group. *Environmental Science and Technology* **2001**, 35, (17), 3576-3583.
52. Bowers, A. R.; Gaddipati, P.; Eckenfelder Jr., W. W.; Monsen, R. M., Treatment of Toxic or Refractory Wastewaters with Hydrogen Peroxide. *Water Science and Technology* **1989**, 21, 477-486.
53. Satoh, A. Y.; Trosko, J. E.; Masten, S. J., Epigenetic Toxicity of Hydroxylated Biphenyls and Hydroxylated Polychlorinated Biphenyls on Normal Rat Liver Epithelial Cells. *Environmental Science and Technology* **2003**, 37, (12), 2727-2733.
54. Sedlak, D. L. The Abiotic Reactions of Polychlorinated Biphenyls (PCBs). Doctoral Dissertation, University of Wisconsin, Madison, 1992.
55. Hauser, B.; Schrader, G.; Bahadir, M., Dependence of Genotoxicity of Benzo[a]pyrene Suspensions in MutaTox Test on Dissolved Concentration and S9 Addition. *Ecotoxicology and Environmental Safety* **1997**, 38, (3), 224-226.
56. Lambert, M.; Kremer, S.; Anke, H., Antimicrobial, Phytotoxic, Nematicidal, Cytotoxic, and Mutagenic Activities of 1-Hydroxypyrene, the Initial Metabolite in Pyrene Metabolism by the Basidiomycete *Crinipellis stipitaria*. *Bulletin of Environmental Contamination and Toxicology* **1995**, 55, (2), 251-257.

Chapter 6. Modeling

Introduction

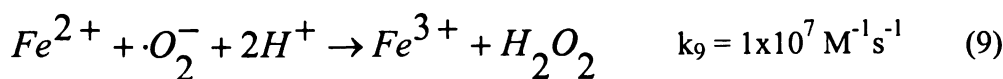
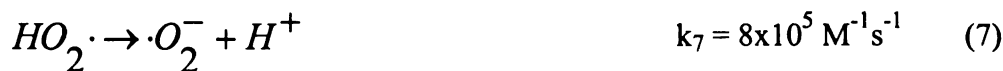
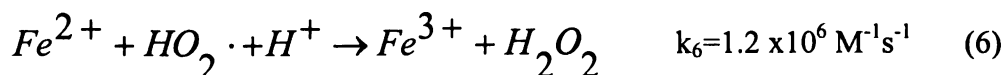
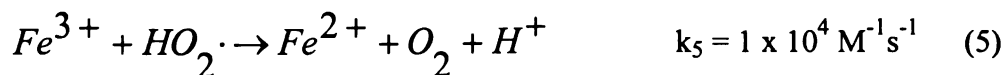
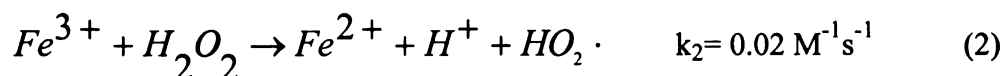
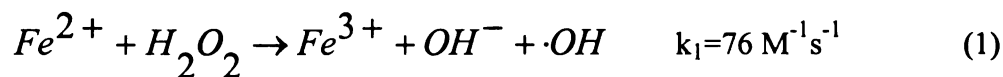
The modeling of CHP systems is a difficult task because of the complexity of the chemical reactions that take place in the environment during remediation and the fact that advection and dispersion become important for incompletely mixed systems. Usually Fenton systems are modeled using kinetic reactions^{1-4, 5-9} and completely mixed conditions are assumed. Unfortunately when remediation of soil and groundwater is performed, completely mixed systems are rarely if ever achieved. Kinetic modeling is required to determine the optimal catalyzer and oxidant ratios for field applications.

This chapter will deal with building three models for the CHP systems tested. The first will be a completely mixed kinetic model, the second a diffusive-reaction model and finally an advection-dispersion model will be created for remediation of aromatics in porous media.

Kinetic Model

A kinetic model that describes the concentrations of multiple species during the reaction for each of the catalyzed hydrogen peroxide propagations used has been developed. This model was developed in order to verify the rate of hydrogen peroxide decomposition to oxygen in Fenton reactions and thus determine how much hydroxyl radicals are being produced from these reactions.

The key to modeling the behavior of Fenton's Reagent reactions is to be able to accurately predict the rate of OH radical production. This prediction can be approximated by modeling the concentrations of hydrogen peroxide and catalyzer with time in the system, as well as knowing the possible hydroxyl radical sinks present. Using known catalyzed hydrogen peroxide reaction and rate constants from the papers by Walling ¹⁰; Pignatello ^{11, 12} and Rivas ⁴; the concentrations of hydrogen peroxide, ferrous and ferric ions may be determined using the following equations for classic Fenton's system:



From these reactions we can write an equation for the concentration of hydrogen peroxide, ferrous ion, ferric ion, hydroxyl radical, superoxide radical, and perhydroxyl radical. If we add the hydrogen peroxide decomposition reaction we can also calculate oxygen production from the system.



Hydrogen Peroxide:

$$\begin{aligned} \frac{dC_{H_2O_2}}{dt} = & -(k_1 C_{Fe^{2+}} + k_2 C_{Fe^{3+}} + k_d) C_{H_2O_2} \\ & + (k_6 C_{HO_2\cdot} + k_9 C_{O_2^{\cdot-}}) C_{Fe^{2+}} \end{aligned} \quad (11)$$

Ferrous ion:

$$\begin{aligned} \frac{dC_{Fe^{2+}}}{dt} = & -(k_1 C_{H_2O_2} + k_6 C_{HO_2\cdot} + k_9 C_{O_2^{\cdot-}}) C_{Fe^{2+}} \\ & + (k_2 C_{H_2O_2} + k_5 C_{HO_2\cdot} + k_8 C_{O_2^{\cdot-}}) C_{Fe^{3+}} \end{aligned} \quad (12)$$

Ferric Ion:

$$\begin{aligned} \frac{dC_{Fe^{3+}}}{dt} = & (k_1 C_{H_2O_2} + k_6 C_{HO_2\cdot} + k_9 C_{O_2^{\cdot-}}) C_{Fe^{2+}} \\ & - (k_2 C_{H_2O_2} + k_5 C_{HO_2\cdot} + k_8 C_{O_2^{\cdot-}}) C_{Fe^{2+}} \end{aligned} \quad (13)$$

Hydroxyl Radical

$$\frac{dC_{OH\cdot}}{dt} = k_1 C_{Fe^{2+}} C_{H_2O_2} - (k_4 C_{Fe^{3+}} + k_3 C_{H_2O_2}) C_{OH\cdot} \quad (14)$$

Perhydroxyl Radical

$$\frac{dC_{HO_2\cdot}}{dt} = k_2 C_{Fe^{3+}} C_{H_2O_2} - (k_5 C_{Fe^{3+}} + k_6 C_{Fe^{2+}} + k_7) C_{HO_2\cdot} \quad (15)$$

Superoxide

$$\frac{dCO_2^-}{dt} = k_7 C_{HO_2} - (k_8 C_{Fe^{3+}} + k_9 C_{Fe^{2+}}) CO_2^- \quad (16)$$

Oxygen

$$\frac{dCO_2}{dt} = 2k_d C_{H_2O_2} + k_5 C_{Fe^{3+}} C_{HO_2} + k_5 C_{Fe^{3+}} CO_2^- \quad (17)$$

Similar equations may be written for the byproducts found during these reactions. The addition of sinks such as bicarbonate (HCO_3^-) and carbonate (CO_3^{2-}) ions may be added to the model to create a more accurate model.

Temperature

The temperature of the reaction solution is not constant in CHP reactions because hydrogen peroxide decomposition to oxygen is an exothermic reaction, releasing 98 kJ/mole of heat. Since the reaction constants are temperature dependent, the rate constants in our model need to be corrected throughout the experiment. Temperature of the reactions can be calculated using the empirical equations obtained from regression analysis in Chapter 2.

$$\frac{T}{T_o} = a \cdot e^{b \cdot t} + c \cdot e^{d \cdot t} \quad (18)$$

Table 6-1: For the regression analysis on the normalized temperature for soluble iron catalyzed reactions described in chapter 2. Molar concentrations of iron and hydrogen peroxide are given along with the coefficients for the regression line and the R^2 .

	H ₂ O ₂	Fe	a	CI	b	CI	c	CI	d	CI	R ²
Ferric											
Trial1	0.11	0.06	1.102	0.004	-0.0012	0.0002	-0.105	0.006	-0.406	0.053	0.98
Trial2	0.62	0.06	1.612	0.032	-0.0094	0.0011	-0.639	0.047	-0.539	0.086	0.97
Trial3	0.11	0.34	1.096	0.004	-0.0013	0.0002	-0.096	0.006	-0.694	0.099	0.98
Trial4	0.62	0.34	1.505	0.013	-0.0090	0.0005	-0.506	0.029	-1.739	0.315	0.99
Trial6	0.73	0.20	1.696	0.017	-0.0122	0.0008	-0.659	0.038	-3.525	1.935	0.99
Trial8	0.37	0.41	1.282	0.005	-0.0053	0.0002	-0.283	0.012	-1.622	0.200	0.99
Trial9-13	0.37	0.20	1.331	0.005	-0.0054	0.0001	-0.332	0.010	-1.833	0.119	1.00
Ferrous											
Trial1	0.11	0.06	1.122	3.0E-04	-0.0031	0.0002	-0.122	0.007	-7.343	4.100	0.99
Trial2	0.59	0.06	1.557	0.013	-0.0011	0.0006	-0.558	0.023	-1.734	0.165	0.99

The value of K is then corrected by the equation:

$$K_T = K_{20} \theta^{T-20} \quad (19)$$

Where

K_T is the kinetic constant for temperature, T

K_{20} is the kinetic constant at 20 °C

θ is a constant that is estimated from the activation energy of the reaction and was found to be 1.058

T is the new temperature for the reaction in °C

Modeling Iron Species and Concentration

The speciation of iron in solution is very difficult to ascertain especially during Fenton Reagent reactions, where both ferric and ferrous ions catalyze the reactions and are the basis of the cycling process. Morel¹³ describes the speciation of iron as a basis of the hydrogen ion concentration.

$$[Fe^{3+}] = 10^{3.2} [H^+]^3 \quad (20)$$

$$[FeOH^{2+}] = 10^1 [H^+]^2 \quad (21)$$

$$[Fe(OH)_2^+] = 10^{-2.5} [H^+] \quad (22)$$

$$[Fe(OH)_4^-] = 10^{-18.4} [H^+]^{-1} \quad (23)$$

$$[Fe_2(OH)_2^{4+}] = 10^{3.5} [H^+]^4 \quad (24)$$

$$[Fe_3(OH)_4^{5+}] = 10^{3.3} [H^+]^5 \quad (25)$$

Oxidation of Ferrous ion by Oxygen

Ferrous ion oxidizes to ferric ions in the presence of oxygen. Since CHP reactions produce oxygen, this reaction may become important for modeling purposes. The equation for this oxidation is:

$$k_{obs} = \frac{k_{f0}[Fe^{2+}] + k_{f1}[FeOH^+] + k_{f0}[Fe^{2+}]}{[Fe^{2+}]} \quad (26)$$

Or

$$k_{obs} = \left(k_{f0} + k_{f1} \frac{K_1 K_w}{[H^+]} + k_{f2} \frac{\beta_2 K_w^2}{[H^+]^2} \right) \left(1 + \frac{K_1 K_w}{[H^+]} + \frac{\beta_2 K_w^2}{[H^+]^2} \right)^{-1} \quad (27)$$

K_1 and β_2 are the formation constants of the mono and dihydroxy species of ferrous ion in water and k_f is the rate constant for the reaction of oxygen with the different iron species in solution. The values for k_f , k_{f0} , k_{f1} and k_{f2} are found in Table 2

The equation can also be written as:

$$\begin{aligned} \frac{dC_{Fe^{2+}}}{dt} = & -k_f' [Fe^{2+}] [O_2] = k_{f0}' [Fe^{2+}] [O_2] \\ & + k_{f1}' [FeOH^+] [O_2] + k_{f2}' [Fe(OH)_2] [O_2] \end{aligned} \quad (28)$$

Table 6-2: Rate Constants for Reaction of Fe^{2+} Species with O_2 from Morel 1993¹³.

Fe^{2+} Species	Pseudo First Order Rate Constant (s^{-1})**	Second-Order Rate Constant ($\text{M}^{-1} \text{s}^{-1}$)***
Fe^{2+}	1.0×10^{-8}	7.9×10^{-6}
FeOH^+	3.2×10^{-2}	25
$\text{Fe}(\text{OH})_2$	1.0×10^4	7.9×10^6
$\equiv \text{Fe}^{2+} *$	6.3×10^{-3}	5.0

* $\equiv \text{Fe}^{2+}$ denotes iron on Goethite surface

** For a constant $P_{\text{O}_2} = 1 \text{ atm}$

*** Derived from first order rate constants using a Henry's constant of $10^{2.9} \text{ M atm}^{-1}$

RMSE

To determine k_d for soluble iron reactions, the kinetic reactions described by equations 11-17 were solved using a stiff ordinary differential equation solver in Matlab (ODE23s), that solves a fourth order Runge-Kutta method, while optimizing the objective function:

$$RMSE = \sqrt{\sum (C_{sim} - C_{obs})^2} \quad (63)$$

where

C_{sim} is the concentration of hydrogen peroxide calculated by the model

C_{obs} is the concentration of hydrogen peroxide obtained from iodometric titrations shown in Chapter 3.

For

sta

M

R

Th

in

op

F

sp

at

o

th

For optimization, the PsearchTool in Matlab running a genetic algorithm was used, with starting point $0.001 \times 10^{-3} \text{ M s}^{-1}$ and minimum and maximum boundaries of 1×10^{-8} to 10 M s^{-1} .

Results

The results from the optimization of the kinetic model are in are shown in Figure 6-1 and in Figure 6-2. The model parameters obtained are then shown in Table 4. The optimization tool was run for both systems, with and without temperature correction. Figures 6-3 and 6-4 show the change in concentration and the production of the other species involved in the reaction: ferrous and ferric ion, OH radical, perhydroxyl radical, and superoxide. These were found not be substantially different between the different oxidant/catalyzer reactions tested. A comparison of the oxygen production predicted by the kinetic model and the data collected in the lab is shown in Figure 6-5.

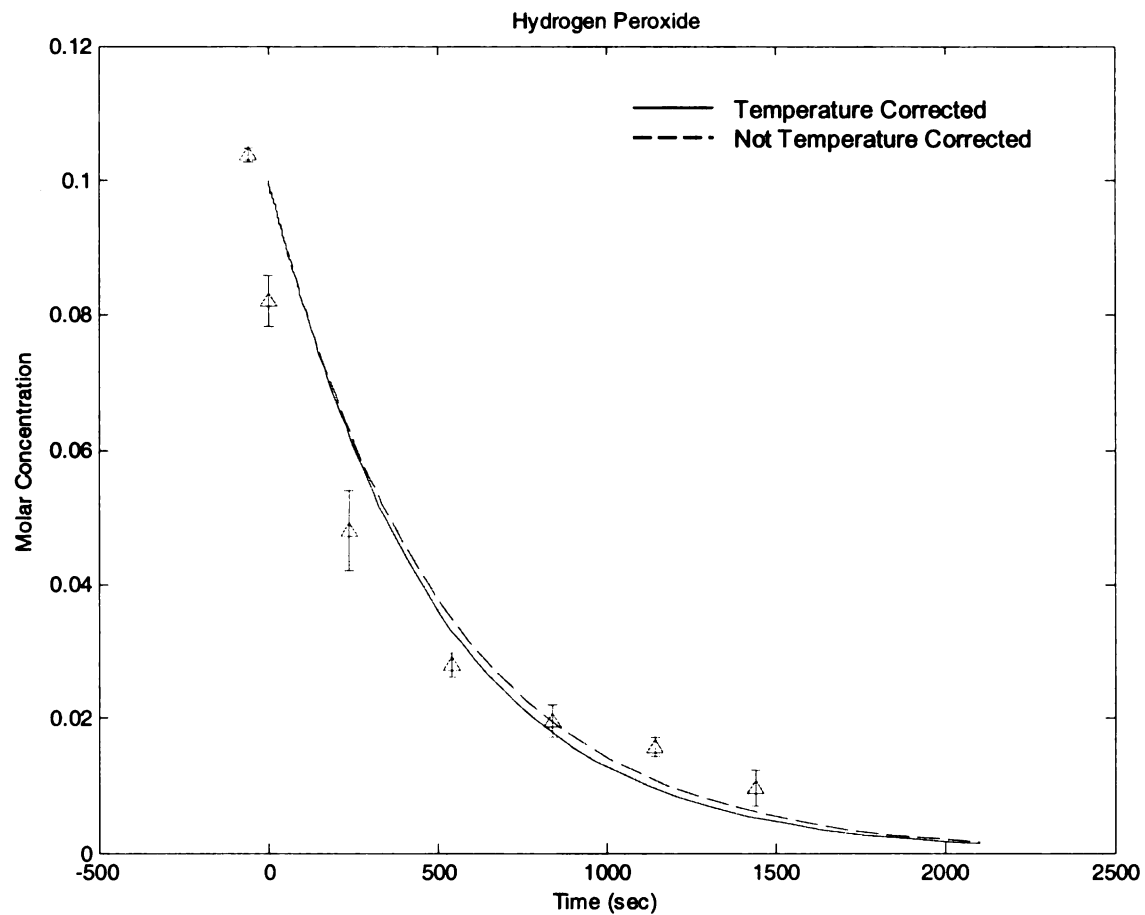


Figure 6-1: Plot showing the result from the optimization of the kinetic model described by equations 11-17 for an initial hydrogen peroxide concentration of 0.1 M and ferric ion concentration of 0.06 M. The lines represent the simulated concentrations obtained by the model and the Δ represent the hydrogen peroxide concentration obtained from iodometric titration.

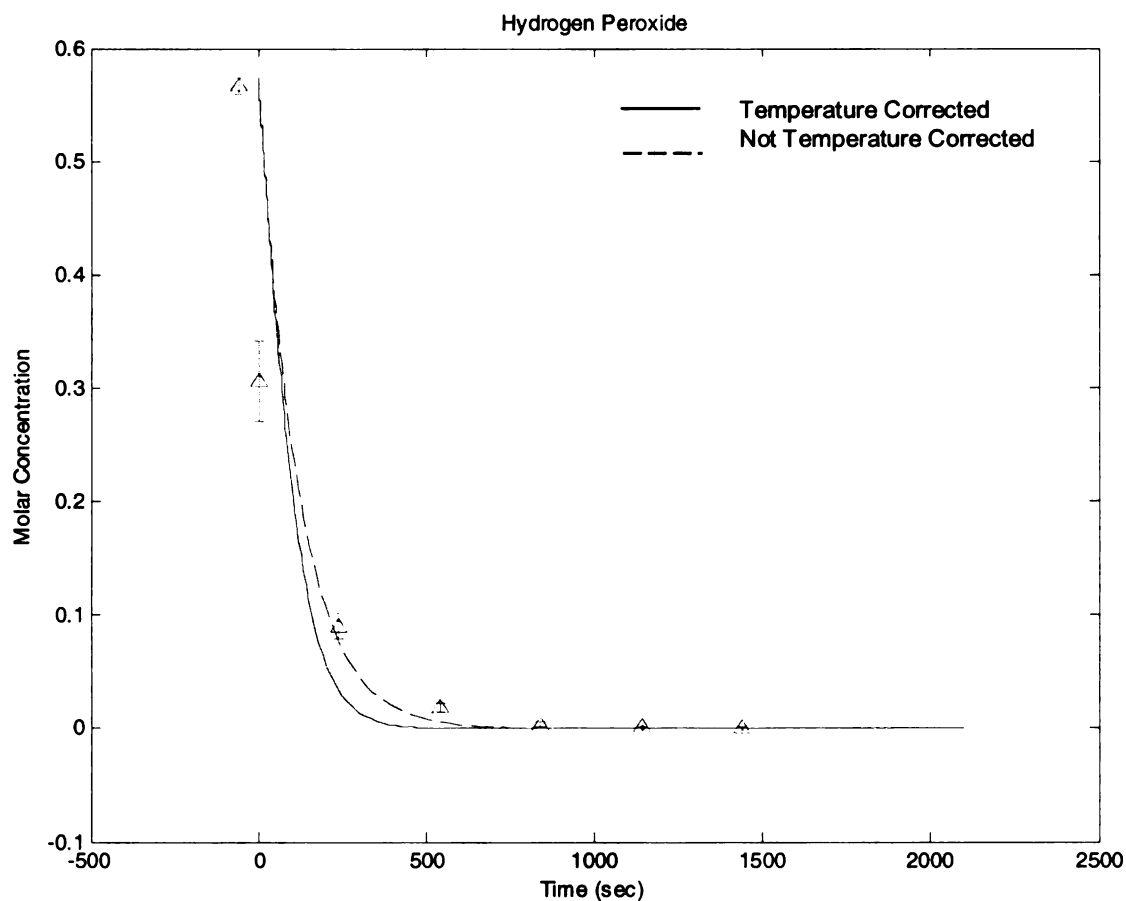


Figure 6-2: Plot showing the result from the optimization of the kinetic model described by equations 11-17 for an initial hydrogen peroxide concentration of 0.57 M and ferric ion concentration of 0.07 M. The lines represent the simulated concentrations obtained by the model and the Δ represent the hydrogen peroxide concentration obtained from iodometric titration.

Table 6-3: Values for the hydrogen peroxide decomposition rate constant determined from the optimization of the objective function in equation 63 for reactions corrected and not corrected for temperature.

H2O2	Fe	kd			
		Temperature correctd	RMSE	Not Temperutue corrected	RMSE
0.10	0.07	0.00194	0.014323126	0.00203	0.0136
0.57	0.07	0.00841	0.081772679	0.9854	0.3199

Figure
GMP re
accent
correcti

Figure 6-3: Graph showing the change in concentration of ferrous and ferric ions during CHP reactions with initial hydrogen peroxide concentration of 0.1 M and ferric ion initial concentration of 0.07 M for reactions modeled with equations 11-17 with temperature correction. The graph illustrates the cycling of ferric ion to ferrous ion and back.

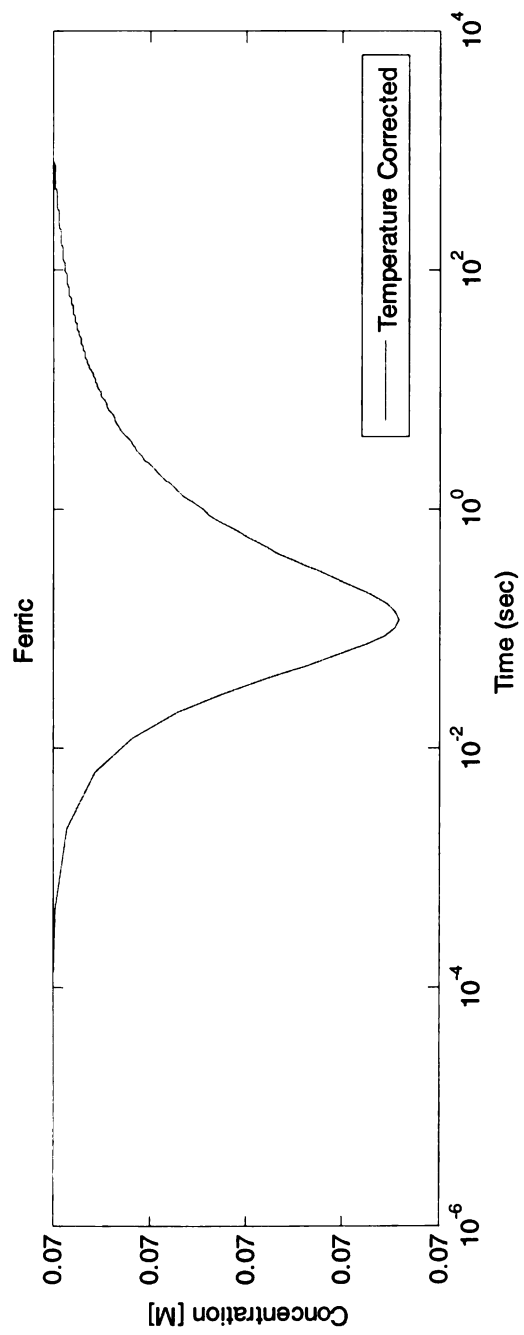
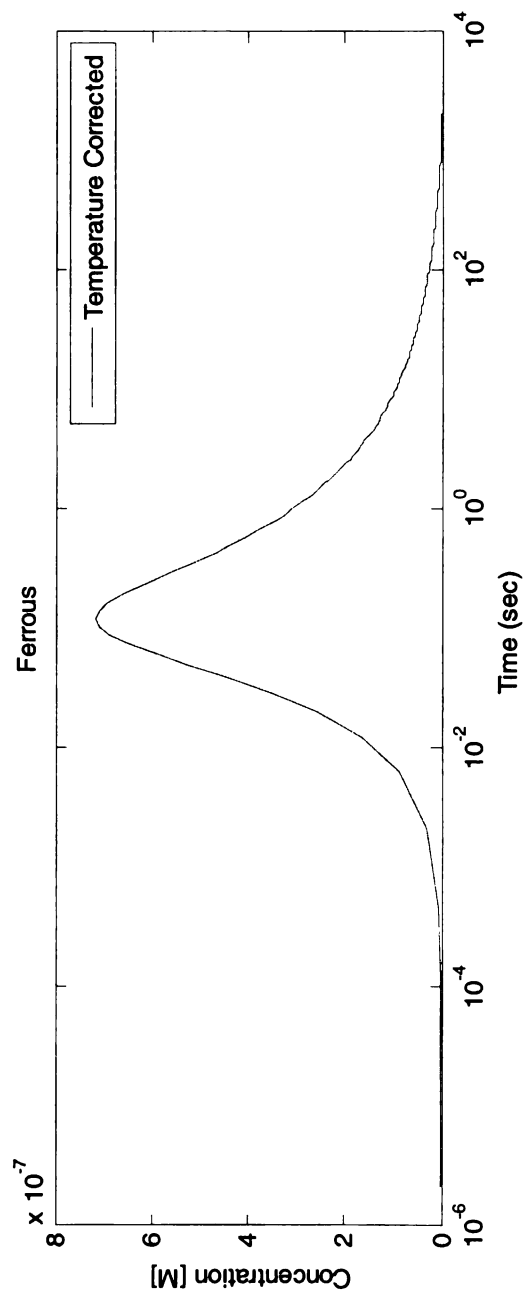


Figure 6-4: Graphs showing the simulated concentrations of hydroxyl radical, perhydroxyl radical, and superoxide formed during CHP reactions for initial hydrogen peroxide concentration of 0.1 M and initial ferric ion concentration of 0.07 M. The model is described by equations 11-17 with temperature correction.

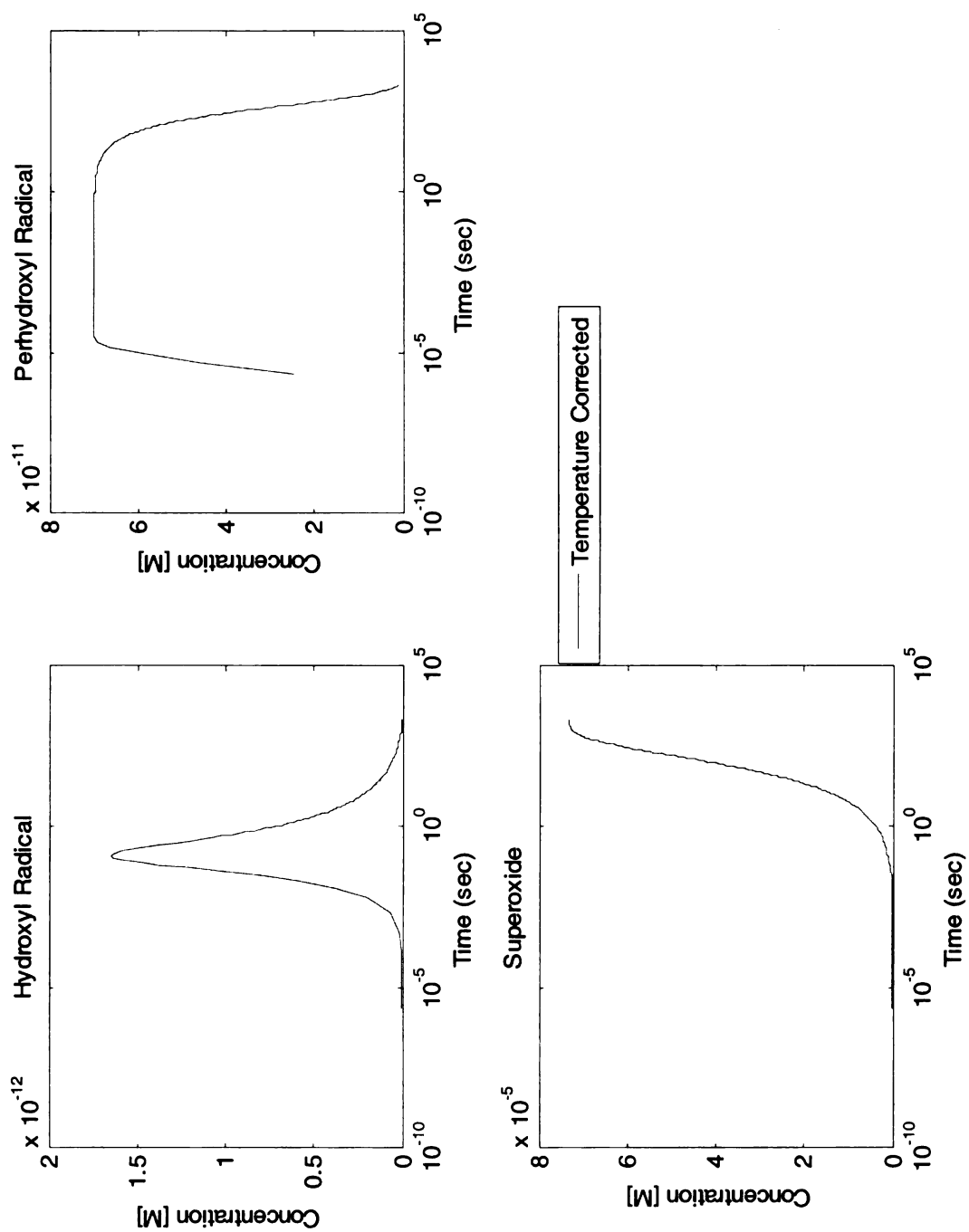
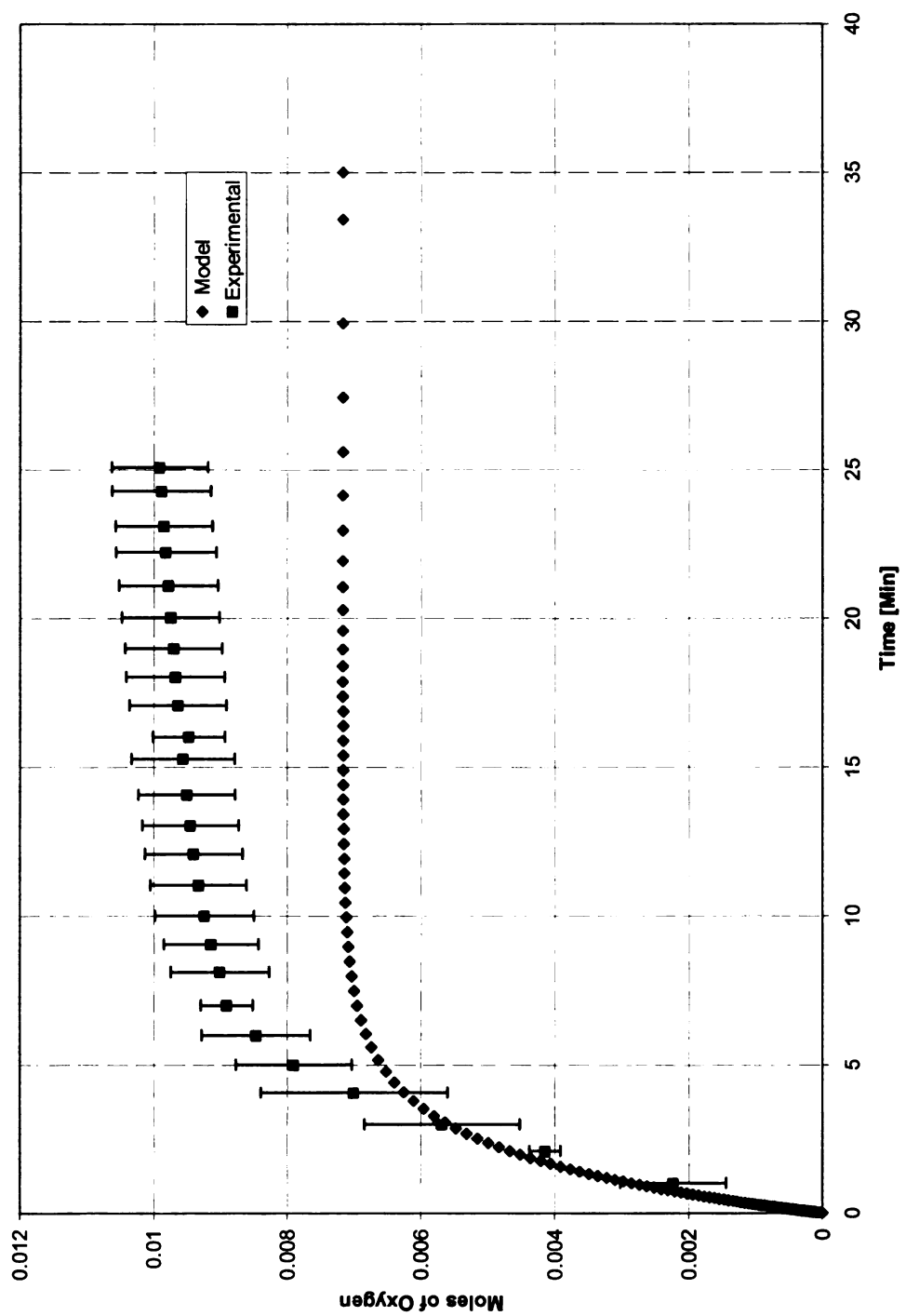


Figure 6-5: Comparison of the oxygen production calculated by the kinetic model and experimental data collected for hydrogen peroxide concentration of 0.57 M and ferric ion concentration of 0.07 M



Discussion

The optimization of the kinetic model yielded rate constants for the decomposition of hydrogen peroxide in ferric ion catalyzed reactions that appear to be dependent on the hydrogen peroxide concentration. For solutions with initial hydrogen peroxide concentration of 0.1 M, the rate constant was found to be 0.0194 M s^{-1} ; while for an initial hydrogen peroxide concentration of 0.57 M the RMSE was found to be one order of magnitude higher, from 0.3199 to 0.0817. This can be explained by the fact that samples with 0.1M initial hydrogen peroxide concentration did not have a significant increase in the temperature of the solution (from 19 to 22 °C, Chapter 2) but samples with 0.6 M did result in a significant increase in temperature, i.e., from 19 to 30 °C.

The value of the rate constant may vary because of the errors that accompany the measurement of hydrogen peroxide in these reactions and the effects that a drastic change in temperature would have on the reactions. Since titration requires time to terminate, the CHP may still be reacting during the titration, adding error to the measurement. Also, a change in temperature of the solution results in a change in sample concentration, due to the change in volume of a liquid and the kinetic energy of the ions, and may lead to additional errors. Still we believe the data collected and the optimization of the model is a good way of fine tuning our system.

Figure 6-5 shows a comparison of the oxygen production predicted by the model and the data collected in the laboratory from gravimetric tests (Chapter 2). The models is under predicting the amount of oxygen produced, according to the data collected. There may be

several explanations for this: the data after 5 minutes of reaction time may be the result of a supersaturated solution releasing oxygen in order to equilibrate with the environment. Another explanation is that the model requires the incorporation of the oxygen mass transfer coefficient and therefore, the model should be calibrated to the oxygen production.

From Figure 6-3 we can see that the ferrous ion concentration in solution during the reactions is insignificant, when compared to the ferric ion concentration (5 orders of magnitude less), so we can conclude that most Fenton Reagent reactions are ferric catalyzed and not ferrous catalyzed. This condition may show that ferrous ion concentration is the limiting factor in hydroxyl radical production and the recycling of ferric ion to ferrous ion is the rate limiting step of the process. This issue becomes even more important when high hydrogen peroxide concentrations are used because if we include the oxidation of ferrous ion by molecular oxygen, as shown in equations 26 through 28, the ferrous ion concentration will decrease even more. More robust analysis is being performed on the data presented in this chapter to determine if this is indeed correct, the results will be published in a future paper along with the data already shown

Conclusions

A kinetic model was constructed for the CHP reactions tested, in which temperature was used to correct the rate constants for the reaction. Values for the hydrogen peroxide decomposition rate constant were determined using the data from iodometric titration of hydrogen peroxide in Chapter 3. Although the values varied for different hydrogen peroxide concentrations, the order of magnitude remained constant at 10^{-3} min^{-1} for all samples.

These models help create a more comprehensive representation of catalyzed hydrogen peroxide behavior under different environmental conditions, and should allow us to estimate concentrations of the major components of this system during remediation. The present model can be expanded to encompass the concentration of the target contaminant and to incorporate the role of oxygen in the oxidation of the ferrous ion.

References

1. Gallard, H.; De Laat, J., Kinetic Modeling of Fe(III)/H₂O₂ Oxidation Reactions in Dilute Aqueous Solution Using Atrazine as Model Organic Compound. *Water Research* **2000**, 34, (12), 3107-3116.
2. Beltran, F. J.; Gonzalez, M.; Rivas, F. J.; Alvarez, P., Fenton Reagent Advanced Oxidation of polynuclear Aromatic Hydrocarbons in Water. *Water Air and Soil Pollution* **1998**, 105, (1998), 685-700.
3. Beltran, F. J.; Ovejero, G.; Rivas, J., Oxidation of Polynuclear Aromatic Hydrocarbons in Water.4. Ozone Combined with Hydrogen Peroxide. *Industrial Engineering and Chemistry Research* **1996**, 35, (3), 891-898.
4. Rivas, F. J.; Beltran, F. J.; Frades, J.; Buxeda, P., Oxidation of p-Hydroxybenzoic Acid by Fenton's Reagent. *Water Resources* **2001**, 35, (2), 387-396.
5. Augusti, R.; Dias, A. O.; Rocha, L. L.; Lago, R. M., Kinetics and Mechanism of Benzene Derivative Degradation with Fenton's Reagent in Aqueous Medium Studied by MIMS. *Journal of Physical Chemistry* **1998**, 102, (52), 10723-10727.
6. Duesterberg, C. K.; Cooper, W. J.; Waite, T. D., Fenton-Mediated Oxidation in the Presence and Absence of Oxygen. *Environ. Sci. Technol.* **2005**, 39, (13), 5052-5058.
7. Duesterberg, C. K.; Waite, T. D., Process Optimization of Fenton Oxidation Using Kinetic Modeling. *Environ. Sci. Technol.* **2006**, 40, (13), 4189-4195.
8. Duesterberg, C. K.; Waite, T. D., Kinetic Modeling of the Oxidation of p-Hydroxybenzoic Acid by Fenton's Reagent: Implications of the Role of Quinones in the Redox Cycling of Iron. *Environ. Sci. Technol.* **2007**, 41, (11), 4103-4110.
9. Godala, M.; Nowicki, L., Determining the Kinetics of a Chemical Reaction from Calorimetric Measurements and the Amount of Gaseous Products. *Inzynieria Chemiczna I Procesowa (Chemical Engineering and Process)* **2005**, 26, (2), 363-376.
10. Walling, C., Fenton's Reagent Revisited. *Accounts of Chemical Research* **1974**, 8, 125-131.

11. Pignatello, J. J., Dark and Photoassisted Fe³⁺ Catalyzed Degradation of Chlorophenoxy Herbicides by Hydrogen Peroxide. *Environmental Science and Technology* **1992**, 26, (5), 944-951.
12. Pignatello, J. J.; Baehr, K., Ferric Complexes as Catalysts for "Fenton" Degradation of 2,4-D and Metolachlor in Soil. *Journal of Environmental Quality* **1994**, 23, (March-April), 365-370.
13. Morel, F. M.; Hering, J. G., *Principles and Applications of Aquatic Chemistry*. John Wiley & Sons, Inc.: New York, 1993; p 588.

Chapter 7.

Conclusions

Fenton's Reagent systems or catalyzed hydrogen peroxide propagations are a complex set of reactions of which have been extensively studied. Still there are many unanswered questions. The complexity of the system leads most users to approaching it as a black box. The studies described in this work will add some clarity to the use of this reagent, especially where high end hydrogen peroxide concentrations are used or where oxygen production may become a hindrance.

In this study we have found that the decomposition of hydrogen peroxide to oxygen is an important oxidant sink during CHP reactions, especially when high concentrations of hydrogen peroxide are used. This reaction should be incorporated into models to account for hydrogen peroxide loss. The empirical relations determined in this study can be used for predicting the decomposition rate of hydrogen peroxide or the formation rate of oxygen in an in-situ environment. There may be a limit to the maximum oxidant and catalyzer concentrations that can be used; when high concentrations of hydrogen peroxide ($\geq 8\%$ or 2.5×10^{-3} M) and soluble ferrous ion (0.5 M) meet, the reactions become diffusion limited.

The rate of oxygen production was found to be independent of the concentration and oxidative state of soluble iron catalyzer when no chelating agents are added; the relation appears to be first order with respect to hydrogen peroxide concentration. The temperature of the reaction may be estimated using the empirical equations derived in this study.

There are many variables that may have impact on the reactions. The use of a complexing agent such as EDTA would help minimize the loss of hydrogen peroxide through its decomposition to oxygen when soluble iron catalysts are used. Completely saturated Ottawa sand does not affect oxygen production in soluble iron catalyzed reactions. The increase in solution temperature leads to an increase in the rate of reactions and thus increases the rate at which oxygen decomposes. A change in pH of the solution during reaction may lead to the loss of catalyzer due to the formation of insoluble salts.

Goethite catalyzed systems appear to have two rates of oxygen production; an initial rate which occurs during the first hour of reaction and a secondary linear rate which was found to be constant. Oxygen production during the first 24 hours of reaction appears to inhibit hydroxyl radical production during that time span.

Hydroxyl radicals can be measured with SA as a radical probe for mineral iron catalyzed reactions. In goethite systems reactions at pH 7 were less efficient at removing SA than reactions carried out at pH 3. The ionization of the SA at pH 3 appears to have some effect on the hydroxyl radical reactions. Byproducts are formed during CHP reactions for both pH 3 and pH 7 experiments. Six different byproducts were identified using LC and GC/MS analysis, some of which are more oxidized forms than those found in the literature. One of the byproducts found 2,3 DHBA is a known byproduct of the reaction. In order to make a more accurate determination of the actual amount of hydroxyl radicals produced we need to determine the concentration of at least one of these products.

We found that PAHs can be removed from soil using catalyzed hydrogen peroxide reactions. Pyrene was removed from several soil matrices with the removal efficiency decreasing with increasing matrix complexity. Reactions in Ottawa sand achieved the highest level of removal, followed by reactions in soil containing organic matter. Temperature became increasingly important in the system. The temperature of the matrix may increase substantially during reaction, and may cause an acceleration of all the reactions involved, including hydrogen peroxide decomposition.

The remediation of PAHs using CHP systems in both aqueous solutions and soil slurries was found to produce byproducts. Eleven byproducts have been identified from the chemical oxidation of pyrene in these systems. The byproducts found are consistent with hydroxyl radical interaction with aromatics and are similar to those found in bioremediation and ozonation of pyrene under similar conditions. Three different catalyzers were used for the CHP reactions in the two matrices. Byproducts were found in all of the systems, therefore we may conclude that byproducts are produced whenever CHPs are used for remediation of PAHs.

Very little is known about these byproducts after they are formed, because of this we investigated the fate of these byproducts during and after remediation. Parameter estimation software was used to estimate the chemical properties of the byproducts found. As a general trend K_{ow} decreased for all byproducts when compared to pyrene, leading us to conclude that the byproducts are more mobile than the parent compound; aqueous solubility some cases increases by 3 orders of magnitude. This increase in mobility is a potential health risk as some of the byproducts found are known to be toxic or to interrupt GJIC communication.

Incorporating all this information into a useful tool lead us to create a kinetic model for the CHP reactions tested, in which temperature data collected was used to correct the rate constants for the reaction. Values for the rate constant of hydrogen peroxide decomposition in soluble iron systems were determined using the data from iodometric titration of hydrogen peroxide in Chapter 3. This model helps create a more comprehensive representation of catalyzed hydrogen peroxide behavior under different environmental conditions, and should allow us to estimate concentrations of the major components of this system during remediation. The next step is to expand the model to encompass the concentration of the target contaminant and to incorporate the role of oxygen in the oxidation of the ferrous ion.

Appendix A

Appendix A: Pyrene Oxidation Byproducts

LC/MS DATA:

Sample of LC/MS chromatogram of m/z 233 vs. TIC from Pyrene oxidation using CHPs.....	197
Sample of LC/MS chromatogram of m/z 260 vs. TIC from Pyrene oxidation using CHPs.....	198
Sample of LC/MS chromatogram of m/z 217 vs. TIC from Pyrene oxidation using CHPs.....	199
Sample of LC/MS chromatogram of m/z 265 vs. TIC from Pyrene oxidation using CHPs.....	200
Sample of LC/MS chromatogram of m/z 205 vs. TIC from Pyrene oxidation using CHPs.....	201
Sample of LC/MS chromatogram of m/z 204 vs. TIC from Pyrene oxidation using CHPs.....	202
Sample of LC/MS mass spectrum for peak at 27.91 minute retention time from soluble iron hexane extract.....	203
Sample of LC/MS mass spectrum for peak at 13.17 minute retention time from soluble iron hexane extract.....	204
Sample of LC/MS mass spectrum for peak at 1.58 minute retention time from soluble iron hexane extract.....	205
Sample of LC/MS mass spectrum for peak at 1.57 minute retention time from soluble iron acetonitrile extract.....	206
Sample of LC/MS mass spectrum for peak at 1.81 minute retention time from soluble iron acetonitrile extract.....	207
Sample of LC/MS mass spectrum for peak at 22.15 minute retention time from goethite catalyzed hexane extract.....	208
Sample of LC/MS mass spectrum for peak at 31.23 minute retention time from goethite catalyzed hexane extract.....	209

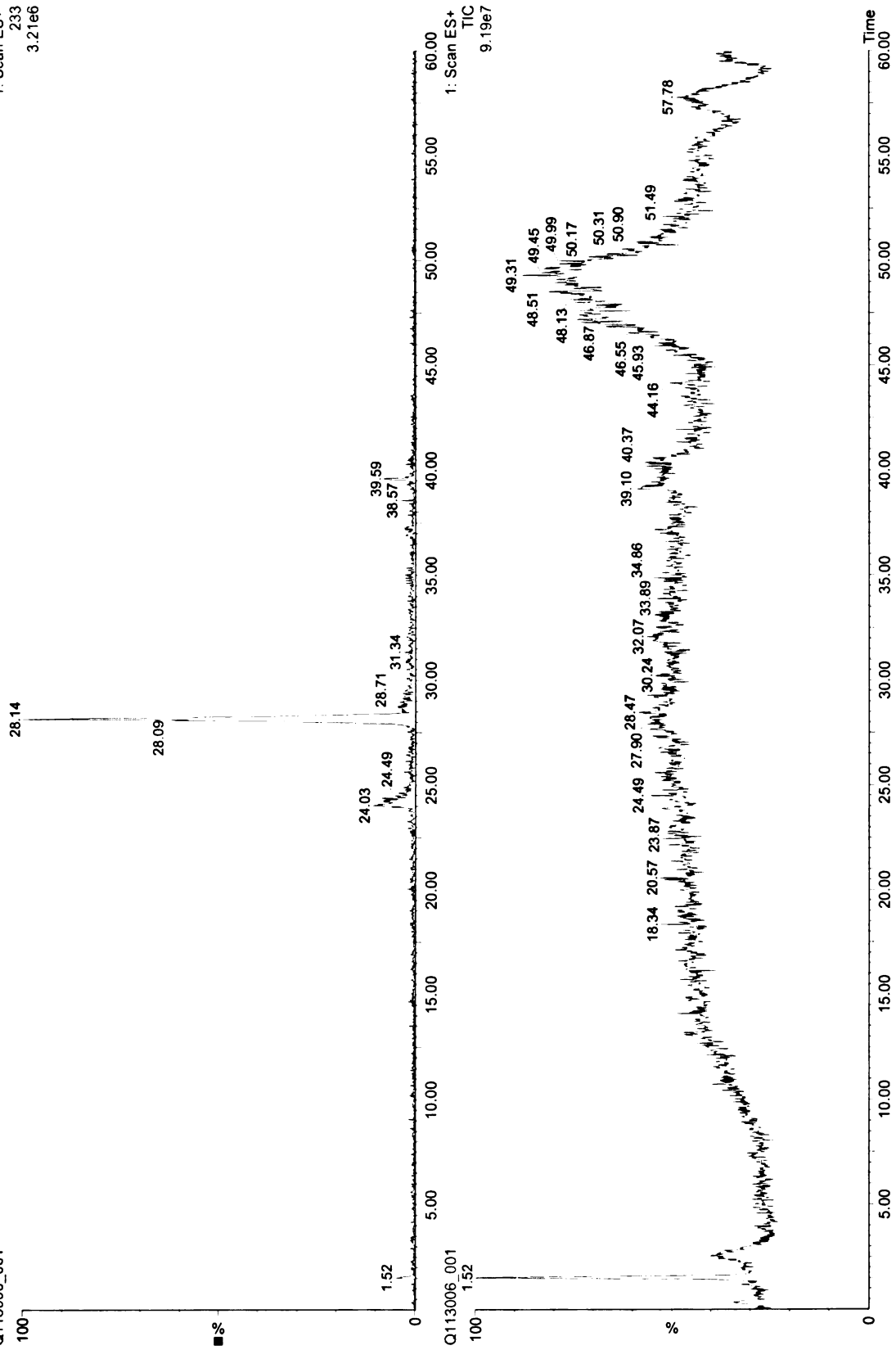
MS/MS DATA:

- Sample of MS/MS spectrum for m/z 218 from soluble iron catalyzed systems..210
- Sample of MS/MS spectrum for m/z 235 from soluble iron catalyzed systems..211
- Sample of MS/MS spectrum for m/z 267 from soluble iron catalyzed systems..212
- Sample of MS/MS spectrum for m/z 247 from soluble iron catalyzed systems..213
- Sample of MS/MS spectrum for m/z 204 from mineral iron catalyzed systems.214
- Sample of MS/MS spectrum for m/z 221 from mineral iron catalyzed systems 215
- Sample of MS/MS spectrum for m/z 260 from mineral iron catalyzed systems.216
- Sample of MS/MS spectrum for m/z 223 from mineral iron catalyzed systems.217
- Sample of MS/MS spectrum for m/z 219 from mineral iron catalyzed systems.218

Carlos/Susan #1 FC-HEX as Rcd (7680)

Q113006_001

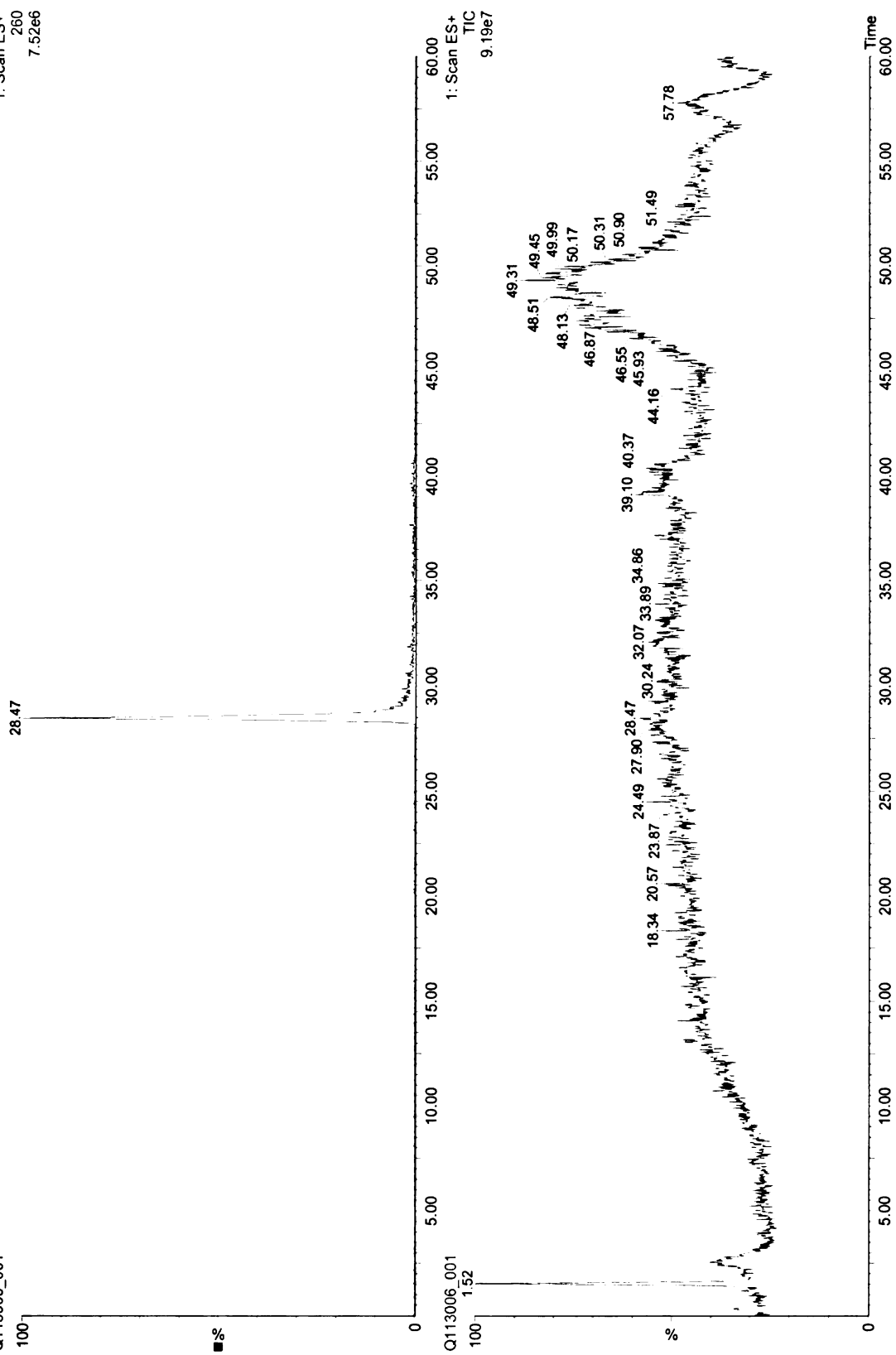
1: Scan ES+
233
3.21e6



Carlos/Susan #1 FC-HEX as Rcd (7680)

Q113006_001

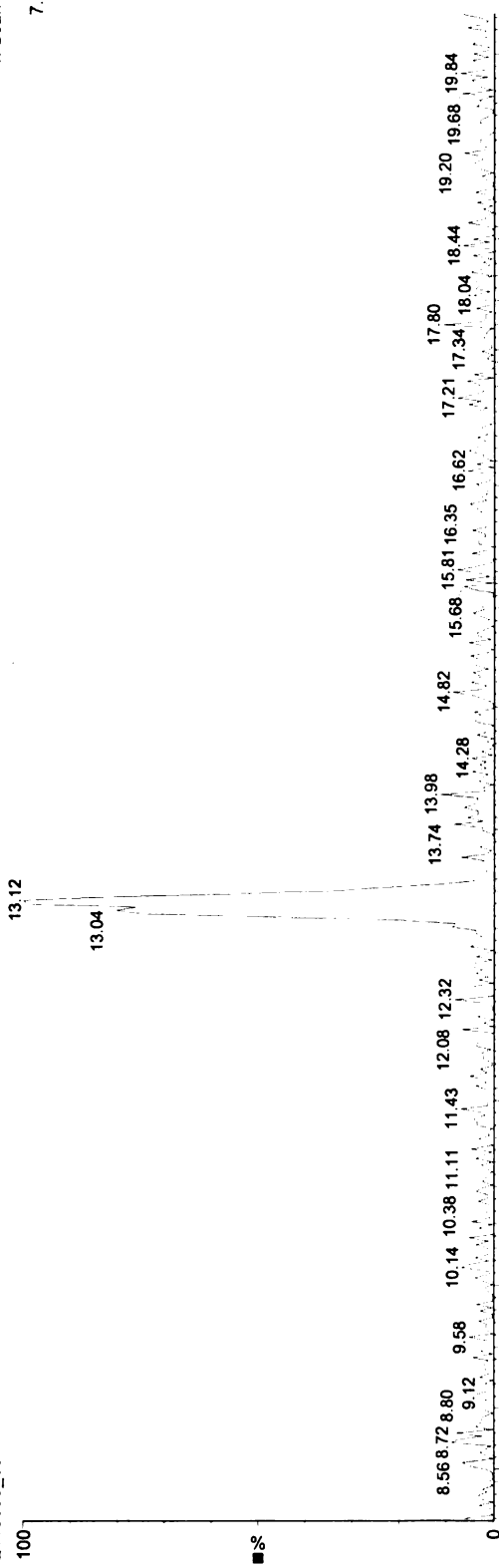
1: Scan ES+
260
7.52e6



Carlos/Susan #1 FC-HEX as Rcd (7680)

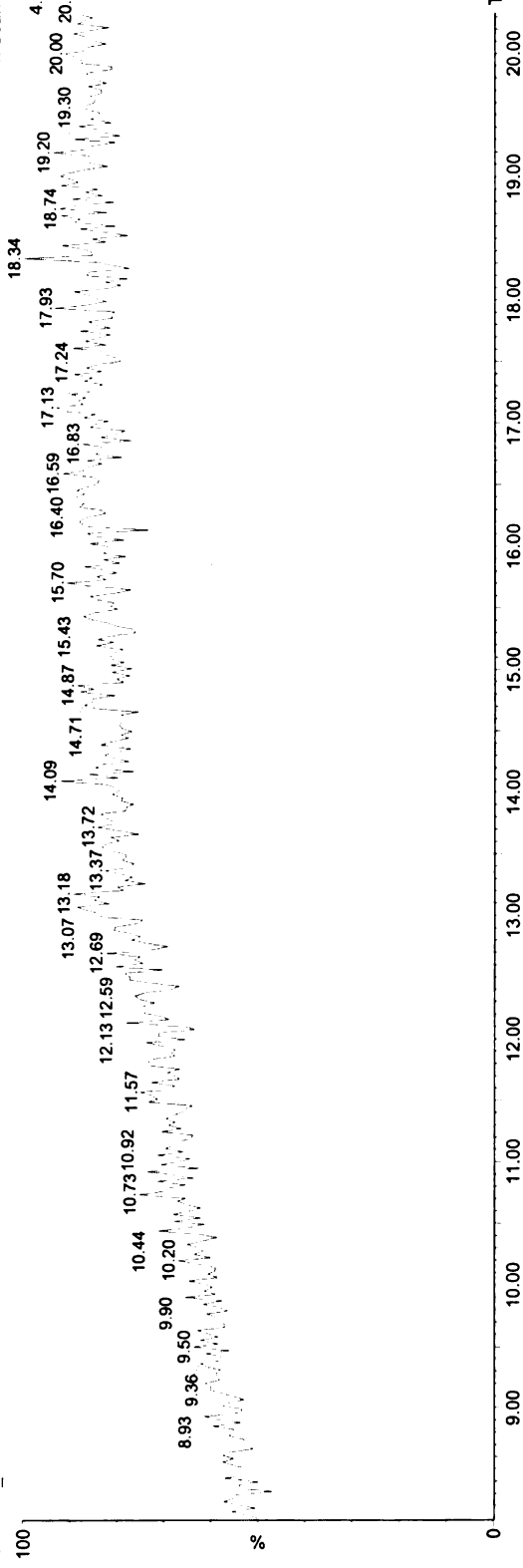
Q113006_001

1: Scan ES+
217
7.66e5



Q113006_001

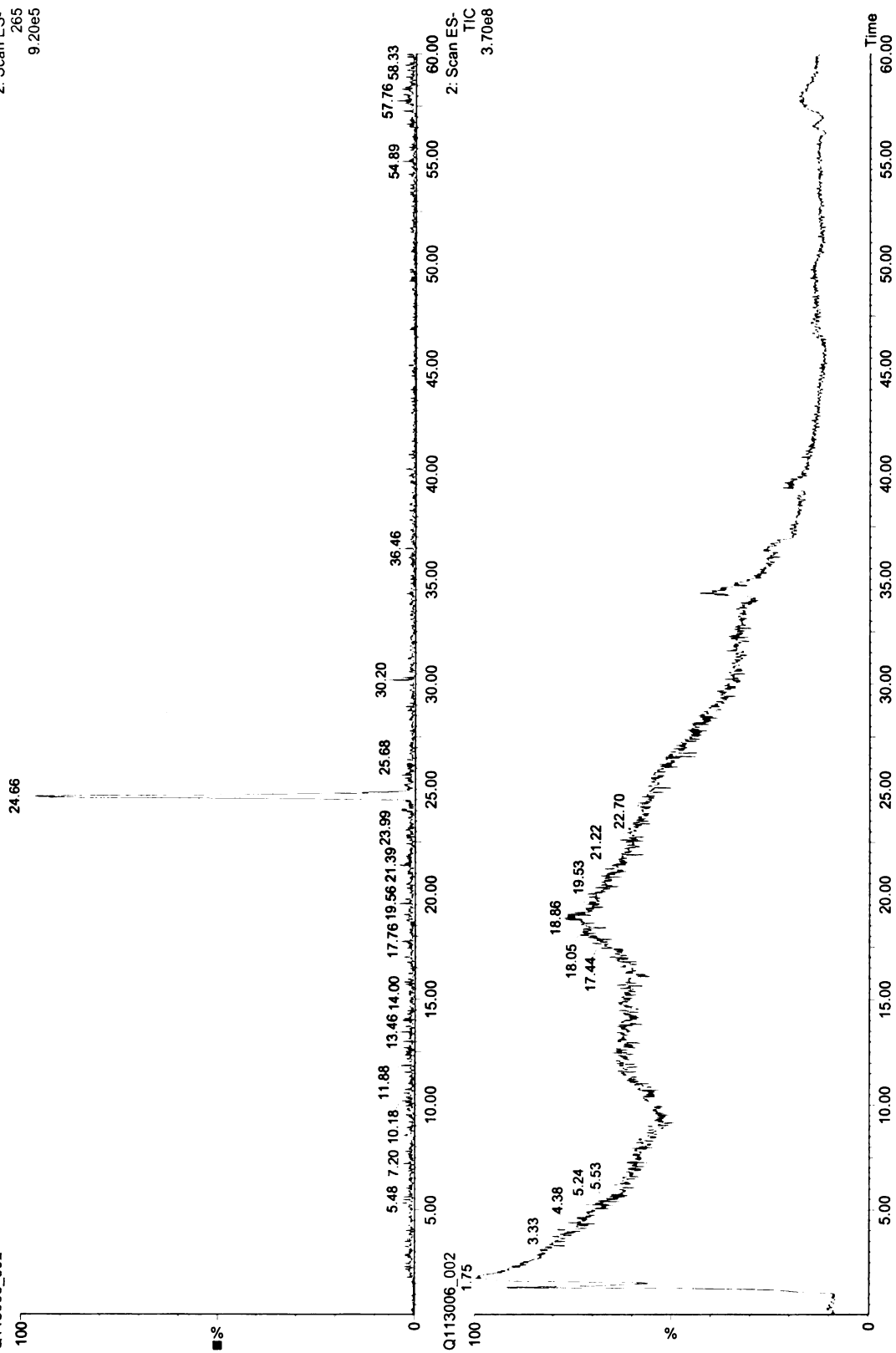
1: Scan ES+
TIC
4.86e7



Carlos/Susan #2 FC-ACN as Rcd (7680)

Q113006_002

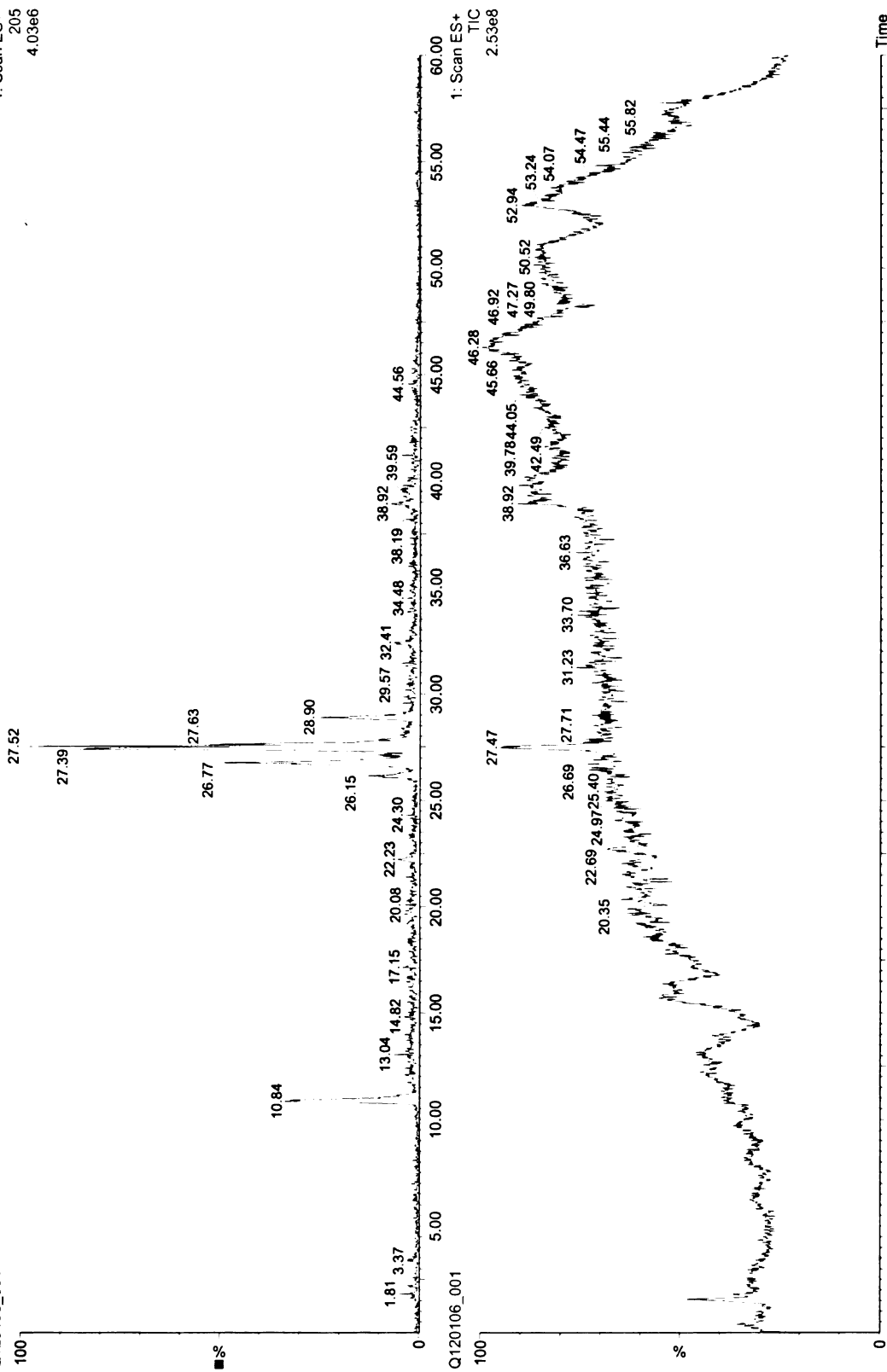
2: Scan ES-
265
9.20e5



Carlos/Susan #3 HEX-GOE as Rcd (7680)

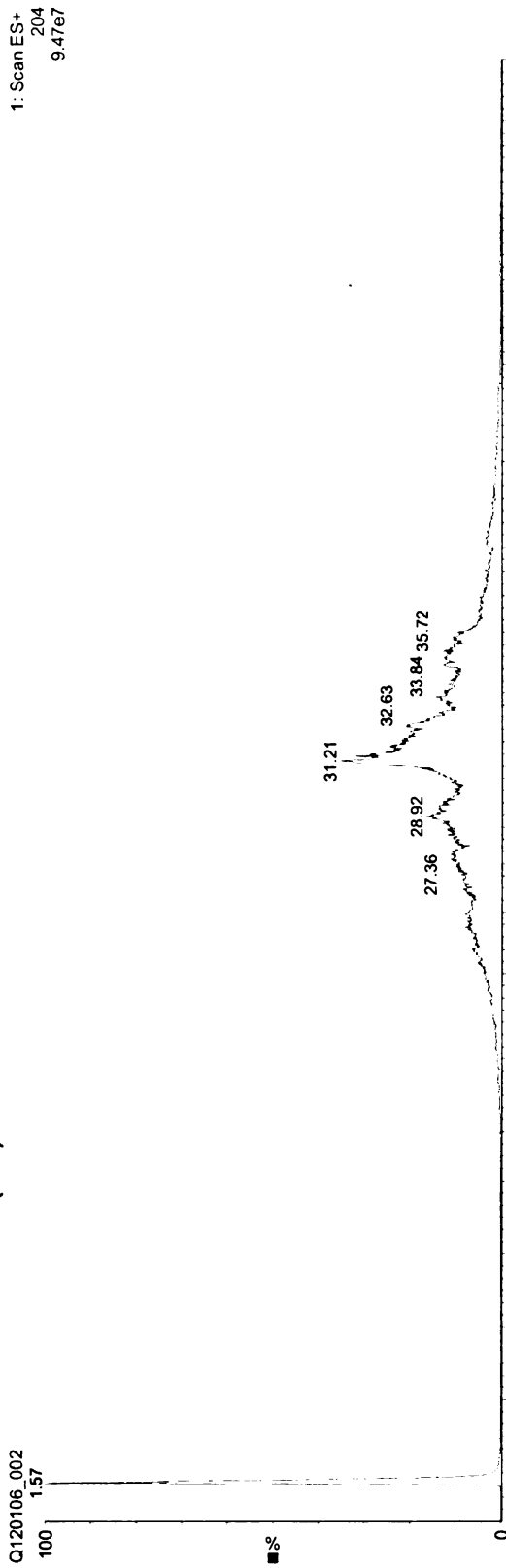
Q120106_001

1: Scan ES+
205
4.03e6

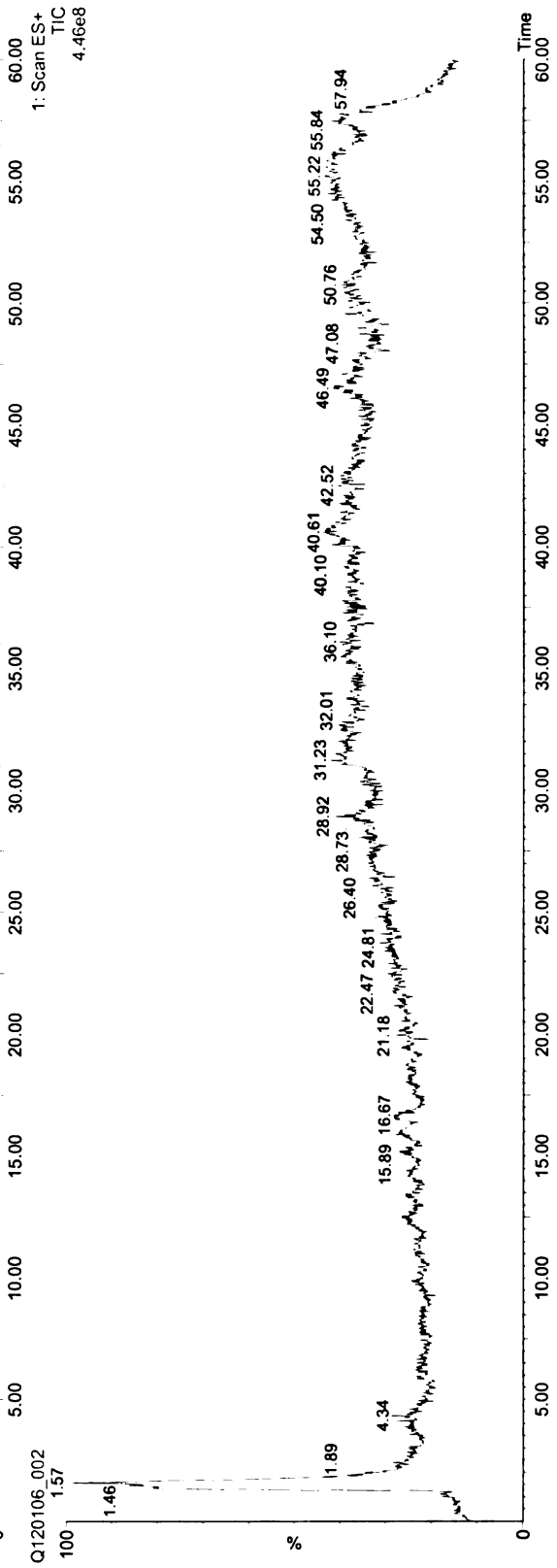


Carlisle/Susan #4 ACN-GOE as Rcd (7880)

1: Scan ES+
204
9.47e7

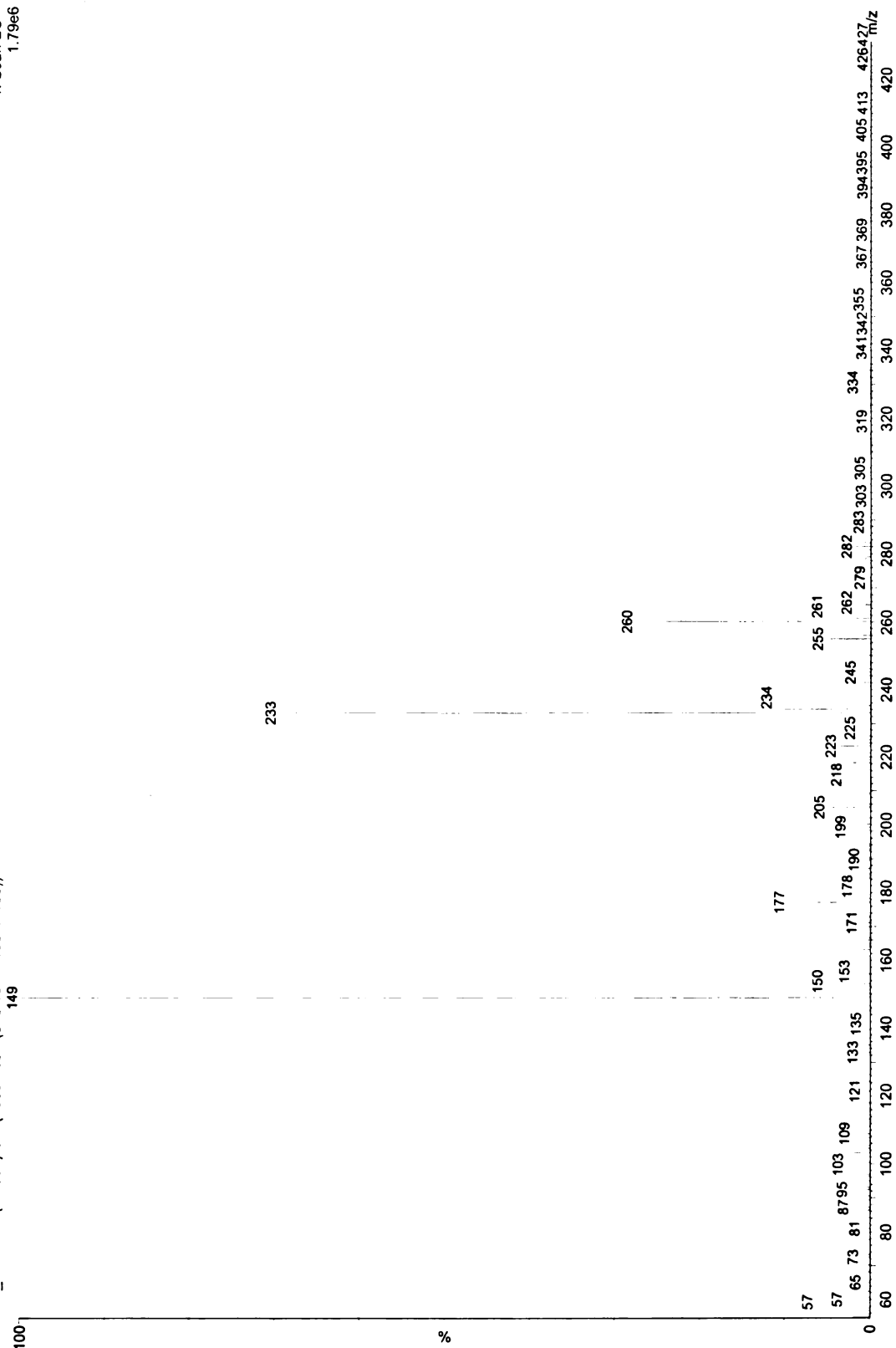


1: Scan ES+
TIC
4.46e8



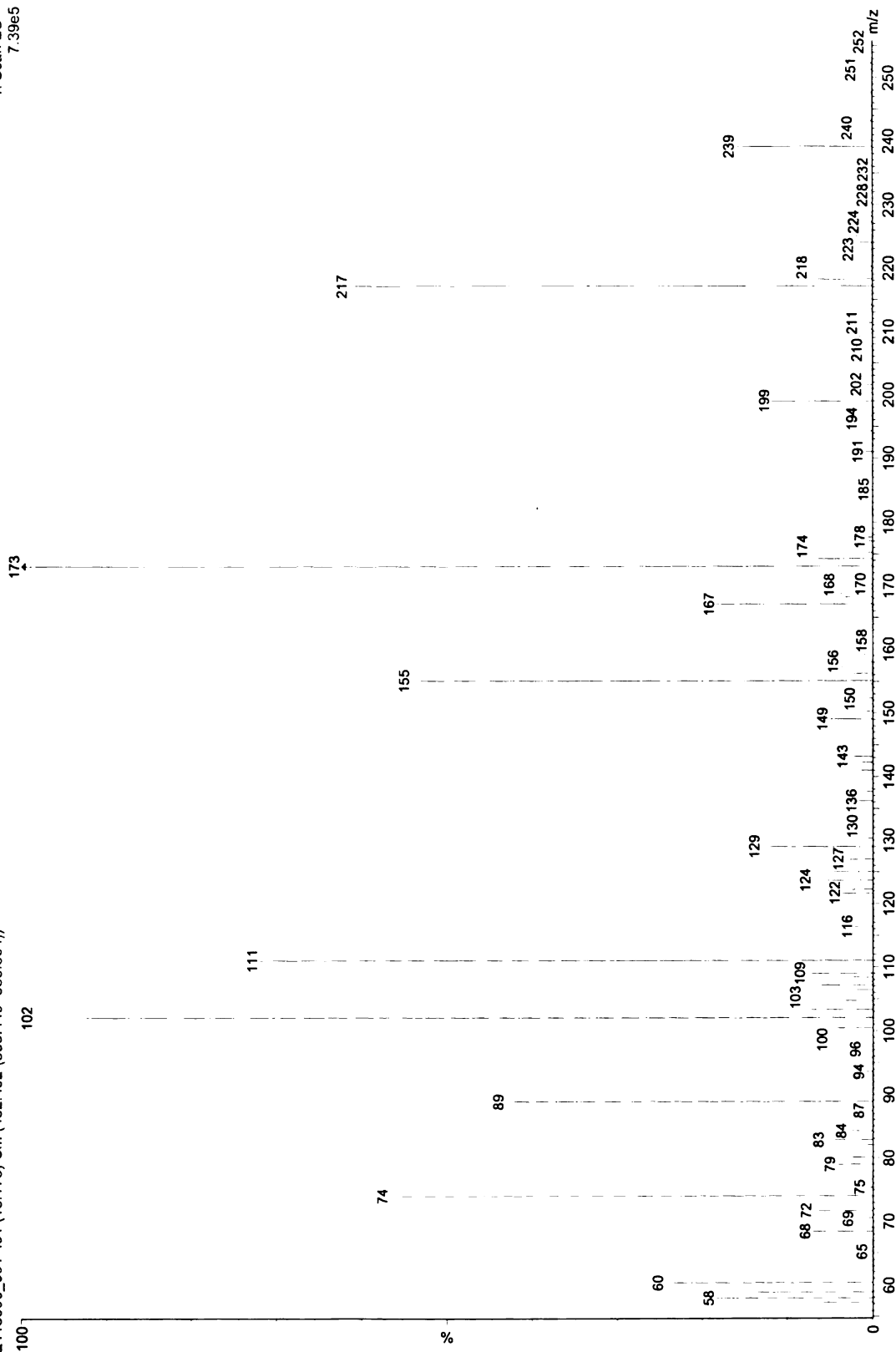
Carlos/Susan #1 FC-HEX as Rcd (7680)
Q113006_001 1039 (27.901) Cm (1039:1057-(948:1014+1084:1186))

1: Scan ES+
1.79e6



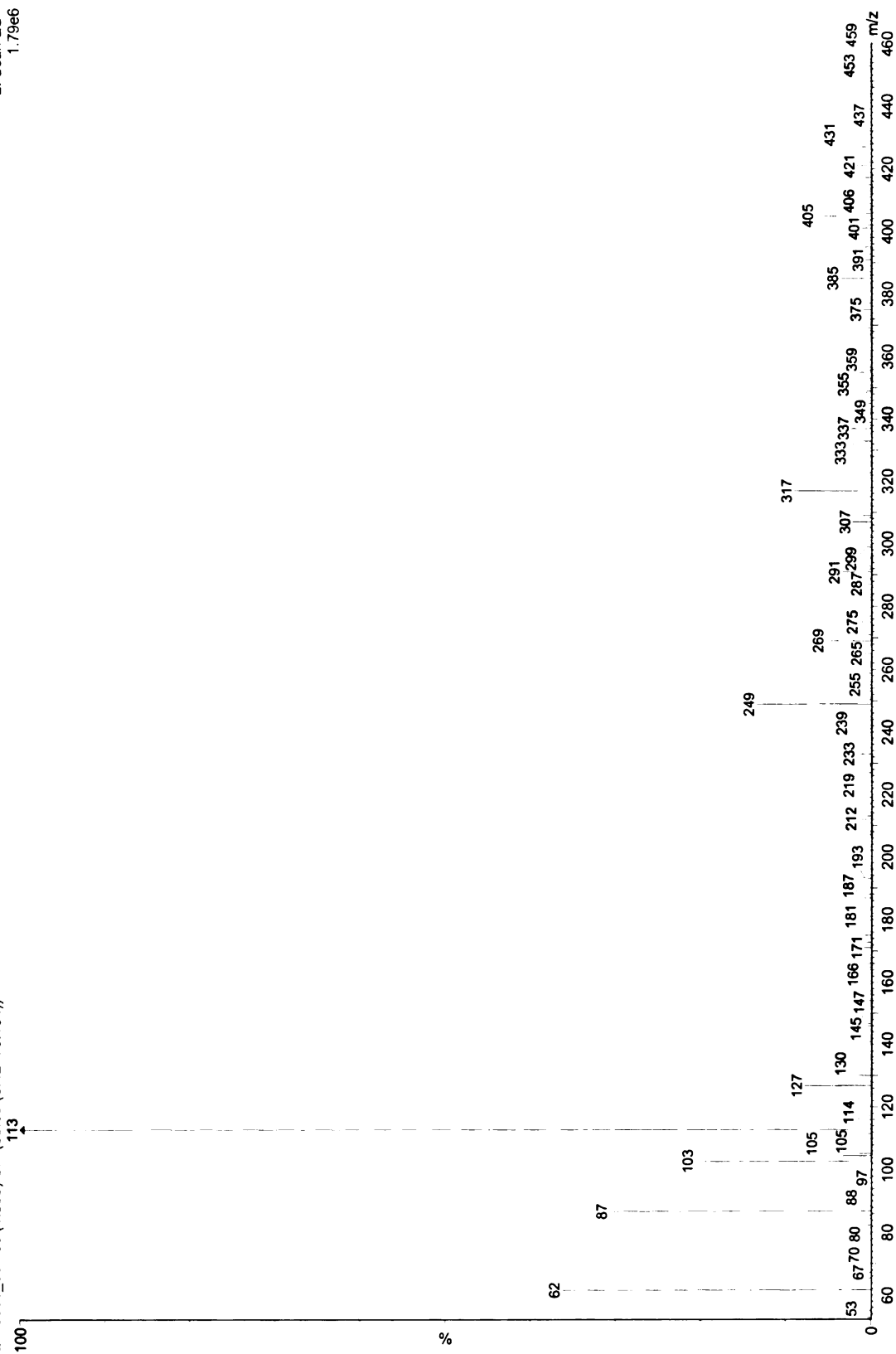
Carlos/Susan #1 FC-HEX as Rcd (7680)
Q113006_001 491 (13.178) Cm (482.492-(368.449+535.664))

1: Scan ES+
7.39e5



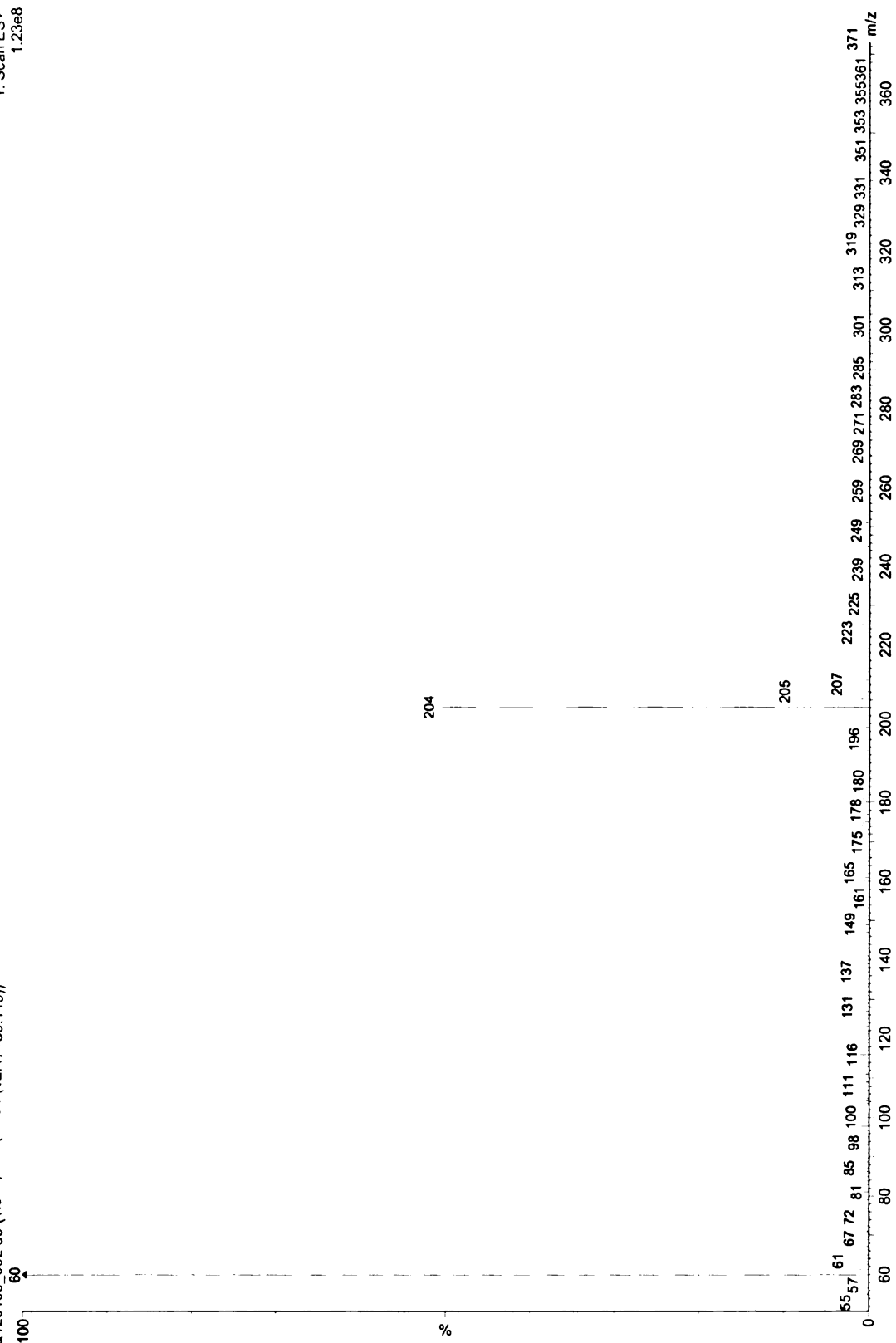
Carlos/Susan #1 FC-HEX as Rcd (7680)
Q113006_001 59 (1.585) Cm (55:59-(8:42+70:104))

2: Scan ES-
1.79e6



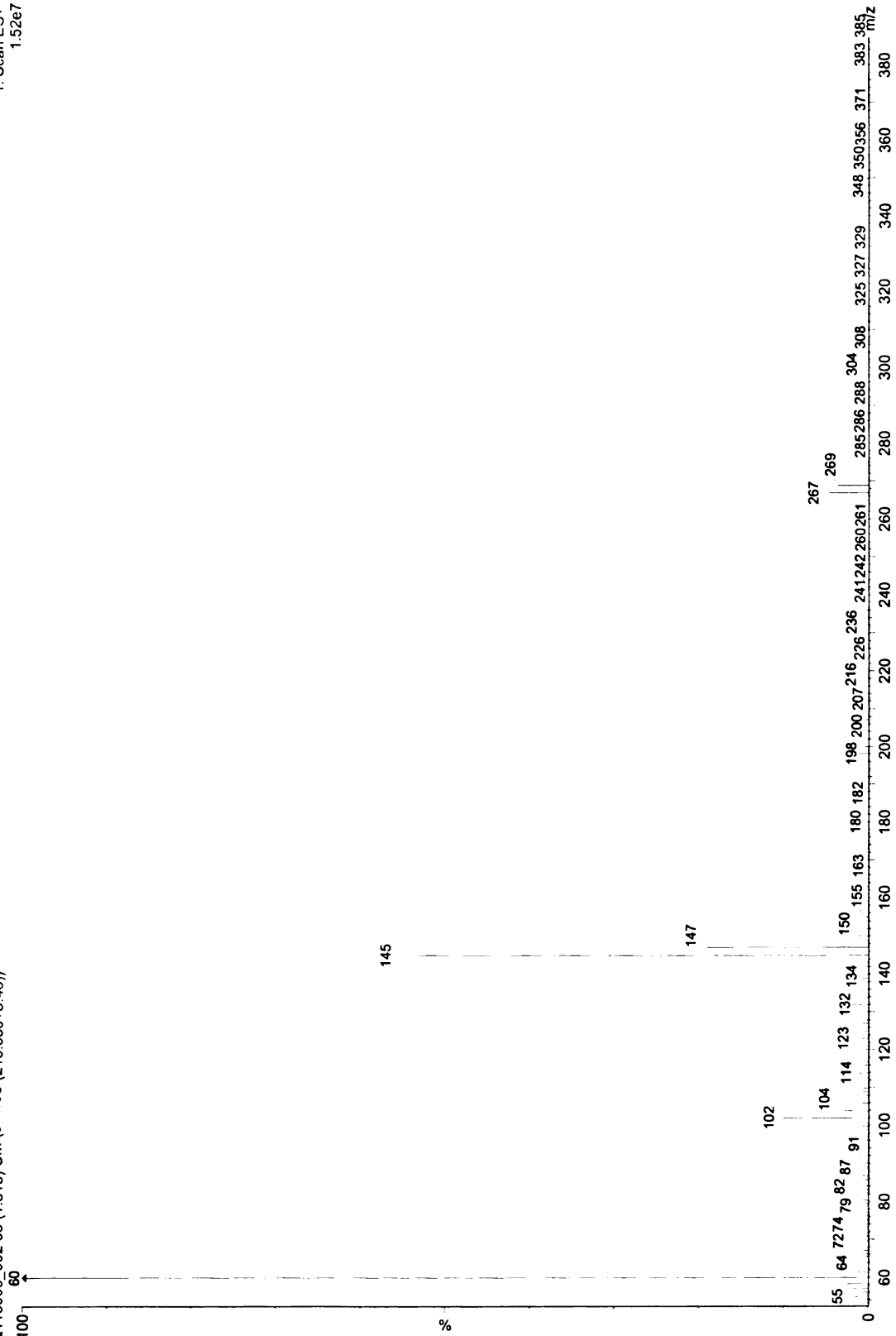
Carlos/Susan #4 ACN-GOE as Rcd (7680)
Q120106_002 59 (1.572) Cm (57.64-(12.47+80.119))

1: Scan ES+
1.23e8



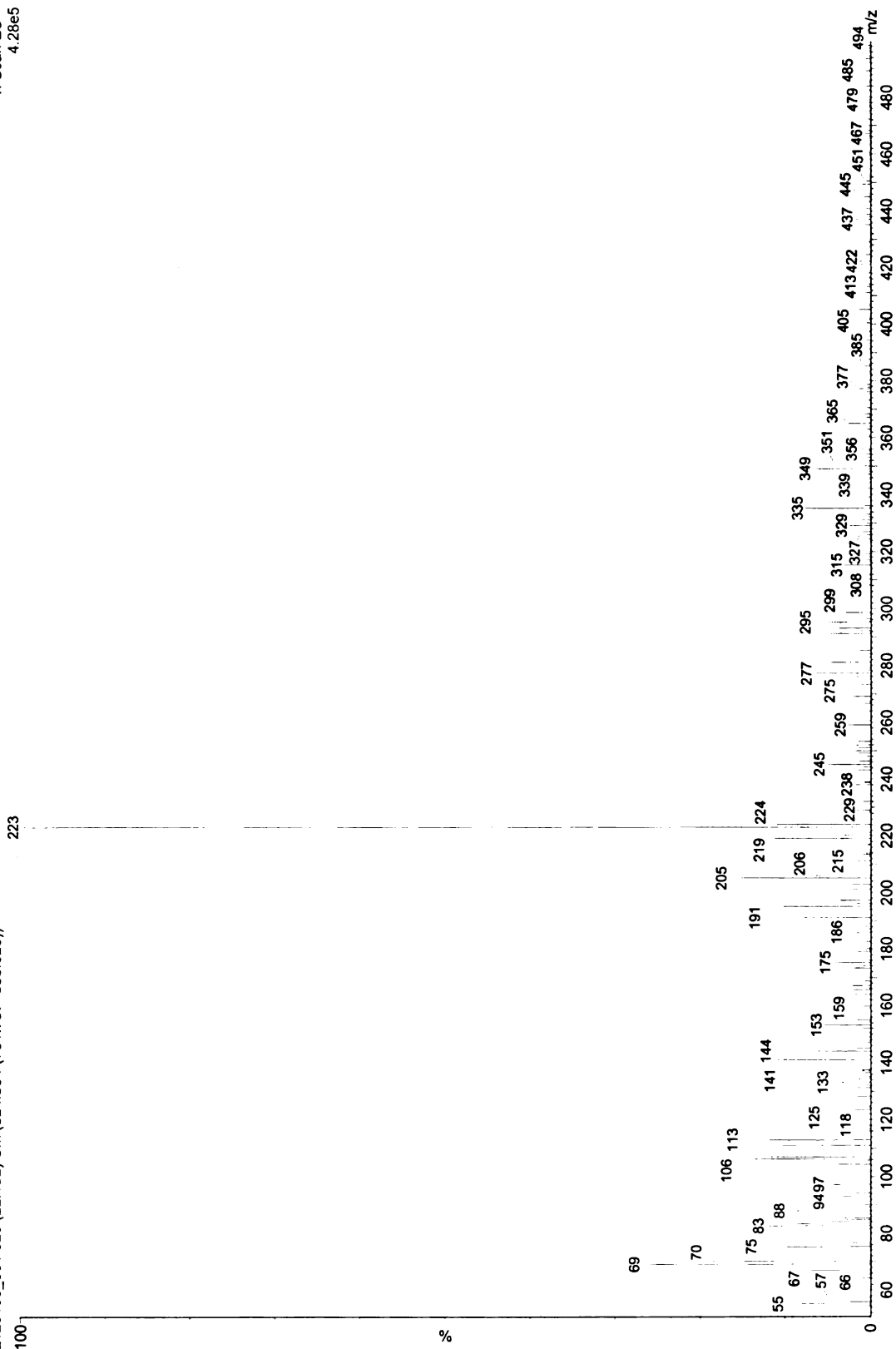
Carlos/Susan #2 FC-ACN as Rcd (7680)
Q113006_002 68 (1.813) Cm (57:108-(215:680+8:43))

1: Scan ES+
1.52e7



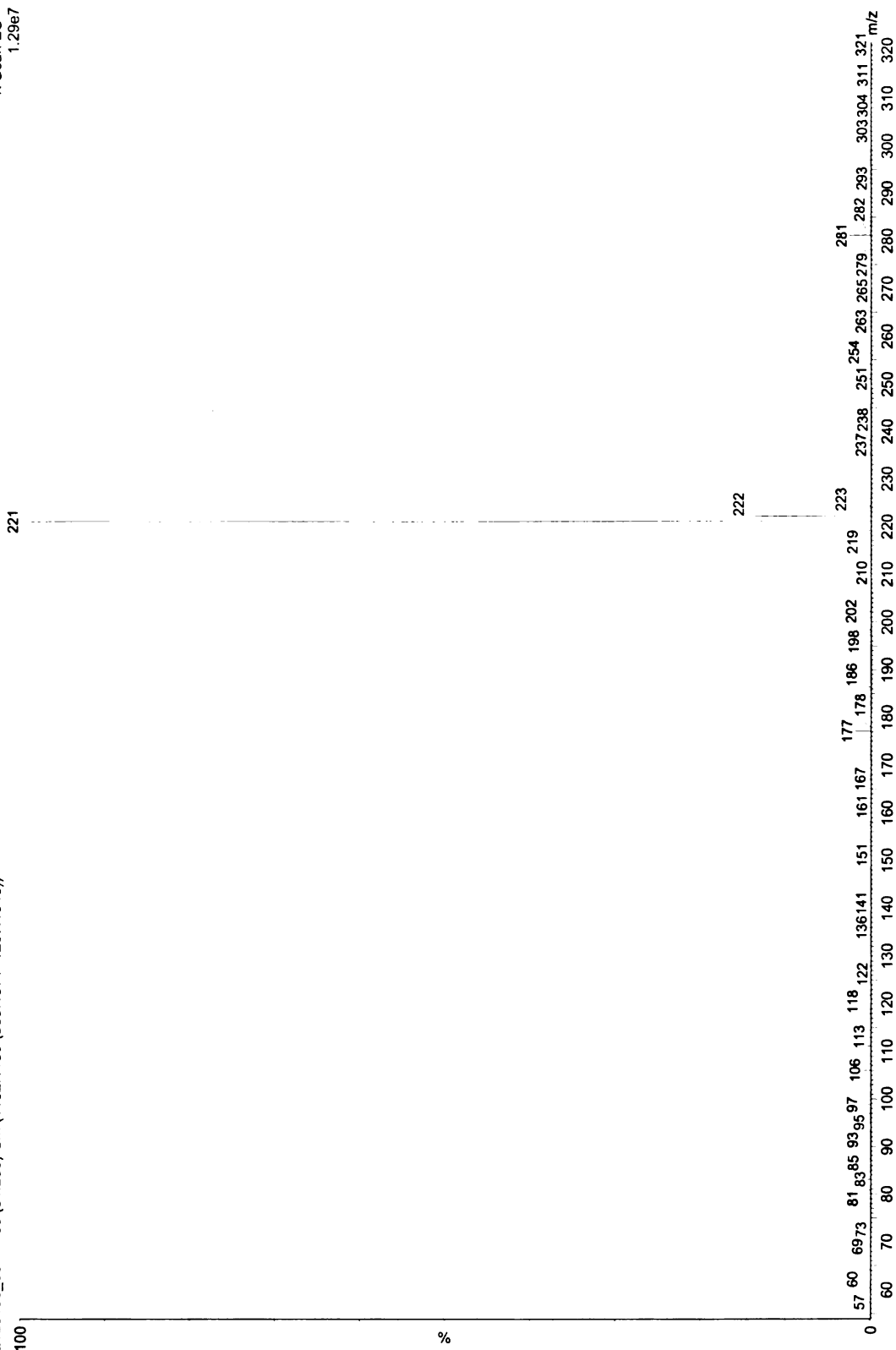
Carlos/Susan #3 HEX-GOE as Rcd (7680)
Q120106_001 825 (22.152) Cm (824:834-(701:787+858:928))

1: Scan ES+
4.28e5

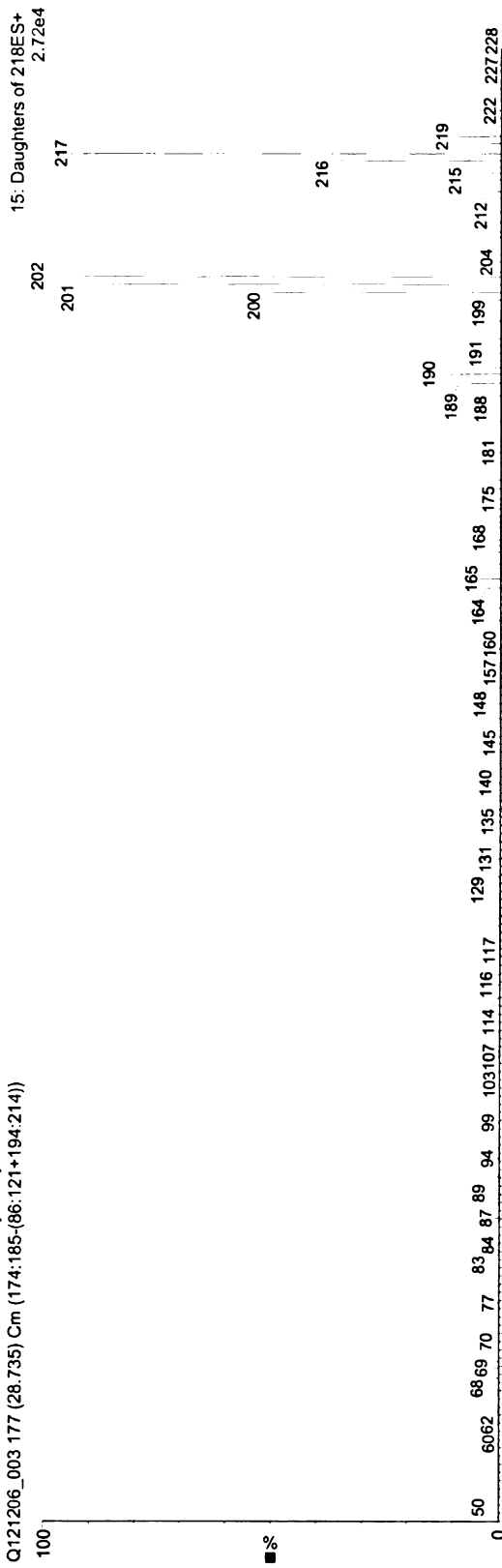


Carlos/Susan #3 HEX-GOE as Rcd (7680)
Q120106_001 1163 (31.233) Cm (1162:1180-869:1071+1267:1548))

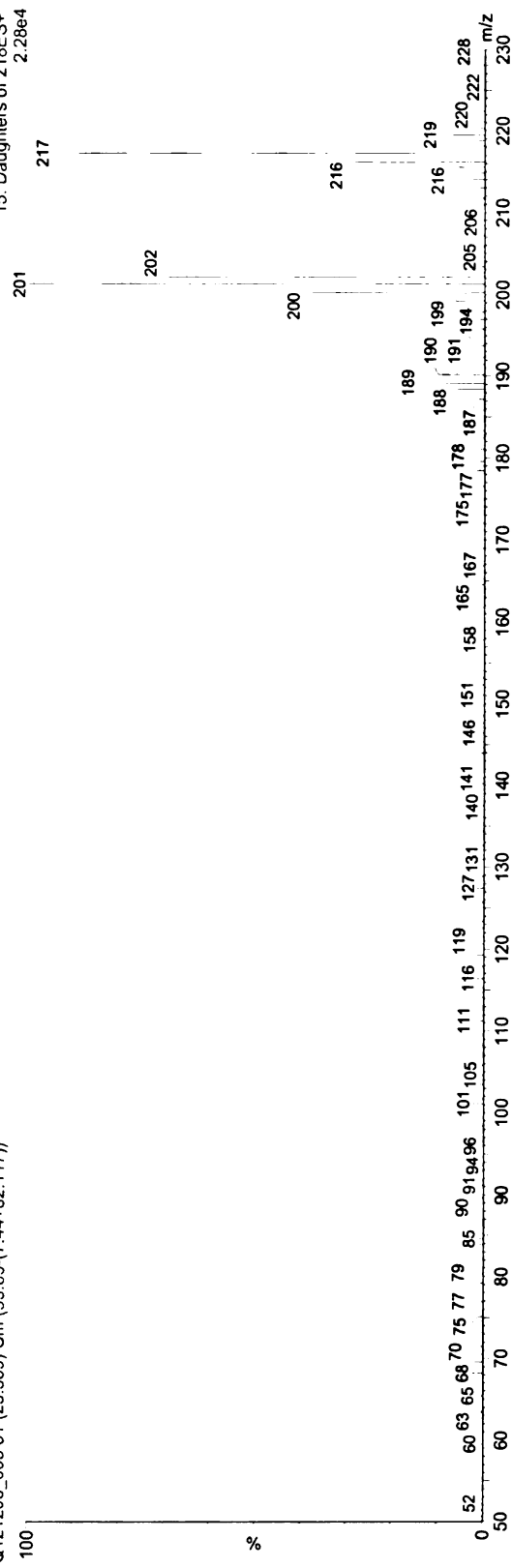
1: Scan ES+
1.29e7



Carlos/Susan #1 FC-HEX as Rcd (7680) MSMS
 Q121206_003 177 (28.735) Cm (174:185-(86:121+194:214))



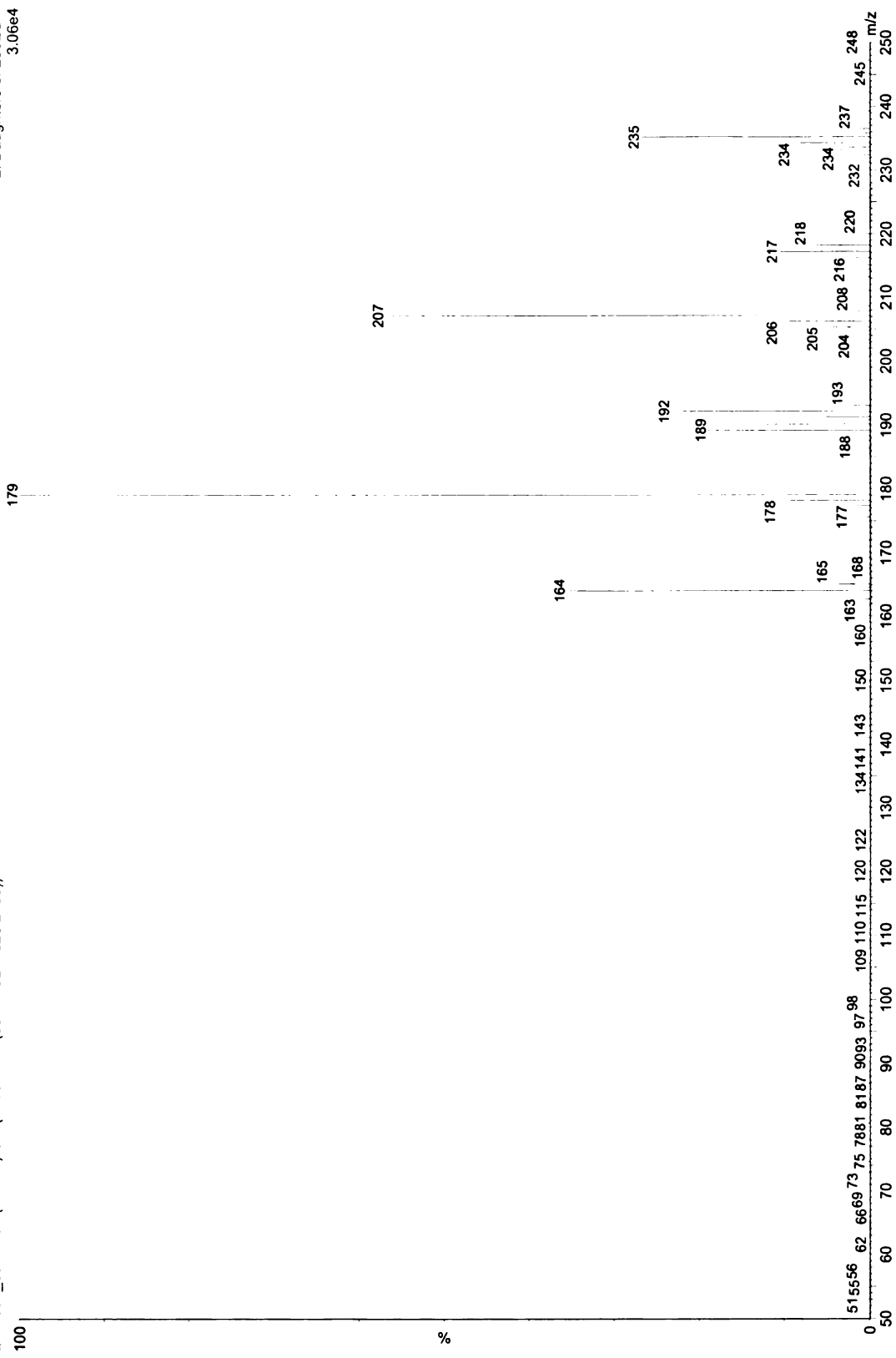
Q121206_003 61 (23.369) Cm (59:69-(7:44+82:117))



Fe (+2) 0.001

Q032907_004 1739 (24.628) Cm (1563:1771-(397:1192+1826:2159))

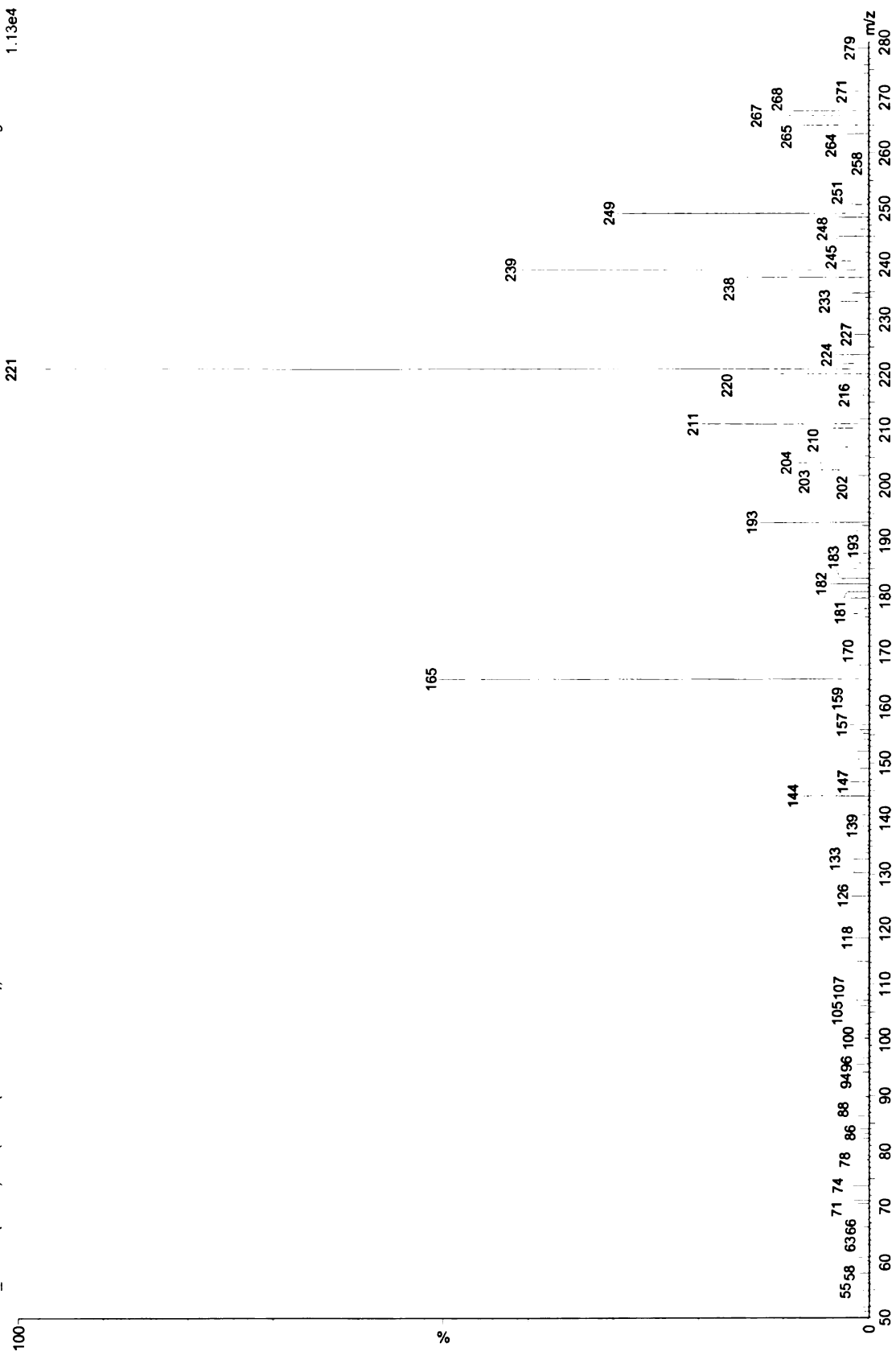
2: Daughters of 235ES+
3.06e4



Fe (+3) 0.001

Q032907_002 75 (1.886) Cm (68.85-(14.61+124.247))

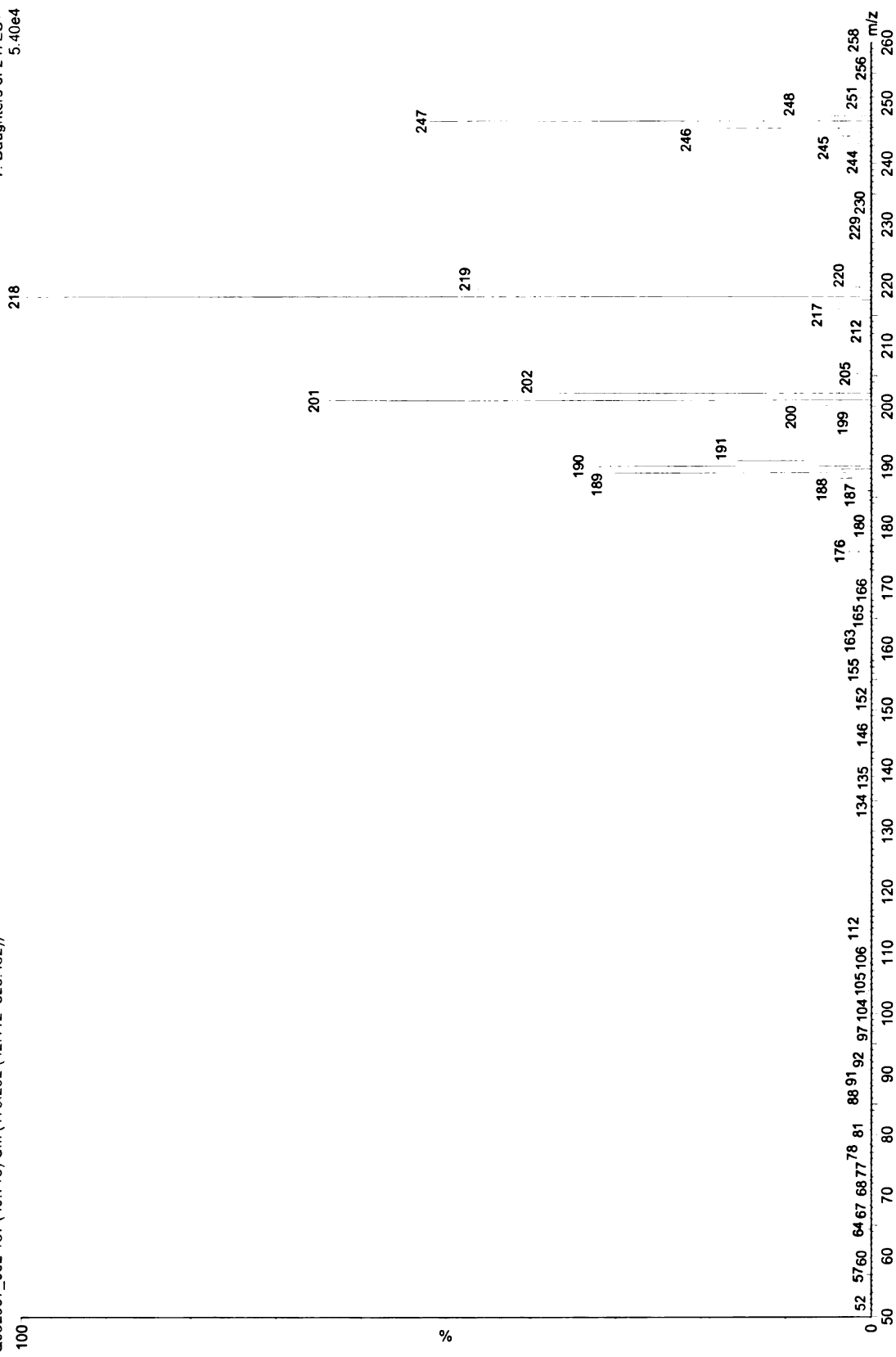
2: Daughters of 267ES+
1.13e4



Fe (+3) 0.001

Q032907_002 187 (40.715) Cm (179:202:(42:112+325.482))

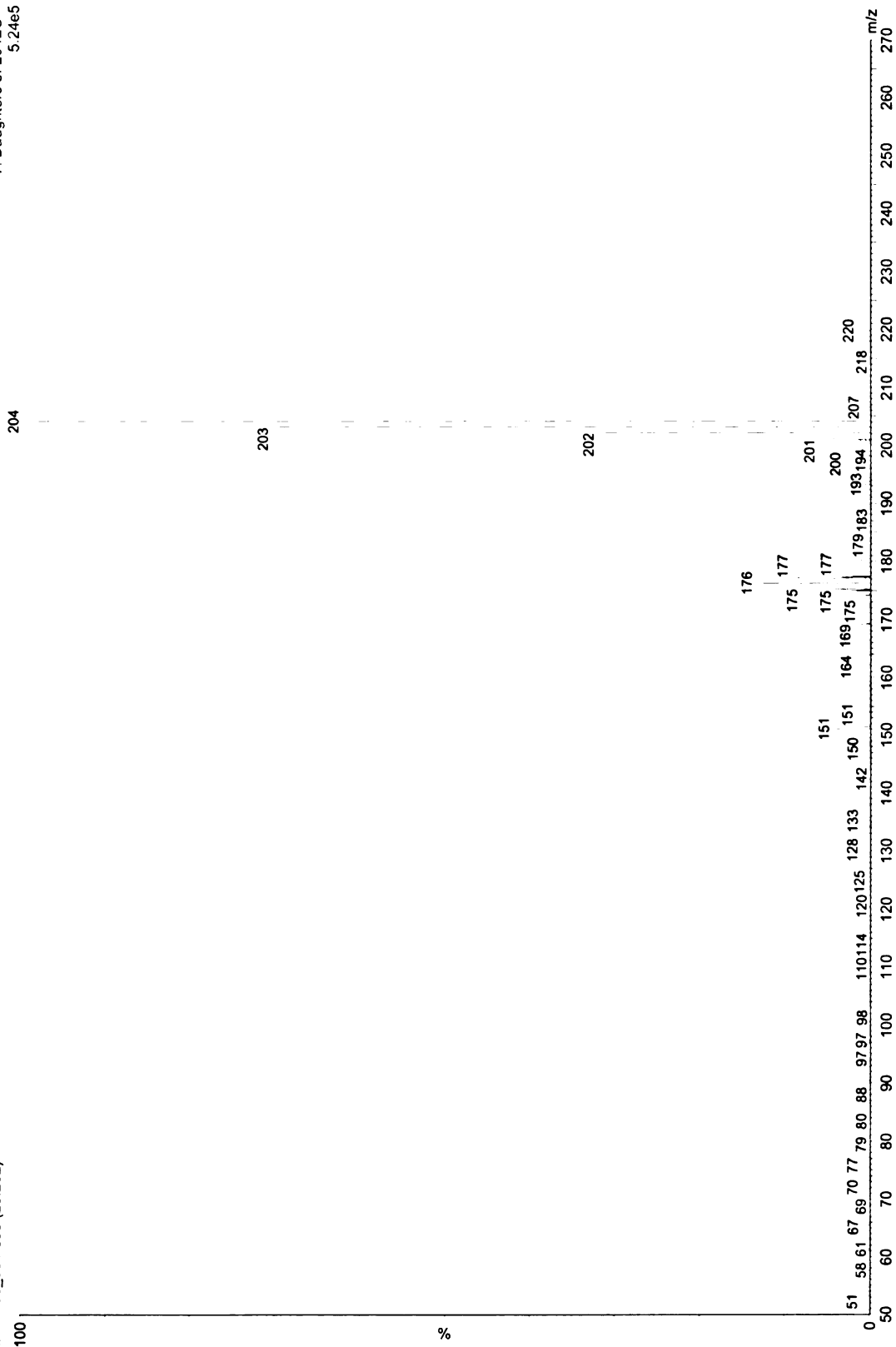
7: Daughters of 247ES+
5.40e4



Carlos/Susan #4 ACN-GOE as Rcd (7690) MSMS

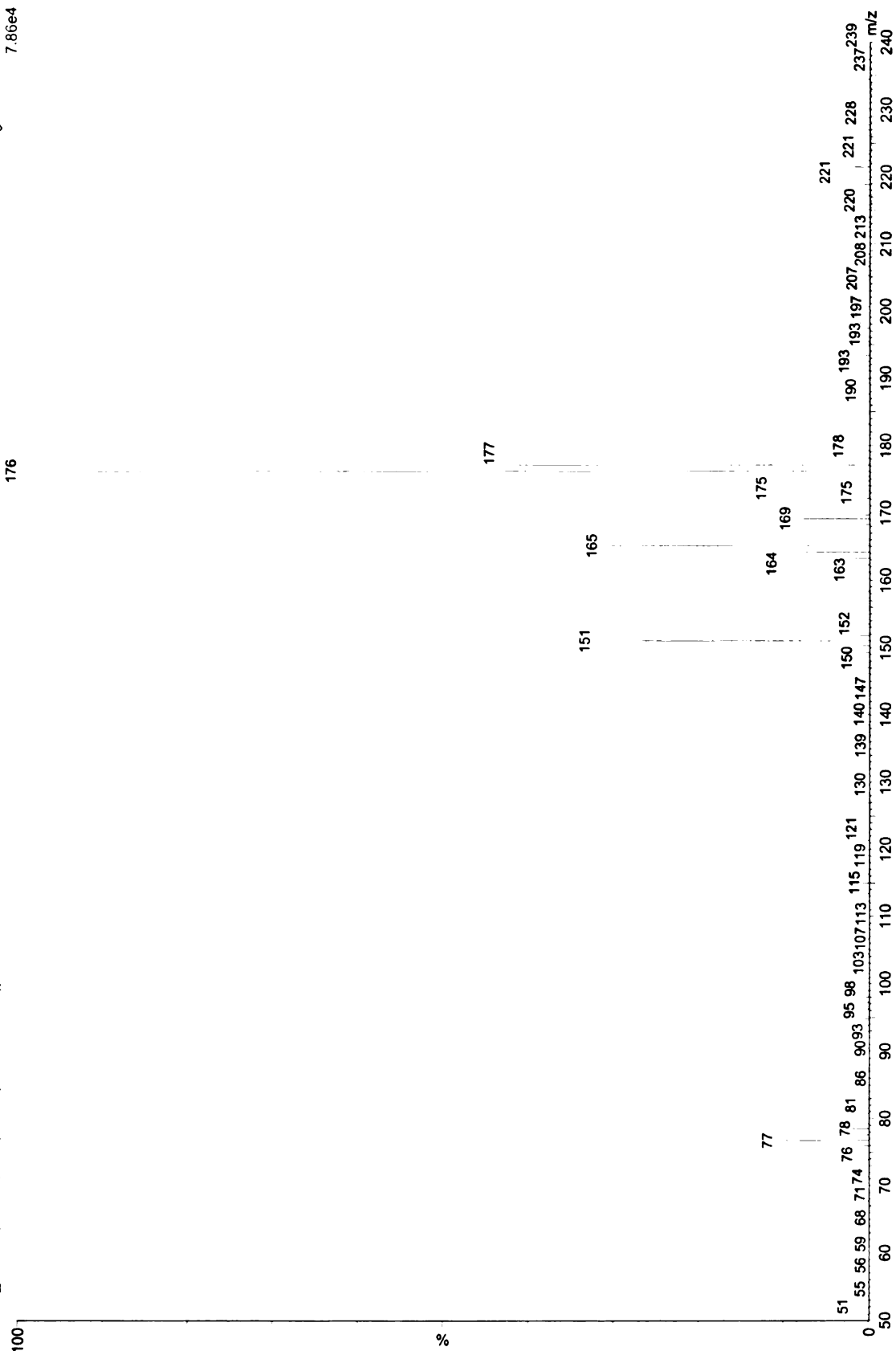
Q121406_001 605 (29.202)

7: Daughters of 204ES+
5.24e5



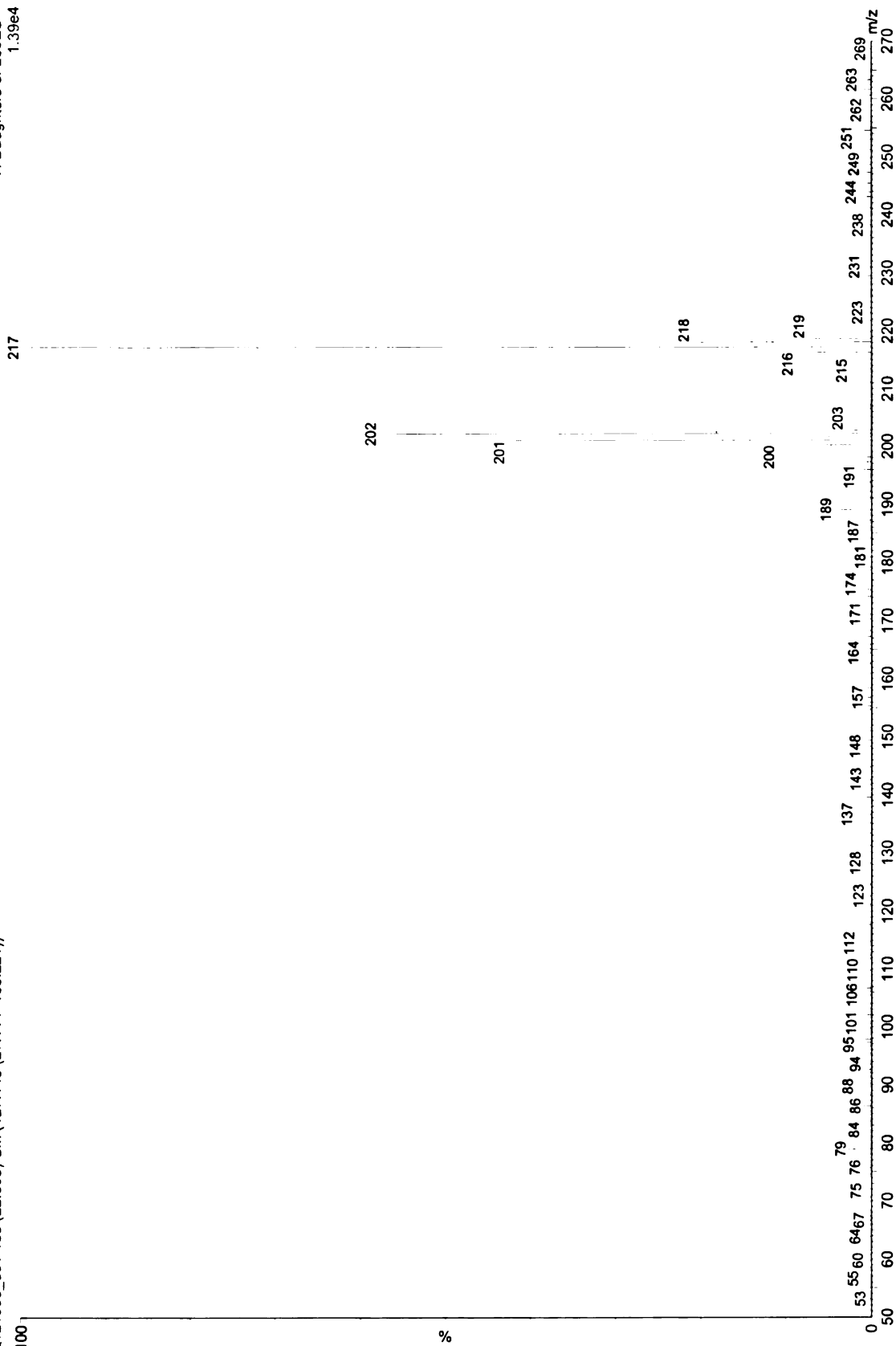
Carlos/Susan #3 HEX-GOE as Rcd (7680) MSMS
Q121306_001 60 (26.094) Cm (54.73-(7:33+140:228))

9: Daughters of 221ES+
7.86e4



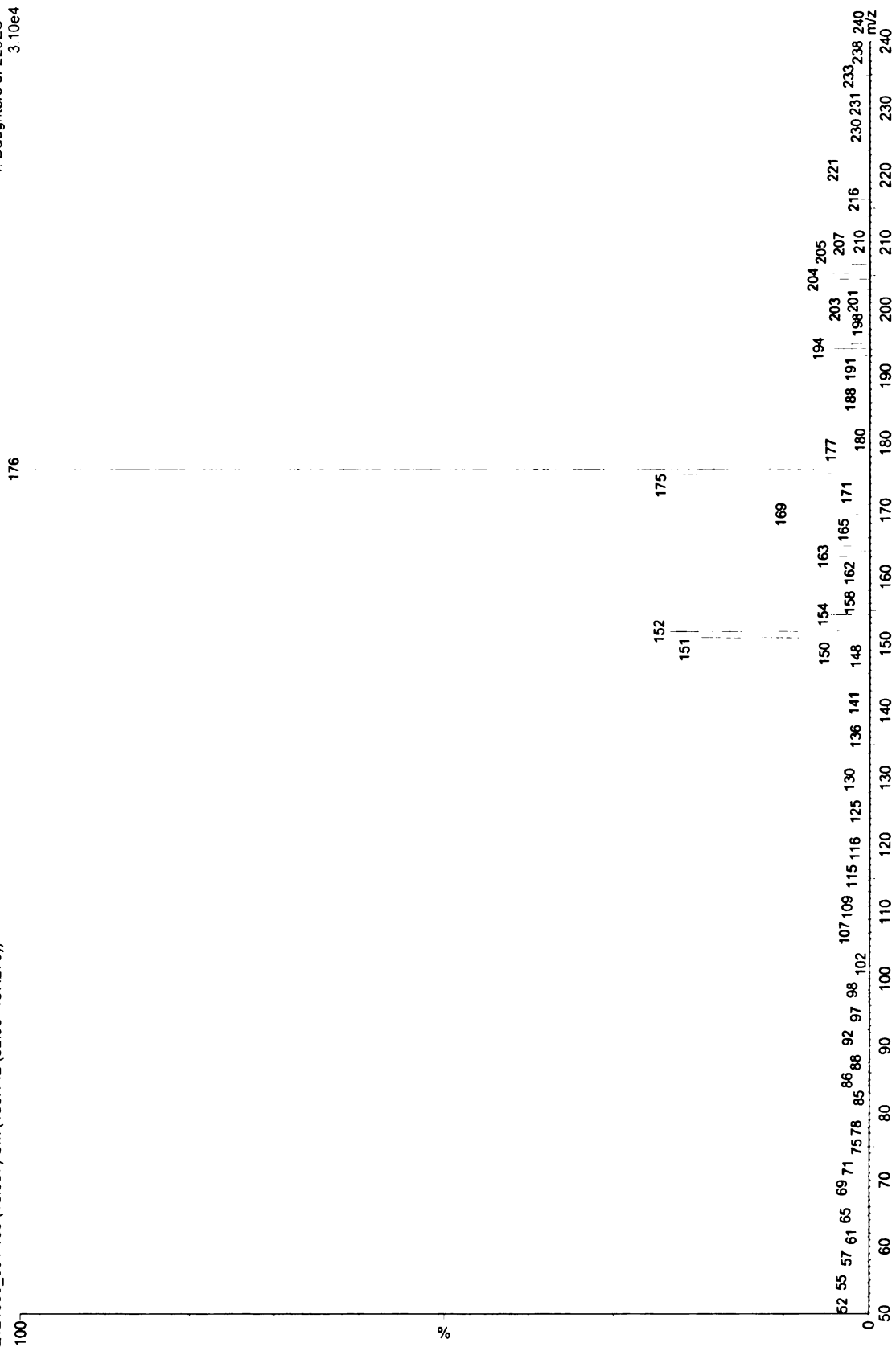
Carlos/Susan #3 HEX-GOE as Rd (7680) MSMS
Q121306_001 136 (22.608) Cm (127:148-(27:114+166:221))

7: Daughters of 260ES+
1.39e4



Carlos/Susan #3 HEX-GOE as Rcd (7680) MSMS
Q121306_001 138 (18.387) Cm (136:142(32:93+157:270))

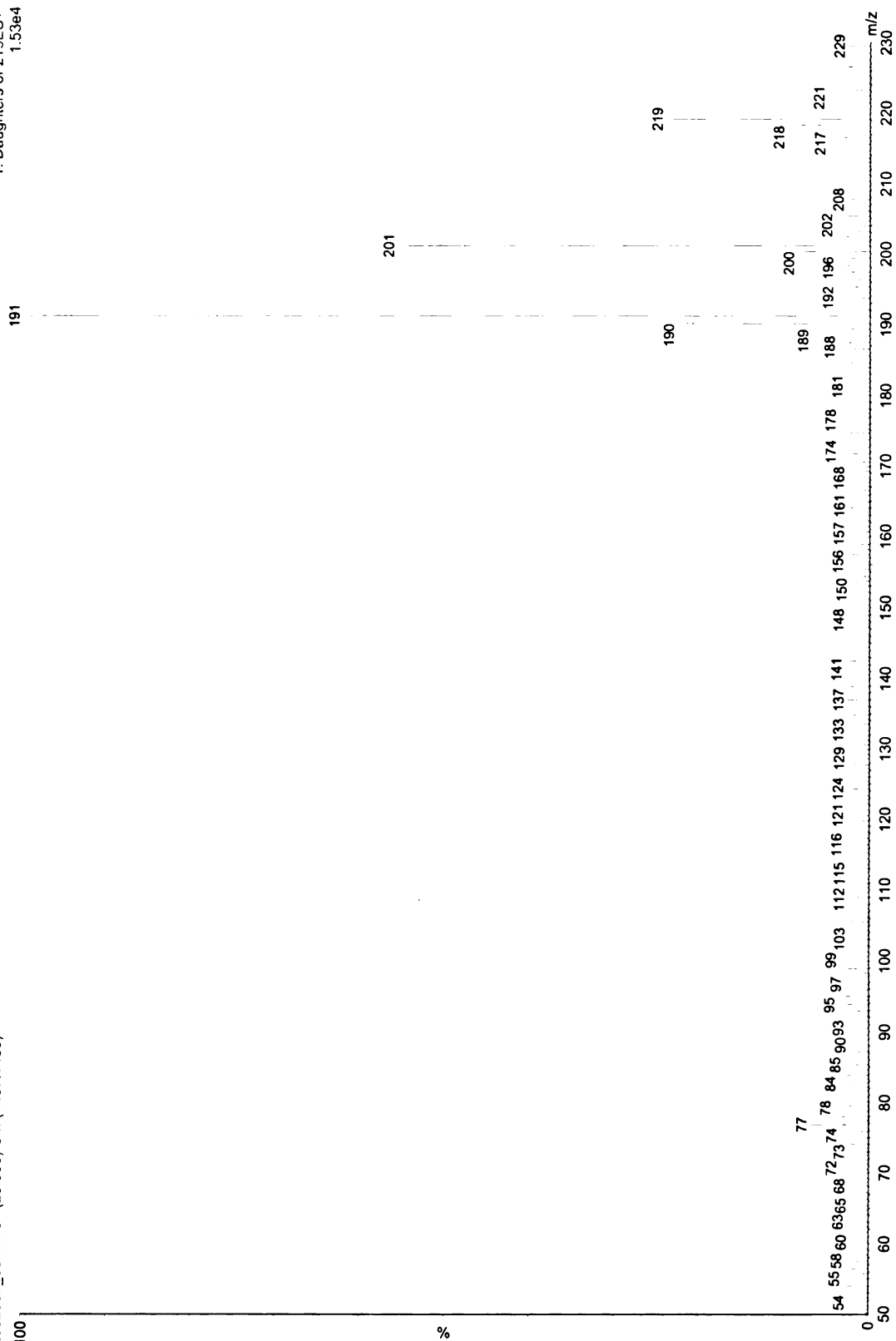
4: Daughters of 223ES+
3.10e4



GOE 0.06

Q032907_001 1451 (20.906) Cm (1407:1465)

1: Daughters of 219ES+
1.53e4



Appendix B

Appendix B: Salicylic Acid Byproducts

LC/MS DATA

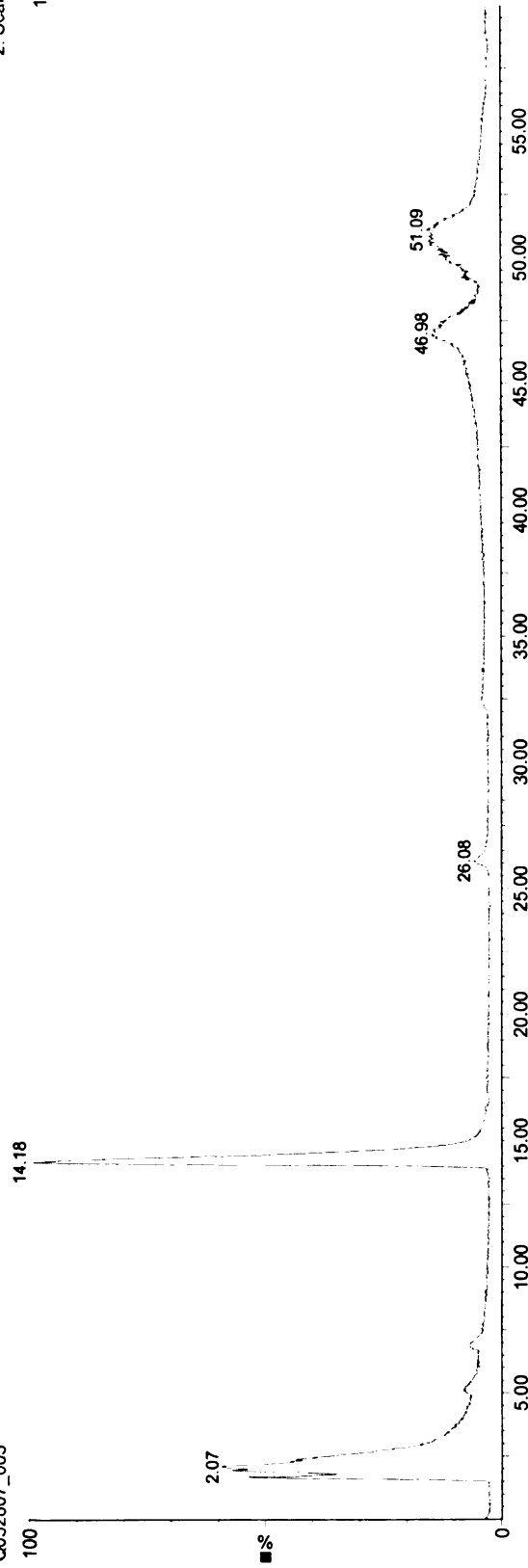
Typical chromatogram of salicylic acid byproducts obtained from Goethite catalyzed CHPs at pH 7.....	221
Typical chromatogram of m/z 93 vs. TIC obtained from Goethite catalyzed CHPs at pH 7.....	222
Typical chromatogram of m/z 153 vs. TIC obtained from Goethite catalyzed CHPs at pH 7.....	223
Typical chromatogram of m/z 169 vs. TIC obtained from Goethite catalyzed CHPs at pH 7.....	224
Mass Spectrum for m/z 169 obtained from Goethite catalyzed CHPs at pH 7...	225
Typical chromatogram of salicylic acid byproducts obtained from Goethite catalyzed CHPs at pH 3.....	226
Typical chromatogram of m/z 153 vs. TIC obtained from Goethite catalyzed CHPs at pH 3.....	227
Typical chromatogram of m/z 169 vs. TIC obtained from Goethite catalyzed CHPs at pH 3.....	228
Mass Spectrum for m/z 169 obtained from Goethite catalyzed CHPs at pH 3...	229

GC/MS DATA

Typical GC/MS chromatogram for salicylic acid samples after CHP Goethite catalyzed reactions.....	230
Close up for peaks with retention time of 15.5 and 16. 2 minutes.....	231
Close up for peaks with retention time of 18.9 and 19.20 minutes.....	232
GC/MS mass spectrum for peak with retention time of 15.5 min.....	233
GC/MS chromatogram showing to compounds eluding at the same retention time of 15.5 min.....	234
GC/MS mass spectrum for peak with retention time of 16.2 min.....	235
GC/MS mass spectrum for peak with retention time of 18.9 min.....	236

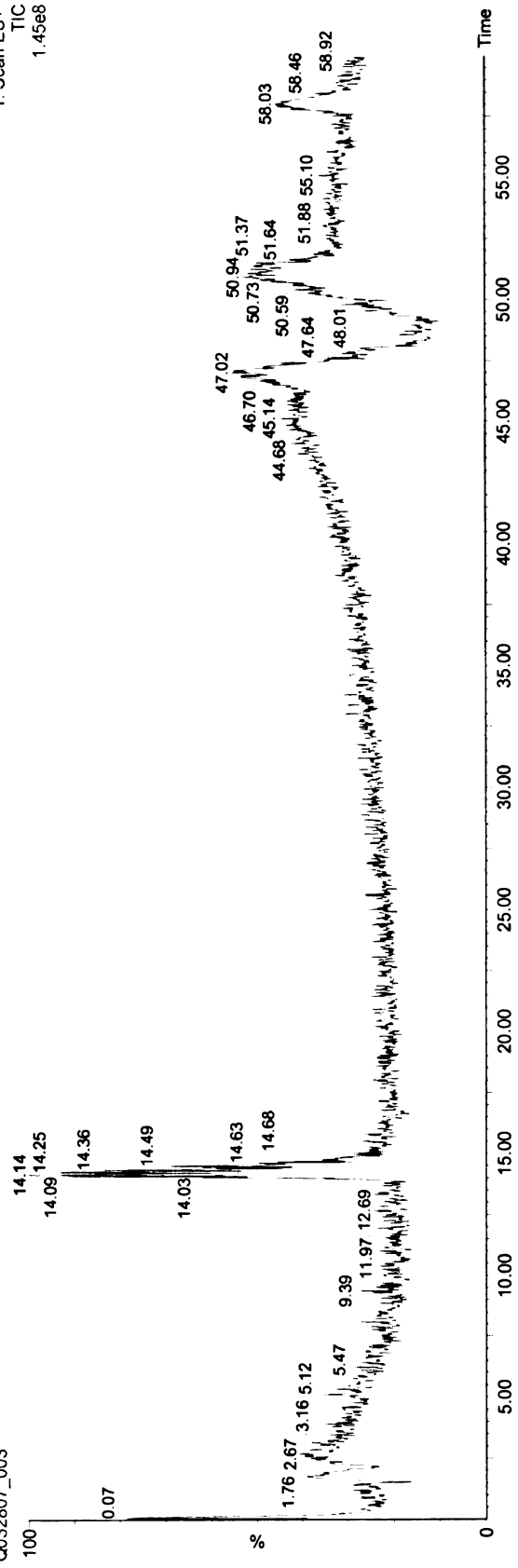
Salicylic Acid pH7
Q032807_003

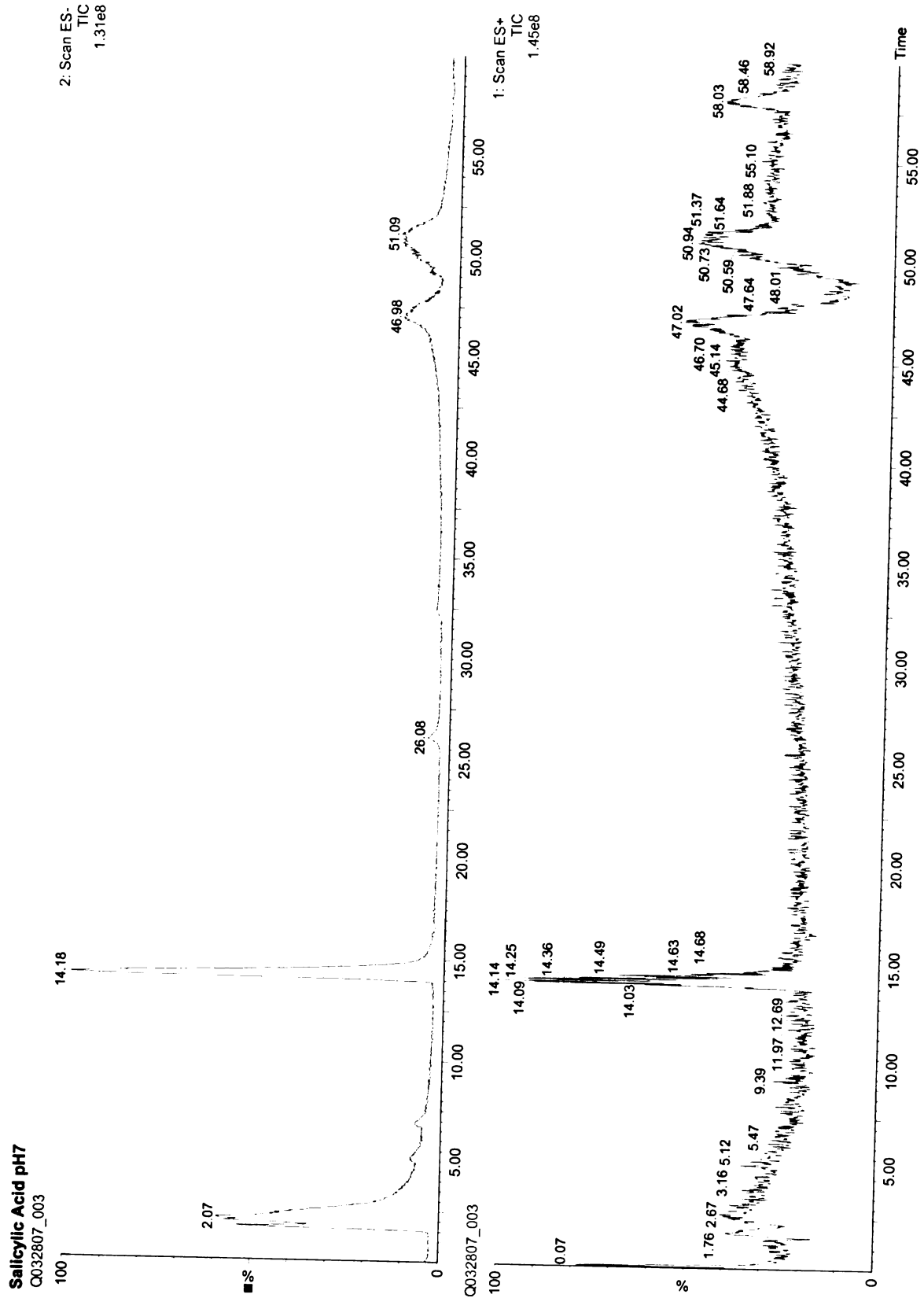
2: Scan ES-
TIC
1.31e8



Q032807_003

1: Scan ES+
TIC
1.45e8

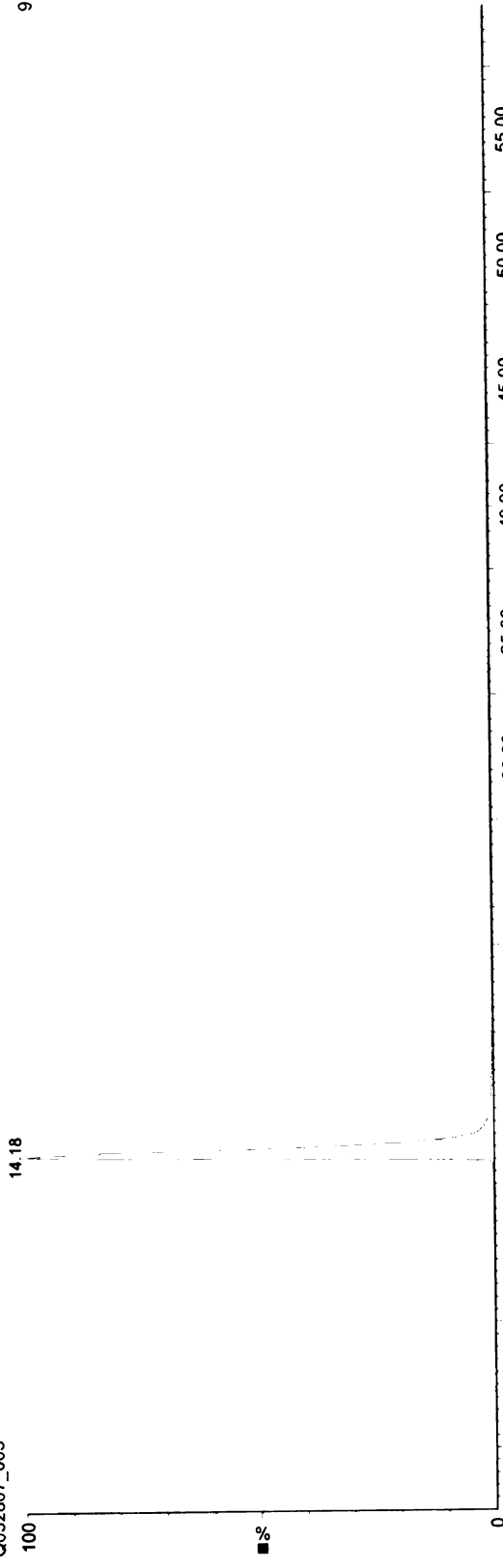




Salicylic Acid pH7

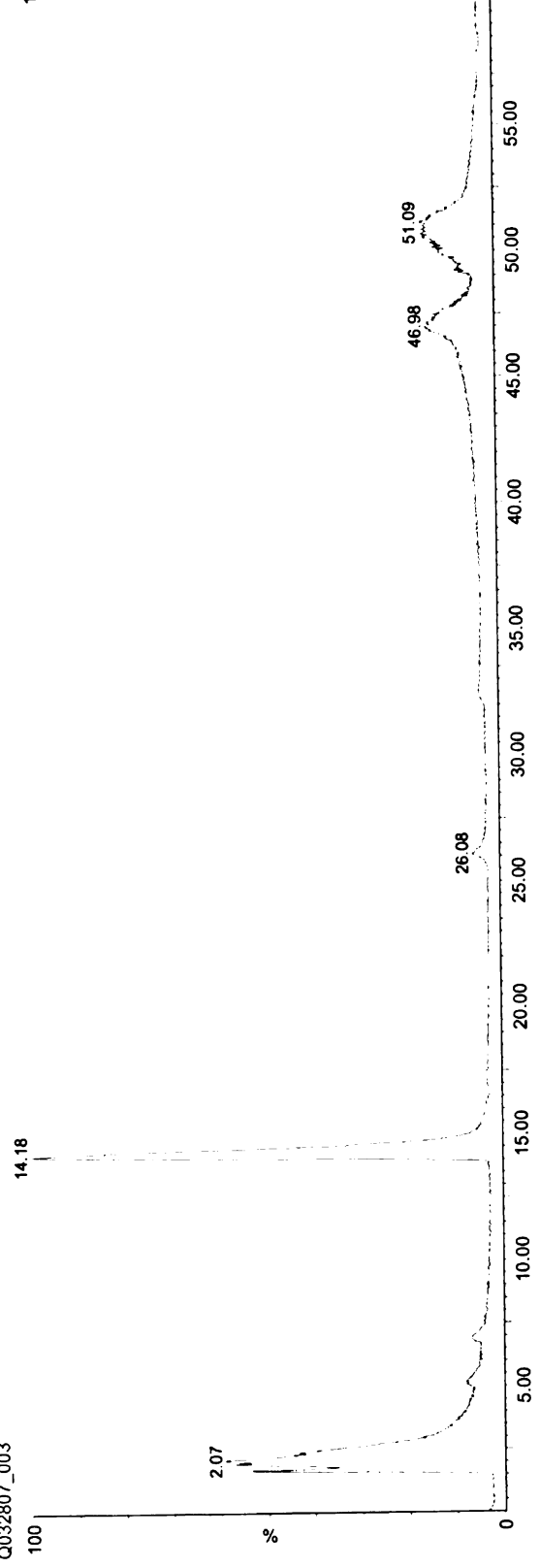
Q032807_003

2: Scan ES-
93
9.18e7



Q032807_003

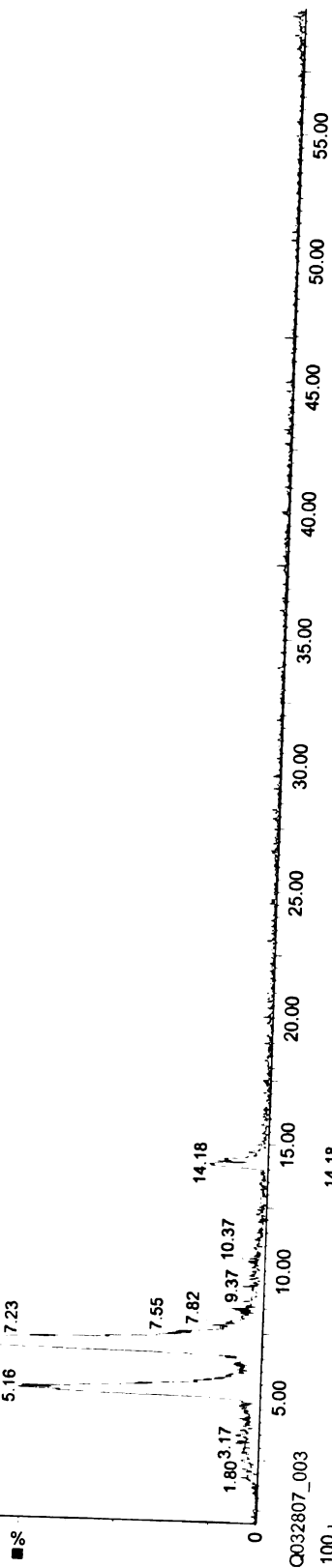
2: Scan ES-
TIC
1.31e8



Salicylic Acid pH7
Q032807_003

2: Scan ES-
153
1.39e6

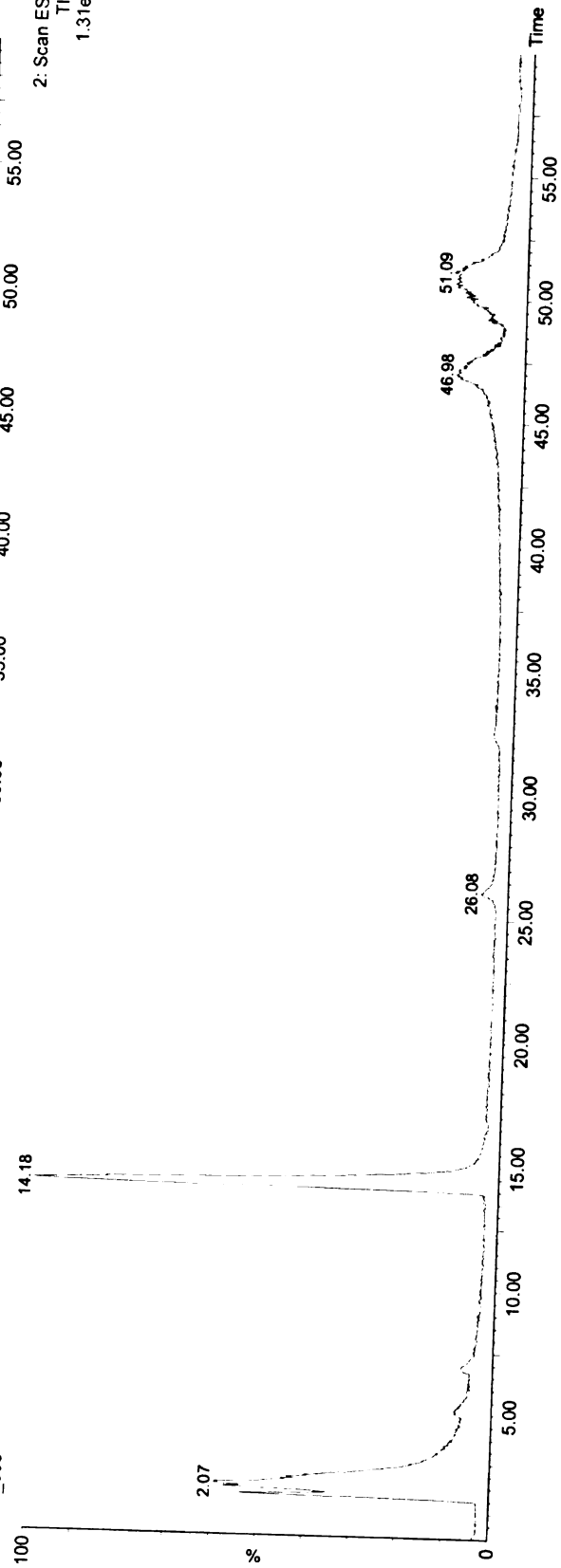
■ %



Q032807_003

%

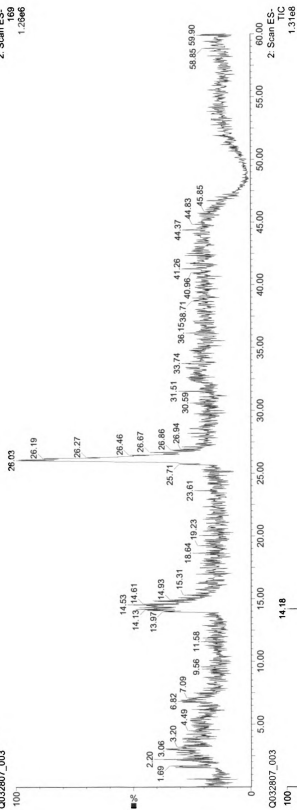
2: Scan ES-
TIC
1.31e8



Salicylic Acid pH7

Q032807_003

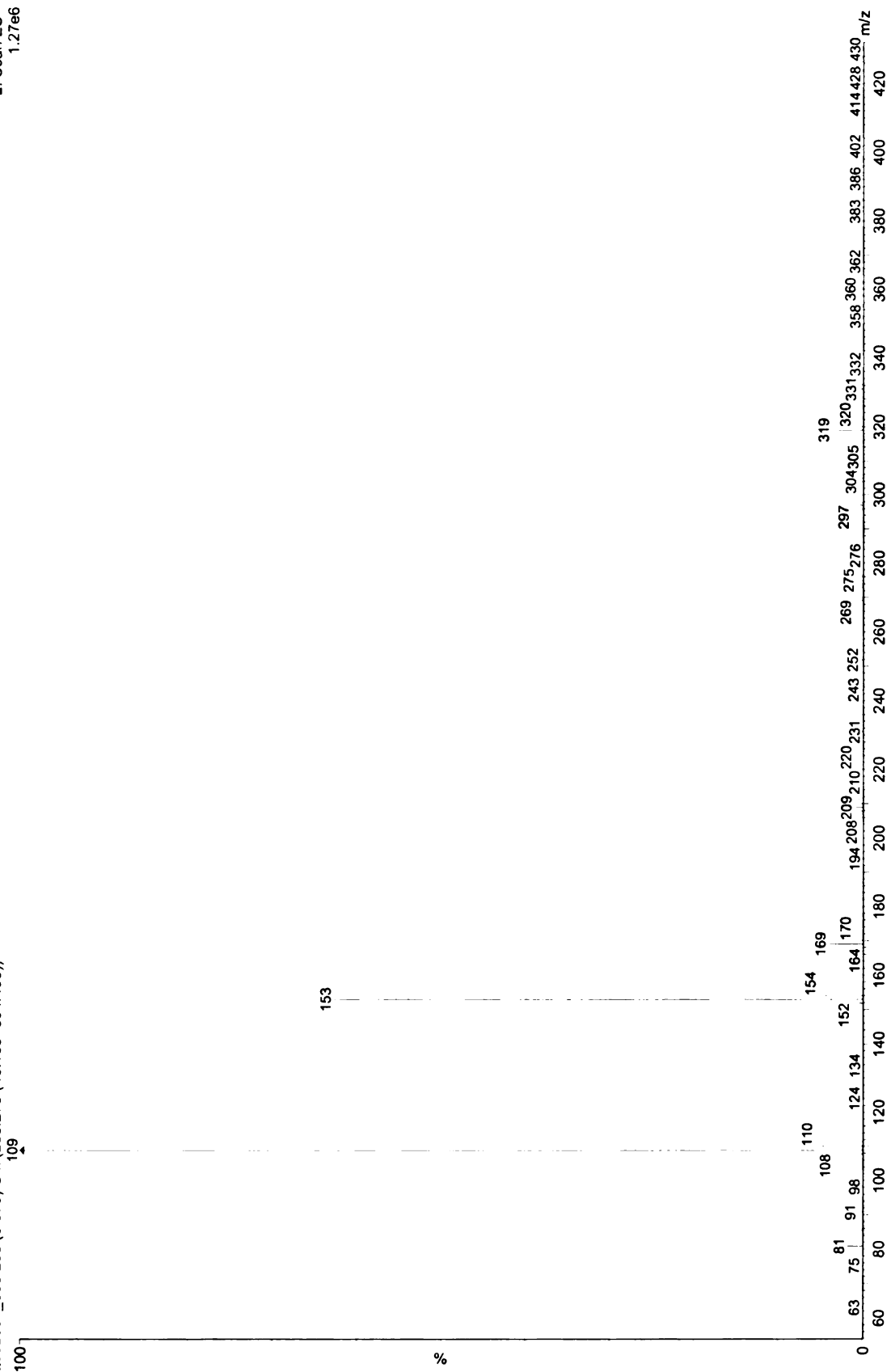
2 Scan ES-
169
1.26e6



Salicylic Acid pH7

Q032807_003 256 (6.876) Cm (250.275-(46:135+364:463))

2: Scan ES-
1.27e6



Salicylic Acid pH3

Q032807_004

2: Scan ES-
TIC
2.81e8

100
0
%

1.69

14.24

47.06 50.87

Q032807_004

1: Scan ES+
TIC
1.09e8

100
0
%

0.09

2.27

2.40

2.67

2.75

2.99

1.79

47.02

46.83 47.23 51.32

46.67 47.29 51.59

50.54 50.38 51.69

45.33 50.38 51.69

58.03 54.30 55.02 58.46 59.29

Time

60.00

55.00

50.00

45.00

40.00

35.00

30.00

25.00

20.00

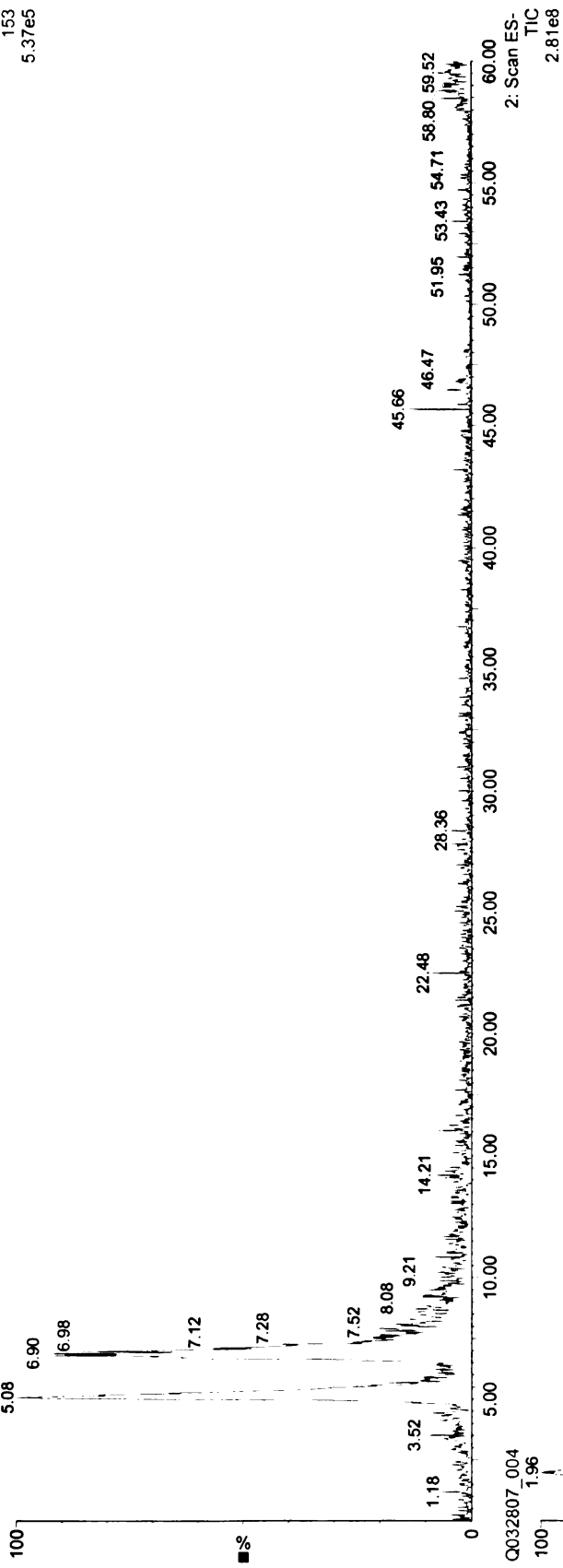
15.00

10.00

5.00

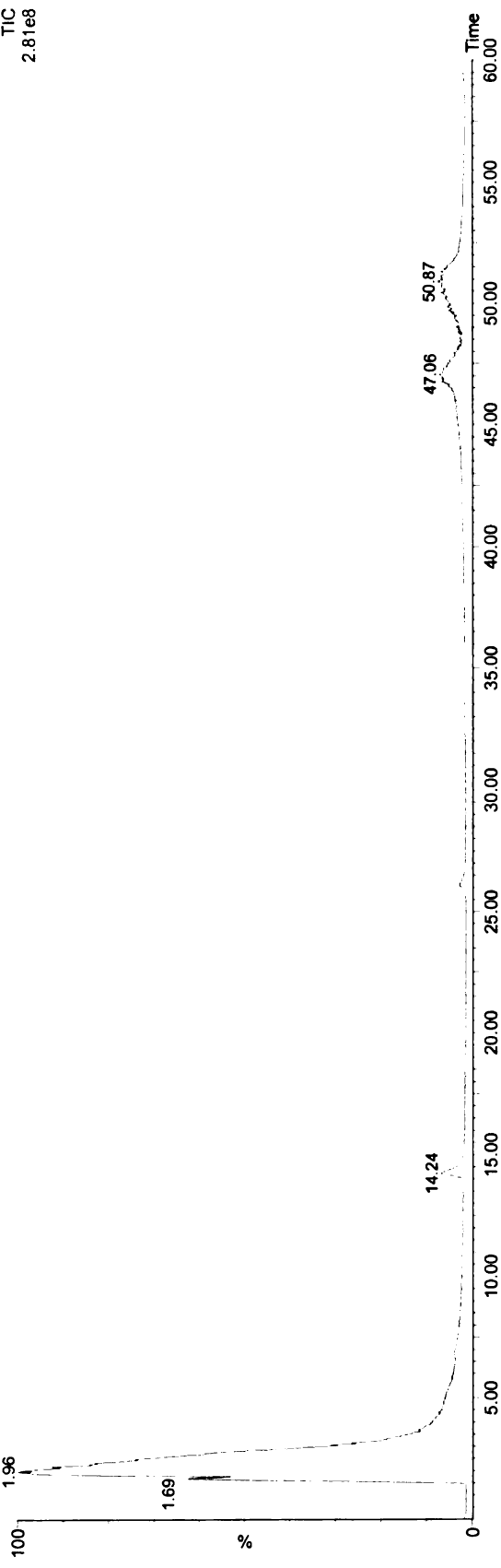
Salicylic Acid pH3
Q032807_004

2: Scan ES-
153
5.37e5

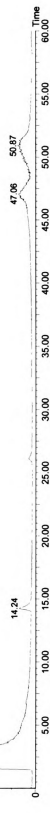
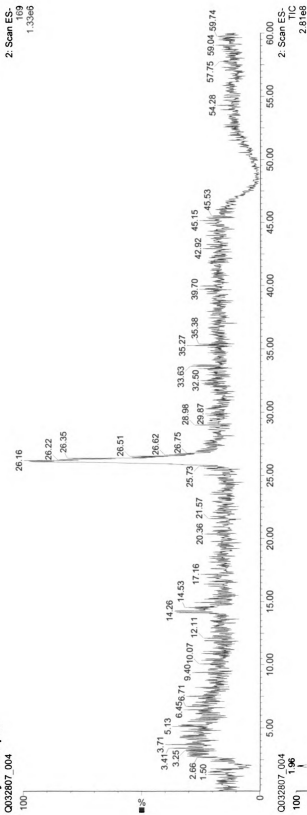


Q032807_004

2: Scan ES-
TIC
2.81e8



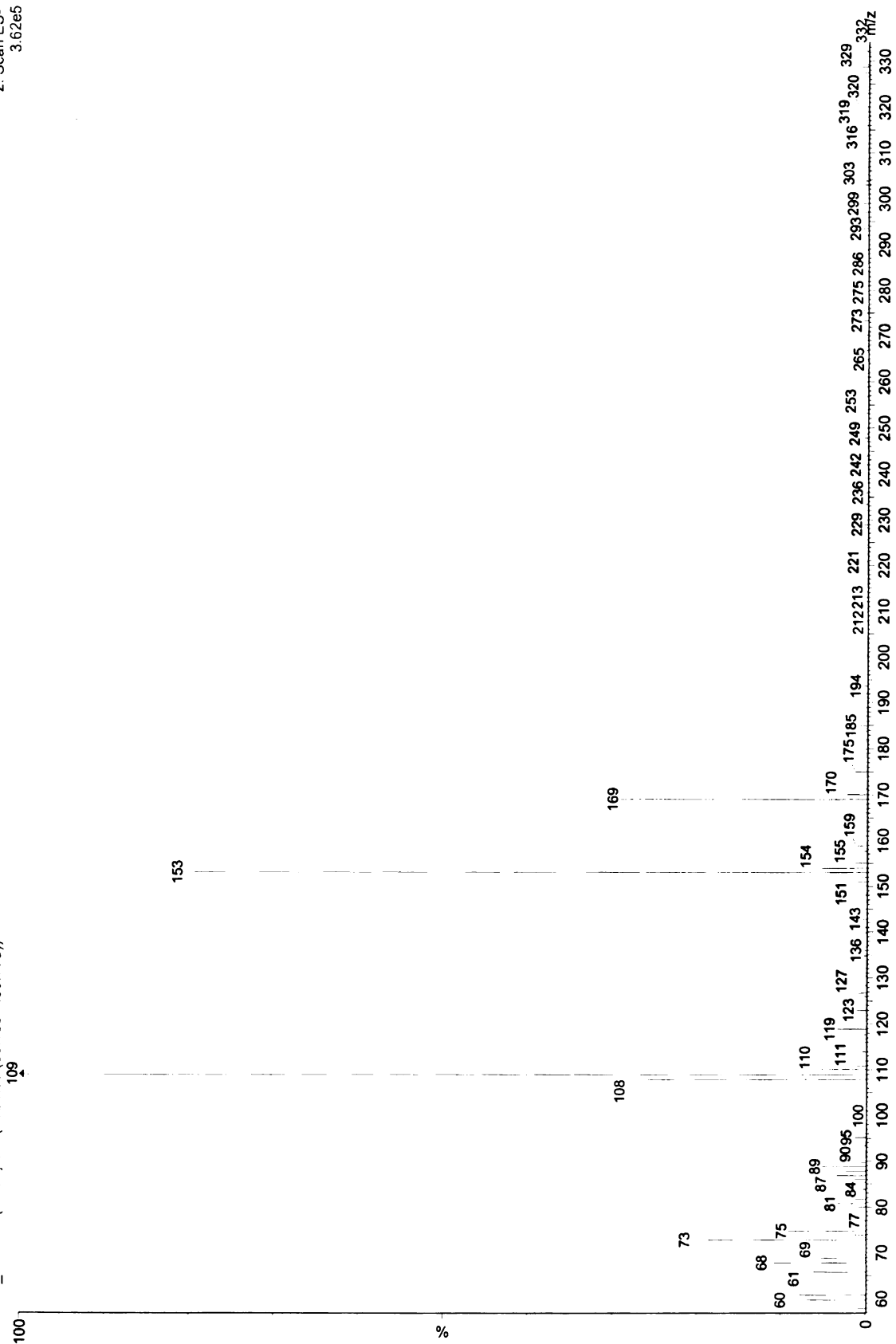
Salicylic Acid pH3
Q032807_004

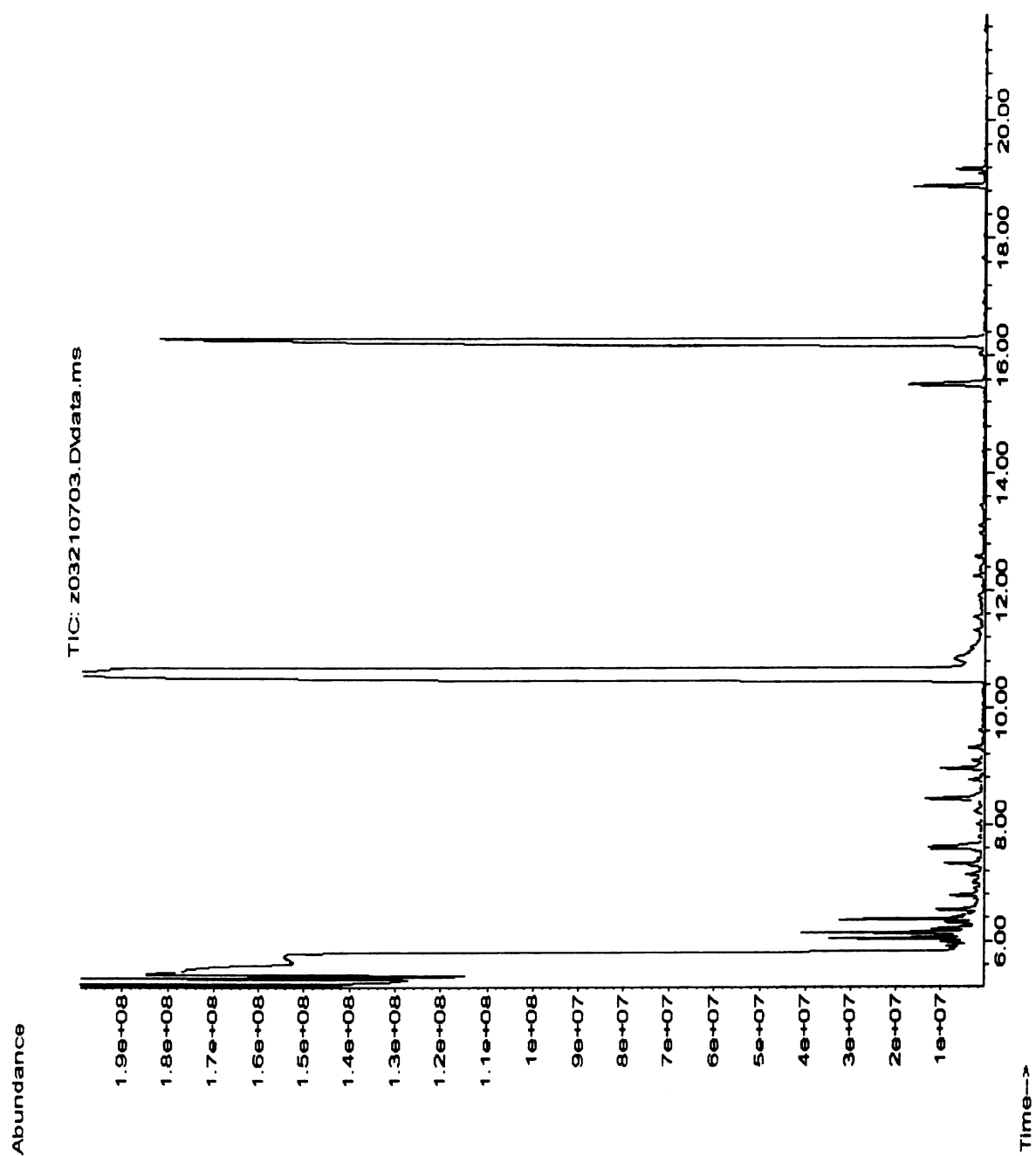


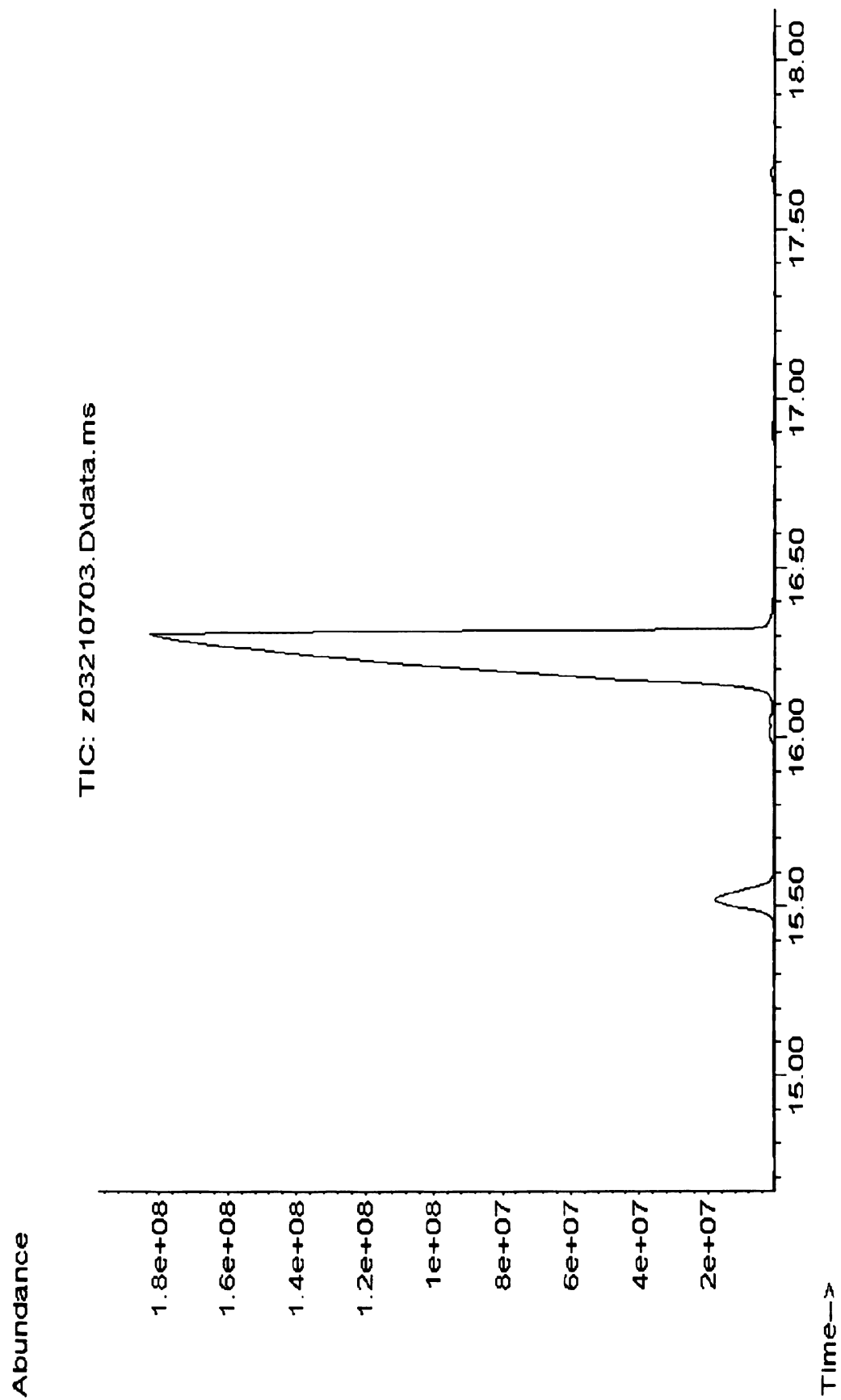
Salicylic Acid pH3

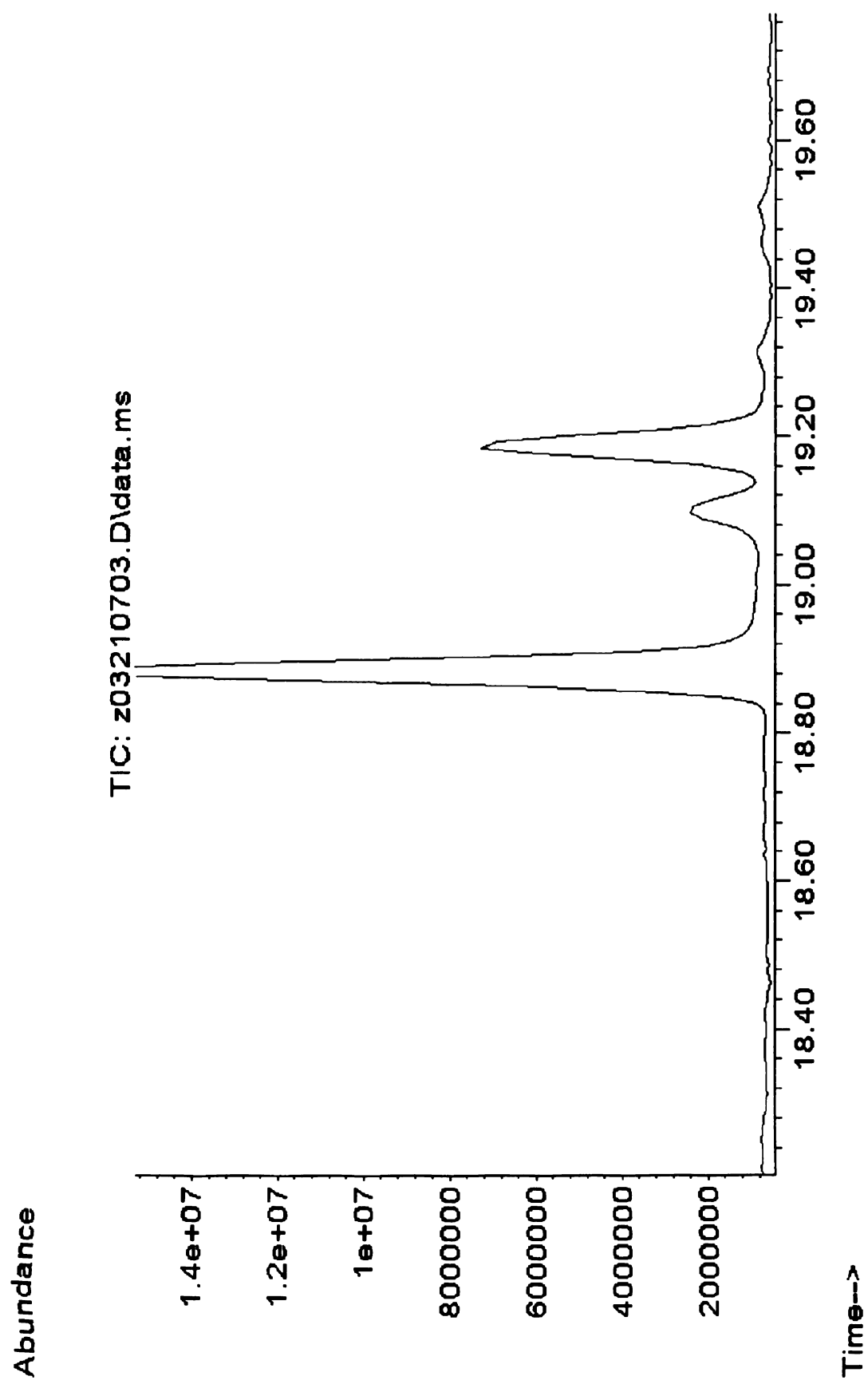
0032807_004 190 (5.103) Cm (188:208-(50:165+433:778))

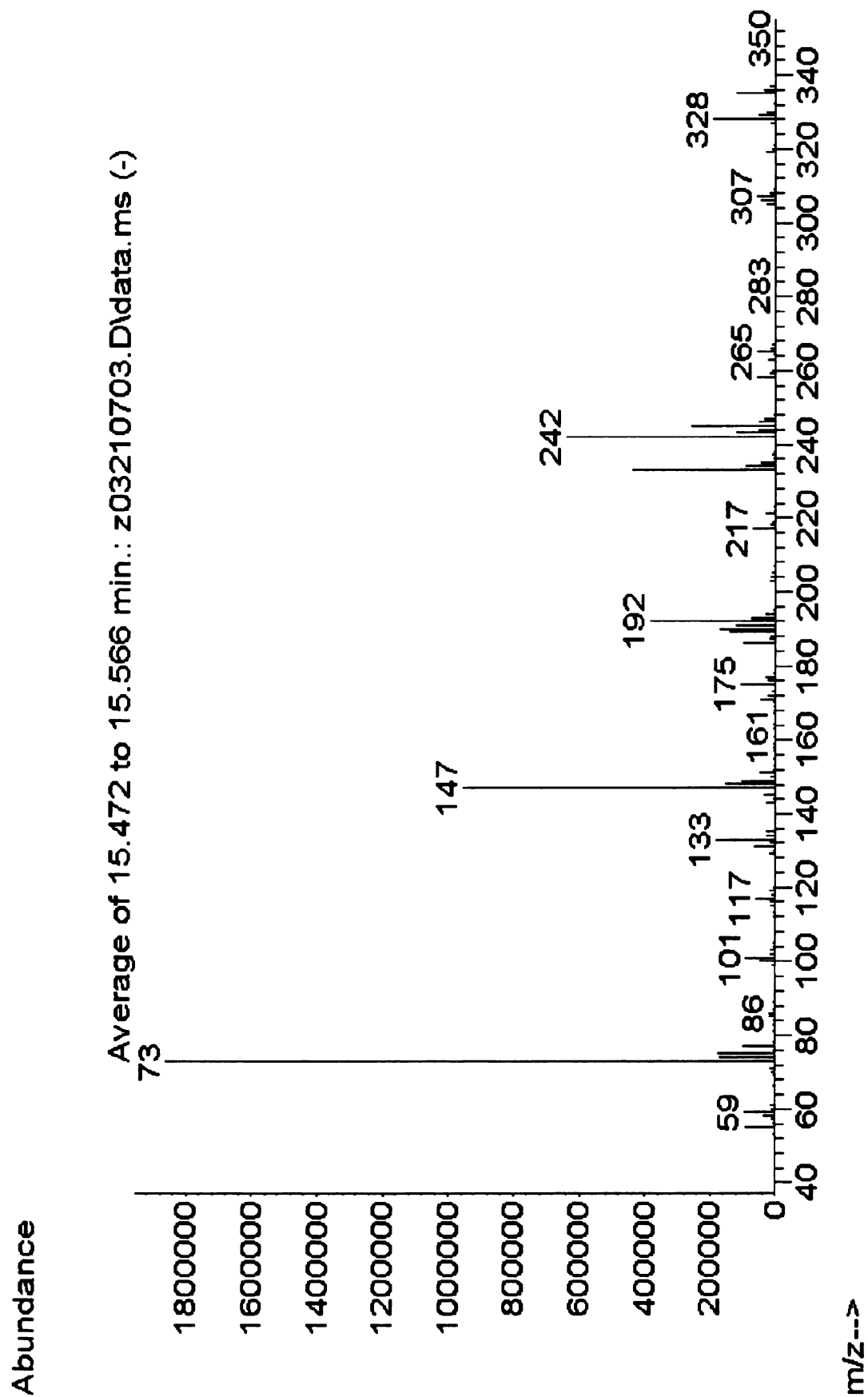
2: Scan ES-
3.62e5

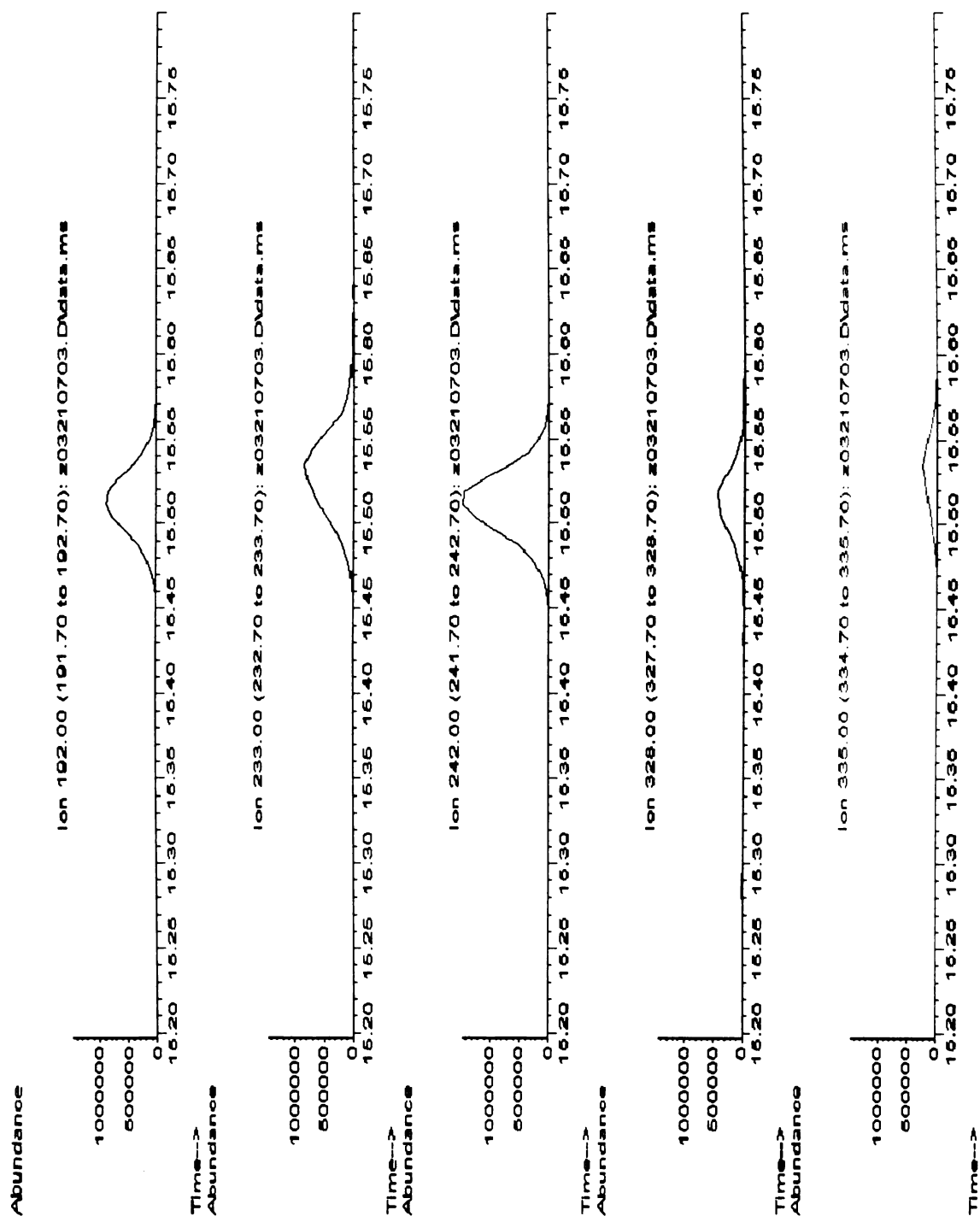




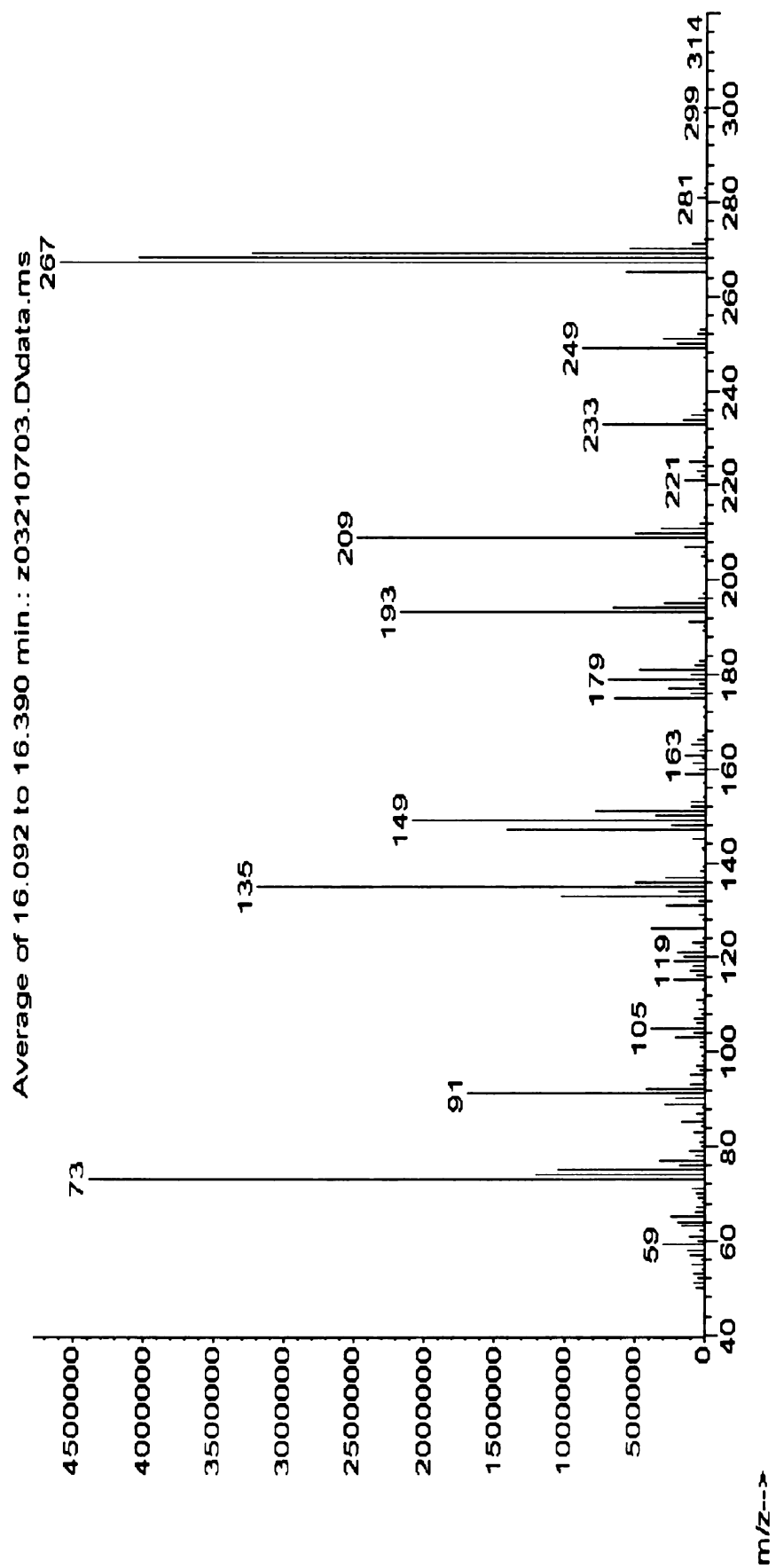




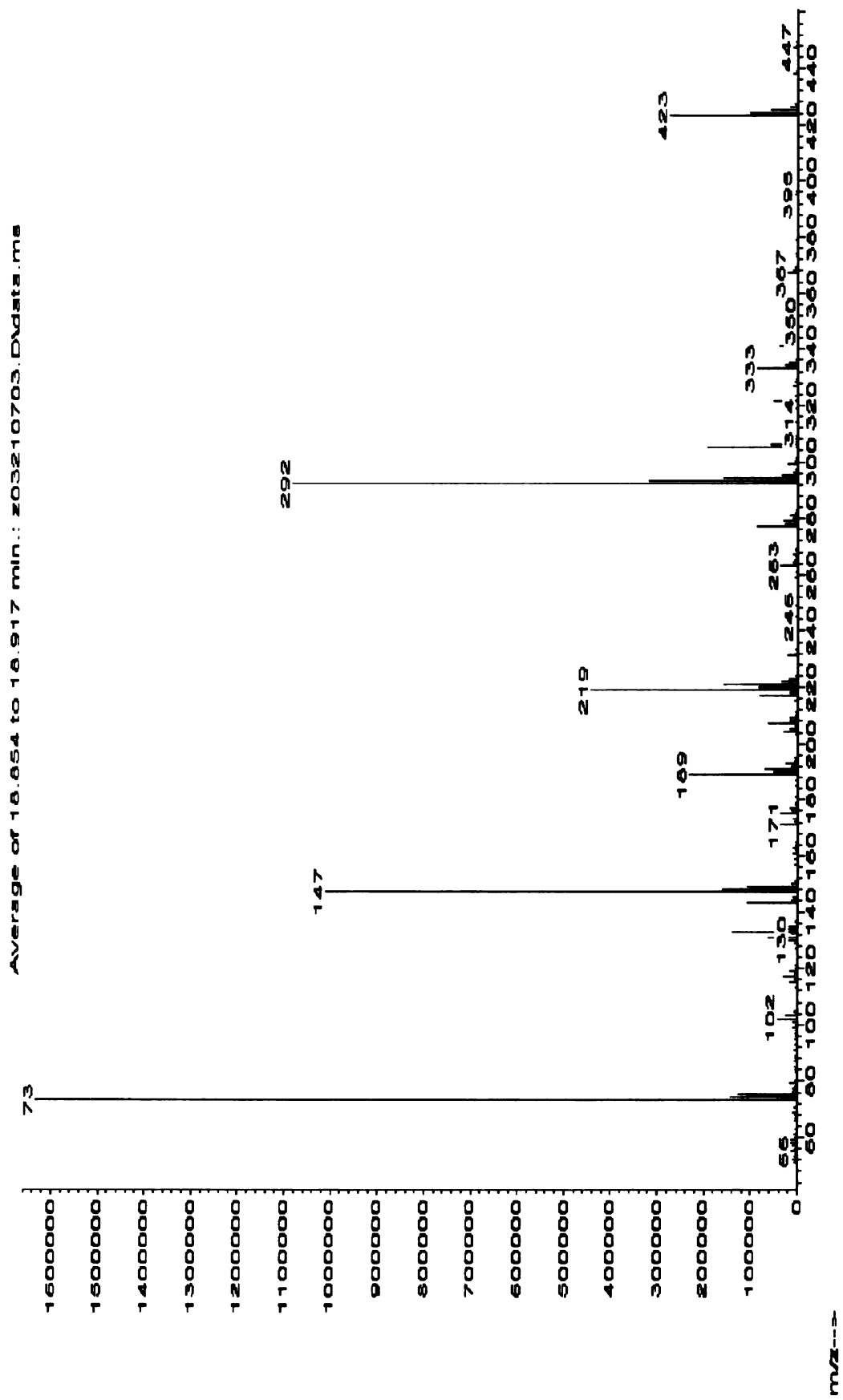




Abundance



Abundance



Appendix C

Appendix C: HPLC Chromatograms

HPLC chromatograms of hexane and acetonitrile extracts from CHP reactions extracted from both soluble and mineral iron catalyzed reactions in aqueous matrices.

Hexane Extracts

Soluble iron catalyzed: chromatogram using ultraviolet detector (254nm).....239

Soluble iron catalyzed: chromatogram using fluorescence detector (ext: 310nm, em: 400nm).....240

Goethite catalyzed: chromatogram using ultraviolet detector (254nm).....241

Goethite catalyzed: chromatogram using fluorescence detector (ext: 310nm, em: 400nm).....242

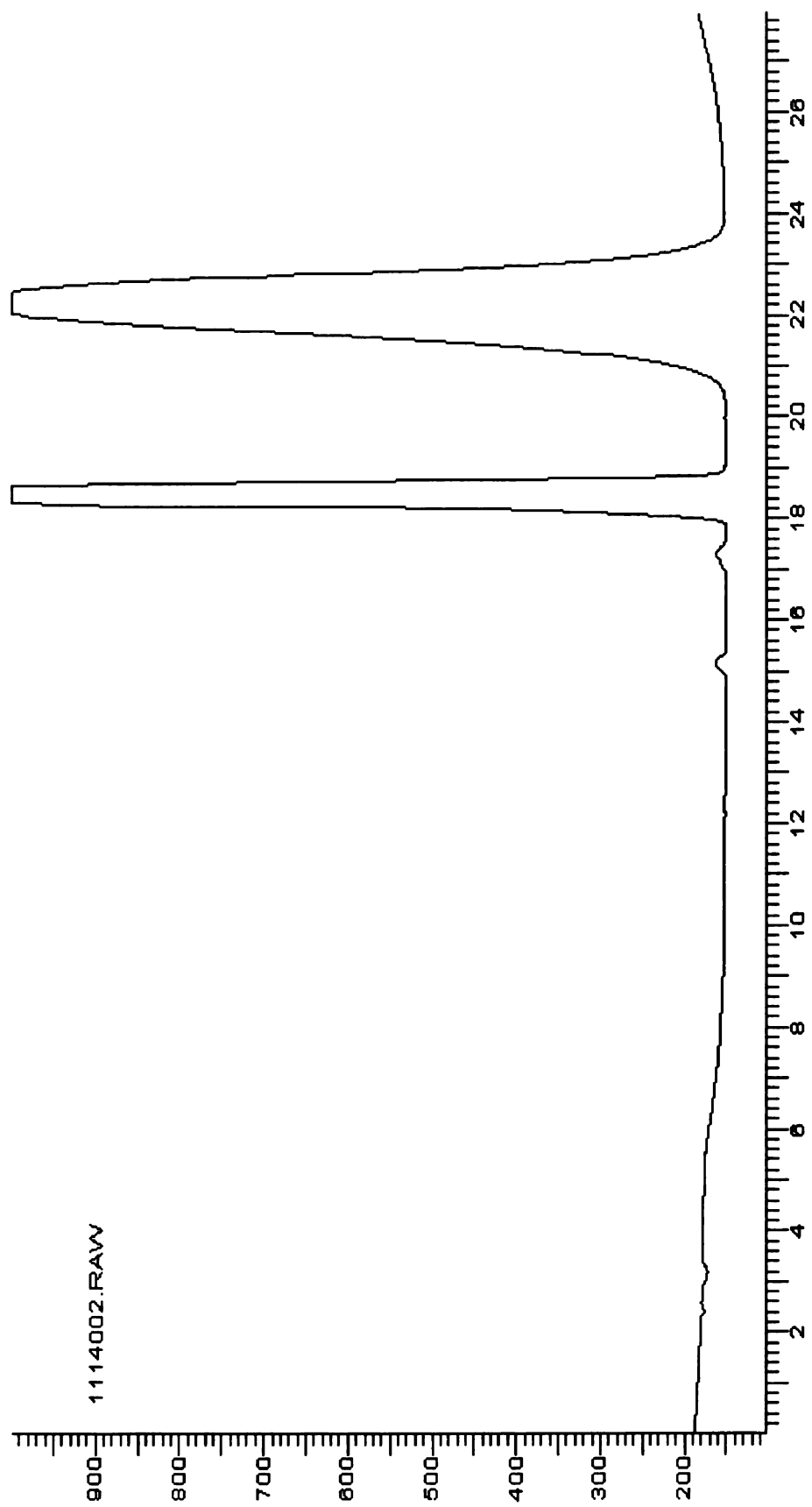
Acetonitrile Extracts

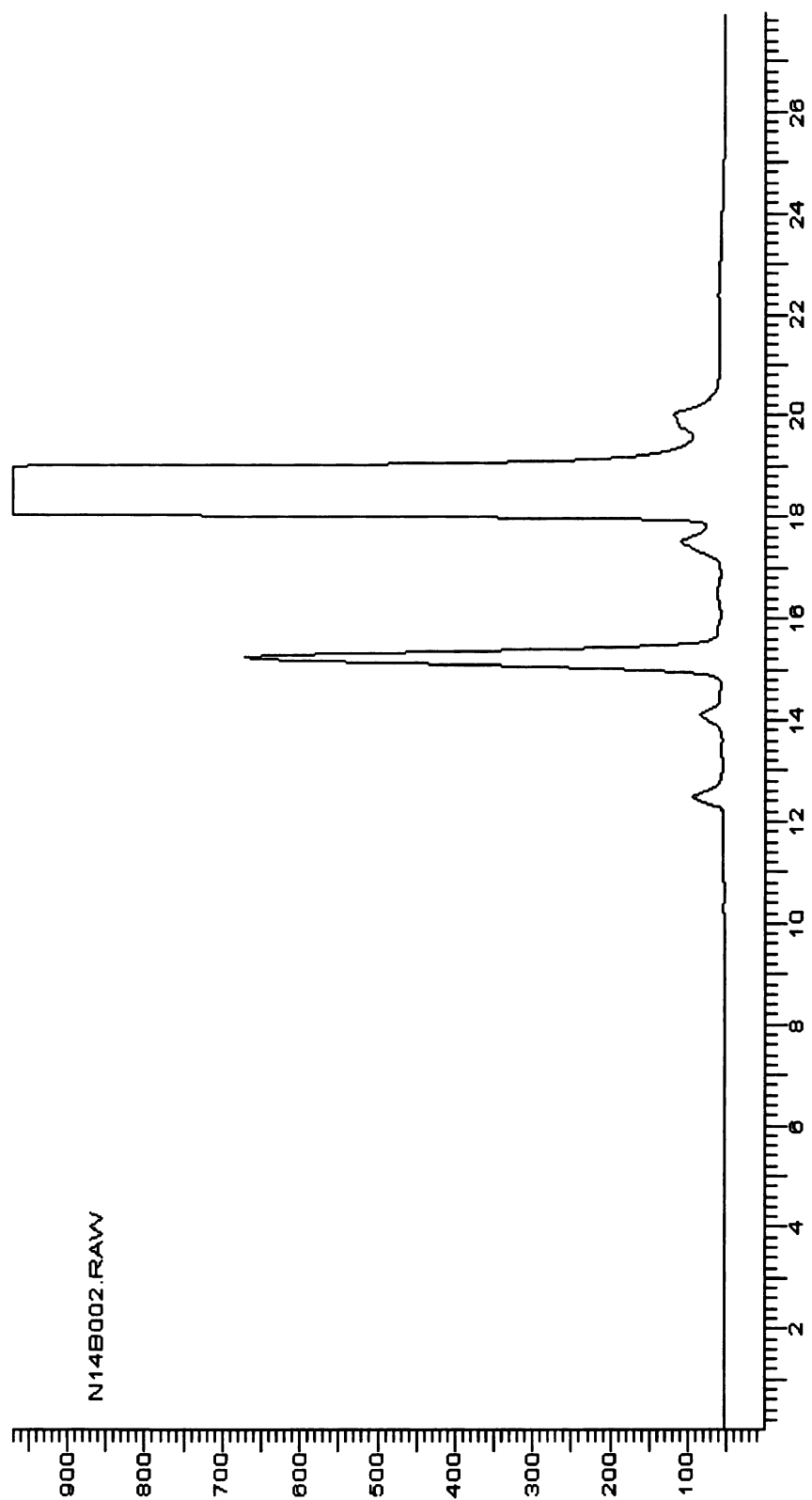
Soluble iron catalyzed: chromatogram using ultraviolet detector (254nm).....243

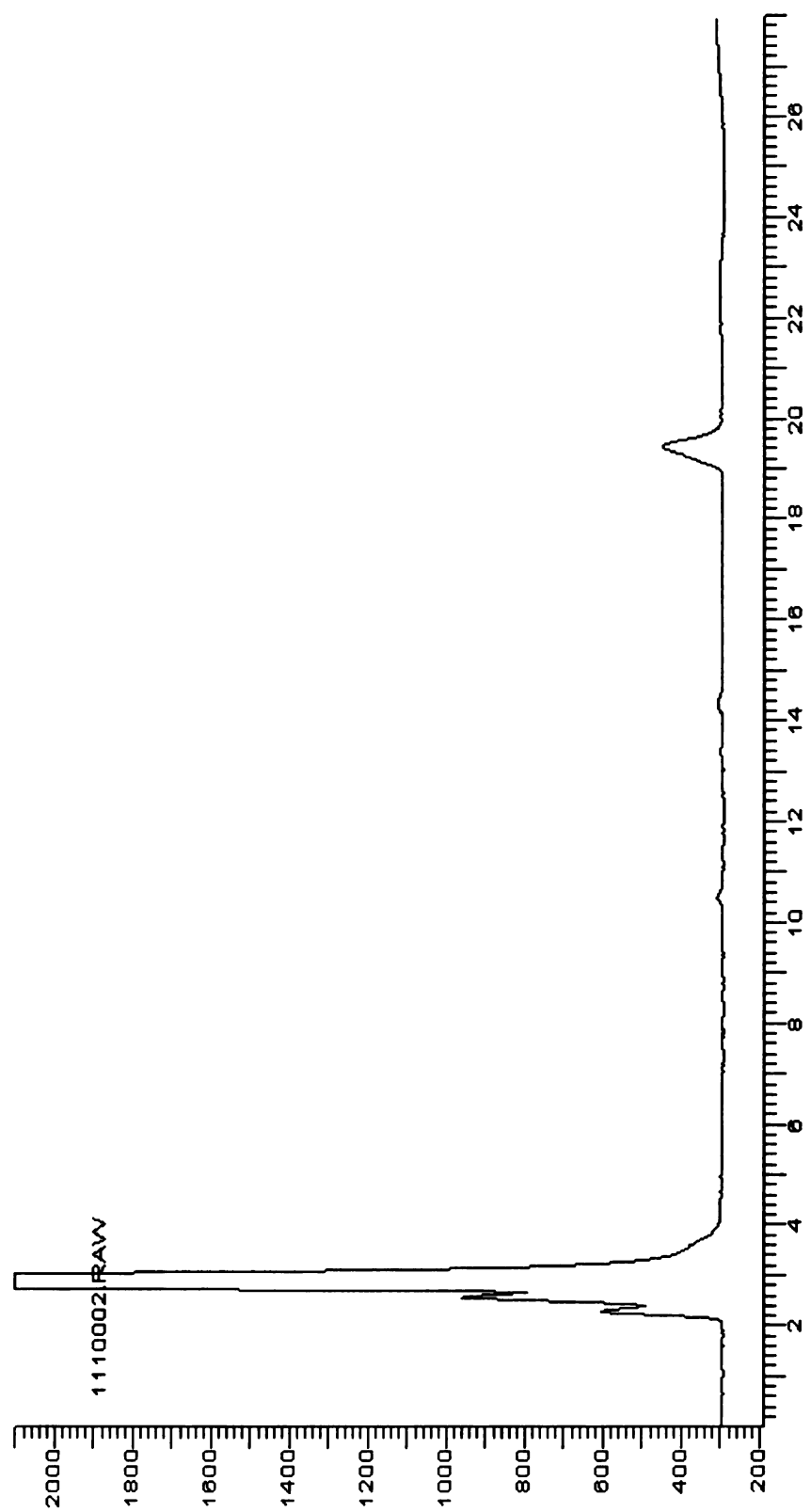
Soluble iron catalyzed: chromatogram using fluorescence detector (ext: 310nm, em: 400nm).....244

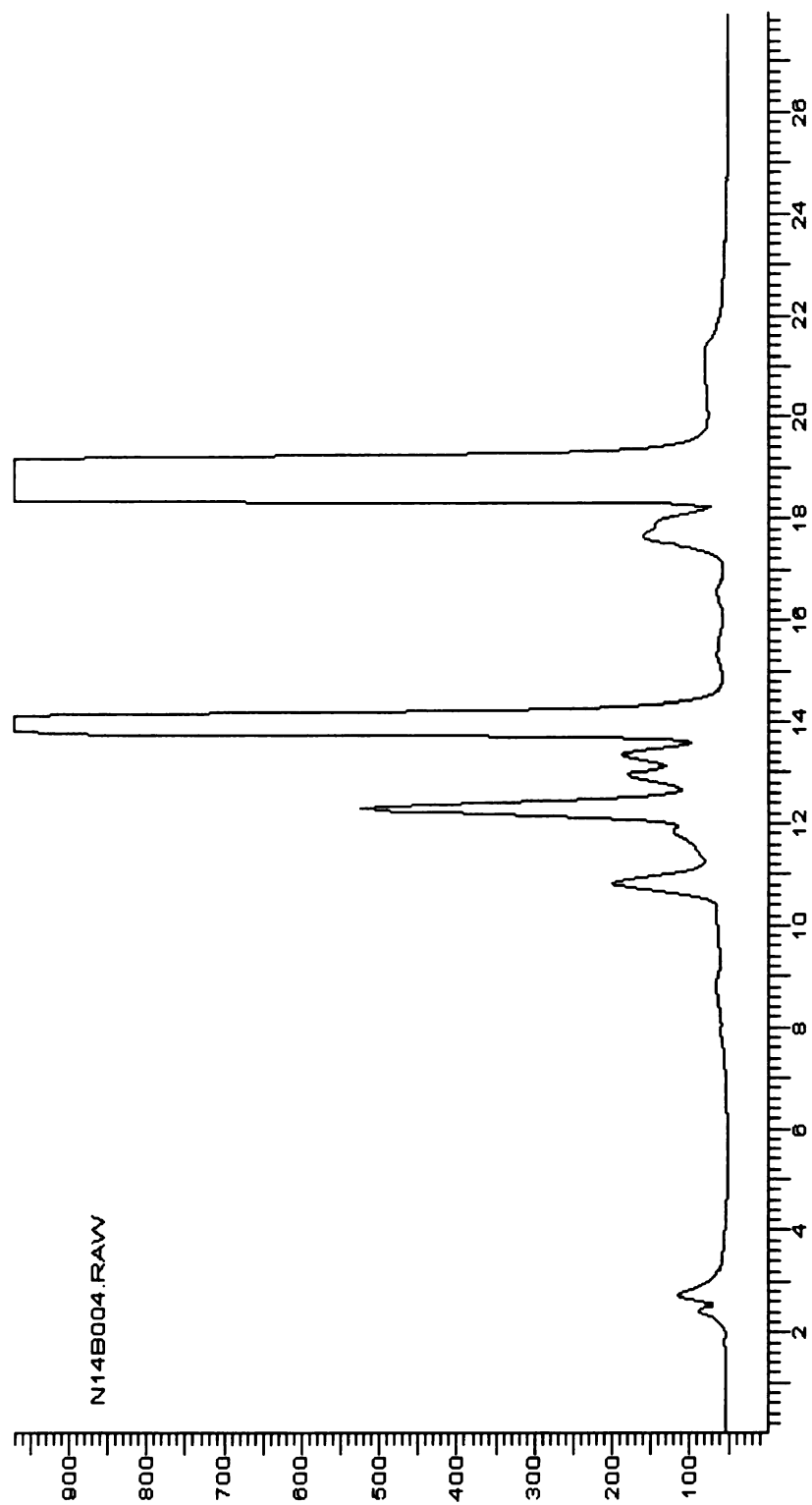
Goethite catalyzed: chromatogram using ultraviolet detector (254nm).....245

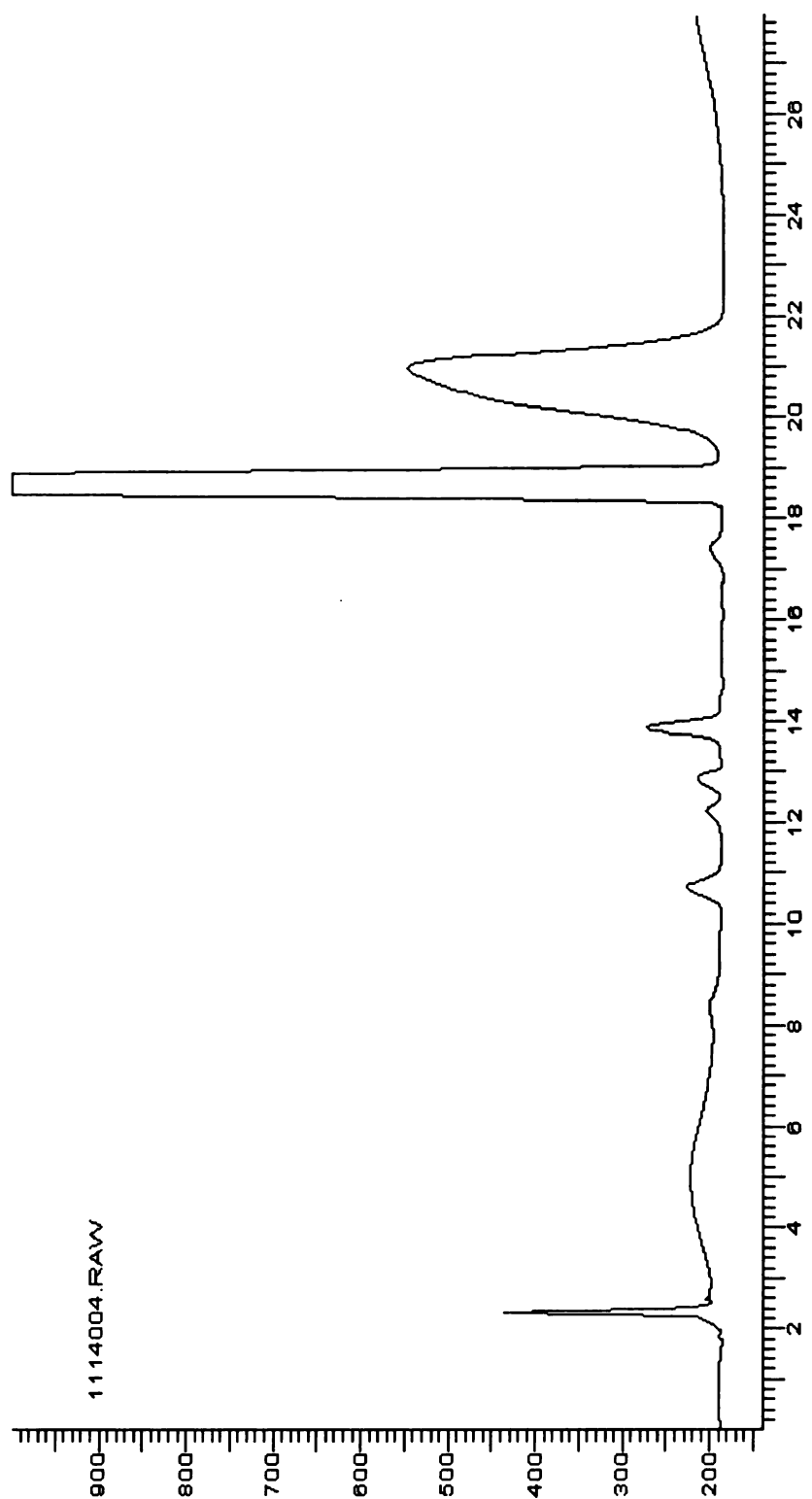
Goethite catalyzed: chromatogram using fluorescence detector (ext: 310nm, em: 400nm).....246

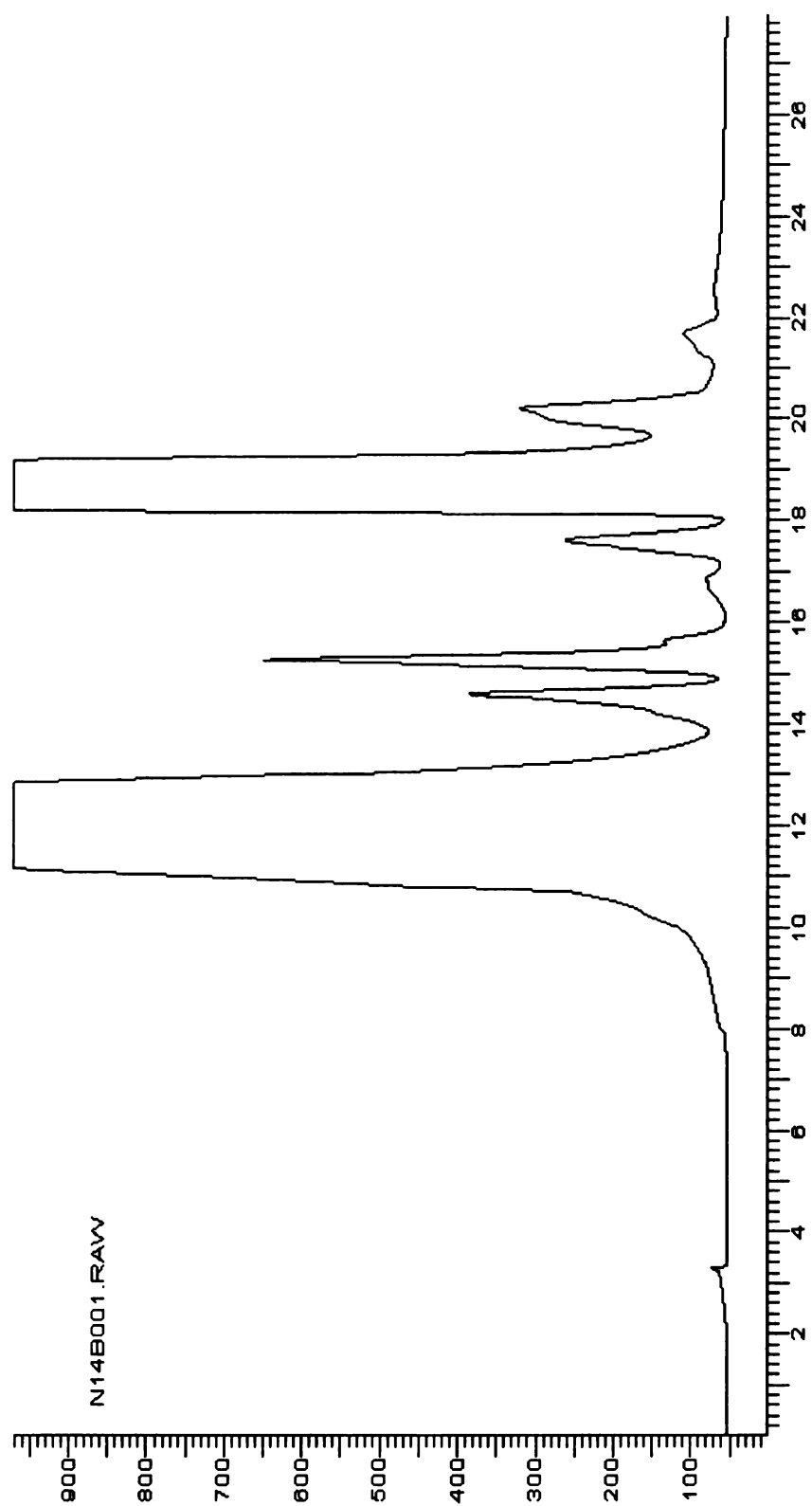


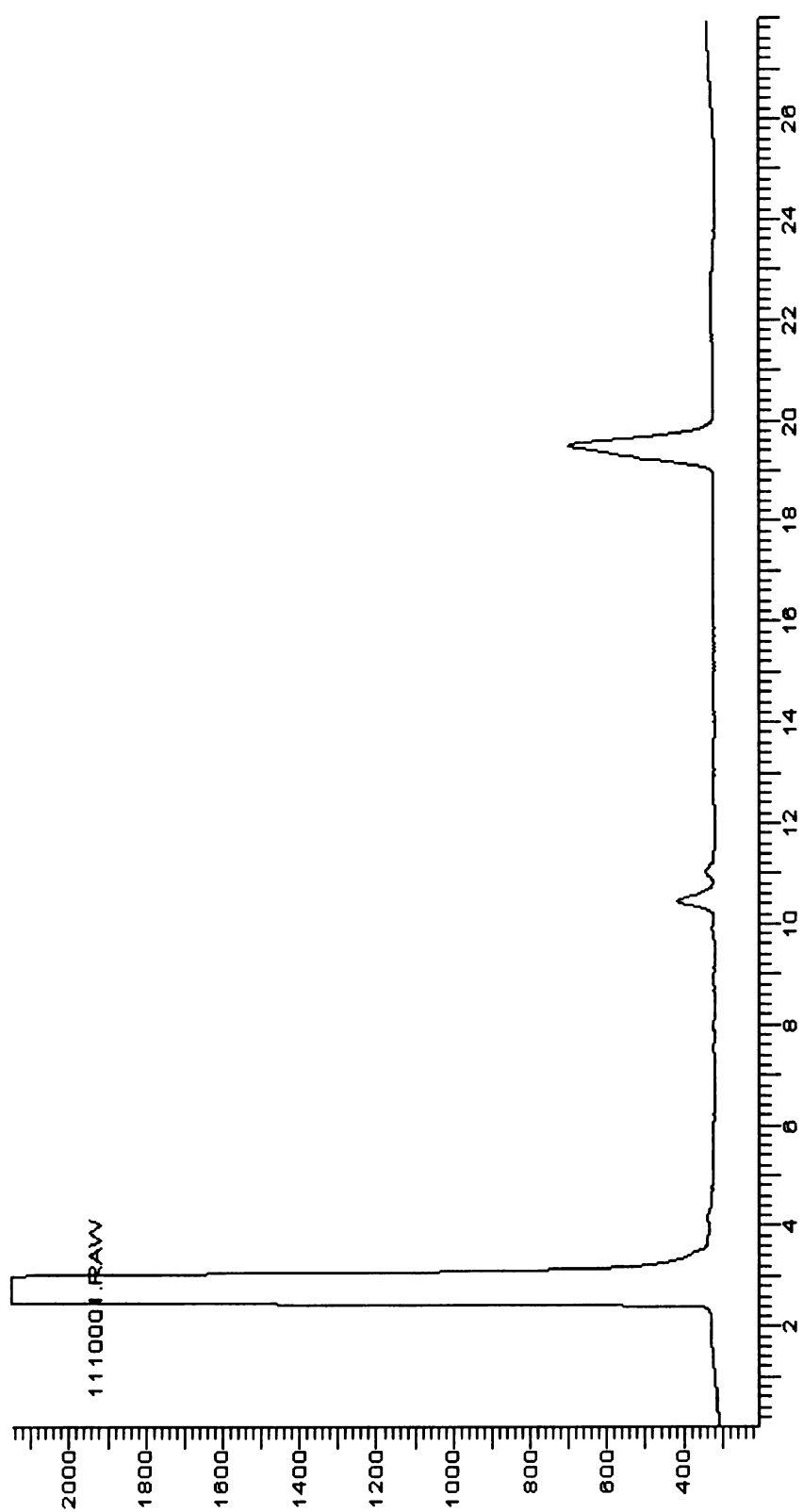


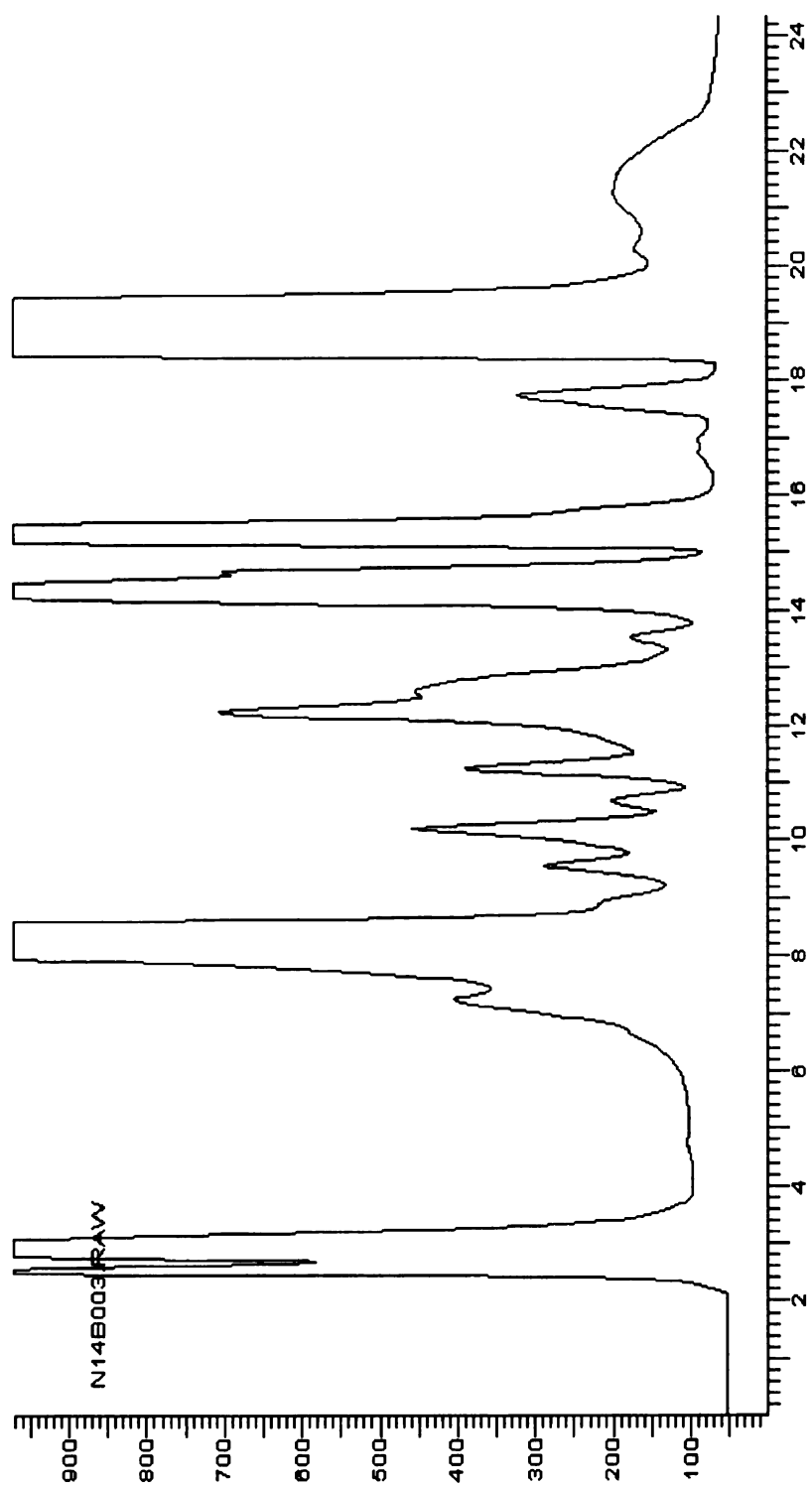












Appendix D

Appendix D: MATLAB Code for Kinetic Model:

This model was run using the data collected from the oxygen production data and the hydrogen peroxide titrations. The RMSE was obtained using the Genetic Algorithm function. Authors: Geneva Hulslander and Carlos Sanlley

```
function [cpr,T] = FentonFerric2T(t,c);
global c0 tspan k1 T;
cpr = zeros(7,1);
% c0=[0.1,0,0.07,0,0,0,0]; %Trial 1
%decomposition of h2o2 in 1/s
%fenton reaction k's;
k2=76;
k3=2*10^-3;
k4=1*10^-3;
k5=5*10^-7;
k6=2*10^5;
k7=3.3*10^7;
k8=(1.2)*10^6;
k9=1*10^7;
V=25*10^-3;
To=19.5;
theta=1.058;
%T=20; %Not temperature corrected
T=To*(1.102.*exp(-(0.0012./60).*t)-0.105.*exp(-(0.406./60).*t)); %Trial
1
%T=To*((1.612.*exp((-0.0094./60).*t))-(0.639.*exp((-0.539./60).*t)));
%Trial 2
%k1=0.00194; %From optimization Trial 1
k1=0.00841; %From optimization Trial 2

% hydrogen peroxide
cpr(1)=- (k1.*theta.^(T-20)+k2*theta.^(T-20)*c(2)+k3*theta.^(T-
20)*c(3)+k7*theta.^(T-20)*c(4))*c(1)+k9*theta.^(T-20)*c(6)*c(2);
% Ferrous Ion
cpr(2)=-k2.*theta.^(T-20).*c(1).*c(2)+k3.*theta.^(T-
20).*c(3).*c(1)+k4.*theta.^(T-20).*c(3).*c(5)+k5.*theta.^(T-
20).*c(6).*c(3)-k8.*theta.^(T-20).*c(2).*c(5)-k9.*theta.^(T-
20).*c(2).*c(6);
% ferric ion
cpr(3)=- (-k2.*theta.^(T-20).*c(1).*c(2)+k3.*theta.^(T-
20).*c(3).*c(1)+k4.*theta.^(T-20).*c(3).*c(5)+k5.*theta.^(T-
20).*c(6).*c(3)-k8.*theta.^(T-20).*c(2).*c(5)-k9.*theta.^(T-
20).*c(2).*c(6));
% hydroxyl radical
cpr(4)=k2.*theta.^(T-20).*c(1).*c(2)-k7.*theta.^(T-20).*c(1).*c(4);
% perhydroxyl radical
cpr(5)=k3.*theta.^(T-20).*c(1).*c(3)-k4.*theta.^(T-20).*c(3).*c(5)-
k6.*theta.^(T-20).*c(5)-k8.*theta.^(T-20).*c(2).*c(5);
% superoxide
cpr(6)=k6.*theta.^(T-20).*c(5)-k5.*theta.^(T-20).*c(6).*c(3)-
k9.*theta.^(T-20).*c(2).*c(6);
% Oxygen
```



```

cpr(7)=(2.*k1.*theta.^(T-20).*c(1)+k4.*theta.^(T-
20).*c(3).*c(5)+k5.*theta.^(T-20).*c(3).*c(6)).*V;

function [rmse]=fentonobj(kk)
global c0 tspan k1 X;
k1=kk(1);
X=kk(2);
tspan = [0:15:2100];
c0=[0.1,0,0.07,0,0,0,0]; %Trial 1
%c0=[0.5736,0,0.07,0,0,0,0]; %Trial 2
options=odeset('AbsTol',[1e-7,1e-12,1e-7,1e-12,1e-12,1e-12,1e-7]);
[t,c]=ode23s(@FentonFerric2T,tspan,c0, options);
load work
time=b(:,1)*60;
simc=interp1(t,c(:,7),time);
obs=b(:,2);
rmse=sqrt(sum((simc-obs).^2));
plot(t,c(:,7),'-g');hold on
%errorbar((a(:,1))*60,a(:,2),a(:,3)./2,'r^');
errorbar((b(:,1))*60,b(:,2),b(:,3)./2,'bp');
% title('Oxygen');
% xlabel('Time (sec)');
% ylabel('moles');
hold off

global c0 tspan k1;
k=fminbnd(@fentonobj,1e-6,1);

```

MICHIGAN STATE UNIVERSITY



3 1293 03062 59